Fluctuations of Global Quantites in Highly Correlated Systems

SUBMITTED BY

Simon Trevor Banks

FOR THE DEGREE OF

Doctor of Philosophy

SUPERVISED BY

Professor Steven T. Bramwell

University College London, 2005

ProQuest LLC
789 East Eisenhower Parkway
P.O. Box 1346
Ann Arbor, MI 48106-1346

Abstract

This thesis addresses the nature of global (many body) fluctuations in highly correlated systems. We begin with the question of temperature dependence in finite two dimensional XY (2dXY) model magnets. Such systems have a fully critical low temperature phase. It is shown analytically, backed up by extensive Monte Carlo simulations, that the non-Gaussian distribution of order parameter fluctuations is not strictly universal but has an explicit temperature dependence – contrary to previous findings. The temperature dependence is used to explain why past studies derived the same distribution for fluctuations of the full order parameter and an approximate linearized form. The appearance of spin vortices in the related Harmonic model is discussed and an argument is presented for why these defects must always appear as bound pairs.

The linearized order parameter of the 2dXY model leads to a family of dimensionally dependent models defined in reciprocal space. An argument is presented for the interpretation of these systems as being critical and a direct space Hamiltonian is derived for the one dimensional case. This model has order parameter fluctuations distributed according to the Fisher-Tippett-Gumbel distribution from extreme value statistics (EVS). The link between criticality and EVS is investigated, as are the origins of the non-Gaussianity. The ability to distinguish between critical distributions is discussed. It is seen that for one, two and three dimensions the critical models presented lead to functionally similar fluctuation distributions.

A previously reported link between EVS and $1/f$ noise is investigated. Our one dimensional critical model is mapped onto the action used to generate $1/f$ signals and we propose an alternative interpretation of the link in the context of a $1/q$ dispersion of spatial normal modes. The experimental observability of the FTG distribution in $1/f$ signals is considered with emphasis on imperfections in the noise. A physically relevant method of generating $1/f$ noise from the superposition of random telegraph signals is also examined.

Contents

List of Figures

List of Tables

Notation

The following symbols and abbreviations appear frequently throughout this thesis:

§	A label used to refer to other sections of the thesis.
arXiv	Used in the bibliography to denote pre-prints available from the e-print archive, http://arxiv.org/.
$\langle x \rangle$	The mean average value of x.
$\langle i, j \rangle$	Used in sums to denote the set of all pairs of variables with $i \neq j$.
(i, j)	Used in sums to denote the set of all pairs of variables with $i = j$ permitted.
β	Used as both the inverse temperature and the order parameter critical exponent. The context should make it clear in which sense it is being used.
BHP	Bramwell-Holdsworth-Pinton (probability density function).
CLT	Central Limit Theorem.
d	The dimensionality of the system.
FBC	Free Boundary Conditions.
f.s.s.	Finite size scaling.
FTG	Fisher-Tippett-Gumbel (probability density function).

k_B	The Boltzmann constant. Throughout this thesis we use units with $k_B = 1$ unless stated otherwise.
$\Im$	The imaginary part of a complex number.
id	Identically distributed.
iid	Independent and Identically Distributed.
J	The magnetic exchange interaction. All the systems considered here are ferromagnetic so J is always positive.
L	The 'linear' size of a discrete system. Generally applied in the case of a hypercubic lattice where it represents the length of one side of the hypercube.
MLG	Multiple Loop Graph.
N	The system size for discrete systems. Equal to the number of degrees of freedom. For a hypercubic lattice $N = L^d$.
PBC	Periodic Boundary Conditions.
PDF	Probability Density Function. Often loosely refered to as the Probability Distribution Function.
$\Re$	The real part of a complex number.
SLG	Single Loop Graph.
T	Temperature. Unless stated otherwise T is in units of J, the exchange interaction.
WBC	Window Boundary Conditions.

Acknowledgements

It is undoubtedly true that no work is done in isolation and I am grateful for this opportunity to say thank you to all those who have helped me in so many ways over the past three years...

First and foremost I must say a very big thank you to my parents, Alva and Trevor, though thank you hardly seems enough. The backup and support they have given has been incredible. This thanks is not just for the practical things that have eased the preparation of this thesis, but, more importantly, for the constant flow of sound advice from two of the wisest people I know.

My thanks extends to the rest of my family too; to Katy, Alex and (more recently!) Emily, a big thank you.

To Steve, my supervisor, I owe thanks on many levels. Firstly for introducing me to the topics that form the basis for the work presented here, about which I knew nothing before. For the interest and enthusiasm with which he spent many hours discussing the finer details of statistical physics – invariably helping me to surmount the apparently insurmountable barriers along the way. But most of all for his generosity with time and of spirit.

And thanks also to my 'second supervisor' Mike Ewing for his continued support.

For my funding I thank the University College London Graduate School for a Graduate School Research Scholarship.

Sincere thanks to all those friends who have provided a place to stay in London thereby easing the occasional woes of commuting. In particular thanks to Dimitris and Stella for their friendship and overwhelming hospitality. Dimitris also deserves special thanks for his frequent help with all manner of computer related problems. His knowledge is apparently unbounded!

To the old guard of G25: Linnea, Emma, Natalie and Katherine – my thanks for being so nice to the only man in the office!

And thanks also to...

...the members of G19: Andrea, Giusy, Kieran, and Luke; to Alexandra, Masae, Andrew Wills, Nik Kaltsoyannis (for helping to resurrect Bismuth), Maxime, Camilla, Charles and Frank Johnson; finally thanks to Charlie Cleary and Maggie Allgrove (Waller) – two great scientists and inspirational teachers.

Chapter 1

Introduction

Fluctuations inherent in physical systems can sometimes make it impossible to assign constant values to observables[1, 2]. Instead these are quantified by a distribution function describing the probability that a measurement will yield a particular result. For a quantum system, when the wavefunction is not an eigenstate of some operator $\hat{A}$, repeated measurement of the observable corresponding to $\hat{A}$ will necessarily yield a distribution of values [3]. The origins of classical fluctuations are less clearly defined. They depend explicitly on the system and are generally too complex to describe theoretically [2]. Despite this, certain generalizations are possible regarding the form of the fluctuation distributions. A global measure of a system with a large number of degrees of freedom is usually expected to be normally distributed as a result of the central limit theorem (CLT) [4]. For this to be true, the system must be separable into micro- or mesoscopically independent, individually negligible, elements [1]. When these criteria are not met there is no reason to expect fluctuations to adopt a Gaussian form and the distribution of the global measure may be any of a range of suitable probability functions.

Systems at thermodynamic critical points are infinitely correlated and may therefore have non-Gaussian global fluctuations [2, 5]. In regions of phase space away from these points the Landau expansion of the free energy is generally valid*, e.g. for some

*Although there are notable exceptions – the non-critical three dimensional XY model, for example, where non-Gaussian fluctuations occur as a result of the influence of Goldstone modes [6].

global variable x, the chemical potential μ is given by

$$\mu(x,T) \sim a(T) + b(T)x^2 + \ldots, \tag{1.1}$$

and so the probability density function (PDF) is Gaussian, as

$$P(x) \sim \exp(-\mu(x,T)/T). \tag{1.2}$$

The width of this function scales with system size, N, as $\sigma \propto N^{-1/2}$ and is therefore zero in the thermodynamic limit, with $P(x)$ being a delta function centred on the average value [1, 2]. Macroscopic observables are then effectively constant as their values are many orders of magnitude greater than the range of their fluctuations – a fact which underpins the theory of classical thermodynamics [2, 4].

The CLT strictly only applies to the normalized variate $x/\sqrt{N}$ [7] and with this scaling the Gaussian form is extracted from the delta function PDF [8, 9]. At a critical point Landau theory breaks down and the high degree of correlation leads to fluctuations scaling as $N^{-1/2+\rho}$ with $\rho \neq 0$ [6, 8]. The PDF is then expected to be non-Gaussian, as can be shown explicitly for the Ising model [10, 11]. A universal, non-Gaussian PDF of a global quantity is a signature of critical fluctuations and the characterization of the forms of these functions is one of the central problems in the study of critical phenomena [5].

1.1 Motivation for the Present Work

At the heart of the renormalization group (RG) method is the assumption that the PDF of a global measure of a critical system is scale invariant and may be obtained from the appropriate critical fixed point [8, 10, 12]. As such the statistics of critical fluctuations are expected to be the same for all members of a given universality class. Studies of Ising [13, 14] and Potts [15] models provide strong evidence to this effect. These results also show the generic features that have become associated with critical PDFs, such as a skewness with large fluctuations below the mean [6] (Figure 1.1).

If statistical behaviour is characteristic of a universality class, there is no reason to expect that systems belonging to different classes will possess the same critical PDFs.

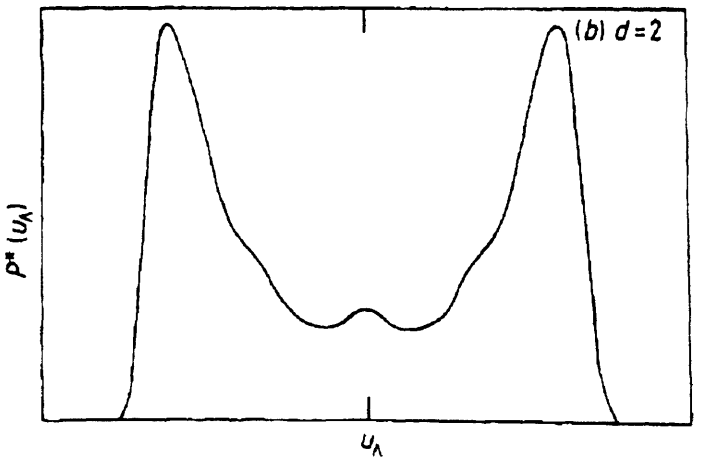

(a)

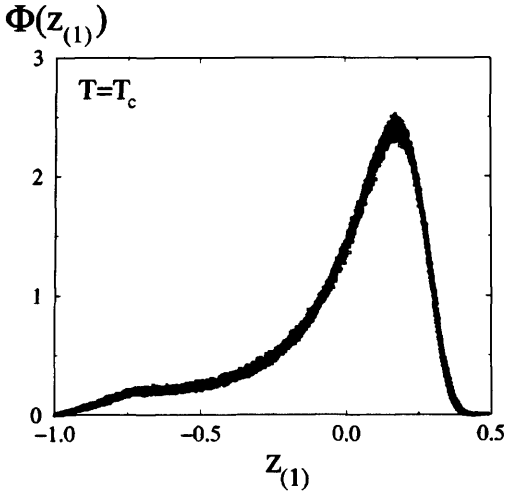

(b)

Figure 1.1: Non-Gaussian Critical PDFs: (a) For the Ising model in two dimensions, from [13]. The plot shows the distribution of the magnetization, including both positive and negative branches. In each case there is a clear skewness with a high probability of large fluctuations for small $|m|$. (b) The scaled distribution of $z = |m|$ for the 3 state two dimensional Potts model, from [15]. The data plotted corresponds to systems with $N = 1024$ (stars) and $N = 2304$ (circles). $\Phi(z)$ corresponds to our $\Pi(z)$.

However in recent years there has been much interest in a distribution function which appears to describe critical fluctuations in systems governed by a range of different fixed points [6, 16–30]. The function, called the BHP (Bramwell-Holdsworth-Pinton) distribution, was first identified in studies of the instantaneous scalar magnetization of the two dimensional XY (2dXY) model of magnetism [16]. This model has the unusual property of a fully critical low temperature region comprised of a line of critical points with a continuously varying exponent $\eta(T) = T/2\pi J$ (Appendix C). The magnetization, m, is not strictly an order parameter as it is non-intensive and becomes identically zero in the thermodynamic limit. However the slow approach to this limit allows m to remain physically relevant for large but finite systems [31, 32]. The temperature dependence of η indicates that each critical point corresponds to a different universality class. However the numerical results in [16] appeared to show a universal distribution of m, independent of both N and T.

This unusual universality is not confined to the critical region of the 2dXY model. The BHP function has been seen to describe global fluctuations in a wide range of model and experimental systems. These include power fluctuations in steady state turbulence [18–20, 33–36] and in liquid crystals undergoing electroconvective flow [37–39], variations in river heights [25], resistance fluctuations near electrical breakdown [29, 40], models of forest fires [21, 41], distributions of model avalanche sizes [21, 42], and global fluctuations in numerous other equilibrium and self-organized critical models [21]. Many of these systems are not critical in the traditional sense as they are far from equilibrium and subject to some sort of driving force. They do however possess strong long range correlations and scale invariance, properties which provide at least a heuristic link with the theory of equilibrium critical phenomena [19, 43, 44].

It appears unlikely that the wide range of systems exhibiting BHP fluctuations all belong to the same universality class – raising questions about why they should exhibit such similar statistical behaviour. An explanation was proposed by Bramwell, Holdsworth and Pinton [19] on the basis of structural similarities between the 2dXY model and closed turbulent flow, where power fluctuations were seen to be BHP like

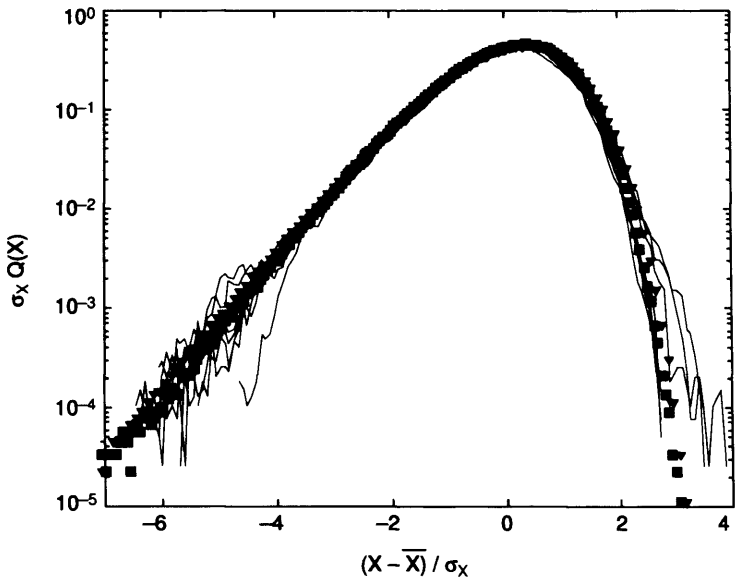

Figure 1.2: The Distribution of Global Fluctuations in the 2dXY Model and Closed Turbulent Flow (from [19]): The continuous lines represent the distribution of power fluctuations for Re=25, 30, 35, 40 and 45. The magnetization data is from Monte Carlo simulations at $T/J = 0.5$ for $N = 100$ (circles), $N = 1024$ (stars) and $N = 10000$ (triangles), and for $T/J = 1.0$ for $N = 1024$ (squares). The semi-logarithmic axes highlight the behaviour in the wings.

and independent of Reynold's number, Re [19, 45] (Figure 1.2). For the magnetic system non-Gaussianity is a consequence of the infinite correlation length leading to fluctuations on all available length scales [6]. In the case of turbulence, power is injected into the system at the macroscopic level to maintain constant Reynold's number [45]. This drives a cascade of fluctuations on all scales down to the microscopic dissipation length and, as in a critical system, each of these is important in determining the fluctuation distribution [19]. A closed experimental system necessarily imposes a finite upper limit on Re, which in turn restricts the number of degrees of freedom. This equivalence with finite N, coupled with the importance of all length scales, was interpreted as indicating a complete analogy with 2dXY critical behaviour – a hypothesis that was later supported analytically [20].

Throughout the literature there are varying claims regarding the universality of the BHP distribution. Perhaps the best interpretation comes at the end of [19]:

> "...it is likely that, for certain universality classes, the departure from Gaussian behaviour at a critical point is described to an excellent approximation by the spin-wave limit of the two-dimensional XY model, with the fine details that characterize and separate the universality classes being concentrated in the central part of the distribution function, or otherwise being hidden by experimental errors."

The usefulness of this generality of functional form remains to be fully established. The fact that so many disparate systems show BHP fluctuations is reminiscent of the CLT. It suggests the possibility that critical PDFs may be governed by a weak equivalent of this theorem, tending toward a general functional form rather than a specific function. This idea is addressed in the present work together with the related question of the effect of this functional similarity on our ability to infer microscopic behaviour from empirically observed PDFs. There may also be consequences for the study of non-equilibrium fluctuations, where the lack of a microscopic theory results in a great emphasis on empirical observations. This has lead to the proposal of a 'picture gallery' of scaling functions which could be used to group experimental results into dynamic universality classes [44]. The development of functions to contribute to this gallery has focused largely on roughness distributions in models of interface growth [46–50]. As the 2dXY model may be mapped onto the two dimensional Edwards-Wilkinson (EW) model of interface growth [51], the BHP 'picture' may be considered as falling into this category. This is perhaps even more significant in the context of the Kadar-Parisi-Zhang (KPZ) equation [52] – a more rigorously non-equilibrium extension to the EW model with non-trivial roughness distributions [53].

Zheng and Trimper have argued that the BHP distribution is a generic bivariate scaling function arising from fourth order mean field theory [22, 54] and not a result of critical behaviour. In support of this they cite the results of Bramwell *et al.* concerning magnetization fluctuations in the Ising model [21]. These simulations were performed for $T^*(L)$ just below T_c, where the correlation length was significantly smaller than L, interpreted by Zheng and Trimper as an indication that the

fluctuations could not be critical. In a reply to this suggestion [23] Bramwell *et al.* emphasized an important facet of the finite size scaling of the 2dXY model, reiterating one of the central results of [16]. The hyperscaling condition, $\sigma/\langle m\rangle$ = constant, is obeyed in the critical regime and, crucially, the value of this constant is very small (approximately $0.04T/J$). Therefore, as m approaches zero with increasing N, the width of the distribution $P(m)$ narrows with the effect that $P(0)$ is effectively zero for all finite N. The result is that the magnetization remains a well defined one dimensional quantity, despite the divergent susceptibility [16]. Another way of interpreting this behaviour is to say that the magnetization never feels the effect of its boundaries at 0 and +1, regardless of the size of the system. In the case of the Ising model simulations, the small value of ξ is analogous to the small value of $\sigma/\langle m\rangle$ in the 2dXY model – it means that the magnetization never reaches the limits of its range. However as ξ scales directly in proportion to L, diverging in the thermodynamic limit, the BHP function does arise as a result of critical fluctuations.

Analytical studies of the BHP distribution have focused on the harmonic spin wave model which completely captures the behaviour of the 2dXY model in the critical regime [55–59]. The Gaussian form of this Hamiltonian allows the moments of the fluctuations to evaluated [6, 16, 17]. Combining the resulting expressions leads to an integral representation of the distribution,

$$P(m) = \int_{-\infty}^{\infty} \frac{\mathrm{d}x}{2\pi\sigma} \exp\left[ix\frac{m-\langle m\rangle}{\sigma} + \sum_{k=2}^{\infty} \frac{g_k}{2k}\left(ix\sqrt{\frac{2}{g_2}}\right)^k\right], \tag{1.3}$$

where g_k are constants (defined in Chapter 4) and the sum and integral may be performed numerically. So far it has proved impossible to find a closed form expression for the distribution, however the large and small m asymptotes are analytically accessible [6], with

$$\Pi(z) \propto |z| \exp\left(4\pi^2\sqrt{\frac{g_2}{2}}z\right) \tag{1.4}$$

for fluctuations below the mean, and

$$\Pi(z) \propto \exp\left[-\frac{1}{8\pi}e^{8\pi\left(\sqrt{\frac{g_2}{2}}z-a\right)} + 8\pi\sqrt{\frac{g_2}{2}}z\right] \tag{1.5}$$

for fluctuations above the mean. Here $a \approx 0.11351444$ is a constant, and the magnetization has been normalized by its standard deviation, in the now accepted manner [6, 16] (see also §2.2.5), with $\sigma P(m) = \Pi(z)$ and $z = (m - \langle m \rangle)/\sigma$.

Knowledge of these asymptotes assists in fitting the BHP form to well defined functions [6]. Over the range of greatest experimental interest (i.e. within a few standard deviations of the mean) it was seen that a generalized log-normal function

$$\Pi(z) = \frac{w}{\sqrt{2\pi\sigma^2}(s-z)} \exp\left\{-\frac{1}{2\sigma^2}[\ln(s-z) - a]^2\right\} \tag{1.6}$$

$$s = 3.45981,\ a = 1.20109,\ \sigma = 0.28325$$

offered the best fit of the possibilities studied. However the asymptotes of this function are incorrect. Perhaps surprisingly, a χ^2_ν distribution with approximately 10 degrees of freedom represents a very good fit to the BHP function over a wide range of m, and has the correct asymptotic behaviour,

$$\Pi(z) = w(s-z)^{\nu/2-1} e^{-a(s-z)} \tag{1.7}$$

$$\nu = 10.07155,\ s = a = 2.24405,\ w = 2.31233.$$

This result indicates that the statistics of a critical 2dXY magnet, a highly correlated many body system, may be reasonably represented by a distribution derived from a small number of independent identically distributed degrees of freedom.

An intriguing result is that the BHP distribution is fitted well by a generalized form of the Fisher-Tippet-Gumbel (FTG) distribution for the a^{th} largest of a sample of random numbers [60, 61],

$$\Pi(z) = \frac{a^a}{\Gamma(a)} \exp\left\{-a\left[\alpha_a(z-u_a) + e^{\alpha_a(z-u_a)}\right]\right\} \tag{1.8}$$

$$a = \pi/2,\ b = 0.938,\ s = 0.374,\ w = 2.14.$$

A link between critical phenomena and extreme value statistics (EVS) is an attractive proposition [62, 63]; however the non-integer value of a for the BHP distribution is difficult to interpret physically [6]. In particular it is unclear which quantity's extreme values should be examined. An approximate 'linearized' form of the magnetization

may be diagonalized in reciprocal space [6]. One of the most remarkable observations in the study of the 2dXY model has been that the distribution of this quantity is precisely the BHP function, even at temperatures when it completely fails to represent the full order parameter [6, 25]. The advantage of the linearized magnetization is that it consists of a set of independent normal modes. Studies showed, however, that the BHP function was not recovered from fluctuations of the largest normal mode [64] and it has been suggested that any physical link with extremal statistics must be via correlated many body objects [21, 24, 28]. Numerical studies of the Sneppen de-pinning model appear to confirm this [42].

It remains an open question whether there is any physical manifestation of extremal statistics present in critical phenomena. Attempts to identify suitable independent extreme quantities have proved unsuccessful [64] (see also Chapter 5). However there is numerical [42] and analytical [65] evidence of a relationship between the BHP distribution and the extreme values of correlated variables. More work is needed before the critical – EVS link is fully understood.

The treatment of the linearized order parameter in [6] may be extended to cover a family of models in general dimension d [25]. In the case $d = 1$ the distribution of the magnetization can be found analytically and is seen to be the 'fundamental' FTG distribution ($a = 1$). In Chapter 5 we present an argument for the interpretation of this model as representing a critical system. This result gives renewed impetus to the idea of a critical – extremal link, though once again the distribution of the largest normal mode is not the FTG function.

The $d = 1$ model also provides a very appealing link to the phenomenon of $1/f$ noise. The breakthrough came in the work of Antal *et al.* who showed analytically that the roughness distribution of Gaussian signals with $1/f$ power spectra was precisely the FTG function [48]. $1/f$ noise was first observed in fluctuations of current in vacuum tubes [66] and has since been seen in a wide range of physical systems from the luminosity of stars [67] to the pitch an volume of many types of music [68]. The temporal scale invariance of these signals is analogous to the spatial behaviour at

equilibrium critical points. It is therefore tempting to associate the two. Combined with the results of [48], [25] and Chapter 5 this suggests a heuristic cycle of connections between critical phenomena, $1/f$ noise and extreme value statistics. Whilst the connection between $1/f$ noise and the FTG distribution is mathematically rigorous it remains physically unexplained. Thus far it has not been possible to identify a suitable extreme quantity in the noise signal [69]. As such it is not yet clear whether there is any physical basis for linking these three fields or whether the appearance of the FTG distribution is a purely mathematical result.

To end this section we note that the universality of the BHP distribution has become widely accepted in the literature [6, 20, 25, 26, 29, 70]. However it has been suggested by Labbé *et al.* that, contrary to previous findings, the distribution is dependent on temperature [30]. This study uses relatively short simulations (it is unlikely that the 5×10^5 MCS/s used would be sufficient to accurately sample the wings of the distribution). It is also possible that their results are subject to vortex corrections [27]. In Chapter 4 we present clear analytical evidence that the 2dXY magnetization fluctuations are dependent on T together with Monte Carlo simulations confirming this result.

1.2 Organization of the Thesis

The rest of this thesis is organized as follows...

Chapter 2 introduces the theoretical background to critical phenomena, from the ideas of classical thermodynamics and statistical mechanics, through critical exponents and universality to the basic ideas of the renormalization group. Probability distributions are discussed, together with the central limit theorem and normalization procedures.

Chapter 3 is in two parts. The first considers the toy model of non-interacting Ising spins as a tractable system for the introduction of certain theoretical techniques. This allows for a direct comparison between statistical and statistical mechanical

methods and leads to the derivation of a number of quite general relations. Part two discusses aspects of series expansion approximations to the Ising partition function. A potentially useful link between zero and finite field expressions is demonstrated. A finite size scaling expression for fluctuations in the specific heat is introduced which, coupled with exact expressions for the finite size partition function, leads to a means for predicting the finite size scaling of T_c.

The work presented in this thesis was inspired by studies of the 2dXY model. Chapter 4 reviews the theoretical development of this model culminating in the derivation of the BHP function. This derivation is re-examined with emphasis on certain assumptions regarding the effect of taking the thermodynamic limit. By showing that these assumptions are invalid we demonstrate an explicit temperature dependence, a result backed up by Monte Carlo simulations. A possible Kosterlitz-Thouless transition in the Harmonic model is discussed in the light of the observation of vortices in this supposedly purely spin-wave system.

The linearized order parameter for the 2dXY model leads to a reciprocal space description in terms of independent normal modes with a large dispersion of amplitudes. This is generalized in Chapter 5 to general dimension and it is argued that the resulting family of systems are all critical. For $d = 1$ the magnetization has been seen previously to be FTG distributed [25]. We introduce and analyse two real space Hamiltonians for this model. It is seen that the distribution of the largest normal mode is not FTG like, and contributions to the PDF from different parts of the Brillouin zone are examined.

Finally, the link with $1/f$ noise is discussed in Chapter 6. We consider the link between $1/f$ noise and extreme value statistics and suggest that this may be better understood in the context of a $1/q$ dispersion of spatial normal modes. The effects of imperfections in the $1/f$ behaviour are considered within the framework of a thought experiment designed to test our ability to observe the $1/f$ – extremal link experimentally. We also provide numerical confirmation of Machlup's theory that $1/f$ noise may result from the superposition of random telegraph (RT) signals, and discuss the effect of varying the boundaries of the energy window for the RT components.

Chapter 2

The Theoretical Background to Critical Phenomena

2.1 The Theory of Critical Phenomena

2.1.1 Phase Transitions

A thermodynamic system has associated with it a set of potentials which are functions of various intensive and extensive variables. Knowledge of one potential completely describes the system as the others may derived from it via a series of Legendre transforms [2]. Of particular interest is the potential whose natural variables* are all intensive, the per unit mass form of which is called the chemical potential, μ [71]. For a system at equilibrium the value of μ is the same for all phases present, however it need not vary smoothly across a coexistence curve. This has led to the functional form of μ being used to characterize different types of phase transition [71, 72] .

A 'first order' transition separates phases which are distinct, occupying different region of thermodynamic configuration space [2]; they have different entropies, resulting in a non-zero latent heat. For example, consider a magnetic system for which the

*The 'natural variables' of a potential X are those that enable $\mathrm{d}X$ to be readily separated into components of heat and work, and that lead to physically relevant partial derivatives of X. For a discussion see Appendix B of [71].

chemical potential is the per particle Helmholtz potential, $\mu = f(T, H)$, a function of temperature and magnetic field.† The entropy is given by $S = \left(\frac{\partial f}{\partial T}\right)_H$ and the latent heat per particle is

$$l = T(S_+ - S_-) = T\left[\left(\frac{\partial f_-}{\partial T}\right)_H - \left(\frac{\partial f_+}{\partial T}\right)_H\right], \tag{2.1}$$

where the $\pm$ subscripts indicate values infinitesimally above and below the transition temperature. From (2.1) it is seen that a first order transition requires a discontinuous first order derivative of the chemical potential, hence the name. The classification of transitions as first order, second order and so on was due to Ehrenfest who categorized a transition as n^{th} order where the n^{th} derivative of μ was the lowest order derivative to be discontinuous [72]. Confusion arose however when systems with logarithmically divergent derivatives were identified (for example in the Ising model [74]). It is now more common to group all non-first order transitions together under the heading 'continuous' [71].

2.1.2 Critical Exponents, Power Laws and Self-Similarity

Critical phenomena are associated with continuous (generally second order) phase transitions. Thus the free energy and its first order derivatives are continuous functions but second order and higher derivatives possess singularities the nature of which characterize the critical behaviour. It is found experimentally that the divergences in these quantities may be represented by power laws. Assuming that all parameters other than temperature are held fixed at their critical values, the distance of the system from its critical point, the point in phase space where the second order transition occurs (Figure 2.1), may be expressed in terms of the reduced temperature $t = (T - T_c)/T_c$ where T_c is the critical temperature. Quantities such as the specific heat, susceptibilities, correlation lengths *etc.* then vary as $\mathcal{F}(t) \sim |t|^{-x}$, were x, a 'critical exponent', generally takes a positive value (see Table 2.1).

†Some confusion arises for magnetic systems over whether μ is the specific Gibbs or Helmholtz potential. The origin of the problem comes in the definition of the first law as either $\mathrm{d}U = \mathrm{d}Q - M\,\mathrm{d}H$ or $\mathrm{d}U = \mathrm{d}Q + H\,\mathrm{d}M$ [73]. Throughout this thesis the first of these definitions will be used.

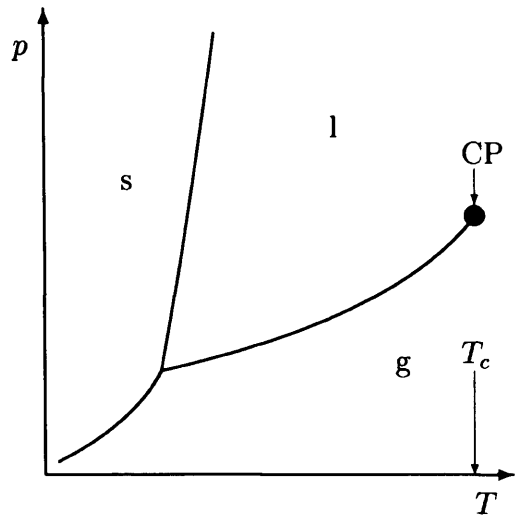

(a)

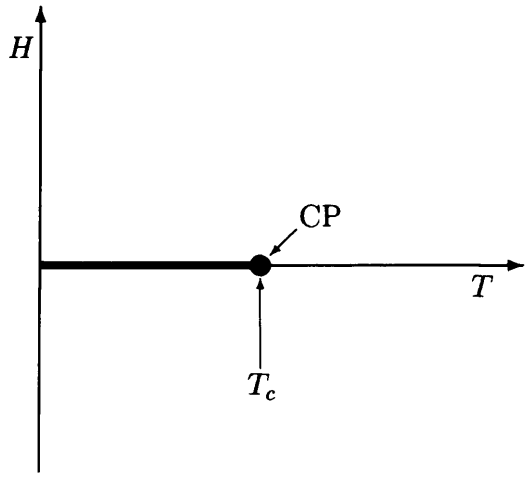

(b)

Figure 2.1: Critical Points: Denoted here CP for (a) fluid and (b) ferromagnetic systems, critical points normally occur at the end of coexistence curves on phase diagrams. For the fluid system the phases are solid (s), liquid (l) and gas (g), the CP terminating the l/g coexistence curve. Beyond this point there is a single fluid phase for all temperatures (T) and pressures (p). For the ferromagnet the phases are defined by the direction of the applied field (H) and are separated by the line $H = 0$ ($T < T_c$). Above T_c the system is in a purely paramagnetic state.

It may be assumed that these power law divergences represent a good first approximation to a more complicated relationship [73]

$$\mathcal{F}(t) = At^{-x}(1 + Bt^{y} + \ldots), \tag{2.2}$$

where the exponent x is defined by

$$x = \lim_{t \to 0} \left(\frac{\ln \mathcal{F}(t)}{\ln t} \right). \tag{2.3}$$

The observation of power laws is of direct physical significance as it is a mathematical expression of scale invariance or self-similarity. This is seen by considering the effect a change of scale has on the appearance of a power law, as opposed to on some other functional form. A plot of $y = x^a$ can always be superimposed on plot of $y = (nx)^a$ by rescaling the x axis by a factor of n and the y axis by a factor of n^a. Thus, if no dimensions are given, it is impossible to tell the scale of an observable from a power law plot. This property, peculiar to power laws, is made manifest in critical systems by the fact that it is impossible to tell the scale of a portion of a critical system when viewed in isolation [12] (Figure 2.1.2).

Table 2.1 gives definitions of the more common critical exponents. As phase transitions may be approached from both high and low temperatures, each physical quantity was originally thought to have two relevant exponents. However the renormalization group has shown that the singularities are symmetric about the transition (this is demonstrated explicitly in Chapter 5 of [71]) and so only one exponent per quantity is listed. The definition of δ makes it clear that power laws need not always be functions of temperature.

The 'order parameter' (OP) is a quantity whose thermal average is zero on one side of a continuous phase transition and finite on the other. Near T_c this quantity varies as a power law with exponent β. As the name suggests, the OP is a measure of the degree of long range order in the system. The complexity of the order parameter varies greatly from simple scalars to complex vector fields [71]. For ferromagnetic systems, the appropriate choice is the magnetization, m (defined in Table 2.1), a derivative of the chemical potential that is zero in the paramagnetic phase but finite

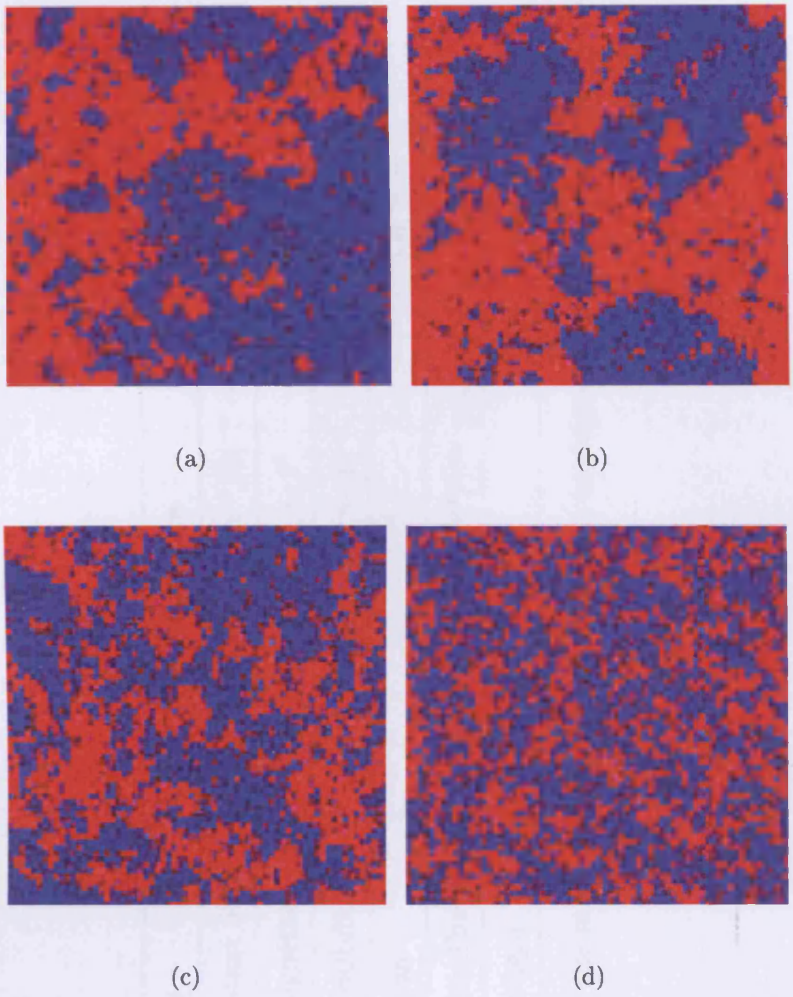

Figure 2.2: Scale Invariance in Critical Systems: These pictures are the results of snapshots of a Monte Carlo simulation of the two dimensional Ising model for a system with $N = 159201$. In (a) and (b) the system is at its critical temperature, $T_c \approx 2.27$. The first of these (a) is simply the top left hand corner (comprising 17689 spins) of the lattice at equilibrium. Picture (b) is formed by splitting the original lattice into squares of 3×3 spins and assigning each square the value ± 1 on the basis of 'majority rule', thus defining a new lattice with $N = 17689$ Ising 'block spins'. The blocking procedure, a sort of real space renormalization (see §2.1.9) causes no apparent change in the distribution of cluster sizes relative to the original lattice. The bottom pictures are for a simulation with $T > T_c$. In (c) we see the top left hand corner of the original lattice. Picture (d) shows the results of the blocking procedure. In this case the blocking clearly results in a change in the distribution of cluster sizes with smaller clusters becoming more prevalent.

Exponent	Quantity	Divergence	Conditions
α	Specific Heat (constant field)	$C_H = -T\left(\frac{\partial^2 f}{\partial T^2}\right)_H \sim \alpha^{-1}(\lvert t\rvert^{-\alpha} - 1)$	$T \to T_c$, $H = 0$
β	Order Parameter (magnetization)	$m = -\left(\frac{\partial f}{\partial H}\right)_T \sim t^{\beta}$	$T \to T_c^-$, $H = 0$
γ	Isothermal Susceptibility	$\chi_T = -\left(\frac{\partial^2 f}{\partial H^2}\right)_T \sim \lvert t\rvert^{-\gamma}$	$T \to T_c$, $H = 0$
δ	Magnetization	$m \sim H^{1/\delta}$	$H \to 0$, $T = T_c$
η	Two Point Correlation Function	$G_c^{(2)}(r) = \langle \mathbf{s}_0.\mathbf{s}_r \rangle - \lvert \langle \mathbf{s}^2 \rangle \rvert \sim \frac{1}{r^{d-2+\eta}}$	$T = T_c$, $H = 0$
ν	Correlation Length	$\xi \sim \lvert t\rvert^{-\nu}$	$T \to T_c$, $H = 0$

Table 2.1: Critical Exponents: Definitions of the most common critical exponents in magnetic systems, and the quantities to which they relate. After Binney *et al.* [71]

below T_c. Although strictly a vector, it is often more useful to consider the magnitude $m = |\mathbf{m}|$ to avoid problems of symmetry [75]. Care must be taken though as minor changes in the definition of the order parameter may have significant effects on the behaviour of quantities derived from it (see for example §4.5.3).

2.1.3 Relationships Between the Critical Exponents

A number of relationships between the critical exponents can be derived from general thermodynamical considerations rather than the specifics of the system [73]. These relationships were originally derived as inequalities from standard thermodynamic expressions and physical constraints. For example, the Rushbrooke inequality, $\alpha + 2\beta + \gamma \geq 2$, is derived for a ferromagnet simply using the relation $\chi_T(C_H - C_M) = T\alpha_H^2$ and the fact that C_M can not be negative [76]. Hence, for $H = 0$ and $T \to T_c$,

$$C_M = C_H - \frac{T\alpha_H^2}{\chi_T} \geq 0 \tag{2.4}$$

$$C_H \geq \frac{T\alpha_H^2}{\chi_T} \tag{2.5}$$

$$\geq \frac{T\left(\frac{\partial m}{\partial T}\right)_H^2}{\chi_T}. \tag{2.6}$$

Recalling $C_H \sim |t|^{-\alpha}$, $\chi_T \sim |t|^{-\gamma}$ and $\left(\frac{\partial m}{\partial T}\right)_H \sim |t|^{\beta-1}$, and using (2.3), the relationship in (2.6) may be expressed as

$$-\alpha \geq 2(\beta - 1) - (-\gamma) \qquad \text{or} \qquad \alpha + 2\beta + \gamma \geq 2. \tag{2.7}$$

Similar considerations lead to the Griffiths [77, 78], Fisher [79] and Josephson [80] inequalities,

$$\alpha + \beta(1 + \delta) \geq 2 \tag{2.8}$$

$$(2 - \eta)\nu \geq \gamma \tag{2.9}$$

$$d\nu \geq 2 - \alpha, \tag{2.10}$$

relating the six major critical exponents. The Josephson inequality is particularly interesting as it links the values of the exponents to the dimensionality, d, of the system. This is an example of a 'hyperscaling' relation and it ties the specific heat to the behaviour of the correlation length (defined in §2.1.5). The linking together of six exponents in just four relationships indicates a reduction in the degrees of freedom. This is only in a weak sense however as these relationships are inequalities rather than equations.

In 1965 Widom proposed the 'scaling hypothesis', a mathematical trick that yields the same exponent relations as above but renders them as rigorous equations [81]. The justification for his approach was, at the time, mainly heuristic, however subsequent theoretical work has enabled scaling to be derived from firmer physical principles [12]. In its simplest form the scaling hypothesis states that, near the critical point, the chemical potential is a generalized homogeneous function of its reduced variables (such as t and $h = H - H_c$). For example a magnetic system would have $f(a^{y_t}t, a^{y_h}h) = af(t,h)$ for any a. Immediately it is seen that only two parameters (y_t and y_h) are required to specify the system, so certain exponent relations must exist. Differentiating the free energy with respect to the field gives,

$$a^{y_h}\frac{\partial f(a^{y_t}t, a^{y_h}h)}{\partial(a^{y_h}h)} = a\frac{\partial f(t,h)}{\partial h} \tag{2.11}$$

so

$$a^{y_h}m(a^{y_t}t, a^{y_h}h) = am(t,h), \tag{2.12}$$

and

$$m(t,0) = a^{y_h-1}m(a^{y_t}t, 0). \tag{2.13}$$

As (2.13) must be true for all values of a, it is possible to set $a = |t|^{-1/y_t}$ such that

$$m(t,0) = |t|^{(1-y_h)/y_t}m(1,0). \tag{2.14}$$

Given that $m(1,0)$ is a constant, the only temperature dependence comes from the first factor so, according to the definition of β,

$$\beta = \frac{1-y_h}{y_t}. \tag{2.15}$$

Setting $a = h^{-1/y_h}$ for $m(0,1)$ one arrives at

$$\delta = \frac{y_h}{1 - y_h}. \tag{2.16}$$

Alternatively, differentiating f twice with respect to h yields the susceptibility exponent

$$\gamma = \frac{2y_h - 1}{y_t}, \tag{2.17}$$

whilst differentiating twice with respect to t gives a similar expression for α,

$$\alpha = \frac{2y_t - 1}{y_t}. \tag{2.18}$$

Equations (2.15), (2.16), (2.17) and (2.18) may then be combined to give some familiar exponent relations in equation form (see, for example, [73]).

2.1.4 Fluctuations

One of the defining characteristics of critical systems is the manner in which certain quantities fluctuate on all length scales. The reasons for this are clear in the context of diverging second derivatives of the free energy. Figure 2.3 shows schematic plots of the specific Gibbs free energy as a function of the magnetization. The plots represent the behaviour of a system whose paramagnetic symmetry is spontaneously broken at T_c as one moves along $h = 0$. Above T_c, $g(T, m)$ has a single well-defined minimum corresponding to $m = 0$. For $T < T_c$ the most stable value of $g(T, m)$ is doubly degenerate with two values of m minimizing the free energy. The two minima are separated by a potential barrier the height of which is diminished as the critical point is approached, leaving, at $T = T_c$, a single broad minimum. Recalling that $\left(\frac{\partial f}{\partial h}\right)_T = -m$ and $\left(\frac{\partial g}{\partial m}\right)_T = h$ gives the relation

$$\left(\frac{\partial^2 g}{\partial m^2}\right)_T = -\left(\frac{\partial^2 f}{\partial h^2}\right)_T^{-1}. \tag{2.19}$$

Therefore, as the second derivative of f with respect to h diverges at the critical point, $\left(\frac{\partial^2 g}{\partial m^2}\right)_T$ must be zero. As there can be no point of inflexion the conclusion must be that $g(m)$ is constant over the range of physical interest. This range then

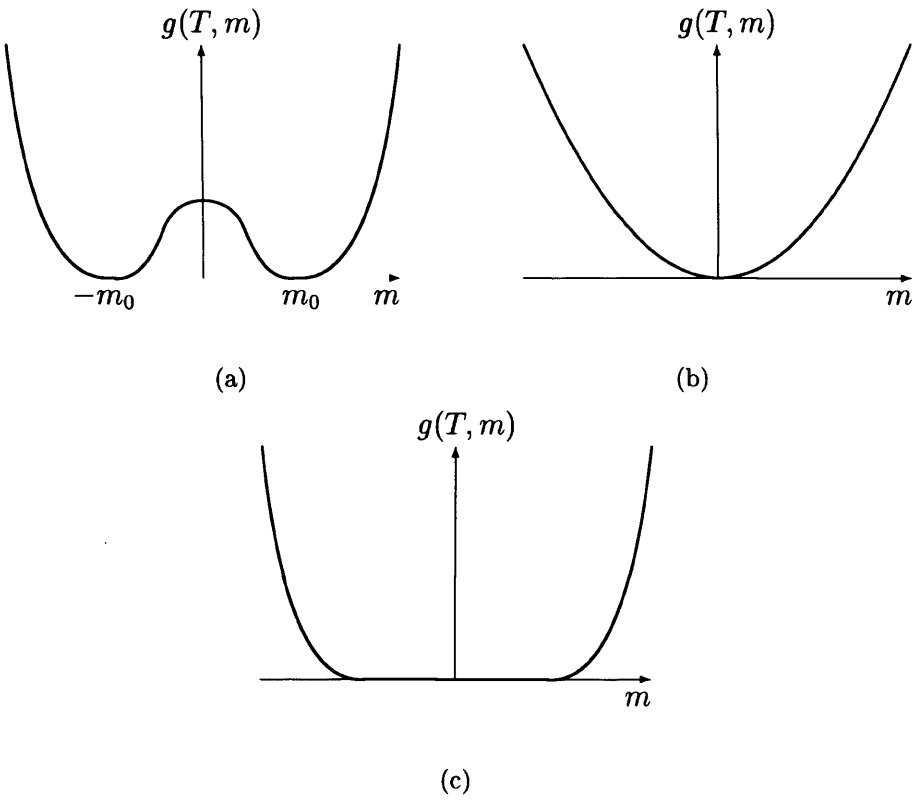

Figure 2.3: The Schematic Gibb's Free Energy for a Ferromagnet: The plots show $g(T, m)$ for (a) $T < T_c$ where a potential barrier separates minima corresponding to two distinct phases, (b) $T > T_c$ where a single phase exists, and (c) $T = T_c$ where the free energy develops a plateau over which many configurations have effectively the same energy and large scale fluctuations occur.

provides a plateau over which m is able to take any value with effectively zero cost in energy, accounting for the fact that m can have such large scale fluctuations. Also, for the same reasons, an arbitrarily small perturbation can produce a substantial change in m, accounting for the divergent susceptibility. As the temperature is increased above T_c the plateau in the potential rapidly narrows to a sharper single minimum and critical behaviour ceases.

Large scale fluctuations are not in themselves confined to critical systems. The important thing for criticality is that, as larger fluctuations become feasible, the small scale variations continue to make their presence felt. This is demonstrated by the phenomenon of critical opalescence - the first [82], and arguably most visually impressive, experimental realization of critical behaviour (Figure 2.4). As the gas/liquid critical point is approached along the coexistence curve, the sizes of the gas and liquid regions begin to fluctuate over an increasingly large range. When the largest fluctuations become comparable in size to the wavelength of visible light, the light is scattered and the fluid mixture starts to appear milky or opalescent. It is possible to get even closer to the critical point though, and correspondingly the sizes of the largest fluctuations continue to increase - even up to centimetre proportions. Importantly, the scattering of light is not diminished, confirming the presence of smaller fluctuations which remain physically relevant [73].

2.1.5 Correlations

Consider a model ferromagnet consisting of a large number, N, of spins confined to a d dimensional hypercubic lattice with linear size L (such that $N = L^d$). The energy of the system typically depends on short range interactions between the spins, often including just nearest neighbours. Being ferromagnetic, each spin influences its neighbours to adopt a similar orientation. These in turn influence the next nearest neighbours and so the effect of the first spin may propagate further than the range of direct interaction. This behaviour is described by the two point correlation function

$$G(\mathbf{r}_i, \mathbf{r}_j) = \left\langle \mathbf{s}_i . \mathbf{s}_j \right\rangle , \tag{2.20}$$

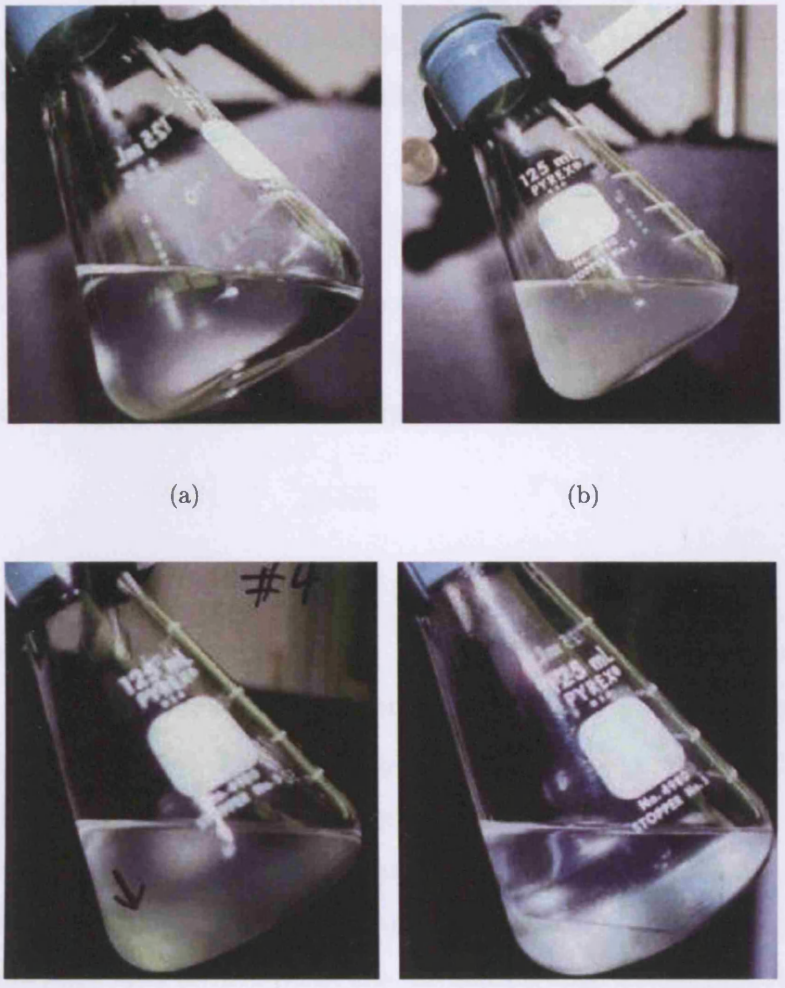

Figure 2.4: Critical Opalescence: This illustration uses a mixture of methanol and hexane in a molar ratio of 435:665. It is therefore fluctuations in the refractive index (rather than the density as in liquid/gas transitions) that give rise to the opalescence. In (a) the solution is above its critical temperature $T_c = 315.55K$ and the components are miscible in all proportions. (b) The mixture has been cooled to the critical point and the milkiness of critical opalescence is visible. (c) As further cooling takes place the miscibility decreases and a meniscus starts to form (indicated by the arrow). (d) Finally, far enough below T_c, the components separate into distinct phases. These pictures may be found on the University of Iowa website [83].

where $\mathbf{r}_i$ and $\mathbf{r}_j$ are the position vectors of the sites of the spins $\mathbf{s}_i$ and $\mathbf{s}_j$. Above T_c correlations between spins become small; below T_c long range order results in little variation of $G(\mathbf{r}_i, \mathbf{r}_j)$ with distance between the spins. For this reason it is useful to remove contributions from the averaged order parameter, defining the connected two point correlation function

$$G_c(r) = \left\langle \mathbf{s}_i.\mathbf{s}_j \right\rangle - |\langle \mathbf{s} \rangle|^2, \tag{2.21}$$

where translational invariance reduces G to a function of a single variable, $r = |\mathbf{r}_i - \mathbf{r}_j|$. For large r, the function $G_c(r)$ behaves as a power law precisely at the critical point, however as T_c is approached, it is as an exponential decay [71],

$$G_c(r) \sim \frac{1}{r^{d-2+\eta}} \qquad T = T_c \tag{2.22}$$

$$\sim e^{-r/\xi} \qquad T \to T_c. \tag{2.23}$$

This introduces ξ, the correlation length, a measure of the distance over which two parts of the system may be considered to be correlated. For $r > \xi$ spins are effectively independent. The fact that $G_c(r)$ falls exponentially to zero away from T_c, but only as a power law at the critical point, suggests that the argument of the exponential must be zero for all r at $T = T_c$, and thus $\xi(T_c) = \infty$. This is indeed the case and the correlation length has a power law divergence, $\xi \sim |t|^{-\nu}$. This really captures the essence of criticality: at a critical point the correlation length is infinite, so every part of the system feels the effect of every other part. A change in any microscopic degree of freedom (e.g. spin) exerts an influence across the infinite range of a thermodynamic system, and fluctuations on all length scales become possible.

2.1.6 Universality

Table 2.2 shows the numerical values of some critical exponents for the Ising model. It is seen that the exponents take different values for each of $d = 2, 3$, however for fixed $d = 2$ they are unaffected by the type of lattice studied[‡]. This is an example of

[‡]This is not always the case. There are examples of frustrated systems where the lattice type affects the critical exponents [84].

System	α	β	γ	δ	η	ν
$d = 2$ Ising Model (square lattice)	0	$\frac{1}{8}$	$\frac{7}{4}$	15	$\frac{1}{4}$	1
$d = 2$ Ising Model (triangular lattice)	0	$\frac{1}{8}$	$\frac{7}{4}$	15	$\frac{1}{4}$	1
$d = 3$ Ising Model (cubic lattice)	0.108	0.327	1.237	4.77	0.0366	0.6298

Table 2.2: Some Critical Exponent Values for the Ising Model: From [73] for $d = 2$ and from [85] $(\alpha, \beta, \gamma, \delta)$ and [86] (η, ν) for $d = 3$.

the fact that critical exponents are insensitive to the much of the microscopic detail of the system. Observations of this behaviour from numerical work on series expansions led to the hypothesis of universality - that critical behaviour may be characterized by only a few macroscopic parameters such as the spatial dimensionality and the symmetry of the ordered phase.

Universality is a useful concept as it enables the grouping of systems into 'universality classes', members of each class sharing a common set of critical exponents. One needs only to solve the simplest member of each class to have a complete description of the critical behaviour of all the other members. That such a simplification as universality is possible is remarkable. It demonstrates that some aspects of the microscopic physics giving rise to the transition in the first place play no part in determining the critical behaviour.

2.1.7 Finite Size Scaling

The experimental relevance of thermodynamic theory relies on the assumption that the thermodynamic limit, $N \to \infty$, is applicable for experimental systems with typically $N = \mathcal{O}(10^{23})$. When dealing with finite systems the divergences associated with phase transitions do not occur and instead one sees finite peaks at temperatures shifted from T_c. As numerical work is necessarily performed on systems with $N \ll 10^{23}$, it is important to be able to quantify the effects of finite size. This is also useful for systems where the thermodynamic limit may not be experimentally accessible (see Chapter 4).

For a critical system that is finite in all dimensions the effect of N may be understood in the context of the diverging correlation length. In such systems there is a restriction on the largest possible fluctuations constraining ξ to the order of L. This provides a link between the system size and the critical exponents – as it assumed that $\xi/L \sim \mathcal{O}(1)$, it must be true that $L \sim |t|^{-\nu}$ [87]. This in turn implies that $|t| \sim L^{-1/\nu}$, and so, for example,

$$\chi \sim L^{\gamma/\nu} \tag{2.24}$$

$$C \sim L^{\alpha/\nu} \tag{2.25}$$

$$m \sim L^{-\beta/\nu}. \tag{2.26}$$

In all these expressions it is assumed that the system is at the shifted critical temperature, $T_c(L) = T_c(\infty) - aL^{-1/\nu}$ for some constant a [12, 87].

More formally, if a general function $f(|t|, L)$ scales as $|t|^x$ for $L = \infty$, then [87]

$$L^{x/\nu} f(|t|, L) = (L^{1/\nu}|t|)^x \phi(L^{1/\nu}|t|), \tag{2.27}$$

the right hand side being a function of a single variable, $L^{1/\nu}|t|$.

When simulating a critical system, care must be taken to ascertain the precise value of $T_c(L)$. It is generally not appropriate to use $T_c(\infty)$ as the behaviour at this temperature may not be strictly critical [14].

2.1.8 Statistical Mechanics

Critical behaviour cannot be explained by thermodynamics [2]. Instead a statistical mechanical approach must be adopted, explicitly considering microscopic interactions. If a system has a state i with energy E_i, the probability of the system being in this state is

$$P_i = \frac{1}{Z} e^{-\beta E_i} \qquad \text{where} \qquad Z = \sum_i e^{-\beta E_i}, \tag{2.28}$$

where $\beta = 1/T$ (in units where the Boltzmann constant $k_B = 1$) and Z is the partition function. This function plays a central role as it provides a link with thermodynamics

via the Helmholtz potential,[§]

$$f(T,H) = -\frac{1}{\beta}\log Z. \tag{2.29}$$

Thus knowledge of Z is sufficient to completely describe a system. The energy of a each microscopic configuration is given by the Hamiltonian. However, even when a suitable Hamiltonian is known, derivation of the partition function using (2.28) is often an intractable problem.

There are a number of model systems of varying complexity for which Z may be determined analytically [88]. In such cases the partition function may be used directly to investigate fluctuations. The average value of a some property, say X, is given by $\langle X\rangle = \sum_i X_i e^{-\beta E_i}/Z$. Assuming there is a term $-aX$ in the Hamiltonian,

$$\langle X\rangle = \frac{1}{\beta Z}\frac{\partial}{\partial a}\left(\sum_i e^{-\beta(E_i'-aX_i)}\right)\Bigg|_{a=0} \tag{2.30}$$

$$= \frac{1}{\beta}\frac{\partial(\log Z)}{\partial a}\Bigg|_{a=0}. \tag{2.31}$$

If the required term is not present in the Hamiltonian, it can always be added (giving $E_i' = E_i$) since a is set equal to 0 after the differentiation. The fluctuations in X are provided by the second differential,

$$\frac{1}{\beta}\frac{\partial^2(\log Z)}{\partial a^2}\Bigg|_{a=0} = \frac{1}{\beta}\frac{\partial}{\partial a}\left(\frac{1}{Z}\frac{\partial Z}{\partial a}\Bigg|_{a=0}\right) \tag{2.32}$$

$$= \frac{1}{\beta}\left[\frac{1}{Z}\frac{\partial^2 Z}{\partial a^2}\Bigg|_{a=0} - \left(\frac{1}{Z}\frac{\partial Z}{\partial a}\Bigg|_{a=0}\right)^2\right] \tag{2.33}$$

$$= \left\langle X^2\right\rangle - \langle X\rangle^2 \tag{2.34}$$

$$= \frac{\chi}{\beta}. \tag{2.35}$$

Equation (2.35), demonstrating the interdependence between probability distributions and thermodynamic potentials, is known as the linear response theorem [71].

[§]This link is assuming the canonical ensemble where, for a system of fixed size at a fixed temperature, the energy is free to vary. See [2] for a good proof.

When X is a product of microscopic variables, e.g. $\mathbf{s}_i$, it is possible to obtain correlation functions using the above method. This time each variable is assumed to have its own linear term in the Hamiltonian, $-J_i\mathbf{s}_i$, and the n point correlation functions are,

$$G^{(n)}(\mathbf{r}_i \ldots \mathbf{r}_n) = \langle \mathbf{s}_i \ldots \mathbf{s}_n \rangle = \frac{1}{Z}\frac{\partial^n Z}{\partial J_i \ldots \partial J_n} \tag{2.36}$$

Harder to prove (see Appendix D of [71]) but more useful are the corresponding expressions for the connected n point correlation functions,

$$G_c^{(n)}(\mathbf{s}_i \ldots \mathbf{s}_n) = \frac{\partial}{\partial J_i} \ldots \frac{\partial}{\partial J_n}(\log Z). \tag{2.37}$$

2.1.9 The Renormalization Group

The development of the renormalization group (RG) represents a major achievement in the study of critical phenomena, providing a sound mathematical footing for many physical observations. The concepts behind the RG are most readily discussed in the context of a specific system and the $d = 2$ Ising model is a straightforward choice (see §3.2 for a description of the model). A 'thought experiment' may be performed where one views the lattice of Ising spins through a window in an otherwise opaque screen. Assuming the lattice is large, only a fraction of it will be visible. For a system at its critical point, there will be clusters of up and down spins of all sizes distributed across the lattice, and this will be reflected in the visible portion. Moving the lattice backward, away from the screen, increases the visible area but results in a loss of definition and the highest resolution detail may be lost. However, as the the system is critical the distribution of clusters will appear the same. For $T < T_c$, clusters with spins in one direction (e.g. up) will be larger, on average, than cluster of spins in the other direction (down). As the lattice is moved away from the screen the loss of high resolution results in the down clusters gradually being obscured and the system appears more ordered than when viewed up close. For $T > T_c$, as the lattice is moved away, large clusters become smaller relative to the visible portion of the lattice indicating that only short range order is present. In very simplistic terms the RG procedure is the mathematical equivalent of moving the lattice back.

Real space renormalization may be understood in terms of Kadanoff's 'block spins' [89], bypassing much of the technical detail of the RG method. The idea is that the degrees of freedom are split into groups, with new degrees of freedom being defined as some function of the members of each group. Consider sectioning a square lattice of magnetic spins, s_i, into blocks of size $b \times b$. Each block is then assigned a value $\sigma_k = f(\{s_i\})$ where the braces indicate the set of spins in block k. The only constraint on the function f is that the σ_k have the same range of values as the original spins [71]. If the PDF of states of the original spins is known then the equivalent distribution of the block spins can be determined by summing the probabilities of simple spin configurations that give rise to each block spin configuration. Therefore if X is a function of the spin configuration its distribution is unaffected by the renormalization procedure [71],

$$\langle X^n \rangle = \frac{1}{Z(\{\sigma_k\})} \sum_{\{\sigma_k\}} X(\{\sigma_k\})^n P(\{\sigma_k\}) = \frac{1}{Z(\{s_i\})} \sum_{\{s_i\}} X(\{s_i\})^n P(\{s_i\}). \qquad (2.38)$$

Renormalization has the effect of introducing more couplings into the system than may have been present initially. It is often said that the renormalization transformation is simply a move from one point, $\{K\}$, to another, $\{K'\}$, in the infinite dimensional space of all possible couplings, such that $\{K'\} = R\{K\}$. If certain fixed points, $\{K^*\}$, exist such that $R(\{K^*\}) = \{K^*\}$, and if the transformation operation R is differentiable in their vicinity, then

$$K'_a - K^*_a \sim \sum_b T_{ab}(K_b - K^*_b) \qquad \text{where} \qquad T_{ab} = \left.\frac{\partial K'_a}{\partial K_b}\right|_{K=K^*}, \qquad (2.39)$$

is the set of equations defining the renormalization group transformation [12]. It is best to think of the original Hamiltonian as depending on all possible couplings, but with many of them being zero. The RG transformation then simply alters the values of the various parameters, not the form of the Hamiltonian itself.

The matrix T_{ab} describes the geometry of the coupling space near K^* and it is this that ultimately controls the behaviour of the system. The eigenvalues of the matrix may be written as $\lambda_i = b^{y_i}$ (with b defined above). For $y_i > 0$ the scaling variables u_i renormalize away from their fixed point values, as $u'_i = \lambda_i u_i$, and are

said to be relevant. For $y_i < 0$, u_i renormalizes to zero and is irrelevant. The sub-space in which all relevant scaling variables are zero is called the critical surface. By tuning the external constraints such that the Hamiltonian lies on this surface, repeated renormalization leads to the fixed point controlling that RG flow.

Figure 2.5 shows a schematic diagram of RG flows in a two dimensional sub-space. This could represent the two dimensional Ising model with K_1 and K_2 being the reduced nearest and next nearest neighbour couplings respectively. The original model then has $K_2 = 0$ and the Hamiltonian is some point along the K_1 axis, exactly where is determined by the temperature.[¶] At T_c the RG flow leads to the critical fixed point. If the original system had $K_2 \neq 0$ varying the temperature could move the Hamiltonian along a line other than the K_1 axis, for example the dotted line shown. This line crosses the critical surface at a different point from the simple Ising model, however both systems renormalize to the same fixed point and so belong to the same universality class.

Exactly how fixed points 'control' critical behaviour depends on the way in which the free energy renormalizes. The singular part of the free energy may be written as a function of the relevant scaling variables[‖] as [12]

$$f_s(u_t, u_h) = b^{-nd} f_s(b^{ny_t} u_t, b^{ny_h} u_h), \tag{2.40}$$

where n is the number of iterations of the RG procedure. Some algebra then gives [12])

$$f_s(t, h) = |t/t_0|^{d/y_t} \phi\left(\frac{h/h_0}{|t/t_0|^{y_h/y_t}}\right), \tag{2.41}$$

(where t_0 and h_0 are constants) which is exactly the prediction of the scaling hypothesis in §2.1.3. Differentiating (2.41) in the appropriate manner then leads to (2.15), (2.16) and (2.17), and therefore to the exponent relations (2.7)-(2.10).

Renormalization of the correlation function makes use of (2.36) giving $G(r) \sim r^{-2(d-y_h)}$. This may then be generalized to correlations of 'scaling operators', ϕ_i, each of which

[¶]There are in fact two relevant scaling variables for the $2d$ Ising model, one related to temperature, the other to field. However, they exist in even and odd sub-spaces respectively and so, working in the even sub-space the Hamiltonian depends only on T [12].

[‖]Irrelevant scaling variables lead to corrections which are considered negligible here, though strictly speaking they may be significant.

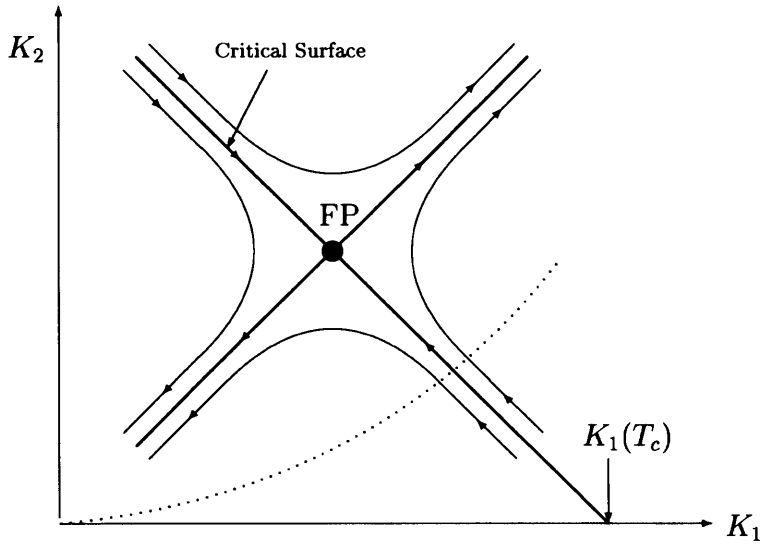

Figure 2.5: RG Flows in a Two Parameter Subspace: For parameter sets lying on the critical surface, renormalization leads to the critical fixed point (FP). Away from the critical surface, renormalization leads to either of the trivial (high or low temperature) fixed points. Any model with T fixed such that K_1 and K_2 lie on the critical surface will renormalize to the same fixed point and thus exhibit the same critical behaviour.

is uniquely coupled to a scaling variable u_i, and is defined by linear combinations of products of the microscopic variables of the system, such that [12]

$$\langle \phi_i(\mathbf{r}_1)\phi_i(\mathbf{r}_2)\rangle \propto |\mathbf{r}_1 - \mathbf{r}_2|^{-2x_i}, \tag{2.42}$$

where

$$x_i = d - y_i. \tag{2.43}$$

This result is completely general and defines the 'scaling dimension', x_i. For systems that may be represented, or approximated, by a Gaussian Hamiltonian, (2.42) is particularly useful as all the averages may be evaluated using Gaussian integration (see Appendix A).

2.2 Probability Distribution Functions

2.2.1 Definitions of Probability Functions

A distribution function, $F(x)$, is a measure of cumulative probability. Simply defined, $F(x')$ is the probability that a variable x will take a value less than or equal to x'. This imposes certain restrictions on the form of $F(x)$. The function must be defined for all values of $x_{\min} \leq x \leq x_{\max}$ with only a finite number of discontinuities. The function must be monotonically non-decreasing between $F(x_{\min}) = 0$ and $F(x_{\max}) = 1$.

A probability density function (PDF)** $f(x)$ is defined such that $f(x')$ is the probability that the variable x takes the value x'. Thus, for discrete and continuous data respectively,

$$F(x) = \sum_{x'=x_{\min}}^{x} f(x') \qquad \text{or} \qquad F(x) = \int_{x_{\min}}^{x} f(x')\,\mathrm{d}x', \tag{2.44}$$

and hence

$$\mathrm{d}F = f(x)\,\mathrm{d}x. \tag{2.45}$$

It is convenient that, as $f(x)$ is zero for all x below $x_{\min}$ and above $x_{\max}$,

$$F(x_{\max}) = \int_{x_{\min}}^{x_{\max}} f(x')\,\mathrm{d}x' = \int_{-\infty}^{\infty} f(x')\,\mathrm{d}x' = 1, \tag{2.46}$$

the last equality indicating that x must assume some value.

2.2.2 Moments

It is often not possible to express PDFs in terms of analytical mathematical functions. Therefore it is useful to define the moments of a distribution, which may be used to compare one distribution with another. The general expression for the r^{th} moment, μ_r of a distribution about a point $x = a$ is

$$\mu_r(a) = \int_{-\infty}^{\infty} (x-a)^r f(x)\,\mathrm{d}x. \tag{2.47}$$

**The nomenclature is often flexible here – sometimes the term 'probability distribution function' is used in place of 'probability density function'. As we are almost never interested in distribution functions, such as $F(x)$, there should be no cause for confusion.

The zeroth moment is always unity and is unimportant. The first moment is simply related to the arithmetic mean. In the discrete case this is easily thought of as the sum over all possible values of the variable $x = x'$ with each value weighted by its probability. In the case of continuous x this becomes

$$\langle x \rangle = \int_{-\infty}^{\infty} x f(x)\,\mathrm{d}x = \mu_1(0), \tag{2.48}$$

and in general,

$$\langle x^r \rangle = \int_{-\infty}^{\infty} x^r f(x)\,\mathrm{d}x = \mu_r(0), \tag{2.49}$$

where $\langle x^r \rangle$ denotes the r^{th} moment about $x = 0$, viz. the average of x^r.

The so-called 'principle' moments (labelled simply μ_r) are defined as those for which $a = \langle x \rangle$ and are usually the quantities of most interest. It is often easier to evaluate moments about a point other than the mean and then relate these to the principle values. This is done by making the substitution $z = x - a$ and using the binomial expansion

$$\mu_r = \sum_{k=0}^{r} (-1)^k \, {}^r\mathrm{C}_k \, \left\langle z^k \right\rangle \mu_{r-k}(a). \tag{2.50}$$

If the functional form of $f(x)$ is known, the moments may be extracted from the moment generating function,

$$G(s) = \int_{-\infty}^{\infty} e^{sx} f(x)\,\mathrm{d}x, \tag{2.51}$$

where, without loss of generality, $a = 0$. Obtaining the moments from $G(s)$ is achieved by expanding the exponential and integrating term by term,

$$G(s) = \int_{-\infty}^{\infty} f(x)\,\mathrm{d}x + s\int_{-\infty}^{\infty} x f(x)\,\mathrm{d}x + \frac{s^2}{2}\int_{-\infty}^{\infty} x^2 f(x)\,\mathrm{d}x + \cdots + \tag{2.52}$$

$$= 1 + s\langle x \rangle + \frac{s^2}{2}\left\langle x^2 \right\rangle + \cdots +, \tag{2.53}$$

thus

$$\langle x^r \rangle = \left. \frac{d^r G(s)}{ds^r} \right|_{s=0}. \tag{2.54}$$

For independent variables x and y with distributions $f_1(x)$ and $f_2(y)$,

$$G_{x+y}(s) = \iint e^{(x+y)s} f_1(x) f_2(y)\,\mathrm{d}x\,\mathrm{d}y \tag{2.55}$$

$$= G_x(s) G_y(s). \tag{2.56}$$

2.2.3 Cumulants

There are circumstances in which the moment generating function, as defined above, does not exist for all real s. An equivalent definition using the pure imaginary variable is (in place of s) gives rise to the more useful 'characteristic function'. It can be shown that, within certain general constraints, this function completely describes the PDF, and is, in turn, totally determined by it [90].

The definition of the characteristic function, $\phi(s)$, shows that it is the Fourier transform of the PDF,

$$\phi(s) = \int_{-\infty}^{\infty} e^{isx} f(x)\,\mathrm{d}x. \tag{2.57}$$

This is still a moment generating function as it obeys all the rules discussed above. It also defines the cumulants – a set of constants similar to the moments (and related to them), which are more directly connected to the shape of the distribution making them descriptively more useful. The r^{th} cumulant, κ_r, is defined by the equation

$$\log(\phi(s)) = \sum_{r=1}^{\infty} \frac{(is)^r}{r!} \kappa_r \tag{2.58}$$

Two properties, true of both moments and cumulants, are worth noting. Firstly, a shift in the origin of the distribution affects only the first cumulant. For example, if the origin is shifted by $+c$,

$$\phi_2(s) = \int_{-\infty}^{\infty} e^{is(x-c)} f(x)\,\mathrm{d}x \tag{2.59}$$

$$= e^{-isc} \int_{-\infty}^{\infty} e^{isx} f(x)\,\mathrm{d}x \tag{2.60}$$

$$= e^{isc} \phi_1(s) \tag{2.61}$$

where ϕ_1 and ϕ_2 are the characteristic functions for the original and shifted distributions respectively. As

$$\log(\phi_2(s)) = -isc + \log(\phi_1(s)) \tag{2.62}$$

only the coefficient of is has changed, so moments with $r > 1$ remain unaffected. Secondly, a change in variable $x \to ax$ does not alter $f(x)\,\mathrm{d}x$ and so the cumulants transform as $\kappa_r \to a^r \kappa_r$.

The infinite set of cumulants will, for most well behaved PDFs, completely define the distribution. However, often only the first four cumulants are needed to obtain a good description of its shape [91]. The mean (μ) and variance (σ^2, where σ is the standard deviation) are just the first and second cumulants respectively. The skewness (γ_3) is a measure of the asymmetry, while the 'defect of kurtosis' (γ_4) is the deviation of the kurtosis, a measure of the sharpness of the peak (sometimes called the 'fatness'), from the Gaussian value of 3. These two quantities are respectively equal to the third and fourth cumulants of the variate normalized to the standard deviation.

Some important relations are:

$$\mu = \frac{\kappa_1}{\sigma} = \frac{1}{\sigma}\langle x \rangle \tag{2.63}$$

$$\sigma^2 = \kappa_2 = \left\langle x^2 \right\rangle - \langle x \rangle^2 \tag{2.64}$$

$$\gamma_3 = \frac{\kappa_3}{\sigma^3} = \frac{1}{\sigma^3}\left(\left\langle x^3 \right\rangle - 3\left\langle x^2 \right\rangle \langle x \rangle + 2\langle x \rangle^3\right) \tag{2.65}$$

$$\gamma_4 = \frac{\kappa_4}{\sigma^4} = \frac{1}{\sigma^4}\left(\left\langle x^4 \right\rangle - 4\left\langle x^3 \right\rangle \langle x \rangle - 3\left\langle x^2 \right\rangle^2 + 12\left\langle x^2 \right\rangle \langle x \rangle^2 - 6\langle x \rangle^4\right). \tag{2.66}$$

2.2.4 Distributions of Compound (Global) Variables

The Central Limit Theorem

A compound variable, or global quantity S, depends on more than one microscopic component, s_i. Generally speaking S is the sum of its microscopic constituents, each of which has its own distribution of values. Therefore the PDF, $P(S)$, depends

both on the individual PDFs of the s_i, and on the manner in which these microscopic components interact with each other. In many physical systems one would expect the microscopic variables to be identically distributed (id), and this makes the statistical analysis somewhat easier.

When the variables s_i do not interact with each other, that is they are statistically independent, the central limit theorem (CLT) applies. This remarkable theorem states that if $S_N = \sum_{i=1}^{N} s_i$ and the s_i have mean μ and variance σ^2, then

$$\lim_{N\to\infty} P\left(a \leq \frac{S_N - N\mu}{\sigma\sqrt{N}} \leq b\right) = \frac{1}{\sqrt{2\pi}} \int_a^b e^{-u^2/2}\, \mathrm{d}u. \tag{2.67}$$

In other words, as the system becomes infinitely large, the distribution of the global measure approaches a Gaussian – regardless of the form of the distribution of the s_i. In fact the result is even more general. Firstly the microscopic variables do not need to be identically distributed, simply to share a common mean and variance. Secondly the s_i do not need to be independent. Instead, any correlation between the microscopic variables must have a sufficiently short range that the global quantity may be expressed as the sum of mesoscopic independent variables [1]. There is however one final criterion that must be fulfilled for the CLT to apply. Each of the constituent parts of the global quantity must make an individually negligible contribution to the sum. Thus there must not be a large spread in values of the s_i [92–94].

Things become very much more complicated when the microscopic variables begin to strongly interact with each other. The limiting example of this is critical behaviour. For a critical system the infinite correlation length prevents the system having even mesoscopically independent regions. Therefore any global measure will be the sum of highly correlated variables and the central limit theorem breaks down [6, 8]. Unfortunately, when this occurs, there is no known equivalent non-Gaussian function toward which distributions tend. Thus, at first sight, the distributions of global quantities in critical systems are limited in form only by the general restrictions that apply to all PDFs.

Universality suggests that the non-trivial PDFs that do occur at critical points are not all different but may be grouped together in universality classes [8, 10, 12–15].

Thus the shape of a critical distribution depends on dimensionality and symmetry rather than on detailed microscopic considerations. As a result it might be reasonable to assume that an experimental system could be assigned to a given universality class by comparing its measured distribution with a gallery of predetermined functions. This idea of a 'picture gallery' has been proposed by Rácz in the context of non-equilibrium scaling functions (see in particular [44]).

2.2.5 Normalization of Global Variables

From (2.67) it is seen that the CLT applies to the normalized global variable $\frac{(S-\langle S\rangle)}{N^{1/2}}$ not simply to S. This is crucial to extract any meaning from the distribution as the thermodynamic limit is taken. The standard deviation of fluctuations in S scales as $N^{1/2}$ when the components s_i are independent [7]. Thus if S is normalized by any power of N other than $1/2$ the distribution of the global quantity will either become infinitely narrow or infinitely wide as $N \to \infty$ (for a detailed discussion see Appendix A of [6]).

For a critical system the fluctuations in the intensive quantity $z = S/N$ may scale in manner other than $N^{-1/2}$ [8]. In fact, finite size scaling leads to the relation [6]

$$\sigma \sim N^{-\frac{1}{2}+\frac{1-\eta/2}{d}}. \tag{2.68}$$

Thus critical variables should be normalized by their standard deviation, not simply $N^{1/2}$, in order to obtain a reasonable limit distribution. The appropriate limit function, shifted to zero mean, is therefore [16, 19]

$$P'\left(\frac{z-\langle z\rangle}{\sigma_z}\right) = \sigma_z P(z). \tag{2.69}$$

Chapter 3

Toy Models and Approximate Methods

This chapter begins by looking at a simple model with no phase transition as an introduction the concepts involved in solving a thermodynamic system. The purpose is two-fold: firstly to demonstrate the approach of statistical mechanics in terms of counting numbers of configurations, and secondly to show that this approach yields exactly the same results as can be obtained directly from purely statistical considerations.

The second half of the chapter focuses on the Ising model in two dimensions, for which a phase transition does exist. A series expansion approach to the problem in finite field is discussed and related to an equivalent expression in zero field using the ideas of graph theory. Also a simple finite size scaling argument is suggested for the variance of the energy fluctuations.

3.1 Non-Interacting Spins - A Simple Precursor to the Ising Model

This section focuses on the susceptibility of a simple toy model of N non-interacting one dimensional (Ising) magnetic spins, $s_i = \pm 1$, in an external field. The only energy

in the system comes from the interaction of each spin with the field,

$$E = -h\mu \sum_{i=1}^{N} s_i, \tag{3.1}$$

where μ is the magnetic moment of an individual spin (which will be taken as 1 from now on). The location of the spins is unimportant so no lattice type needs to be specified.

3.1.1 A Statistical Mechanical Approach

It is possible to solve the model defined in (3.1) by using either statistical mechanics or simple statistics. The latter is the more straightforward, however the former is more informative and leads to the derivation of a number of useful and quite general relations. We begin with the statistical mechanical approach and define the extensive magnetization,

$$M = \sum_{i=1}^{N} s_i, \tag{3.2}$$

thus

$$\frac{\partial E}{\partial h} = -M. \tag{3.3}$$

Expressions for the Magnetic Susceptibilities

The aim is to find expressions for the per spin susceptibilities of this model,

$$\chi_{\text{int}}^{(n)} = \left(\frac{\partial^{n-1} \langle m \rangle}{\partial h^{n-1}} \right)_T, \tag{3.4}$$

where $m = M/N$. The approach taken is to perform the majority of the analysis using the extensive magnetization and then transform the results at an appropriate stage. It will be seen that correct normalization of the resulting distribution makes the distinction between extensive and intensive properties irrelevant. However it is important at each stage of the derivation to be clear with which quantity one is dealing. If the magnetization and energy of a given spin configuration, say α, are M_α and E_α respectively, then

$$\langle M \rangle = \frac{\sum_\alpha M_\alpha e^{-\beta E_\alpha}}{\sum_\alpha e^{-\beta E_\alpha}} \tag{3.5}$$

$$= \frac{1}{Z}\sum_{\alpha} M_\alpha e^{-\beta E_\alpha}, \tag{3.6}$$

where Z is the partition function. Thus

$$\frac{\partial \langle M^a \rangle}{\partial h} = \frac{\partial}{\partial h}\left(\frac{1}{Z}\sum_{\alpha} M_\alpha^a e^{-\beta E_\alpha}\right) \tag{3.7}$$

$$= \frac{1}{Z}\beta \sum_{\alpha} M_\alpha^{a+1} e^{-\beta E_\alpha} - \frac{1}{Z^2}\sum_{\alpha} M_\alpha^a e^{-\beta E_\alpha}\left\{\beta \sum_{\alpha} M_\alpha e^{-\beta E_\alpha}\right\} \tag{3.8}$$

$$= \beta\left\{\left\langle M^{a+1}\right\rangle - \langle M^a \rangle \langle M \rangle\right\}. \tag{3.9}$$

Also, differentiating powers of (3.5) gives

$$\frac{\partial \langle M^a \rangle^b}{\partial h} = \left\{b \langle M^a \rangle^{b-1} \frac{\partial \langle M^a \rangle}{\partial h}\right\} \tag{3.10}$$

Repeated use of (3.9) and (3.10) yields the following expressions for the first three extensive susceptibilities in terms of the moments of M:

$$\frac{\partial \langle M \rangle}{\partial h} = \beta\left\{\left\langle M^2\right\rangle - \langle M \rangle^2\right\} \tag{3.11}$$

$$\frac{\partial^2 \langle M \rangle}{\partial h^2} = \beta^2\left\{\left\langle M^3\right\rangle - 3\left\langle M^2\right\rangle \langle M \rangle + 2\langle M \rangle^3\right\} \tag{3.12}$$

$$\frac{\partial^3 \langle M \rangle}{\partial h^3} = \beta^3\left\{\left\langle M^4\right\rangle - 4\left\langle M^3\right\rangle \langle M \rangle - 3\left\langle M^2\right\rangle^2 + 12\left\langle M^2\right\rangle \langle M \rangle^2 - 6\langle M \rangle^4\right\}. \tag{3.13}$$

Comparing this set of equations with the results of §2.2.3 shows that each right hand side is equal to β^a times κ_{a+1} where κ_r is the r^{th} cumulant of the distribution of M. Hence all that remains is the determination of the forms of $\langle M^a \rangle$.

To this point the exact form of the Hamiltonian has not been referred to and so the independence of the spins has not been a factor. The results are therefore quite general and apply to all magnetic systems.

Evaluation of Averages

The lack of interaction in this model enables contributions from each spin to be treated separately. Thus the sum over all states may be replaced by the product of

sums over all possible values of each variable,

$$\langle M \rangle = \frac{\sum_\alpha M_\alpha e^{-\beta E_\alpha}}{\sum_\alpha e^{-\beta E_\alpha}} \tag{3.14}$$

$$= \frac{\sum_{s_1=\pm1}\sum_{s_2=\pm1}\sum_{s_3=\pm1}(s_1+s_2+s_3+\ldots+)\,e^{-\beta(\varepsilon_1+\varepsilon_2+\varepsilon_3+\ldots+)}}{\sum_{s_1=\pm1}\sum_{s_2=\pm1}\sum_{s_3=\pm1}e^{-\beta(\varepsilon_1+\varepsilon_2+\varepsilon_3+\ldots+)}} \tag{3.15}$$

$$= N\frac{\sum_{s_1=\pm1} s_1 e^{-\beta\varepsilon_1}}{\sum_{s_1=\pm1} e^{-\beta\varepsilon_1}}, \tag{3.16}$$

Having only two terms, the sums may be performed explicitly,

$$\langle M \rangle = N\frac{\sum_{s_1=\pm1} s_1 e^{-\beta\varepsilon_1}}{\sum_{s_1=\pm1} e^{-\beta\varepsilon_1}} \tag{3.17}$$

$$= N\left(\frac{-e^{-\beta h}+e^{\beta h}}{e^{-\beta h}+e^{\beta h}}\right) \tag{3.18}$$

$$= N\left(\frac{2\sinh(\beta h)}{2\cosh(\beta h)}\right) \tag{3.19}$$

$$= N\tanh(\beta h). \tag{3.20}$$

At this point, (3.20) may be differentiated repeatedly to find the susceptibilities. However the following method shows how the desired quantities may be found by counting the different configurations.

The method for evaluating $\langle M^2 \rangle$, $\langle M^3 \rangle$ and $\langle M^4 \rangle$ is essentially the same as used above, however 'cross terms' in the expansion of $(s_1+s_2+s_3+\ldots+)^r$ result in minor complications. Some observations about $\langle M^r \rangle$ make the calculation easier.

- The form of the exponential is unaltered by the power to which M_i is raised. Thus the numerator of the average expression will be of the form $Ae^{\beta h} + Be^{-\beta h}$.

- The coefficients of A and B arise from the multiplication of r terms, each of which is restricted to be ±1. This means that factors in the numerator are restricted to be of the form $2\sinh(\beta h)$ or $2\cosh(\beta h)$. The denominator is always $(2\cosh(\beta h))^N$.

- Whether a given term is $\cosh(\beta h)$ like or $\sinh(\beta h)$ like depends simply on the product of the s_i concerned. If the product of the exponents of the r relevant spins is positive the term is $\cosh(\beta h)$, if negative it is $\sinh(\beta h)$.

- Finally, each free spin (those not explicitly represented in a given term) yields a cosh function from the sum over its states. This applies to distinct spins, so whilst $s_i s_j s_k$ is multiplied by a factor $\cosh^{N-3}(\beta h)$, the term s_i^3 is associated with $\cosh^{N-1}(\beta h)$ because for this term there are $N-1$ free spins.

Hence the problem is reduced to one of evaluating the number of each type of term arising from the expansions of $(\sum_i s_i)^r$, $r = 2, 3, 4$, and thus is a question of combinatorics.

The case with $r = 2$ is simplest, with only two types of term arising from the squaring of the magnetization. Terms are either s_i^2 or $s_i s_j$.

In the expansion of $(s_1 + s_2 + s_3 + \ldots +)^2$ there are N possible choices for the spin to consider from the 'first' bracket. For terms of the form s_i^2 this is the only degree of freedom as the second spin is constrained to equal the first. Hence there are N s_i^2 terms arising from expansion. For the $s_i s_j$ type, the only restriction on the second spin is that it must *not* be the same as the first. Hence there are $N-1$ spins to choose from resulting in $N(N-1)$ terms of the form $s_i s_j$. Therefore, using the observations noted above,

$$\left\langle M^2 \right\rangle = \frac{\sum_\alpha M_\alpha^2 e^{-\beta E_\alpha}}{\sum_\alpha e^{-\beta E_\alpha}} \tag{3.21}$$

$$= N\frac{(\cosh(\beta h))(\cosh^{N-1}(\beta h))}{\cosh^N(\beta h)} + N(N-1)\frac{(\sinh^2(\beta h))(\cosh^{N-2}(\beta h))}{\cosh^N(\beta h)} \tag{3.22}$$

$$= N(1 + (N-1)\tanh^2(\beta h)). \tag{3.23}$$

Similar considerations provide the factors in Table 3.1, and the expression for $\langle M^3 \rangle$ is,

r	Type of term	Factor
2	s_i^2	N
	$s_i s_j$	$N(N-1)$
3	s_i^3	N
	$s_i^2 s_j$	$3N(N-1)$
	$s_i s_j s_k$	$N(N-1)(N-2)$
4	s_i^4	N
	$s_i^3 s_j$	$4N(N-1)$
	$s_i^2 s_j s_k$	$6N(N-1)(N-2)$
	$s_i^2 s_j^2$	$3N(N-1)$
	$s_i s_j s_k s_l$	$N(N-1)(N-2)(N-3)$

Table 3.1: Factors in the Expansion of $\langle M^r \rangle$

$$\langle M^3 \rangle = \frac{\sum_\alpha M_\alpha^3 e^{-\beta E_\alpha}}{\sum_\alpha e^{-\beta E_\alpha}} \tag{3.24}$$

$$= \frac{1}{\cosh^N(\beta h)} \Big\{ N \sinh(\beta h) \cosh^{N-1}(\beta h) + 3N(N-1) \cosh^{N-1}(\beta h) \sinh(\beta h) + N(N-1)(N-2) \sinh^3(\beta h) \cosh^{N-3}(\beta h) \Big\} \tag{3.25}$$

$$= N \tanh(\beta h)(3N - 2 + (N-1)(N-2) \tanh^2(\beta h)). \tag{3.26}$$

For $\langle M^4 \rangle$ one gets,

$$\langle M^4 \rangle = \frac{\sum_\alpha M_\alpha^4 e^{-\beta E_\alpha}}{\sum_\alpha e^{-\beta E_\alpha}} \tag{3.27}$$

$$= \frac{N}{\cosh^N(\beta h)} \Big\{ N \cosh^N(\beta h) + 4N(N-1) \sinh^2(\beta h) \cosh^{N-2}(\beta h) + 6N(N-1)(N-2) \sinh^2(\beta h) \cosh^{N-2}(\beta h) + N(N-1)(N-2)(N-3) \sinh^4(\beta h) \cosh^{N-4}(\beta h) + 3N(N-1) \cosh^N(\beta h) \Big\} \tag{3.28}$$

$$= N\left\{3N - 2 + 4N^2\tanh^2(\beta h) - 6N\tanh^2(\beta h) + 2\tanh^2(\beta h) + (N-1)(N-2)(N-3)\tanh^4(\beta h)\right\}. \quad (3.29)$$

Relating Susceptibilities to Cumulants

It is the fluctuations in the intensive magnetization that are of interest and so it is desirable to express the intensive susceptibilities, $\chi_{\text{int}}^{(n)}$, in terms of the intensive moments, $\langle m^x \rangle$.

$$\chi_{\text{int}}^{(1)} = \frac{\partial \langle m \rangle}{\partial h} \quad (3.30)$$

$$= \frac{1}{N}\left(\frac{\partial \langle M \rangle}{\partial h}\right) \quad (3.31)$$

$$= \frac{1}{N}\beta\left(\left\langle M^2 \right\rangle - \langle M \rangle^2\right) \quad (3.32)$$

$$= \frac{1}{N}\beta\left(\left\langle m^2 \right\rangle N^2 - \langle m \rangle^2 N^2\right) \quad (3.33)$$

$$= \beta N\left(\left\langle m^2 \right\rangle - \langle m \rangle^2\right). \quad (3.34)$$

Similarly

$$\chi_{\text{int}}^{(2)} = \frac{\partial^3 \langle m \rangle}{\partial h^3} = \beta^2 N^2\left(\left\langle m^3 \right\rangle - 3\left\langle m^2 \right\rangle \langle m \rangle + 2\langle m \rangle^3\right) \quad (3.35)$$

$$\chi_{\text{int}}^{(3)} = \frac{\partial^4 \langle m \rangle}{\partial h^4} = \beta^3 N^3\left(\left\langle m^4 \right\rangle - 4\left\langle m^3 \right\rangle \langle m \rangle - 3\left\langle m^2 \right\rangle^2 + 12\left\langle m^2 \right\rangle \langle m \rangle^2 - 6\langle m \rangle^4\right) \quad (3.36)$$

Thus for the first three susceptibilities it is seen that

$$\chi_{\text{int}}^{(a)} = (\beta N)^a \kappa_{a+1}. \quad (3.37)$$

where κ_a is the a^{th} cumulant of the intensive magnetization distribution. Again this result is quite general and does not arise from the independence of the spins. Using the expressions derived for the extensive moments, together with $\langle x^y \rangle = (1/N^y)\langle (Nx)^y \rangle$, gives the dependence of $\chi_{\text{int}}^{(a)}$ on the external field,

$$\chi_{\text{int}}^{(2)} = \beta\left(1 - \tanh^2(\beta h)\right) \quad (3.38)$$

$$\chi_{\rm int}^{(3)} = 2\beta^2\left(\tanh^3(\beta h) - \tanh(\beta h)\right) \tag{3.39}$$

$$\chi_{\rm int}^{(4)} = 2\beta^3\left(4\tanh^2(\beta h) - 1 - 3\tanh^4(\beta h)\right). \tag{3.40}$$

The cumulants of the distribution of m are therefore (note that $\kappa_2 = \sigma^2$)

$$\kappa_2 = \frac{\chi_{\rm int}^{(2)}}{\beta N} \tag{3.41}$$

$$= \frac{1}{N}\left(1 - \tanh^2(\beta h)\right) \tag{3.42}$$

$$\stackrel{H\to 0}{=} \frac{1}{N} \tag{3.43}$$

$$\kappa_3 = \frac{\chi_{\rm int}^{(3)}}{\beta^2 N^2} \tag{3.44}$$

$$= \frac{2}{N^2}\left(\tanh^3(\beta h) - \tanh(\beta h)\right) \tag{3.45}$$

$$\stackrel{H\to 0}{=} 0 \tag{3.46}$$

$$\kappa_4 = \frac{\chi_{\rm int}^{(4)}}{\beta^3 N^3} \tag{3.47}$$

$$= \frac{2}{N^3}\left(4\tanh^2(\beta h) - 1 - 3\tanh^4(\beta h)\right) \tag{3.48}$$

$$\stackrel{H\to 0}{=} -\frac{2}{N^3} \tag{3.49}$$

The mean, μ, variance $\sigma^2 = \kappa_2$, skewness $\gamma_3 = \kappa_3/\sigma^3$ and the defect of kurtosis, $\gamma_4 = \kappa_4/\sigma^4$ may therefore be found. In the limit of zero field they are,

$$\mu = 0 \tag{3.50}$$

$$\sigma^2 = \frac{1}{N} \tag{3.51}$$

$$\gamma_3 = 0 \tag{3.52}$$

$$\gamma_4 = -\frac{2}{N}, \tag{3.53}$$

consistent with the predicted Gaussian form.

3.1.2 The Statistical Route to the Cumulants

In theory, (3.50)–(3.53) may be derived in a simple statistical manner as the distribution function for each individual spin is known,

$$P(s_i) = \frac{1}{2}\left(\delta(-1) + \delta(+1)\right).$$

The characteristic function of this double delta function is

$$\begin{aligned}
\phi(t) &= \frac{1}{2}\int_{-\infty}^{\infty} e^{itx}\left(\delta(-1) + \delta(+1)\right) dx && (3.54)\\
&= \frac{1}{2}\left[e^{it} + e^{-it}\right] && (3.55)\\
&= \cos(t). && (3.56)
\end{aligned}$$

For the distribution of the global quantity, $M = \sum_{i=1}^{N} s_i$, the characteristic function is the product of the contributions from the individual spins. Hence,

$$\begin{aligned}
\Phi_N(t) &= \cos^N(t) && (3.57)\\
\ln\left[\Phi_N(t)\right] &= \ln\left[\cos^N(t)\right] && (3.58)\\
&= N \ln\cos(t) && (3.59)\\
&= N \ln\left[1 - \frac{t^2}{2!} + \frac{t^4}{4!}\cdots\right] && (3.60)\\
&\approx N \ln\left[1 + \left(-\frac{t^2}{2!} + \frac{t^4}{4!}\right)\right] && (3.61)\\
&\approx N\left[-\frac{t^2}{2!} + \frac{t^4}{4!} - \frac{1}{2}\left(-\frac{t^2}{2!} + \frac{t^4}{4!}\right)^2\cdots\right] && (3.62)\\
&\approx N\left[-\frac{t^2}{2!} + \frac{t^4}{4!} - \frac{t^4}{8}\right] && (3.63)\\
&\approx N\left[-\frac{t^2}{2!} - 2\frac{t^4}{4!}\right] && (3.64)\\
&\approx N\left[\frac{(it)^2}{2!} - 2\frac{(it)^4}{4!}\right]. && (3.65)
\end{aligned}$$

The power series expansions used for the cosine and logarithm functions have been truncated at the appropriate points such that the fourth order cumulant remains exact. The r^{th} cumulant of the distribution of M is the coefficient of $(it)^r/r!$,

$$\kappa_1 = 0 \tag{3.66}$$

$$\kappa_2 = N \tag{3.67}$$

$$\kappa_3 = 0 \tag{3.68}$$

$$\kappa_4 = -2N. \tag{3.69}$$

These values refer to the distribution of the extensive magnetization. Only after normalizing by σ_M do the values become the same as (3.50)–(3.53). This highlights the fact that the for correctly normalized distributions it is not important whether one deals with intensive of extensive quantities.

The system being considered has no means for cooperation between variables, so the central limit theorem predicts that the magnetization distribution should be Gaussian in the thermodynamic limit ($N \to \infty$). This is clearly the case; the variance and defect of kurtosis scale as $1/N$, the skewness is identically zero.

3.2 The Two Dimensional Ising Model

The model discussed in the previous section is effectively the Ising model, defined by the Hamiltonian

$$H = -J \sum_{\langle i,j \rangle} s_i s_j - h \sum_i s_i \tag{3.70}$$

in the case of zero exchange interaction, $J = 0$. This model has a long history dating back to Ising's 1925 solution of the one dimensional case [95], and Onsager's solution of the two dimensional model [74] in zero field remains one of the most important breakthroughs in the theoretical development of critical phenomena. For $h \neq 0$ no exact solution has yet been found and so approximate methods must be used.

3.2.1 Series Expansions

There is a wealth of literature regarding series expansions of the Ising model partition function covering all manner of lattices, dimensions, couplings and boundary conditions (see for example [73]). The aim of this section is not to add to the large numbers of terms already evaluated, but rather to draw attention to a link between zero and finite field expansions that we have not seen discussed explicitly elsewhere.

A low temperature expansion discussed by Baxter [88] expands the partition function as a power series in $u = \exp(-4K)$, where $K = \beta J$. This series results in two branches stemming from the minima associated with all spins aligned with the field and all spins aligned against the field. The first few terms in both series are given as,

$$\begin{aligned} Z_N &= e^{2NK+Nh}\left\{1 + Nu^2e^{-2h}\right. \\ &\quad +2Nu^3e^{-4h} + \tfrac{1}{2}N(N-5)u^4e^{-4h} \\ &\quad \left.+6Nu^4e^{-6h} + Nu^4e^{-8h} + \ldots +\right\} \\ &\quad +e^{2NK-Nh}\left\{1 + Nu^2e^{2h}\right. \\ &\quad +2Nu^3e^{4h} + \tfrac{1}{2}N(N-5)u^4e^{4h} \\ &\quad \left.+6Nu^4e^{6h} + Nu^4e^{8h} + \ldots +\right\} \end{aligned} \tag{3.71}$$

where the temperature factor has been absorbed into the field under the transformation $h \rightarrow \beta h$.

More recently, Beale [96] used a similar expansion for a finite $m \times n$ lattice. Using Kaufman's extension [97] to Onsager's solution [74], he managed to obtain the exact, zero field, expansion for systems up to $n = m = 32$. Constraining Beale's lattice to be a square ($m = n = \sqrt{N}$), with a small transformation of variables (Beale expands in $x = \sqrt{u}$) his expansion can be expressed as:

$$\begin{aligned} Z_N &= e^{2NK}\sum_{k=0\ldots}^{N} g_k u^k \\ &= e^{2NK}\left\{2 + 2Nu^2 + 4Nu^3 + (N^2+9N)u^4 + (4N^2+24N)u^5 + \ldots +\right\} \end{aligned} \tag{3.72}$$

Where g_k is the number of possible configurations with energy $4kJ$ above the ground state.

Comparison of the coefficients of u^x in equations (3.71) and (3.72) shows that they are closely linked. Let $\Theta(z)$ denote the coefficient of z and consider $\Theta(u^2)$ in the finite field expansion (3.71):

$$\Theta(u^2) = Ne^{2NK}\left(e^{(N-2)h} + e^{(2-N)h}\right) \tag{3.73}$$

Setting $h = 0$ in (3.73) results in:

$$\Theta(u^2) \stackrel{h\to 0}{=} 2Ne^{2NK} \tag{3.74}$$

which is the same as is obtained directly from the zero field approach as represented by equation (3.72). A similar relationship also holds for u^4 where there are many contributions to the partition function in (3.71) with various h dependencies. Letting $h \to 0$ in this case and cancelling the factor of e^{2NK} common to both expansions gives,

$$2\left[\frac{1}{2}N(N-5) + 6N + N\right] = N^2 + 9N \tag{3.75}$$

This link is quite intuitive as setting $h = 0$ in the finite field expansion must ultimately give rise to the same partition function as one obtains by simply considering the zero field case to start with. The question then arises:

> Is possible to split up the coefficients obtained in zero field to arrive at the correct h dependent terms?

If so, given that the zero field terms are exactly calculable, the finite field coefficients follow directly.

Consider first the expansion in equation (3.72). The Hamiltonian for this system is $H = -J\sum_{\langle i,j\rangle} s_i s_j$ with the ground state energy corresponding to all spins aligned, $E_{gs} = -J(2N)$. The smallest energy interval is $4J$ corresponding to the flipping of a spin with three positive and one negative interactions. Thus all energy levels may be expressed as $E_k = E_{gs} + 4kJ$ where k is an integer. Taking g_k as the number of states with energy E_k then yields equation (3.72).

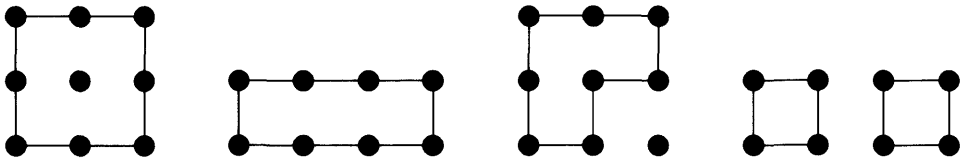

(a) (b) (c) (d)

Figure 3.1: The four types of graph that may be constructed on a square lattice using 8 'bonds': The two sub-graphs of part (d) may be joined at a vertex but must not share any common linkages.

Comparison with Peierls' discussion of spin zone boundaries [98] shows that $\Theta(u^k)$ is related to the number of closed even vertex graphs with $2k$ bonds that can be embedded in a toroidal lattice of size N. Given the symmetry of the system, the number of graphs is precisely half the value of the coefficients, as 'all spins up' is equivalent to 'all spins down'. For example, $\Theta(u^4) = N^2 + 9N$. Now consider the permitted graphs that may be drawn with $2k = 8$ bonds – these are shown in Figure 3.2.1 (a)–(d). Graph (a) may appear N times on the lattice, once at each of the N lattice points, because it is the same in all four orientations. By contrast, (b) has two distinct orientations that it can adopt at each lattice point, and (c) has four such possibilities. Thus these graphs contribute $2N$ and $4N$ respectively. Finally graph (d) consists of two distinct squares with four lines each. These may be joined at the corners but must not share any bonds. The first square may be placed freely at any point on the lattice and has only a single orientation. The second square may be sited anywhere that does not result in a bond overlap with the first. This restricts it to $N - 5$ possibilities. The identical nature of the two squares means either could be chosen as the first, introducing a combinatorial factor of $\frac{1}{2}$. Thus the contribution from graph (d) is $\frac{1}{2}N(N-5)$ giving a total for the number of graphs with eight lines of $\frac{1}{2}N(N+9)$. As predicted this is exactly half the value of the coefficient.

Similar analysis of the finite field expansion (3.71) is made more complicated by

the presence of two terms in the Hamiltonian. If $H = -J\sum_{\langle i,j\rangle} s_i s_j - h\sum_i s_i$ then the ground state energy is given by $E_{gs} = -(J(2N) + hN)$. The smallest energy increments for each term are $4J$ and $2h$ (a single spin flip goes from a contribution of $-h$ to $+h$ or *vice versa*). As expected from topological considerations, only certain values of $\Theta(J)$ are possible for each $\Theta(h)$. For example, if all spins are 'pointing up' then two are flipped, there are only two outcomes. If the spins are neighbours there is a single region of minority spins with a perimeter of 6 bonds. This scenario relates to the term in u^3. Alternatively the spins could be separate as represented by the eight line graph in Fig. 3.2.1(d). This relates to the term in u^4.

Thus the expansion has terms in $u^x e^{-yh}$ corresponding to graphs with 'area' $y/2$ and perimeter $2x$. If the coefficients of graphs with perimeter $2x$ are summed irrespective of the values of y to which they pertain, one obtains the same coefficients as for the zero field expansion, which we can determine precisely numerically for a given value of N.

> **If we can separate the graphs with perimeter $2x$ into groups with area $y/2$, and count the number of graphs in each group, we will be able to split the known zero field coefficients into the contributions required to define the finite field partition function.**

Unfortunately this procedure is practically impossible for all but a few very small lattices. The first problem one encounters is the limitation on the size of system for which the exact zero field coefficients can be obtained. There is no theoretical maximum, only a huge computational expense as the size increases. Currently the largest size for which we have zero field results is $N = 1024$. This expansion contains coefficients of the order 10^{306} – as computational time increases rapidly with system size this is clearly a limiting factor. The next difficulty arises from the sheer number of graphs that must be categorized. This is of the order of the largest coefficient and is prohibitively large even for $N = 1024$. Unless some considerable simplification is achieved the problem appears to remain intractable (see also Chapter 7).

An interesting aside is an observation which possibly simplifies some elements of

graph counting programs, and which we have not seen in previous work. If each point in the perimeter of a graph is assigned a value $\frac{1}{4}, \frac{1}{2}, \frac{3}{4}, 1$, depending on the portion of that point contained *within* the graph, then the sum over all points is equal to the area of that graph.

3.2.2 The Energy Distribution at Zero Field

An extension of Onsager's solution due to Kaufman [97] can be simplified to a sum of products of polynomial factors [96]. Using *Mathematica* it is possible to expand these products - setting precision to $N \ln 2 / \ln 10$ decimal digits ensures that the exact integer values are obtained. The coefficients were evaluated for all square lattices in the range $L = 7$ to $L = 32$ at temperatures from $T/J = 1 - 2.9$ in steps of 0.1 and $T/J = 5 - 50$ in steps of 5.

According to Beale's expansion [96], the energy distribution may be expressed as

$$P(E_k) = \frac{g_k u^k}{\sum_k g_k u^k} \tag{3.76}$$

where $u = \exp(-4\beta J)$ and, as stated previously, state k has energy

$$E_k = -J(2N) + 4kJ. \tag{3.77}$$

Given that the coefficients g_k are known explicitly, the moments of the distribution of energies can be evaluated exactly.

These exact moments provide a useful means for investigating finite size scaling. For example, Onsager's solution shows that the specific heat has a logarithmic singularity in the thermodynamic limit,

$$C \sim -\ln(t), \tag{3.78}$$

which is predicted to scale as (from §2.1.7),

$$C \sim -\ln(\xi^{-\frac{1}{\nu}}) \tag{3.79}$$

$$\sim \frac{1}{\nu d} \ln(N). \tag{3.80}$$

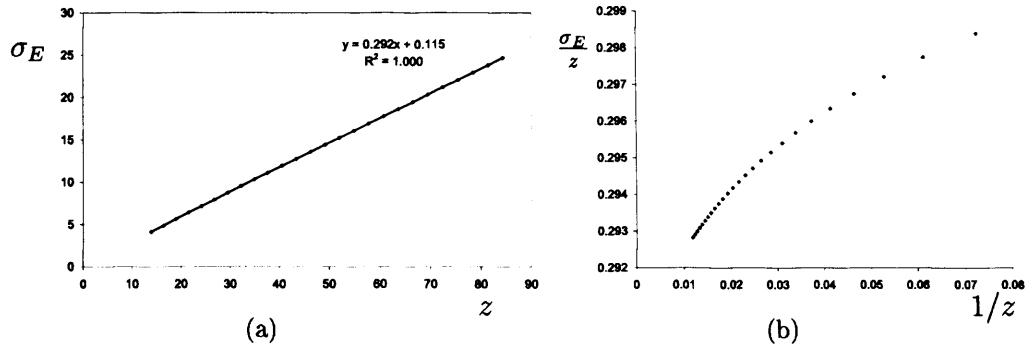

Figure 3.2: Scaling of σ_E in the 2d Ising Model: (a) σ as a function of $\sqrt{N \ln N}$ appears to show good linearity. (b) $\sigma/\sqrt{N \ln N}$ as a function of $1/\sqrt{N \ln N}$ highlights deviation from the predicted scaling. Note, $z = \sqrt{N \ln N}$ and the solid line in (a) is a least squares fit to the data.

But the specific heat is simply proportional to the variance of the energy distribution, and so

$$C = \frac{1}{NT^2}\left(\langle E^2 \rangle - \langle E \rangle^2\right) \tag{3.81}$$

$$= \frac{1}{NT^2}\sigma_E^2. \tag{3.82}$$

Therefore,

$$\sigma_E \sim \sqrt{NC} \tag{3.83}$$

$$\sim \sqrt{N \ln N} \tag{3.84}$$

Thus it is expected that the variance of the energy distribution will vary as $N \ln(N)$. Intuitively this seems reasonable given the weakness of the anomaly in the specific heat (one would not therefore expect strong deviations from normal behaviour). To test this hypothesis, exact values of σ are plotted against $\sqrt{N \ln N}$ in Figure 3.2(a), for L in the range 7–32. A least squares fit to the data is an almost perfect straight line with an R^2 value of 1.00, seeming to confirm the prediction. Plotting $\sigma/\sqrt{N \ln N}$ against $1/\sqrt{N \ln N}$ is a more sensitive way to treat the data, and allows for better

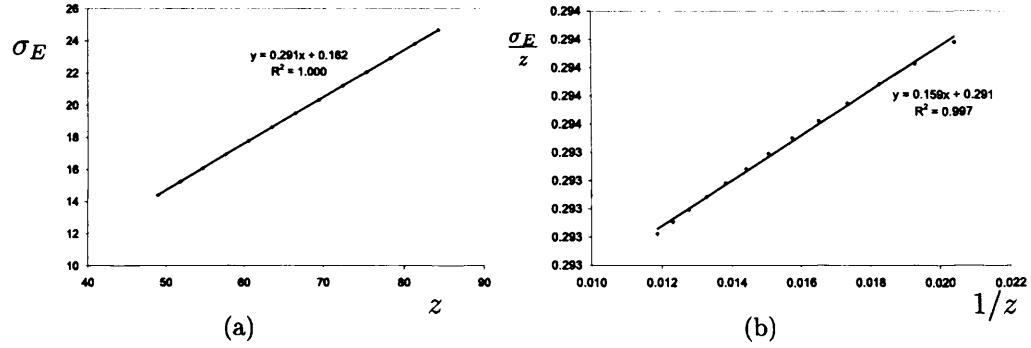

Figure 3.3: Scaling of σ_E, Neglecting Small N: As for Figure 3.2.2 but neglecting systems with $L < 20$. Again, $z = \sqrt{N \ln N}$ and the solid lines are a least squares fit to the data.

interpretation of the behaviour as N becomes large. This plot, shown in Figure 3.2(b), shows a noticeable deviation from linearity. This may be an indication that (3.84) is incorrect, or at least subject to significant corrections, however a major cause of the discrepancy is likely to be the fact that the scaling of T_c has been ignored. Thus, as L decreases, the evaluation of σ is taking place further and further from the effective critical temperature. In order to test the hypothesis exactly, one must therefore know the precise form of the finite size scaling of the temperature.

We suggest that, given the fact σ is known exactly, its dependence on N may be used to go backward and obtain an expression for $T_c(L)$, at least to a first approximation. The procedure is very simple and lacks a rigorous underpinning, however it is open to scrutiny via numerical simulation of other thermodynamic properties. Firstly, it is recognized that the finite size scaling arguments leading to (3.84) assume that L is reasonably large, whilst remaining finite. Thus for very small systems one expects f.s.s. to fail and it is reasonable to reject the values of σ arising from the smallest systems. As shown in Figure 3.3, this leads to a much greater linearity, with the expected relationships between the gradients and intercepts of the two graphs. A good working expression is thus obtained for the scaling of the standard deviation as a function of $\sqrt{N \ln N}$ which may be used to generate 'ideal' values for $\sigma(N)$ at the

appropriate critical temperatures, $T_c(L)$,

$$\sigma(N) \approx 0.29\sqrt{N \ln N} + 0.16. \tag{3.85}$$

Then one needs only to identify the temperature giving rise to the predicted value of $\sigma(N)$ for a range of system sizes, to enable the determination of the dependence of T_c on L. The results are plotted in Figure 3.4, where it is seen that, to a first approximation,

$$T_c(L) = 2.27 + 1.76L^{-1} + 12.7L^{-2}. \tag{3.86}$$

The accepted form of the scaling of T_c is $T_c(L) = T_c(\infty) + bL^{-1/\nu}$, with $T_c(\infty) = 2.269$ and $\nu = 1$ for the 2d Ising model [87]. Thus (3.86) deviates from general theory only by higher order corrections which diminish for large L, and predicts $b \approx 1.76$ for this model with periodic boundary conditions (implicit in the analysis in [96, 97]).

We note that this is by no means the first suggestion that Kaufman's solution could be used to investigate finite size scaling. In particular there is a detailed study by Ferdinand and Fisher [99] which gives a rigorous treatment of the specific heat in finite lattices. Our contribution is to suggest that the energy distribution could be used as a tool in this analysis. The only drawback to this claim is the large discrepancy between our approximate value of $b \approx 1.76$ and the undoubtedly more accurate value of $b \approx 0.68$ reported in [99]. The reasons for this remain unclear. Despite the fact that our study is at an early stage (see "Future Work", §7.1) and the approximations made are quite coarse, such a large error is still surprising.

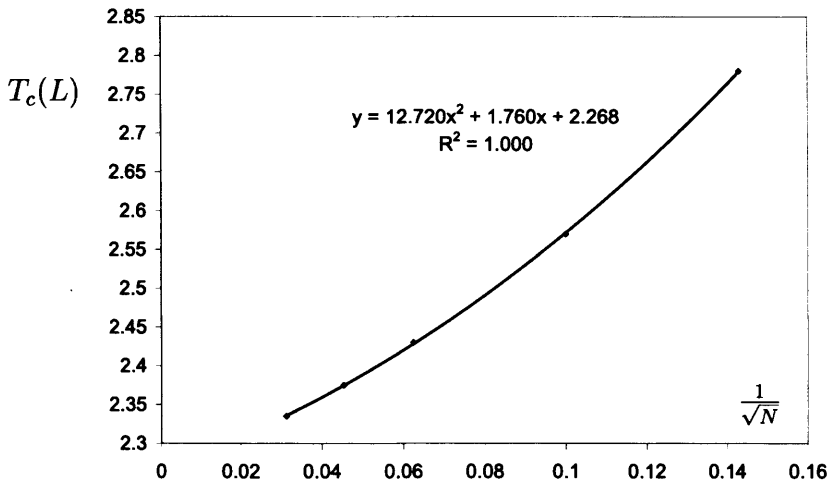

Figure 3.4: Scaling of T_c in the 2d Ising Model: The points represent the temperatures at which σ obeys (3.85) for each system size. The line is a least squares fit showing the quadratic nature of the data.

Chapter 4

Studies of the Two Dimensional XY Model

4.1 Introduction to the 2dXY Model

This chapter introduces and discusses various properties of the two-dimensional XY (2dXY) model of magnetism – a model ideally suited to the study of critical phenomena and fluctuating global quantities. Numerical simulations of critical behaviour are often complicated by finite size shifting of T_c, making it hard to know precisely what temperature to study. The 2dXY model avoids such difficulties as it is critical not at a single point, but over a continuous range of temperatures. Furthermore the model proves analytically tractable, the critical region being completely described by a Gaussian Hamiltonian.

4.1.1 Definition of the Model

The 2dXY model consists of classical spins, $\mathbf{S_r}$, of unit length, lying in the plane of a two dimensional lattice. In this work a square lattice of linear dimension L is used, such that the system size is $N = L^2$. The state of a given spin is then completely described by the angle, $\theta_\mathbf{r}$, that it makes with some arbitrary (but fixed) axis. In the

absence of any external magnetic field the model is defined by the Hamiltonian

$$H = -J \sum_{\langle \mathbf{r},\mathbf{r}' \rangle} \mathbf{S}_{\mathbf{r}}.\mathbf{S}_{\mathbf{r}'} = -J \sum_{\langle \mathbf{r},\mathbf{r}' \rangle} \cos(\theta_{\mathbf{r}} - \theta_{\mathbf{r}'}) \tag{4.1}$$

where the sum runs over all nearest neighbour pairs of spins and J is the ferromagnetic (therefore positive) exchange interaction. Unless otherwise stated the lattice parameter is taken to be $a = 1$.

4.1.2 Lack of Order in the 2dXY Model

A ferromagnet passing from its low temperature phase to a high temperature paramagnetic region is a paradigm of a continuous phase change, with a well defined critical point and associated critical exponents. However, the 2dXY model is unable to support long range order in the face of very low energy excitations, as expressed mathematically by the Mermin-Wagner theorem [100]. This theorem states that $d = 2$ is the 'lower critical dimension' (the highest dimension at or below which long range order is unsustainable) for systems with a continuous symmetry.

The ease with which order is destroyed can be understood by considering the effect of having continuous spins in a low dimensional systems. Even if neighbouring spins have tiny differences in their angular variables – corresponding to vanishingly small energies – it is clear that, in the thermodynamic limit, spins separated by large distances could be pointing in significantly different directions. This is shown schematically in Figure 4.1 which represents a 'spin wave'. It is the excitation of long wavelength (low energy) spin waves that accounts for the destruction of long range order. As the dimensionality is increased the greater number of neighbouring spins negates this effect and long range range order is sustainable.

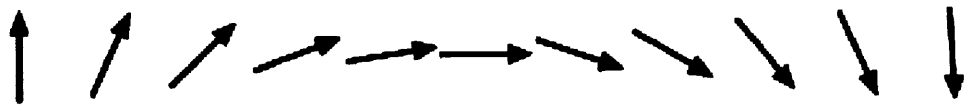

Figure 4.1: Part of a Spin Wave: The spins at the extremities are pointing in opposite directions, however each spin differs only slightly from its neighbours resulting in a minimal energy penalty.

4.2 Theoretical Treatments of the Infinite 2dXY Model

4.2.1 Vortices and the Kosterlitz-Thouless Transition

Numerical studies of the 2dXY model indicated the presence of a phase transition [101–103] and therefore appeared to contradict the Mermin-Wagner theorem [100]. This prompted Kosterlitz and Thouless to propose a new type of transition in which neither phase possesses traditional long range order [55]. They introduced the concept of 'topological long range order' as the absence of topological defects*. Their transition is from such an ordered state to a fully disordered phase in which topological defects occur; it is characterized by the different response of the system to external perturbations in the two phases.

Spin Vortices

The Kosterlitz-Thouless (KT) transition focuses on the role played by spin vortices. A vortex can be defined as a region of spins around which tracing some closed path results in a change in θ of $2n\pi$ where n is its strength or vorticity. Figure 4.2 represents a pair of vortices with $n = 1$ and $n = -1$. In the region immediately surrounding a vortex core it is clear that θ changes rapidly. However, as one moves further away,

*What constitutes a topological defect depends on the system. In crystals they are dislocations, in magnets they are spin vortices *etc.*

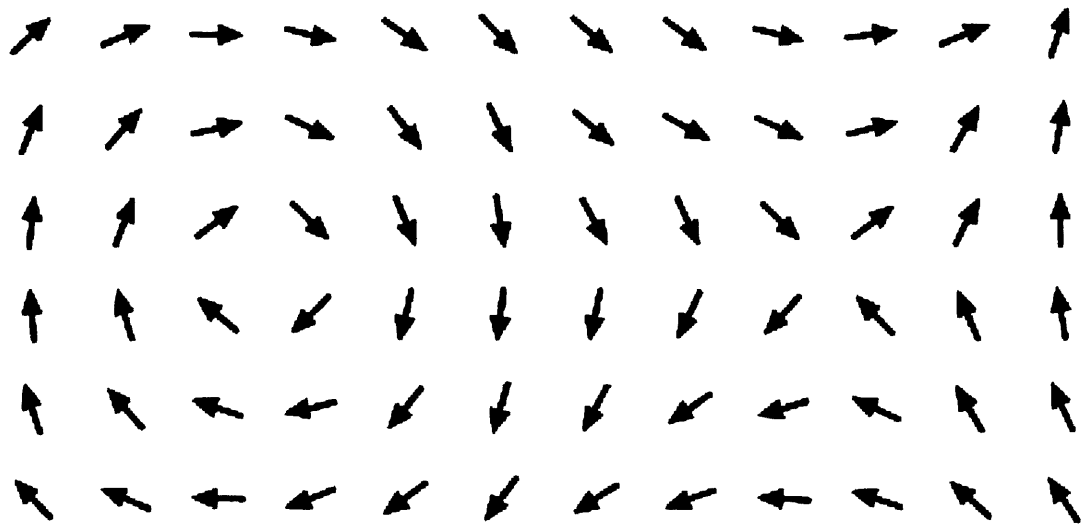

Figure 4.2: A Vortex Anti-Vortex Pair: These two vortices have equal and opposite vorticity (+1 on the left, -1 on the right). On their own each vortex is energetically unstable below the Kosterlitz-Thouless transition temperature, however they may occur as a bound pair.

neighbouring spins align more closely making only a small contribution to the energy.

The energy of an isolated vortex with $n = 1$ is

$$E_v = \pi J \ln L, \tag{4.2}$$

and so diverges logarithmically with system size. As the entropy associated with the introduction of the vortex diverges at the same rate,

$$S_v = 2 \ln L, \tag{4.3}$$

a temperature dependent balance exists between these two contributions to the free energy,

$$F_v = (\pi J - 2T) \ln L. \tag{4.4}$$

Therefore, in the thermodynamic limit, isolated vortices are excluded for all temperatures below the Kosterlitz-Thouless transition temperature, $T_{KT} = \pi/2$, resulting in

a topologically ordered 'phase'. At higher temperatures free vortices are energetically stabilized by their entropy and all order is lost.

It is the behaviour of vortices in response to an applied magnetic field that defines the KT transition. A vortex is a defect analogous to a dislocation in a crystal; thus the transition can be understood in the context of the dislocation theory of melting [104]. A liquid close to its melting point will have a structure similar to that of the crystalline solid, but with a number of dislocations. Application of a small shear stress will effect a viscous flow which brings the defects to the surface. In the solid state, where there are no dislocations at equilibrium, the response to an applied force is markedly different. A magnetic system with free vortices acts like the liquid phase; the vortices move to the surface on application of a small magnetic field. If there are no vortices present the response to the field (the susceptibility) will be of a different form, characteristic of the topologically ordered region. In this way a transition may exist between two magnetic 'phases' despite the fact that spin waves destroy long range order in both of them.

The Spin Wave – Vortex Model of Kosterlitz and Thouless

Thus the 2dXY model has two phases characterized by the form of the susceptibility and separated by the transition temperature T_{KT}. The low temperature phase has no isolated vortices but does have low energy excitations in the form of spin waves. The high temperature region has a mixture of vortices and spin waves, and is disordered in both the conventional and topological sense.

These observations were combined into a simplification of the 2dXY model which relies on two basic assumptions [55]. Firstly, at low temperatures, one expects neighbouring spins to have very similar values of θ. When this is true it is reasonable to expand the cosine in (4.1) and truncate the expansion at the quadratic term. This gives, leaving aside the constant,

$$H = \frac{J}{2} \sum_{\langle \mathbf{r},\mathbf{r}' \rangle} (\theta_{\mathbf{r}} - \theta_{\mathbf{r}'})^2 = \frac{J}{2} \sum_{\mathbf{r}} (\Delta\theta(\mathbf{r}))^2, \tag{4.5}$$

where Δ is the first difference operator and $\theta(\mathbf{r})$ is effectively a continuous field but

is strictly defined only at the lattice sites. The second assumption is that the field defined by the spin variables may be split into two terms, $\theta(\mathbf{r}) = \psi(\mathbf{r}) + \vartheta(\mathbf{r})$, where $\vartheta(\mathbf{r})$ represents spin configurations at local minima (corresponding to vortices), and $\psi(\mathbf{r})$ the spin wave deviations from these minima. From the definition of spin waves and vortices it is clear that

$$\oint \psi(\mathbf{r}) = 0 \qquad\qquad \oint \vartheta(\mathbf{r}) = 2n\pi, \tag{4.6}$$

where the sums are over all closed paths for $\psi(\mathbf{r})$ and at least some closed paths encircling the vortex core for $\vartheta(\mathbf{r})$.[†] The first of these constraints kills the cross term in the Hamiltonian, leaving

$$H = \frac{J}{2}\sum_{\mathbf{r}} (\Delta\psi(\mathbf{r}))^2 + \frac{J}{2}\sum_{\mathbf{r}} (\Delta\vartheta(\mathbf{r}))^2 . \tag{4.7}$$

So the problem is separable into two non-interacting systems, one corresponding to spin waves, the other to vortices.

Berezinskiĭ's Harmonic Spin Wave Model

The spin wave component arising from Kosterlitz and Thouless' work is relatively straightforward to solve analytically. In fact it corresponds exactly to Berezinskiĭ's Harmonic model [56], defined by a Hamiltonian which he proposed completely captured 2dXY behaviour at low temperatures,

$$H - E_0 = \frac{J}{2}\sum_{\langle \mathbf{r},\mathbf{r}' \rangle} (\theta_{\mathbf{r}} - \theta_{\mathbf{r}'})^2, \tag{4.8}$$

where $E_0 = 2JN$ is the energy of the ground state.

The beauty of the Harmonic model lies in the fact that its quadratic nature leads to Gaussian Boltzmann factors and a reciprocal space Hamiltonian that is diagonalized into independent normal modes. By introducing a field term, Berezinskiĭ was able to express the free energy as

$$\frac{F - E_0}{N} = \frac{T}{2}\ln\frac{2\pi}{T} - h + \frac{T}{2}\int \mathrm{d}\mathbf{q}\,\ln(J\Delta(\mathbf{q}) + h), \tag{4.9}$$

[†]Not all paths around the core of a vortex result in a change in θ of $2n\pi$. Consider Figure 4.2 – a path encircling both the vortices leaves θ unchanged. Thus (4.6) is valid only for paths enclosing a region of total vorticity n.

where Δ is a discretized version of the Laplace operator in reciprocal space.

The behaviour of Δ is extremely important and leads to one of the more subtle aspects of the theoretical development of the model. The study of Brownian motion on a d dimensional infinite discrete lattice provides the definition of a Green's function for that lattice,

$$G(\mathbf{r}) = \int \frac{\mathrm{d}^d\mathbf{q}}{(2\pi)^d} \frac{e^{i\mathbf{q}\cdot\mathbf{r}}}{1 - \frac{1}{d}\sum_\mu \cos q_\mu}. \tag{4.10}$$

Here μ is an index for the possible dimensions and q_μ is therefore the component of the wavevector $\mathbf{q}$ in dimension μ. The Green's function is, in this context, a measure of the average amount of time spent at a given lattice site and may also be defined as

$$G(\mathbf{r}) = -\Delta_{\mathbf{r}}^{-1} \tag{4.11}$$

where the real space first difference operator is defined, for some function $f(\mathbf{x})$, as

$$\Delta_{\mathbf{r}} f(\mathbf{x}) = \frac{1}{2d}\sum_{\mu}^{d} \left[f(\mathbf{x}+\mathbf{a}_\mu) + f(\mathbf{x}-\mathbf{a}_\mu) - 2f(\mathbf{x})\right], \tag{4.12}$$

with $\mathbf{a}_\mu$ being the primitive lattice vectors. This analysis translates directly into the language of field theory where $G(\mathbf{r})$ becomes a propagator of a Euclidean free field $\theta(\mathbf{r})$, and

$$G(\mathbf{r}) = \frac{J}{T}\left\langle \theta_{\mathbf{r}}\theta_{\mathbf{r}'}\right\rangle. \tag{4.13}$$

Berezinskiĭ [56] recognized a problem with applying this relation to the Harmonic model. In the field theoretical definition the field must be freely varying between $\pm\infty$. Indeed this must be true as one can see from (4.10) that the propagator diverges logarithmically for $d = 2$, which is only possible (from (4.13)) when the variables $\theta_{\mathbf{r}}$ are unconstrained. However, implicit in the definition of the the magnetic spin variables is their periodicity, with $-\pi \leq \theta_{\mathbf{r}} < \pi$. Imposing this range on the 'field' kills the divergence of Green's function. It was decided therefore to relax the bounds allowing the spins to be infinitely variable. Given that the Harmonic model was only designed to be applicable in the region of the global minimum at low temperatures, this is a reasonable approximation.

The two-spin correlation function for the Harmonic model has a power law behaviour [56],

$$g(\mathbf{r}) = \left\langle \mathbf{S}_0.\mathbf{S}_\mathbf{r} \right\rangle \tag{4.14}$$

$$= |\mathbf{r}|^{-T/2\pi J} \tag{4.15}$$

where the divergence leads to an infinite susceptibility per spin [57],

$$\chi \sim \int g(\mathbf{r})\, \mathbf{dr} \tag{4.16}$$

$$= \infty. \tag{4.17}$$

Such behaviour is unusual as the susceptibility remains infinite at all temperatures, not at an isolated critical point. This is the first evidence of a line of critical points with a temperature dependent exponent $\eta(T)$, and is a defining characteristic of the low temperature region of Kosterlitz and Thouless.

Interacting Vortices

Kosterlitz and Thouless realised that tightly bound vortex-antivortex pairs have finite energy and so are not excluded from the 'ordered' phase. Thus the phase transition does not see the creation of new defects, but is rather a manifestation of the unbinding of pairs of defects already present. In this revised picture one must take into account the interaction between vortices, particularly the relaxation of bound pairs in the field of a larger pair as it separates.

The vortex problem was mapped onto a model of a two dimensional Coulomb gas which was solved using an iterated mean field approach [55]. In the low temperature phase the total vorticity is required to be zero and the infinite susceptibility of the Harmonic model is observed. Inclusion of vortex interactions results in a lowering of the transition temperature, and the spin-spin correlation function vanishes discontinuously at T_{KT}.

Greater weight was given to these findings with the more detailed renormalization approach taken by Kosterlitz in 1974 [57]. The renormalization procedure is

clearly explained by Cardy [12] on the basis of a Gaussian model modified to include a contribution from vortices, associated with a scaling operator y. The scaling dimension of a single isolated vortex is $x_V = \pi K$ (where K is the inverse temperature or spin wave stiffness) and so the renormalization group eigenvalue for the vortex is $y_V = 2 - \pi K$ which is relevant only for temperatures above $T = \pi/2$. In addition, the presence of bound pairs of vortices in the low temperature region is confirmed. These pairs are integrated out by the coarse graining effect of renormalization, and the RG trajectories flow, at low temperatures, toward Gaussian fixed points.

What constitutes 'low temperatures' in this context depends on the energy of the vortex core, C, which controls the initial value of the expansion parameter $y = y_0 e^{-\pi KC}$, where y_0 is the vortex fugacity. For a given value of y there is a temperature $T \leq \pi/2$ below which RG flows are toward the Gaussian fixed points. Above this value the flows are toward a high temperature fixed point controlling the truly paramagnetic region. The renormalization flows are labelled by the parameter K_{eff}, the effective value of the reciprocal temperature at the fixed point controlling the flow. Thus $T_{\text{eff}} = 1/K_{\text{eff}}$ is the renormalized temperature for a system with no vortices – i.e. the Harmonic model. So the RG analysis provides a link between the vortex/spin wave model at temperature T and the Harmonic model at T_{eff}. Starting at $K_{\text{eff}} = 2/\pi$ the vortices renormalize in a self-similar manner giving rise to a universal exponent $\eta = 1/4$. The ordered phase with $K_{\text{eff}} > 2/\pi$ is completely described by the Harmonic model, with $\eta(T) = 1/4\pi K_{\text{eff}}$ being temperature dependent. A schematic diagram of the RG flows is shown in Figure 4.3.

The parameter y is a function of the temperature T. Thus at some point the function $y(T)$ coincides with the trajectory $K_{\text{eff}} = \pi/2$. It is this temperature that will be referred to as T_{KT} as it corresponds to the point at which isolated vortices become energetically viable. K_{eff} jumps discontinuously to zero at this point [105].

Renormalization of the harmonic component is slightly complicated by the periodicity of the spin variables. This prevents simple rescaling of θ so that $K = 1$ as would normally be the case. Instead, K is an exactly marginal variable and so corresponds to a line of fixed points [12]. The result is precisely as predicted by spin

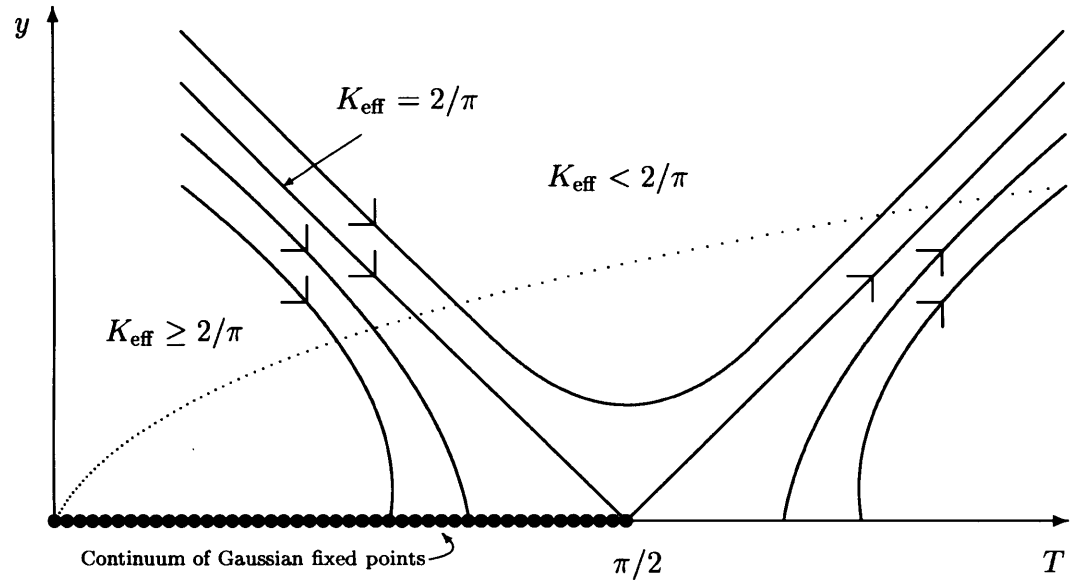

Figure 4.3: Schematic Renormalization Group Trajectories for the Kosterlitz-Thouless Approximation to the 2dXY Model: The trajectories are labelled according to the effective inverse temperature after all vortices have been renormalized out (corresponding to $y = 0$). For $K_{\text{eff}} \geq 2/\pi$ the flows are toward a line of Gaussian fixed points. For higher temperatures y increases under renormalization and free vortices emerge. The dotted line represents the behaviour of the expansion parameter $y(T)$ for a particular value of C.

wave analysis, except the inclusion of vortices terminates the line of critical points at T_{KT}.

As well as confirming the mean field and spin wave results, the RG analysis yields information regarding the correlation length,

$$\xi \sim \exp(b\tau^{-1/2}) \qquad \tau > 0 \tag{4.18}$$

$$\sim \infty \qquad \tau < 0 \tag{4.19}$$

which diverges faster than any power of $\tau = (T - T_{KT})/T_{KT}$ making the exponents ν and γ undefined for the 2dXY model. The infinite correlation and infinite susceptibility are the defining characteristics of the critical low temperature phase.

The Villain Model

The mapping of vortices onto a Coulomb gas and the expansion of the cosine interaction in the Hamiltonian both make the qualitative assumption of low temperature. There is no clear evidence that these approximations are appropriate in the region of the Kosterlitz-Thouless transition, as discussed by Villain in 1975 [58]. He proposed a new model in which the cosine interaction of equation (4.1) is replaced by another function altogether, rather than a simplification of the cosine form. This new potential,

$$V_{\mathbf{r}\mathbf{r}'}(\theta) = \frac{1}{2}T \ln \left\{ \sum_{n=-\infty}^{\infty} \exp\left(-\frac{J}{T}A_{\mathbf{r}\mathbf{r}'}\,(\theta - 2\pi n)^2\right)\right\}, \tag{4.20}$$

maintains the full symmetry properties of the 2dXY model yet corresponds to a Hamiltonian which may be expressed exactly in quadratic form,

$$H = \frac{1}{2}\sum_{\langle \mathbf{r},\mathbf{r}'\rangle} A_{\mathbf{r}\mathbf{r}'}(\theta_{\mathbf{r}} - \theta_{\mathbf{r}'} - 2\pi n_{\mathbf{r}\mathbf{r}'})^2, \tag{4.21}$$

where $A_{\mathbf{r}\mathbf{r}'}$ is a function of J and T. The Fourier transformed Hamiltonian then consists of two non-interacting parts which are seen to correspond to the spin wave and vortex contributions discussed above. The vortices arise as a result of the variables $n_{\mathbf{r}\mathbf{r}'}$ which have no strict physical interpretation, but may be thought of as relating the number of times $\theta_{\mathbf{r}}$ and $\theta_{\mathbf{r}'}$ have been 'wound'. In this model the spin variables are

once again constrained to be in the range $\pm\pi$ with the divergence of the correlation function being managed by $n_{\mathbf{r}\mathbf{r}'}$.

Villain acknowledged that the similarity between his Hamiltonian and that of the full 2dXY model was not self-evident, however he was able to make a good case for the rigorous equivalence of the two models, as well as re-deriving the results of Kosterlitz and Thouless. A later renormalization group treatment of the Villain model [59] yielded the same scaling functions as those derived by Kosterlitz, with $T_{KT} \approx 1.351$ in excellent agreement with numerical results [106].

4.3 Pseudo Ordering in Finite Size Systems – The Physical Relevance of the 2dXY Model

The scalar instantaneous magnetization per spin (or simply the 'magnetization'),

$$m = \frac{1}{N}\sqrt{\left(\sum_{\mathbf{r}} \mathbf{S}_{\mathbf{r}}\right)^2}, \tag{4.22}$$

is the usual choice of order parameter for ferromagnetic systems. As this quantity depends on the sum over the spin variables, its average is zero in the paramagnetic phase and finite only when there is ferromagnetic ordering. In the 2dXY model, the destruction of long range order by low energy spin waves means that $\langle m \rangle$ goes to zero in the thermodynamic limit for all finite T [100]. However, the manner in which this limit is approached is of great physical significance [31, 32].

Taking a large, but finite, system and applying periodic boundary conditions leads to a reciprocal space Hamiltonian of the form (note detailed derivations of all the equations in this section may be found in Appendix C)

$$H = \frac{J}{2}\sum_{\mathbf{q}\neq 0} \gamma_{\mathbf{q}} |\varphi_{\mathbf{q}}|^2, \tag{4.23}$$

where, $\varphi_{\mathbf{q}}$ is the Fourier transform of the spin variable $\theta_{\mathbf{r}}$, and in two dimensions, $\gamma_{\mathbf{q}}$ is defined in terms of the orthonormal components of the wavevector $\mathbf{q}$ as,

$$\gamma_{\mathbf{q}} = 4 - 2\cos q_x - 2\cos q_y. \tag{4.24}$$

It is convenient to move to a reference frame in which the Goldstone (zero frequency) mode is excluded. This is achieved by defining a new variable, $\psi_{\mathbf{q}} = \theta_{\mathbf{r}} - \overline{\theta}$, where $\overline{\theta}$ is the instantaneous magnetization direction [16],

$$\overline{\theta} = \tan^{-1}\left(\frac{\sum_{\mathbf{r}} \sin\theta_{\mathbf{r}}}{\sum_{\mathbf{r}} \cos\theta_{\mathbf{r}}}\right). \tag{4.25}$$

An alternative definition of the magnetization is

$$m = \frac{1}{N}\sum_{\mathbf{r}} \cos\psi_{\mathbf{r}}, \tag{4.26}$$

which differs only slightly from (4.22) with the corrections disappearing for large N. This makes the analysis tractable and yields

$$\langle m\rangle = \left(\frac{1}{CN}\right)^{\frac{T}{8\pi J}}, \tag{4.27}$$

where $C \approx 1.8456$ [6]. The spin-spin correlation function is therefore

$$g(\mathbf{r}) = \langle m\rangle^2 \exp\left(\frac{T}{J}G(\mathbf{r})\right), \tag{4.28}$$

and the susceptibility

$$\chi = \frac{\langle m\rangle^2}{T}\sum_{\mathbf{r}}\left[\exp\left(\frac{T}{J}G(\mathbf{r})\right) - 1\right]. \tag{4.29}$$

Using equation (4.27) it can be shown that $\langle m\rangle$ decreases so slowly with system size that its thermodynamic limit is experimentally inaccessible, with a magnet the size of Texas retaining a measurable finite value [31, 107]! This result indicates that although the thermodynamic limit is essential to classify the macroscopic behaviour, it may be too extreme an approximation to capture the detailed behaviour of real systems. In this way, m may be considered as a pseudo order parameter arising directly as result of finite size.

Interest in the behaviour of finite 2dXY magnets began in earnest with a renormalization group treatment modified to account for finite size scaling [31]. Given the critical nature of the low temperature region, and the absence of long range order, the exponent β is undefined in the thermodynamic limit. However, for a finite system, there is a region slightly above T_{KT} where an effective β is seen to exist and the magnetization varies with T as a power law.

For a finite system the effective spin wave stiffness does not have a discontinuous jump at T_{KT} but rather goes smoothly, albeit steeply, to zero. The temperature above which $K_{\text{eff}} = 0$ is essentially the Curie temperature, $T_C = T_c$. This is defined in the usual manner as the point at which the correlation length becomes equal to the linear dimension, $\xi = L$. A second relevant characteristic temperature is T^*, defined such that $K_{\text{eff}}(T^*(L)) = 2/\pi$. RG analysis shows that both T_C and T^* are shifted values of T_{KT} with a logarithmic dependence on L,

$$T^*(L) = T_{KT} + \frac{\pi^2}{4c(\ln L)^2} \tag{4.30}$$

$$T_C(L) = T_{KT} + \frac{\pi^2}{c(\ln L)^2}. \tag{4.31}$$

Thus for an infinite system the two temperatures converge on T_{KT} accounting for the jump in K_{eff}.

Empirical observations in layered magnets [31] and thin films [108] show that the excitation of vortices slightly above T_{KT} lead to a deviation of $\langle m \rangle$ from the form predicted by spin wave theory. Instead the magnetization is well described by a power law with a universal exponent $\beta \approx 0.23$, the best fit occurring at T^*. Furthermore the power law behaviour was observed over a range of temperatures, not just asymptotically close to T_C, explaining numerical and practical observations of critical behaviour well below the Curie point.

The power law behaviour can be seen analytically if T_{eff} replaces T in the magnetization expression (4.27). This is valid when the spin wave stiffness varies little with wavelength, as is the case at T^* [32]. Defining

$$\beta = \frac{\partial \ln m(L,T)}{\partial \ln t}, \tag{4.32}$$

where $t = T_C - T$, it is seen that $\beta(L, T^*) = 3\pi^2/128 = 0.231\ldots$ which is a universal value. Indeed T^* may be regarded as a universal point where it is seen that the magnetization scales with size, field and temperature [32].

It is clear that only finite 2dXY systems are of any physical relevance. There can be no physical manifestation of the infinite systems which have been the focus

of the bulk of theoretical work. The effective β has been measured for a number of layered Heisenberg magnets with planar anisotropy, which may be considered as quasi-2dXY systems [31]. Many of the compounds studied (covering a range of spin values and lattice types) had the predicted value $\beta = 0.23$. For other systems there were small deviations with the exponent in the range $0.18 \leq \beta \leq 0.26$. The theoretical predictions of T^* and T_c have also been confirmed [32, 109].

A later paper by Elmers *et al.*, looking at the critical behaviour of an ultra-thin layer of Fe(100) on W(100), is even more emphatic. This epitaxial system has been shown to be unequivocally two dimensional. The magnetization was seen to obey a power law with $\beta = 0.22 \pm 0.01$, achieving much greater accuracy than previous studies. Perhaps most significantly, the first analysis of the critical susceptibility for this class of system was also reported. Close to T_C the susceptibility was extremely large. Above $1.02T_C$ it was seen to diverge as $\chi \propto \exp(b\tau^{-0.5})$ with $b = 1.6 \pm 0.1$. This is of the same order of magnitude as predicted by Kosterlitz, $b \approx 2.6$.

4.3.1 Magnetization Distributions in the Harmonic XY Model: The Universal Nature of the Critical Region

Prompted by the interesting behaviour and physical relevance of the finite magnetization, numerical studies were performed with a view to determining the distribution function, $P(m)$ [16]. Given that m is a global variable, depending on microscopic contributions from all spins, one would generally expect it to be normally distributed, as a result of the central limit theorem (CLT). At a critical point, however, the infinite correlation length leads to a breakdown of the CLT and non-Gaussian fluctuations may be observed. Thus non-Gaussian behaviour is expected to be possible throughout the low temperature region of the 2dXY model.

Finite size scaling predicts that the magnetization should scale as $\langle m \rangle \sim L^{-\beta/\nu}$ (see §2.1.7). Therefore, whilst β and ν are undefined, their ratio is well behaved and is given by spin wave theory as [57]

$$\frac{\beta}{\nu} = \frac{T}{4\pi J} \tag{4.33}$$

The temperature dependence of this ratio implies that the fixed points governing the spin wave region belong to different universality classes. Thus, not only can $P(m)$ be non-Gaussian below T_{KT}, but there is nothing to suggest that it should adopt the same functional form at each critical point.

The model studied in [16] was a simplified version of that put forward by Villain [58], called the Harmonic XY (HXY) model. The Hamiltonian is,

$$H = \frac{J}{2} \sum_{\langle \mathbf{r},\mathbf{r}' \rangle} (\theta_{\mathbf{r}} - \theta_{\mathbf{r}'} - 2\pi n)^2 \tag{4.34}$$

where the thermodynamic 'vortex variables' used by Villain have been replaced by integers, $n = 0, \pm 1$, such that $(\theta_{\mathbf{r}} - \theta_{\mathbf{r}'} - 2n\pi)$ remains bounded by $\pm\pi$.

This Hamiltonian requires some discussion. The implication of the definition of the n variables is that the $\theta_{\mathbf{r}}$ are restricted to between $\pm\pi$ in the same way as in the original 2dXY model. This ignores the divergence of $G(\mathbf{r})$ discussed by Berezinskiĭ which is not dealt with by the restricted n parameter as in the Villain model. However, if n is allowed to vary freely whilst keeping the θ variables constrained, the effect of the periodicity is lost and the model reduces to a simple spin wave system [59]. Allowing $n = \pm 1$ permits vortices to enter the system but not with arbitrarily high vorticity. This is an extremely effective approximation (see §4.5.2 for a comparison between simulations of the 2dXY and HXY models) as renormalization shows that below T_{KT} vortices with $|n| > 1$ are irrelevant. At higher temperatures the approximation remains valid only when evaluating periodic functions of the spin variables.

Somewhat surprisingly the simulations [16] clearly showed a non-Gaussian distribution of the magnetization which was, without fitting, the same for all temperatures up to the point at which vortex pair unbinding becomes an issue (Figure 4.4(a)). This remarkable observation suggested that $P(m)$ was universal in a way that transcends the boundaries between universality classes. In addition, it was subsequently realised that this PDF, termed the BHP distribution, is of a very similar form to that describing fluctuations of power consumption in closed turbulent flow [19] (Figure 4.4(b)). Three dimensional turbulence and two dimensional magnets in equilibrium appear to have relatively little in common. What was clear, however, was that both systems

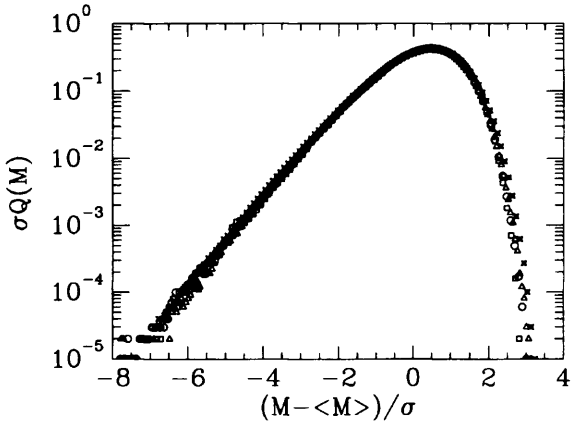

(a)

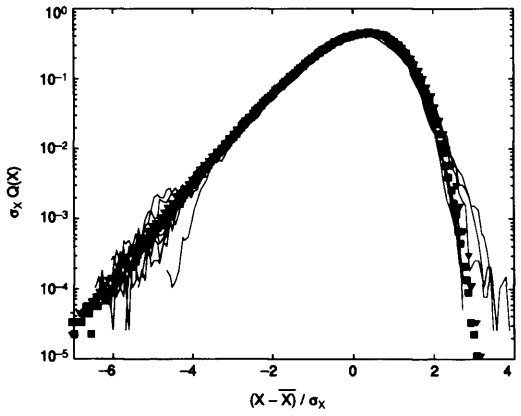

(b)

Figure 4.4: Demonstrating the Apparent Universality of the BHP Distribution: Part (a) shows the magnetization distribution from Monte Carlo simulations [16] of the Harmonic XY model at $T/J = 0.5$, for $N = 100$ (stars), $N = 1024$ (circles), $N = 10000$ (squares), and for $T/J = 1.0$ for $N = 1024$ (triangles). Part (b) shows a direct comparison (without fitting) between the power distribution in a closed turbulent flow and the magnetization distribution in the 2dXY model (from [19]). The turbulence measurements (lines) are for rotation rates Ω of 25, 30, 35, 40 and 45Hz where Ω is proportional to the Reynolds number of the flow. The magnetization results are taken at $T/J = 0.5$, for $N = 100$ (circles), $N = 1024$ (stars), $N = 10000$ (triangles), and for $T/J = 1.0$ for $N = 1024$ (squares). The variable X is the power or magnetization as appropriate. Parts (a) and (b) are both plotted on semi-log axes to highlight the behaviour in the wings of the distributions. Note that $Q(X)$ is simply the distribution function called $P(X)$ in this work. Taken from Bramwell *et al.*, *Nature* **396**, 552 (1998).

are, in a sense, critical. The criticality of the low temperature HXY model has been explained in terms of the divergent susceptibility and infinite correlation length. The idea of the turbulent system being critical comes from its inherent self-similarity, with eddies on all scales, from the dissipation length to the chamber size, being significant. Put simply, the characteristic shared by the two systems is scale invariance with a finite size cut off. The magnet is constrained by the length L, while for the turbulent flow the size of the apparatus prevents the system from reaching the limit of infinite Reynold's number.

It was proposed that this link provided an explanation for the similarity of the two distribution functions. The CLT results in the Gaussian distribution describing many disparate quantities, but links them together via the concepts of mesoscopic independence and individual negligibility of microscopic components (see §2.2.4). Why then should not critical systems have a similar distribution, characteristic of their scale invariance and high degree of correlation? In other words is it not reasonable to infer the existence of an alternative set of universal limit functions for cases when the CLT fails? This is the implication of the work of Bramwell *et al.* [19] who suggested that the spin wave limit of the 2dXY model may describe, to a good approximation, non-Gaussian critical behaviour for a number of universality classes.

In order to test this hypothesis, numerical simulations were performed on many critical and self-organized critical (SOC) systems. These included order parameter fluctuations in the two-dimensional Ising and percolation models, as well as fluctuations of global quantities in models of forest fires and avalanches in SOC states [21]. The distribution functions obtained in each case were good fits to the BHP form in confirmation of the proposition in [19]. A cautionary note in [6] warns against the conclusion that the distributions for all these systems are analytically the same. The more likely justification for the results is that many universality classes share common features which account for the functional form of the PDF, with differences either appearing outside the range of observation or being masked by experimental error.

4.3.2 Normalization of the Order Parameter

Calculations of $P(m)$ make use of the thermodynamic limit, in contrast to simulations which are necessarily performed on finite systems. In order to avoid spurious results with $P(m)$ having either zero or infinite width, normalization of the order parameter must render the distribution of the normalized quantity independent of N [6, 16]. This is discussed more generally in §2.2.5; for magnetic systems the distribution has been suggested to scale as [14]

$$P(m, L) \sim L^{\beta/\nu} P_L(mL^{\beta/\nu}, \xi/L). \tag{4.35}$$

In finite critical systems the correlation length is constrained by the finite size, fixing the ratio of ξ/L. This reduces (4.35) to a function of a single variable and rescaling $m \to mL^{-\beta/\nu}$ produces a PDF which is independent of the size of the system.

The spin wave expression for the susceptibility is [16] (see also Appendix C)

$$\chi = \frac{\langle m \rangle^2}{T} \sum_{\mathbf{r}} \left[\exp\left(\frac{T}{J} G(\mathbf{r}) \right) - 1 \right] \tag{4.36}$$

$$= \frac{N}{T} \left(\langle m^2 \rangle - \langle m \rangle^2 \right) \tag{4.37}$$

$$= \frac{N}{T} \sigma^2, \tag{4.38}$$

where σ is the standard deviation of the magnetization. If the exponential is expanded and truncated at the quadratic term,

$$\chi \simeq \frac{T \langle m^2 \rangle}{2J^2} \sum_{\mathbf{r}} G(\mathbf{r})^2 \tag{4.39}$$

$$\simeq \frac{NT \langle m^2 \rangle}{2J^2} g_2 \tag{4.40}$$

where (4.40) follows from (4.13) and g_2 is as defined in §4.4.1, having a value of approximately $1/259$ in two dimensions. On this basis the susceptibility diverges as $\chi \sim N^{1-T/4\pi J}$ such that $\sigma \sim N^{-T/8\pi J}$. This yields the important result that the average value of the magnetization scales with N in the same way as the standard deviation,

$$\frac{\sigma}{\langle m \rangle} \sim \mathcal{O}(1). \tag{4.41}$$

Equation (4.41) is a demonstration of the hyperscaling relation $d\nu = \gamma + 2\beta$, as finite size scaling requires

$$\frac{\sigma}{\langle m \rangle} \sim L^{(\gamma - d\nu + 2\beta)/2\nu}. \tag{4.42}$$

To obtain a well behaved distribution function in the thermodynamic limit, one must therefore normalize the variate to the standard deviation [6, 16, 19]. This result is quite general (indeed the CLT strictly applies to the normalized variate X/σ_X[90]), and is confirmed by equations (4.33), (4.35) and (4.41). In this work, following [16] and [6], the distribution is also shifted with respect to the mean giving the PDF

$$\Pi(z) = \sigma P(m) \tag{4.43}$$

where

$$z = \frac{m - \langle m \rangle}{\sigma} \tag{4.44}$$

As discussed in Chapter 1, it is not simply that the ratio in (4.41) is constant that is important, but the fact this ratio is numerically very small. This prevents the magnetization feeling its physical boundaries and m behaves, to an excellent approximation, as a one dimensional quantity.

4.4 The Question of Temperature Independence

This section introduces new work concerning the observed temperature independence of the magnetization distribution. Following the surprising numerical indications of a temperature independent $P(m)$, and spurred on by the relevance of the BHP form to a wide range of highly correlated systems, an attempt was made to derive an analytical expression for the function [6, 21]. The first moment, $\langle m \rangle$, may be derived from spin wave theory. In [6] this calculation is extended providing a general expression for $\langle m^p \rangle$ which was used to construct a size and temperature independent integral expression for the distribution. In the following discussion this derivation is re-examined in detail, with particular emphasis placed on certain assumptions that were made regarding the effect of taking the thermodynamic limit. Terms previously thought to be negligible are shown to make a significant and, crucially, temperature dependent, contribution

to the moments. The effect this has on the scaling function is considered with the conclusion that the dependence on the sole, temperature dependent, critical exponent, η, is very weak. In fact it is so weak that it has little visible effect on the distribution function which remains *apparently* universal until vortex corrections become relevant [27].

4.4.1 Evaluation of the Constants g_k

For reasons that will become apparent, it is useful to define a set of constants

$$g_k = \frac{1}{N^k} \sum_{\mathbf{q}\neq 0} \left(\frac{1}{\gamma_\mathbf{q}}\right)^k . \tag{4.45}$$

The first of the set, g_1, has already been useful (in the guise of $G(0)$, equation (4.13)) in defining $\langle m \rangle$ where it was claimed to diverge logarithmically. This can be seen by taking the continuum limit and converting the sum to an integral over the first Brillouin zone (BZ),

$$g_1 = \frac{1}{N} \sum_{\mathbf{q}\neq 0} \frac{1}{\gamma_\mathbf{q}} \tag{4.46}$$

$$\overset{N\to\infty}{=} \frac{1}{(2\pi)^d} \int_{\mathrm{BZ}} \frac{\mathrm{d}^d\mathbf{q}}{\gamma_\mathbf{q}} . \tag{4.47}$$

As the sum is dominated by contributions with small $|\mathbf{q}|$, the cosine terms in $\gamma_\mathbf{q}$ may be expanded and truncated in the normal way, approximating $\gamma_\mathbf{q} \approx q_x^2 + q_y^2$. To proceed further requires conversion to polar coordinates and, ignoring the geometry of the Brillouin zone, that the integral be performed over a circle. This last move seems, at best, questionable, however it is justified *a posteriori* by the numerical accuracy of the value of g_1, accuracy that benefits from the flexibility of the integral limits.

$$g_1 = \frac{1}{4\pi^2} \int_0^{2\pi} \int_{r_{\min}}^{r_{\max}} \frac{\mathrm{d}r\,\mathrm{d}\theta}{r} \tag{4.48}$$

$$= \frac{1}{2\pi} \ln\left(\frac{r_{\max}}{r_{\min}}\right) \tag{4.49}$$

This leaves the question how best to choose the limits of r. The Brillouin zone is split into blocks of area $(2\pi/L)^2$ centred at coordinates $(2x\pi/L, 2y\pi/L)$, where x and

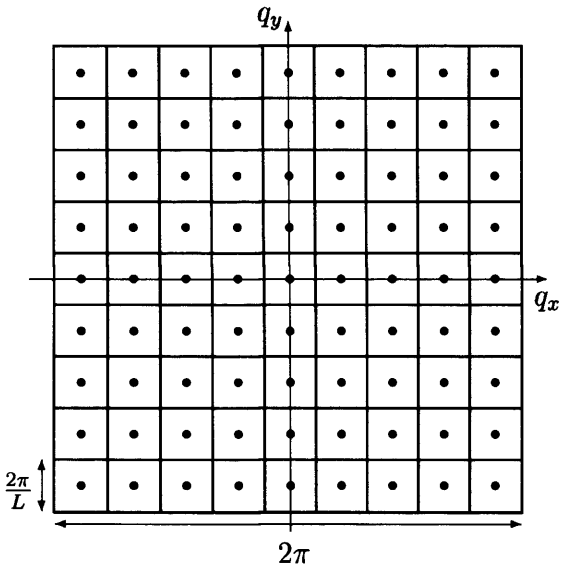

Figure 4.5: The First Brillouin Zone for a Two Dimensional Square Lattice with $N = 81$ spins: The integer parameters x and y have the range $\pm(L-1)/2$ which is ± 4 for this lattice. The area is $4\pi^2$ regardless of the system size; each reciprocal space cell occupies an area of $(2\pi/L)^2$.

y take integer values in the range $-(L-1)/2 \rightarrow (L-1)/2$, as in Figure 4.5 (it is easiest to consider systems where L is odd).

Setting the upper limit to $\pi\sqrt{2}$ and the lower limit to π/L represents the best circular approximation such that no values of $\mathbf{q}$ allowed in the sum are excluded from the integral. The result is that the shaded regions in Figure 4 5 are erroneously counted. This leads to

$$g_1 = \frac{1}{2\pi} \ln \frac{\pi\sqrt{2}}{\pi/L} \tag{4.50}$$

$$= \frac{1}{4\pi} \ln (2N), \tag{4.51}$$

which, until recently, was the generally accepted result [16, 110]. Appendix C of [6] presents a much more rigorous analytical treatment, concluding that the logarithmic divergence goes as $\ln(CN)$ with $C \approx 1.8456$ rather than 2 as previously thought.

For $k > 1$ the sum over $\mathbf{q}$, which may be viewed as a double summation over x and y, must be simplified. In order to avoid $\mathbf{q} = 0$ the sums run from 1, contributions from the axes being reintroduced by means of a second sum corresponding to a one

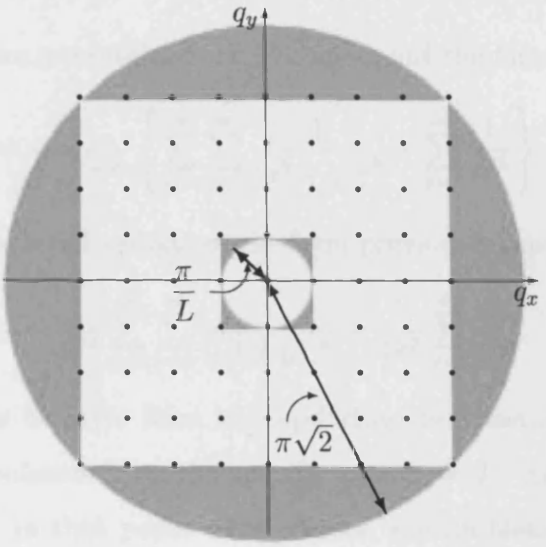

Figure 4.6: Integration Over the First Brillouin Zone: This figure shows the effect of integrating over a circular region rather than the square Brillouin zone. Taking limits such that no possible $\mathbf{q}$ vectors are excluded results in the unwanted inclusion of the shaded areas.

dimensional system (note $\gamma_{\mathbf{q}}^{d=1} = (2 - 2\cos\mathbf{q})$, where $\mathbf{q}$ is now a one dimensional vector, see Appendix C). Both terms are multiplied by 4 to account for the symmetrically equivalent quadrants of the BZ. The upper limits on the sums are simply $Q = (L-1)/2$.

$$g_k = \frac{4}{N^k}\sum_{x=1}^{Q}\sum_{y=1}^{Q}\frac{1}{\left(4 - 2\cos\left(\frac{2\pi x}{L}\right) - 2\cos\left(\frac{2\pi y}{L}\right)\right)^k} + \frac{4}{N^k}\sum_{x=1}^{Q}\frac{1}{\left(2 - 2\cos\left(\frac{2\pi x}{L}\right)\right)^k} \quad (4.52)$$

Replacing the cosine terms by their power series, the constants cancel and, letting $N \to \infty$, the denominator in the first term in (4.52) takes the form

$$\left(\sum_{i=1}^{\infty}\frac{2(-1)^i\left(\frac{2\pi x}{L}\right)^{2i}}{(2i)!} + \sum_{i=1}^{\infty}\frac{2(-1)^i\left(\frac{2\pi y}{L}\right)^{2i}}{(2i)!}\right)^k$$

with a similar expression in the second term. In both cases the denominators contain terms in L^{-a} where $a \geq 2k$. Bringing the factor of $N^k = L^{2k}$ inside the sums leaves the denominators with a constant plus terms dependent on inverse powers of L, all of which disappear in the thermodynamic limit. Hence only the squared terms in the

expansions of the cosines are retained, and bringing out the factor of $(2\pi)^{2k}$ gives

$$g_k = \frac{1}{4^{k-1}\pi^{2k}} \left\{ \sum_{x=1}^{\infty} \sum_{y=1}^{\infty} \frac{1}{(x^2+y^2)^k} + \sum_{x=1}^{\infty} \frac{1}{x^{2k}} \right\}. \tag{4.53}$$

This expression is a corrected version of the form previously reported in [6],

$$g_k = \frac{1}{4\pi^4} \sum_{x=1}^{\infty} \sum_{y=1}^{\infty} \frac{1}{(x^2+y^2)^k} + \frac{1}{4\pi^2} \sum_{x=1}^{\infty} \frac{1}{x^{2k}}. \tag{4.54}$$

The discrepancy seems to arise from not updating the constants when the result for general k is extrapolated from the specific case $k = 2$. As the numerical values reported elsewhere in that paper were correct, the problem appears to be only typographical.

The importance of (4.53) is that $g_{k>2}$ are simply numerical constants with definite determinable values.

4.4.2 Evaluation of the Moments $\langle m^p \rangle$

Probability theory enables the definition of a distribution function in terms of its moments via the relation [90]

$$P(m) = \int_{-\infty}^{\infty} \frac{\mathrm{d}x}{2\pi} e^{imx} \sum_{p=0}^{\infty} \frac{(-ix)^p}{p!} \langle m^p \rangle . \tag{4.55}$$

Following from the definition of the order parameter in (4.26),

$$\langle m^p \rangle = \left\langle \left(\frac{1}{N} \sum_{r=1}^{N} \cos(\psi_r) \right)^p \right\rangle \tag{4.56}$$

$$= \frac{1}{N^p} \left\langle \left(\frac{1}{2} \sum_{r=1}^{N} \left(e^{i\psi_r} + e^{-i\psi_r} \right) \right)^p \right\rangle \tag{4.57}$$

$$= \frac{1}{(2N)^p} \left\langle \left(\sum_{r=1}^{N} \sum_{\sigma=\pm 1} e^{i\sigma\psi_r} \right)^p \right\rangle \tag{4.58}$$

$$= \frac{1}{(2N)^p} \left\langle \sum_{r_1=1}^{N} \sum_{r_2=1}^{N} \cdots \sum_{r_p=1}^{N} \sum_{\sigma_1=\pm 1} \sum_{\sigma_2=\pm 1} \cdots \sum_{\sigma_p=\pm 1} e^{i\sigma_1\psi_{r_1}} e^{i\sigma_2\psi_{r_2}} \cdots e^{i\sigma_p\psi_{r_p}} \right\rangle . \tag{4.59}$$

where, without loss of generality, the index r replaces the position vector $\mathbf{r}$ and i is the imaginary unit $\sqrt{-1}$. Introducing the trace operator

$$\mathrm{Tr} = \sum_{r_1=1}^{N}\sum_{r_2=1}^{N}\cdots\sum_{r_p=1}^{N}\sum_{\sigma_1=\pm1}\sum_{\sigma_2=\pm1}\cdots\sum_{\sigma_p=\pm1}$$

simplifies the notation and equation (4.59) becomes

$$\langle m^p\rangle = \frac{1}{(2N)^p}\mathrm{Tr}\left\langle \exp\left(\sum_{a=1}^{p} i\sigma_a\psi_{r_a}\right)\right\rangle. \tag{4.60}$$

The form of the reciprocal space Hamiltonian (4.23) shows that $|\phi_{\mathbf{q}}|$ is normally distributed. This implies (Appendix C) that θ_r is also Gaussian, as it arises from multiple convolutions of Gaussian functions. The nature of θ_r, and therefore ψ_r, mean that the techniques of Gaussian integration described in Appendix A may be used to evaluate the average in (4.60).

$$\left\langle \exp\left(i\sum_{a=1}^{p}\sigma_a\psi_{r_a}\right)\right\rangle = \exp\left(-\frac{\tau}{2}\sum_{(a,b)}^{p}\sigma_a\sigma_b G_{ab}\right) \tag{4.61}$$

$$= \exp\left(-\frac{\tau}{2}\sum_{a=1}^{p}\sigma_a^2 G_{aa}\right)\exp\left(-\frac{\tau}{2}\sum_{a}^{p}\sum_{b\neq a}^{p}\sigma_a\sigma_b G_{ab}\right) \tag{4.62}$$

$$= \exp\left(-\frac{\tau}{2}pG(0)\right)\exp\left(-\frac{\tau}{2}\sum_{a}^{p}\sum_{b\neq a}^{p}\sigma_a\sigma_b G_{ab}\right) \tag{4.63}$$

$$= \langle m\rangle^p \exp\left(-\frac{\tau}{2}\sum_{a\neq b}^{p}\sigma_a\sigma_b G_{ab}\right) \tag{4.64}$$

In this expression G_{ab} represents $G(r_a - r_b)$, $\tau = T/J$ is the reduced temperature, (a,b) represents all possible pairs of a and b and the shorthand $\sum_{a\neq b} = \sum_a \sum_{b\neq a}$ is introduced. The upper limits of the sums are included explicitly as a reminder that they run over p spins, not the entire lattice.

Combining equations (4.60) and (4.64) gives

$$\langle m^p\rangle = \left(\frac{\langle m\rangle}{2N}\right)^p \mathrm{Tr}\left\{\exp\left(-\frac{\tau}{2}\sum_{a\neq b}^{p}\sigma_a\sigma_b G_{ab}\right)\right\}, \tag{4.65}$$

and the exponential under the trace may be expanded to give

$$\langle m^p\rangle = \left(\frac{\langle m\rangle}{2N}\right)^p \mathrm{Tr}\left\{\sum_{k=0}^{\infty}\frac{1}{k!}\left(-\frac{\tau}{2}\sum_{a\neq b}^{p}\sigma_a G_{ab}\sigma_b\right)^k\right\} \tag{4.66}$$

$$= \left(\frac{\langle m \rangle}{2N}\right)^p \mathrm{Tr}\left\{\sum_{k=0}^{\infty}\left(\frac{1}{k!}\left(-\frac{\tau}{2}\right)^k \underbrace{\sum_{a\neq b}^{p}\sigma_a G_{ab}\sigma_b \sum_{c\neq d}^{p}\sigma_c G_{cd}\sigma_d \ldots}_{k^{\text{th}}\text{ order product}}\right)\right\}. \quad (4.67)$$

This expression is exact. To proceed further one must develop a means of expressing the sums so that they may either be evaluated exactly, or approximated in a controlled manner. The approach adopted in [16] was to introduce a graphical interpretation of the sums. In the re-summation that followed, certain terms were excluded on the assumption that they made no contribution in the thermodynamic limit. We now re-examine this method and show that the assumption is invalid – with the result that an explicit temperature dependence is observed.

4.4.3 A Graphical Representation of the Moments

It is possible to interpret equation (4.67) diagrammatically by letting G_{ab} represent a line joining two *different* points a and b on a sublattice of p points chosen from the original lattice of size N. The expanded exponential contains contributions from all k from zero to infinity, and for each k there is a multiple sum of the form

$$\overbrace{\sum_{a\neq b}\sum_{c\neq d}\cdots}^{2k\text{ sums}}\overbrace{(\sigma_a G_{ab}\sigma_b)\,(\sigma_c G_{cd}\sigma_d)\cdots}^{k\text{ brackets}}.$$

Each bracket corresponds to a line joining two points on the sublattice, thus:

> **the k^{th} term in the expansion is the sum over all possible graphs with k lines on a sublattice of p points chosen from a parent lattice of size N.**

The total number of graphs may be cut considerably by noting certain constraints.

- As already stated, graphs with a line beginning and ending at the same point are disallowed by virtue of the $a \neq b$ condition in the sums.
- Any graph containing odd vertices (points with an odd number of connected lines) will contribute zero when the trace is performed. This can been seen by

considering the effect of the σ parameters. The trace operation sums over all possible values (that is, ± 1) of each σ. Therefore, if any of the σ_a are raised to an odd power (corresponding to the presence of an odd vertex) the sum over that parameter is zero, killing the contribution from that graph.

- Graphs with 'free' points (no connected lines) are interesting. It has been argued [111] that they make zero contribution to the moments of the normalized order parameter, z, as defined in (4.44). However they do contribute to $\langle m^p \rangle$, so will be evaluated here.

- Disconnected graphs are those for which it is not possible to trace a continuous route through all the points using the connecting lines. The graphs in Figure 4.7(d) are all of this type, as is the left hand side of Figure 4.7(c). It is always possible to construct disconnected graphs from a set of connected graphs. It is seen that the contribution made by a disconnected graph is simply the product of the contributions of its connected constituents. Graphs with free points come under this definition.

- Graphs with the same topology make equal contributions to the sums. Thus only contributions from a small subset of all possible graphs need to be evaluated with weightings corresponding to the number of times each topology appears. For example the graphs in Figure 4.7(d) have $p = 4$ all make the same contribution, whereas the $p = 4$ graph in Figure 4.7(a) is topologically different and must be treated separately.

After reducing the set of graphs whose values need to be determined, the following two categories can be identified.

1. **Single Loop Graphs (SLGs)**... contain only points with no more than two lines attached. Thus, each point participates in at most one loop.

2. **Multiple Loop Graphs (MLGs)**... may have points with any (even) number of lines attached.

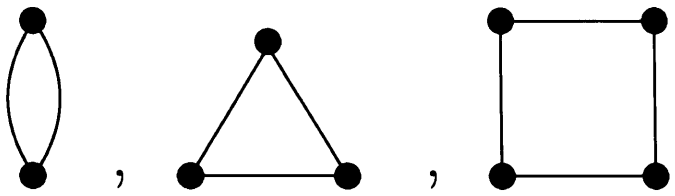

(a)

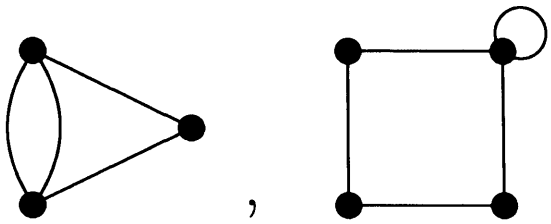

(b)

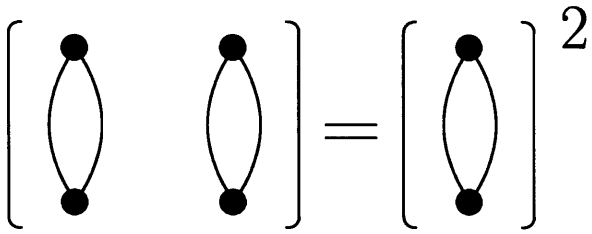

(c)

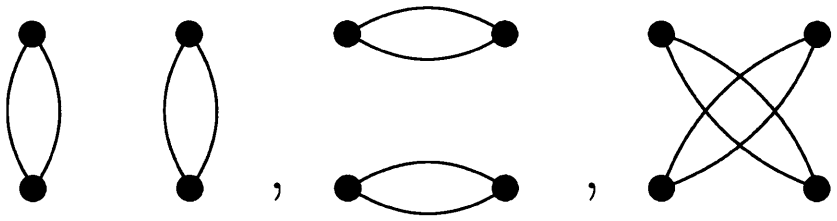

(d)

Figure 4.7: Graphs in the Expansion of $\langle m^p \rangle$: (a) shows examples of allowed connected graphs with $p = 2, 3, 4$ and $k = p$ as considered in [6]. The graphs in (b) are disallowed as they contain either odd vertices or loops involving a single point. In (c) there is an example of a disconnected graph (left hand side) which makes the same contribution as the product of its constituent connected parts. Finally, (d) shows examples of topologically identical graphs with $p = k = 4$. The 'value' of these graphs differs from the $p = k = 4$ graph in (a), which is topologically distinct.

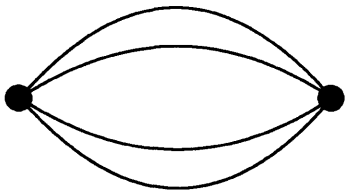

Figure 4.8: An example of a Multiple Loop Graph (MLG): In MLGs each vertex may have more than two lines connected to it. This particular graph is discussed in detail in §4.4.4.

The assumption made in [6] was that the contributions from MLGs go to zero in the thermodynamic limit. Here we begin by reviewing the SLG only approach, to show how this yields a temperature independent form of $\Pi(z)$, before returning to consider the validity of this approximation.

The Value of Single Loop Graphs

Starting with (4.66), changing the order of the sums and bringing the trace inside the sum over k, enables definition of a new quantity S, such that

$$\langle m^p \rangle = \left(\frac{\langle m \rangle}{2N}\right)^p \sum_{k=0}^{\infty} \left\{ \frac{1}{k!} \left(-\frac{\tau}{2}\right)^k \mathrm{Tr} \left[\left(\sum_{a \neq b}^{p} \sigma_a G_{ab} \sigma_b \right)^k \right] \right\} \tag{4.68}$$

$$= \left(\frac{\langle m \rangle}{2N}\right)^p \sum_{k=0}^{\infty} \frac{1}{k!} \left(-\frac{\tau}{2}\right)^k S \tag{4.69}$$

For connected SLGs, all vertices must be connected to two lines. Thus it is always possible to rearrange the order of the G_{ab} so that they form a simple closed loop,

$$S = \mathrm{Tr} \left\{ \sum_{a \neq b}^{p} \sum_{c \neq d}^{p} \cdots (\sigma_a G_{ab} \sigma_b)(\sigma_c G_{cd} \sigma_d) \ldots \right\} \tag{4.70}$$

$$= \mathrm{Tr} \left\{ C(k) \sum_{a}^{p} \sum_{b \neq a}^{p} \sum_{c \neq (a,b)}^{p} \cdots (\sigma_a G_{ab} \sigma_b)(\sigma_b G_{bc} \sigma_c)(\sigma_c G_{cd} \sigma_d) \ldots \right\} \tag{4.71}$$

$$= C(k) S' \tag{4.72}$$

The $\sum_a \sum_{b\neq a}(\sigma_a G_{ab}\sigma_b)$ remains unchanged, however the other $(k-1)$ factors are the result of a contraction of sums with more degrees of freedom. $C(k)$ is therefore a combinatorial factor accounting for the suppressed, topologically identical, graphs.

In going from (4.70) to (4.71) 'disallowed' graphs and topological repeats are excluded from the sums, the latter being counted instead in the pre-factor. To determine the value of $C(k)$ consider a lattice with k points (connected SLGs all have $k = p$). As all points are initially identical, the first of k lines may be placed between any two points. This placement defines the values of a and b and, since the number of choices available are contained within $\sum_a \sum_{b\neq a}$ (which does not change on going from (4.70) to (4.71)), this does not affect $C(k)$. There remain $(k-1)$ lines to place, sequentially, in such a way that a closed loop is formed. It is readily seen that there are $(k-1)!$ ways to achieve this. Bearing in mind that the lines are actually vectors, originating at one point and terminating at another, and that G is an even function,

$$C(k) = 2^{k-1}(k-1)!. \tag{4.73}$$

This leaves the effect of the trace to be established. Given that all of the σ parameters are raised to even powers, the sums over $\sum_{\sigma_a=\pm 1}$ *etc.* yield a factor of 2^p. The remaining sums over the various r_a are most easily dealt with by Fourier transforming the Green's functions G according to

$$G(\mathbf{r}) = \frac{1}{N}\sum_{\mathbf{q}\neq 0} e^{-i\mathbf{q}\cdot\mathbf{r}} G(\mathbf{q}), \tag{4.74}$$

where $G(\mathbf{q})^{-1} = \gamma_{\mathbf{q}}$. It is convenient now to consider the effect of free points on the SLGs, as without them the sum over k becomes meaningless. Clearly p must be greater than k and the argument of the trace in (4.71) is unaffected by their presence. This gives

$$\begin{aligned} S' \;=\; & \frac{2^p}{N^k}\sum_{\mathbf{r}_1=1}^{N}\cdots\sum_{\mathbf{r}_p=1}^{N}\sum_{a=1}^{p}\sum_{b\neq a}^{p}\cdots \\ & \times \sum_{\mathbf{q}_1\neq 0} e^{-i\mathbf{q}_1\cdot(\mathbf{r}_a-\mathbf{r}_b)} G(\mathbf{q}_1)\sum_{\mathbf{q}_2\neq 0} e^{-i\mathbf{q}_2\cdot(\mathbf{r}_b-\mathbf{r}_c)} G(\mathbf{q}_2)\cdots\sum_{\mathbf{q}_k\neq 0} e^{-i\mathbf{q}_k\cdot(\mathbf{r}_k-\mathbf{r}_1)} G(\mathbf{q}_k). \end{aligned} \tag{4.75}$$

The sums over the indices a, b, c *etc.* have the effect of labelling the p points. The same result is achieved by fixing $a = 1$, $b = 2$, and so on, then evaluating the number of permutations of the labels, which is simply ${}^{p}\mathrm{P}_{k}$.

Each sum of the form $\sum_{\mathbf{r}_j=1}^{N}$ for $j > k$ introduces a factor of N as $\mathbf{r}_{j>k}$ does not appear in any G. Thus, re-grouping and changing the order of the sums,

$$S' = 2^p \, {}^{p}\mathrm{P}_{k} \, N^{p-2k} \sum_{\mathbf{q}_1 \neq 0} \sum_{\mathbf{q}_2 \neq 0} \cdots \sum_{\mathbf{q}_k \neq 0} \left(\sum_{\mathbf{r}_1=1}^{N} e^{-i\mathbf{r}_1 \cdot (\mathbf{q}_1 - \mathbf{q}_k)} \right) \left(\sum_{\mathbf{r}_2=1}^{N} e^{-i\mathbf{r}_2 \cdot (\mathbf{q}_2 - \mathbf{q}_1)} \right) \cdots$$

$$\times \left(\sum_{\mathbf{r}_k=1}^{N} e^{-i\mathbf{r}_k \cdot (\mathbf{q}_k - \mathbf{q}_{k-1})} \right) G(\mathbf{q}_1) G(\mathbf{q}_2) \ldots G(\mathbf{q}_k). \tag{4.76}$$

Using identity $\sum_{\mathbf{r}}^{N} e^{i\mathbf{q}.\mathbf{r}} \overset{N \to \infty}{=} N\delta(\mathbf{q})$, all terms disappear unless $\mathbf{q}_1 = \mathbf{q}_2 = \ldots = \mathbf{q}_k$. And so,

$$S' = 2^p \, {}^{p}\mathrm{P}_{k} \, N^{p-k} \sum_{\mathbf{q} \neq 0} G(\mathbf{q})^k \tag{4.77}$$

$$S' = 2^p \, {}^{p}\mathrm{P}_{k} \, N^{p} g_k, \tag{4.78}$$

explaining the relevance of the constants g_k and providing the expression

$$\langle m^p \rangle_{\mathrm{SLG}} = \langle m \rangle^p \sum_{k=0}^{\infty} \frac{(-\tau)^k}{2k} \, {}^{p}\mathrm{P}_{k} \, g_k. \tag{4.79}$$

Disconnected SLGs in General

A disconnected SLG may be viewed as having j constituent connected parts with $k_1, k_2, \ldots, k_j$ lines each, where $k_1 + k_2 + \ldots + k_j = k$. Splitting the argument of the trace in (4.71) into j non-interacting parts, each one contributes $2^{k_a - 1}(k_a - 1)!$ to $C(k_1, k_2, \ldots, k_j)$. It is then necessary to take into account the number of ways of splitting up (4.71) that give the required topology. This involves recognizing two symmetries under which the graphs are invariant. Firstly, there is no change to a graph resulting from the permutation of its k points. Secondly, the order in which the j SLGs are placed is unimportant. Thus the most convenient definition of the factor C is,

$$\frac{1}{j!}\sum_{\{\varsigma\}} C(k_1,\ldots,k_j) = \frac{1}{j!}\,{}^{k}\mathrm{C}_{k_1}\,{}^{k-k_1}\mathrm{C}_{k_2}\ldots 2^{k_1-1}2^{k_2-1}\times\ldots$$

$$\ldots\times(k_1-1)!(k_2-1)!\ldots \tag{4.80}$$

$$= \frac{1}{j!}2^{k-j}(k_1-1)!(k_2-1)!\ldots(k_j-1)!$$

$$\times\frac{k!}{(k-k_1)!k_1!}\frac{(k-k_1)!}{(k-k_1-k_2)!k_2!}\times\ldots$$

$$\ldots\times\frac{(k-k_1-k_2-\ldots-k_j)!}{(k-k_1-k_2-\ldots-k_j)!k_j!} \tag{4.81}$$

$$= \frac{1}{j!}\frac{2^{k-j}(k_1-1)!(k_2-1)!\ldots(k_j-1)!k!}{k_1!k_2!\ldots k_j!} \tag{4.82}$$

$$= \frac{1}{j!}\frac{2^{k-j}k!}{k_1k_2\ldots k_j}. \tag{4.83}$$

Here $\{\varsigma\}$ represents the set of permutations of the SLG elements of the graph. The $1/j!$ factor emphasizes the lack of order dependence. Combining (4.69), (4.72), (4.78) and (4.83) leads to an expression for the moments (note that $k=1$ makes no contribution)

$$\frac{\langle m^p\rangle}{\langle m\rangle^p} = 1+\sum_{k=2}^{p}\left(-\frac{\tau}{2}\right)^k\frac{{}^{p}\mathrm{P}_k}{k!}\sum_{j=1}^{k}\sum_{k_1+\ldots+k_r=k,k_x\geq 2} C(k_1,\ldots,k_j)g_{k_1}\ldots g_{k_j} \tag{4.84}$$

$$= 1+\sum_{k=2}^{p}\sum_{j=1}^{k}\sum_{k_1+\ldots+k_j=k,k_x\geq 2}\frac{{}^{p}\mathrm{P}_k}{j!}\frac{(-\tau)^k}{2}\frac{g_{k_1}g_{k_2}\ldots g_{k_j}}{k_1k_2\ldots k_j} \tag{4.85}$$

$$= \exp\left(\sum_{k=2}^{\infty}\frac{g_k}{2k}(-\tau)^k\left.\frac{\partial^k}{\partial z^k}z^p\right|_{z=1}\right). \tag{4.86}$$

Equation (4.86) is arrived at by making the substitution ${}^{p}\mathrm{P}_k = \left.\frac{\partial^k}{\partial z^k}z^p\right|_{z=1}$ which not only provides the permutative factor but also negates all terms with $k>p$ which arise from letting the sum over k run to infinity. The standard deviation is thus

$$\sigma = \sqrt{\frac{g_2}{2}}\tau\,\langle m\rangle\,, \tag{4.87}$$

from which it is seen that the hyperscaling condition (4.41) is obeyed. Substituting (4.86) into (4.55) and making the transformation $x \rightarrow x/\sigma$ gives

$$P(m) = \int_{-\infty}^{\infty} \frac{\mathrm{d}x}{2\pi\sigma} \exp\left\{ \frac{ix(m - \langle m \rangle)}{\sigma} + \sum_{k=2}^{\infty} \frac{g_k}{2k} \left(ix\sqrt{\frac{2}{g_2}} \right)^k \right\}, \tag{4.88}$$

which is independent of temperature. This is the BHP distribution.

It is worth noting here that (4.88) may be obtained via an entirely different route. If the order parameter is redefined such that $m = (1/N)\sum_r \psi_r^2$, then it is relatively straightforward to evaluate (4.55) directly in reciprocal space, giving (4.88) [6]. However, this approach is essentially looking at an entirely different physical property. This is discussed in greater depth in §4.5.3 and Chapter 5.

4.4.4 The Effect of Introducing MLGs

The simplest MLG consists of a sublattice with p points, only two of which are connected by k lines. The contributions from such graphs were ignored in [6]. There is no longer the restriction that $k \leq p$ so any even number of lines is permitted. The exponential in (4.65) is expanded in the same way as before, with this time,

$$S = \mathrm{Tr}\left\{ \sum_{a \neq b} (\sigma_a G_{ab} \sigma_b)^k \right\} \tag{4.89}$$

$$= 2^{p+k-1} \sum_{\mathbf{r}_1,\ldots,\mathbf{r}_p} \sum_{a=1}^{p} \sum_{b \neq a}^{p} G_{ab}^k. \tag{4.90}$$

Transforming to reciprocal space does not now give rise to the simplifications seen for SLGs. There is an imbalance between the number of wavevectors (of which there are k) and the number of real space coordinates (of which there are only 2).

$$S = 2^{p+k-1} \sum_{\mathbf{r}_1,\ldots,\mathbf{r}_p} \sum_{a=1}^{p} \sum_{b \neq a}^{p} G_{ab}^k \tag{4.91}$$

$$= 2^{p+k-1} \sum_{\mathbf{r}_1,\ldots,\mathbf{r}_p} \sum_{a=1}^{p} \sum_{b \neq a}^{p} \frac{1}{N} \sum_{\mathbf{q}_1 \neq 0} e^{-i\mathbf{q}_1 \cdot (\mathbf{r}_a - \mathbf{r}_b)} G(\mathbf{q}_1) \frac{1}{N} \sum_{\mathbf{q}_2 \neq 0} e^{-i\mathbf{q}_2 \cdot (\mathbf{r}_a - \mathbf{r}_b)} G(\mathbf{q}_2) \cdots$$

$$\ldots \times \frac{1}{N} \sum_{\mathbf{q}_k \neq 0} e^{-i\mathbf{q}_k \cdot (\mathbf{r}_a - \mathbf{r}_b)} G(\mathbf{q}_k) \tag{4.92}$$

$$= 2^{p+k-1}N^{p-2-k}({}^{p}\mathrm{P}_2)\sum_{\mathbf{r}_1}\sum_{\mathbf{r}_2}\sum_{\mathbf{q}_1\neq 0}\sum_{\mathbf{q}_2\neq 0}\cdots\sum_{\mathbf{q}_k\neq 0} e^{-i(\mathbf{q}_1+\ldots+\mathbf{q}_k).\mathbf{r}_1}e^{i(\mathbf{q}_1+\ldots+\mathbf{q}_k).\mathbf{r}_2}$$

$$\ldots\times G(\mathbf{q}_1)\ldots G(\mathbf{q}_k) \tag{4.93}$$

$$= 2^{p+k-1}N^{p}\ {}^{p}\mathrm{P}_2\ \Theta_k \tag{4.94}$$

where

$$\Theta_k = \frac{1}{N^k}\sum_{\mathbf{q}_1\neq 0,\ldots,\mathbf{q}_k\neq 0} G(\mathbf{q}_1)\ldots G(\mathbf{q}_k)\delta\left(\sum_i \mathbf{q}_i\right). \tag{4.95}$$

Thus the contribution to the magnetization from graphs with k lines joining only two points on a sublattice of p points (admittedly a highly specific set) is,

$$\langle m\rangle^p \sum_{k=0,2,4\ldots}^{\infty} \frac{(-\tau)^k}{2k!}\ {}^{p}\mathrm{P}_2\ \Theta_k. \tag{4.96}$$

The problem is then reduced to evaluating the sum Θ_k.

Do Multiple Loop Graphs Contribute to $\langle m^p\rangle$?

The reason for deriving (4.94) is to test the hypothesis proposed in [6] that MLGs do not contribute to the moments in the thermodynamic limit.

Consider the second moment $\langle m^2\rangle$. All sublattices for this moment have only 2 points, therefore if MLGs can be ignored the only terms remaining from the expansion of the exponential are quadratic, giving $\langle m^2\rangle = \langle m\rangle\,(1 + g_2\tau^2/2)$. Allowing MLGs however gives a very different expression,

$$\left\langle m^2\right\rangle = \langle m\rangle^2\left(1 + g_2\tau^2 + \frac{1}{24}\Theta_4\tau^4 + \ldots\right) \tag{4.97}$$

from which two things are immediately apparent. Firstly, in the low temperature limit only the single loop graphs are significant as all MLGs correspond to higher powers of T. Secondly, the N dependence of the MLGs is tied up in the sum Θ_k.

Evaluating 'the Sum' Θ_k

Θ_k (4.95) may be treated in a similar manner to the constants g_k from §4.4.1. Substituting $G(\mathbf{q}) = 1/\gamma_{\mathbf{q}}$ gives

$$\Theta_k = \frac{1}{N^k} \sum_{\{x_i\}=-\infty}^{\infty} \sum_{\{y_i\}=-\infty}^{\infty} \frac{1}{(4 - 2\cos(2x_1\pi/L) - 2\cos(2y_1\pi/L))} \times \ldots \tag{4.98}$$

$$\ldots \times \frac{1}{(4 - 2\cos(2x_k\pi/L) - 2\cos(2y_k\pi/L))} \times \delta\left(\sum_i x_i\right) \delta\left(\sum_i y_i\right).$$

The sum over $\{x_i\}$ is used to indicate a multiple sum over all members of the set $\{x_1, x_2, \ldots, x_k\}$. The delta function constraint has been separated into its component parts however it can be included simply by requiring $x_k = -\sum_{i=1}^{k-1} x_i$, and similarly for y_k. This way the sums are now of order $k-1$, though there remain k factors in the denominator.

Once again the cosine functions are expanded to give a power series in $(1/L)$. All terms are therefore zero in the thermodynamic limit except those which cancel with the factor N^k outside the sum. This gives

$$\Theta_k = \frac{1}{(2\pi)^{2k}} \sum_{\{x_i\}=-\infty}^{\infty} \sum_{\{y_i\}=-\infty}^{\infty} \frac{1}{(x_1^2 + y_1^2)} \frac{1}{(x_2^2 + y_2^2)} \times \ldots \tag{4.99}$$

$$\ldots \times \frac{1}{\left((-\sum_{i=1}^{k-1} x_i)^2 + (-\sum_{i=1}^{k-1} y_i)^2\right)}.$$

Equation (4.99) indicates that Θ_k is not identically zero, as there are a number of non-zero terms in the sums, all of which are positive (consider, for example, $x_i = 0$ for all i and $y_i = 1$ for all $i < k$, giving a contribution of $(k-1)^{-2}$ to the sum). This provides evidence which contradicts the assumption in [6] that all MLGs go to zero in the thermodynamic limit. Furthermore Θ_k *contains* g_k. This can be seen by recognizing that there are contributions to the sums in (4.99) coming from terms where all absolute values of x_i are equal, as are all absolute values of y_i. These terms, taken by themselves, define the constants g_k. So not only are the Θ_k finite, but they must be larger than the corresponding value of g_k. This follows directly from the definition of S for MLGs which does not preclude the presence of SLGs in the sum. Importantly, removing the g_k contribution still leaves a number of finite terms (this is important as otherwise the Θ_k would just reduce to the SLG contributions).

Unfortunately we have not been able to demonstrate the convergence of Θ_k analytically. Numerical results appear to confirm that it is converges to a finite value

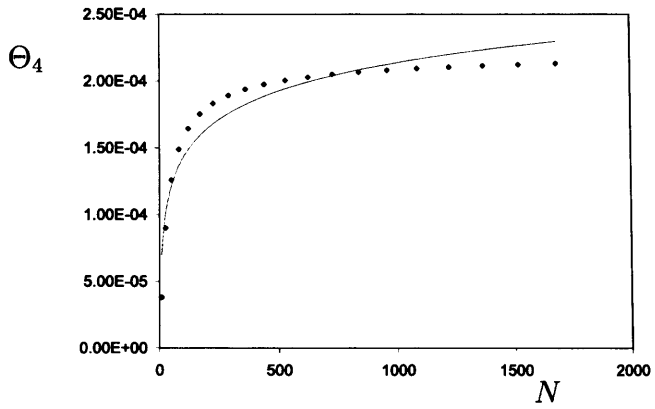

Figure 4.9: Θ_k as a Function of N for $k = 4$: The solid line represents the best logarithmic fit to the data and is clearly more rapidly divergent. It appears from this numerical evaluation of Θ_k that the sum converges in the thermodynamic limit.

(Figure 4.9), with even a logarithmic fit diverging rapidly from the sum as N is increased. It must also be acknowledged that the analysis presented here is based on the extremely specific subset of MLGs defined above, inclusion of which represents only the first stage toward improving the expressions obtained from SLGs alone. This is not a problem though as contributions from different graphs are additive and so more MLGs will simply increase their importance. Suffice to say that an analytical treatment including all possible graphs has proved intractable. However it is clear that the effect of MLGs is to significantly modify the expressions for $\langle m^p \rangle$ in a temperature dependent manner.

4.5 Monte Carlo Simulations

A number of Monte Carlo simulations have been performed in order to test the analytical results presented in §4.4 and to attempt to quantify their consequences for the magnetization distribution. Previous numerical studies appeared to have confirmed the prediction of a temperature independent $P(m)$ [6]. These studies were

performed on the full 2dXY model up to $T/J = 0.7$, some way below T_{KT} in order to avoid having a significant vortex density. The lack of variation of $P(m)$ in this previous study serves as an indication that the temperature dependence predicted above must be relatively weak.

4.5.1 Simulations of the Harmonic Model

The Harmonic model has no vortices and so is purely spin wave in nature at all temperatures. As such, if the assertion of temperature independence is correct then the BHP form should be recovered for $\Pi(z)$ from simulations of this model regardless of T.

Standard single spin-flip Monte Carlo simulations were performed, using a Metropolis [112] update algorithm. The system sizes considered were from $L = 10$ up to $L = 32$, over a range of temperatures from $T/J = 0.5$ to as high as $T/J = 50$. Given the critical nature of the system a large number of Monte Carlo steps per spin (MCS/s) are required for accurate statistics in the wings of the distribution. These simulations use 10^7 MCS/s, the first 10^6 of which are used for equilibration.

The results are shown in Figure 4.10. Parts (a) and (b) show the change in the distribution as a function of temperature for system sizes $N = 100$ and $N = 1024$ spins respectively, with the BHP function plotted for reference. The behaviour is very similar in each case as is confirmed in part (c) which shows some of the results from (a) and (b) superimposed. This is an early indication of agreement with previously reported observation of size independence [6, 16]. Figure 4.10 shows that the low temperature form of the distribution follows that of the BHP function very closely. However, as T is increased, the distribution becomes progressively less skewed, apparently becoming Gaussian in the limit of high temperature. Such behaviour is exactly as expected. The BHP function arises as a result of neglecting MLGs from the moment expansion. In that case, normalization of each cumulant to the appropriate power of the standard deviation results in a cancelling out of all factors of T. However, including MLGs allows higher powers of temperature into the moment (and therefore cumulant) expressions. For κ_r/σ^r at high temperatures the denominator

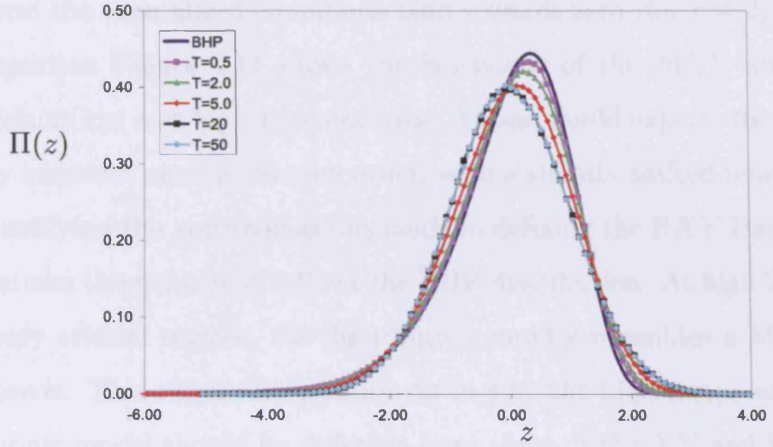

(a)

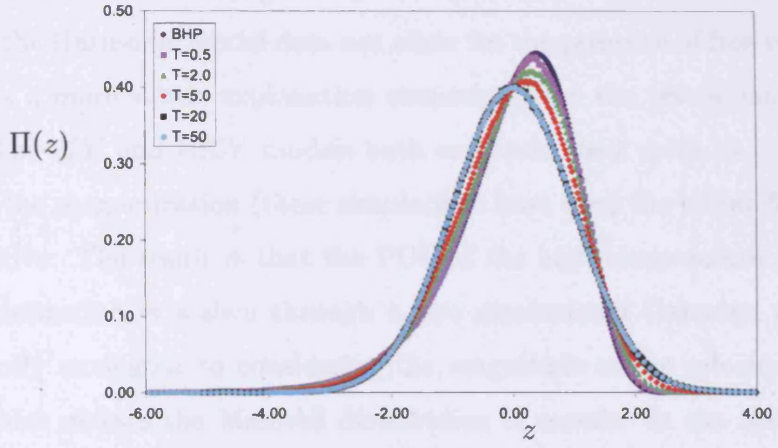

(b)

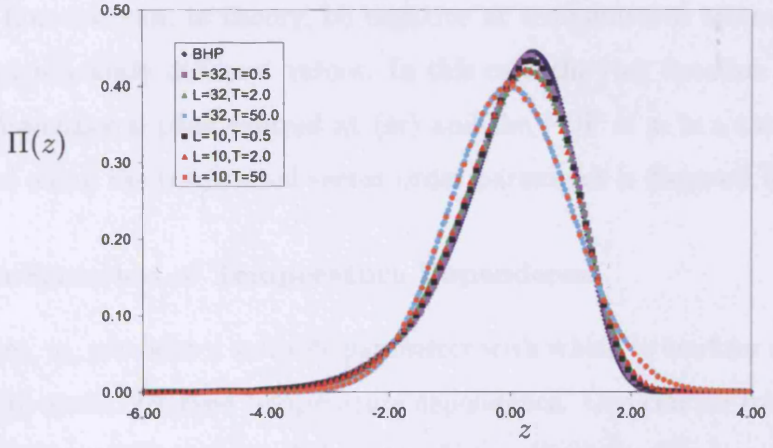

(c)

Figure 4.10: Monte Carlo Simulations on the Harmonic Model: Part (a) shows the variation in $\Pi(z)$ as T is varied for fixed $L = 10$. Part (b) is the same but with $L = 32$. Part (c) shows selected curves from (a) and (b) superimposed

dominates and the normalized cumulants tend towards zero (for $r \neq 2$).

For comparison Figure 4.11 shows the behaviour of the 2dXY and HXY (see §4.3.1) models at low and high temperatures. As one would expect, they behave in a qualitatively identical manner to each other, with a slightly shifted relative temperature scale, justifying the approximations made in defining the HXY Hamiltonian. At low temperatures the behaviour follows the BHP distribution. At high T, outside the spin wave only critical regime, the distribution rapidly resembles a Maxwell distribution of speeds. This raises the question as to why the high temperature statistics of the Harmonic model should be different from those of the XY and HXY models. Firstly one can say that the high temperature states of these models are inherently different as the Harmonic model does not allow for the presence of free vortices. However there is a more subtle explanation stemming from the restrictions on the spin variables. The XY and HXY models both constrain their spins to be in the range $\pm\pi$, and so the magnetization (these simulations have used the cosine form (4.26)) is always positive. The result is that the PDF of the high temperature instantaneous scalar magnetization is a slice through a two dimensional Gaussian ring function. This is exactly analogous to considering the magnitude of the velocity of molecules in a gas, which defines the Maxwell distribution of speeds. In the Harmonic model there are no limits on the values of the spins. Thus, the scalar magnetization defined as a cosine function can, in theory, be negative at temperatures where neighbouring spins have significantly different values. In this case the ring function collapses to a single one dimensional peak centred at $\langle m \rangle$ and the PDF of m is a simple Gaussian. The effect of using the traditional vector order parameter is dicussed in §4.5.3.

$\gamma_3(T)$ - Confirmation of Temperature Dependence

The skewness, γ_3, provides a suitable parameter with which to confirm and characterize the nature of the observed temperature dependence. One can see from Figure 4.10 that this tends towards zero as T becomes large. However there was concern that the restricted sizes of the lattices studied may obscure the true behaviour of other larger, but still finite, systems. Studying γ_3 as a function of $1/N$ shows that this

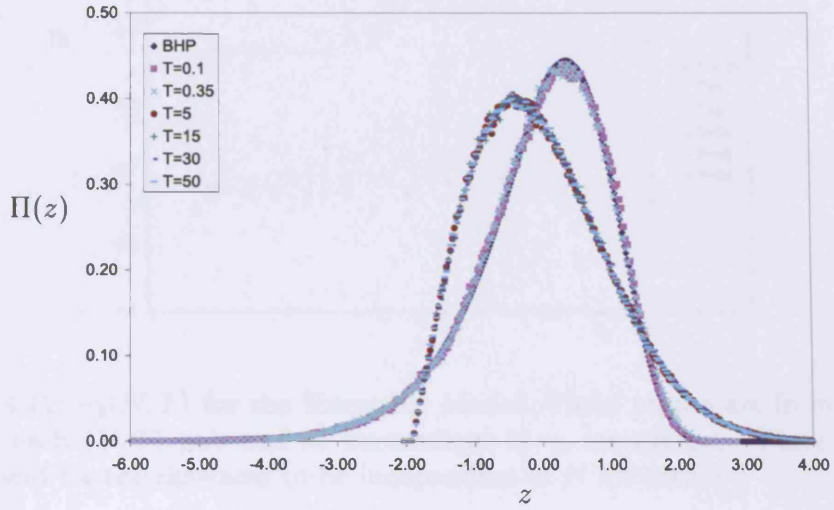

(a)

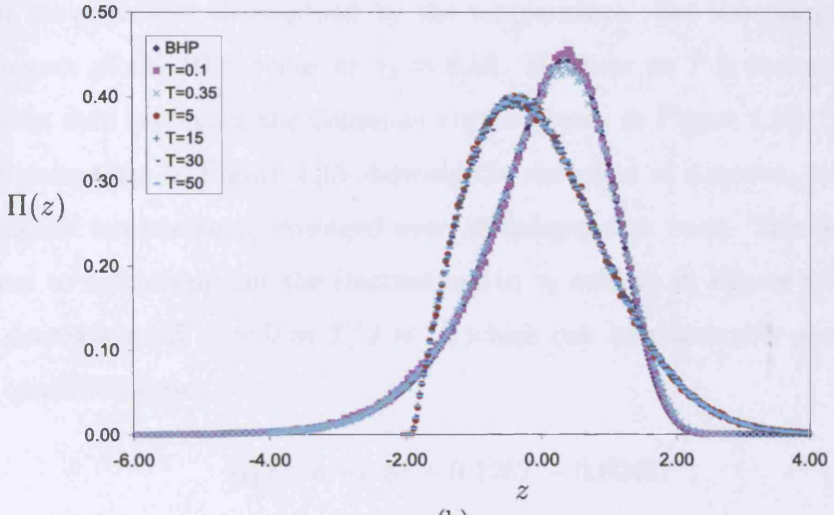

(b)

Figure 4.11: Monte Carlo Data for the 2dXY and HXY Models: Part (a) shows the different statistical regimes at high and low temperature for the 2dXY model. The function is an excellent fit to the BHP form at low T, becoming Maxwellian at high temperatures. Part (b) shows the same behaviour for the HXY model. That both models exhibit high temperature behaviour that is markedly different from that seen for the Harmonic model in Figure 4.10 is a consequence of the definition of m, as discussed in the text.

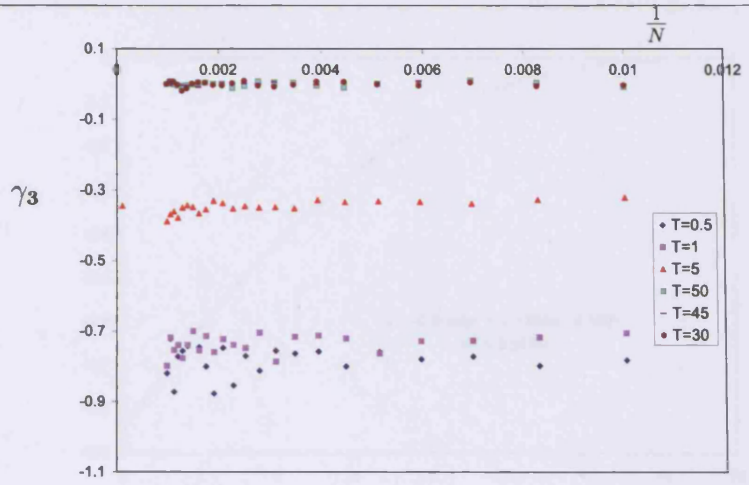

Figure 4.12: $\gamma_3(N,T)$ for the Harmonic Model: These results are from a single MC run for each (N,T) pair and so fluctuations in γ_3 are evident. There is however a clear trend for the skewness to be independent of N for each T.

is not the case. One can see in Figure 4.12 that the trend is for a size independent value of the skewness, determined by the temperature. For low temperatures γ_3 is in the region of the BHP value of $\gamma_3 \approx 0.89$. However as T is increased this value approaches zero reflecting the Gaussian curves shown in Figure 4.10. The picture is clarified somewhat in Figure 4.13 showing the skewness of a system with $L = 16$ as a function of temperature, averaged over 10 independent runs. This averaging goes some way to smoothing out the fluctuations in γ_3 evident in Figure 4.12. There is a steady decrease until $\gamma_3 = 0$ at $T/J \approx 12$ which can be reasonably accurately fitted by the quadratic form,

$$\gamma_3(T) = -0.85 + 0.126T - 0.0048T^2, \tag{4.100}$$

up to the point at which the skewness becomes zero. There is a limit to how closely the γ_3 axis in Figure 4.12 can be approached. Therefore it can not be stated with absolute certainty that there is not a sudden dip in the skewness at a given temperature for larger values of N. However, coupled with the analytical work, the results of these simulations suggest this is very unlikey. Further evidence is provided by a single calculation of a much larger system, $N = 10000$, at $T/J = 5$, which shows no significant deviation from the constant behaviour of the smaller systems at the same temperature.

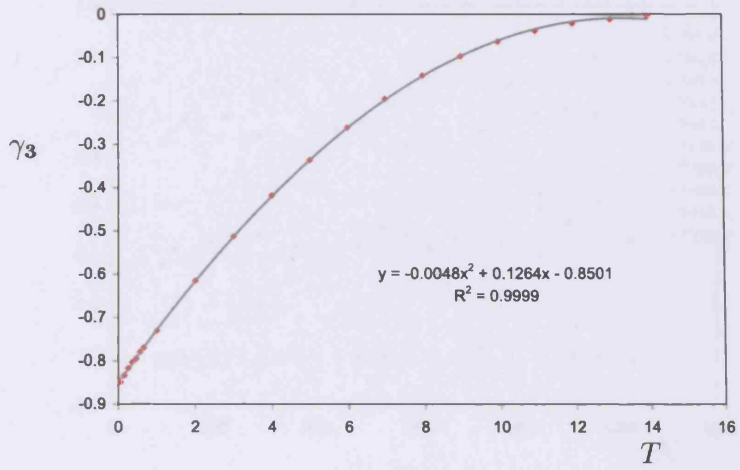

Figure 4.13: $\gamma_3(T)$ for the $L = 16$ Harmonic Model: The diamonds are the results of the averaging over 10 independent MC runs. The solid line is a quadratic least squares fit described by the equation given. The fit is effectively linear at low temperatures.

The Defect of Kurtosis

The behaviour of the defect of kurtosis should be relatively straightforward, and similar to that of the skewness. However, the kurtosis is a much 'softer' quantity and tends to have large fluctuations from one simulation to another. In order to obtain sufficiently reliable statistics one would need to perform numerous runs and average the results.

The output from a set of one off simulations over a range of system sizes is given in Figure 4.14. The general form is akin to that seen in Figure 4.12 for the skewness, however the data is not nearly as well behaved. It can be stated unequivocally though that the defect of kurtosis becomes zero for all system sizes at high temperatures, in line with the observations of a Gaussian distribution.

The Behaviour of $\langle m \rangle$

Figure 4.15 shows $\langle m \rangle$ as a function of $1/N$ for a selection of the temperatures studied. Each plot includes the behaviour predicted by spin wave theory, as given in (4.27). The agreement is excellent at low temperatures, and remains good up to around $T/J = 25$. Beyond this significant deviations start to appear, along with the onset of

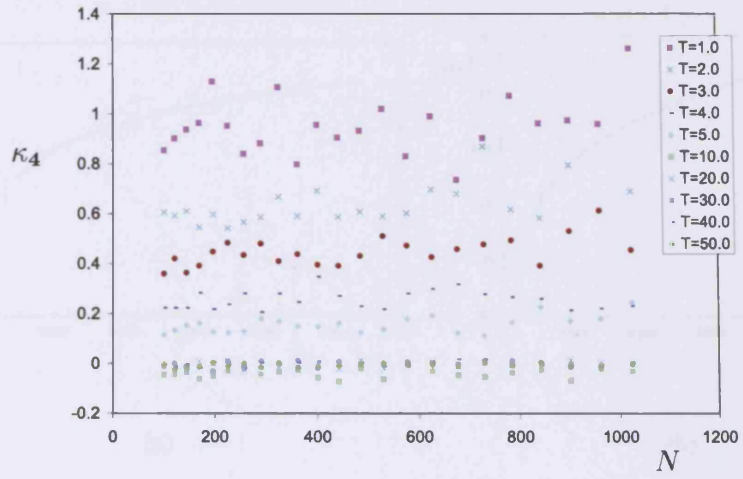

Figure 4.14: $\gamma_4(N,T)$ for the Harmonic Model: These results are from a single MC run for each (N,T) pair and so the softness of the defect of kurtosis is manifest. However the trends for size independence and high T Gaussianity can be made out.

unphysical, negative, values of $\langle m \rangle$. By the time the temperature reaches $T/J = 50$ all semblance of a pattern has been lost. These observations are surprising as the spin wave theory from which (4.27) is derived is rigorous at all temperatures. It seems that the apparent breakdown is a result of insufficient sampling of configuration space at high T. The magnetization, as defined in (4.26), is bounded between ± 1 regardless of the values of the spin variables. The values of $\psi_{\mathbf{r}}$ are, however, unconstrained. These variables are Gaussian as discussed before, and the width of their distribution grows with increasing temperature.

Figure 4.16 shows two possible scenarios. At low temperatures (green line) the distribution of $\psi_{\mathbf{r}}$ is quite narrow as the system minimizes the energy by aligning spins. In this case the vast majority of spins will be in the range for which $\cos\psi_{\mathbf{r}}$ is positive giving a guaranteed positive value for m. By contrast the red line corresponds to a higher temperature at which the spins sample a much larger range of values. Now the distribution of $\psi_{\mathbf{r}}$ is wide enough to cover many periods of the cosine function, giving numerous negative contributions to the average magnetization. If the system is large enough such that all periods of the cosine function are sampled with the correct statistical weighting, defined by the distribution of $\psi_{\mathbf{r}}$, then $\langle m \rangle$ is necessarily positive.

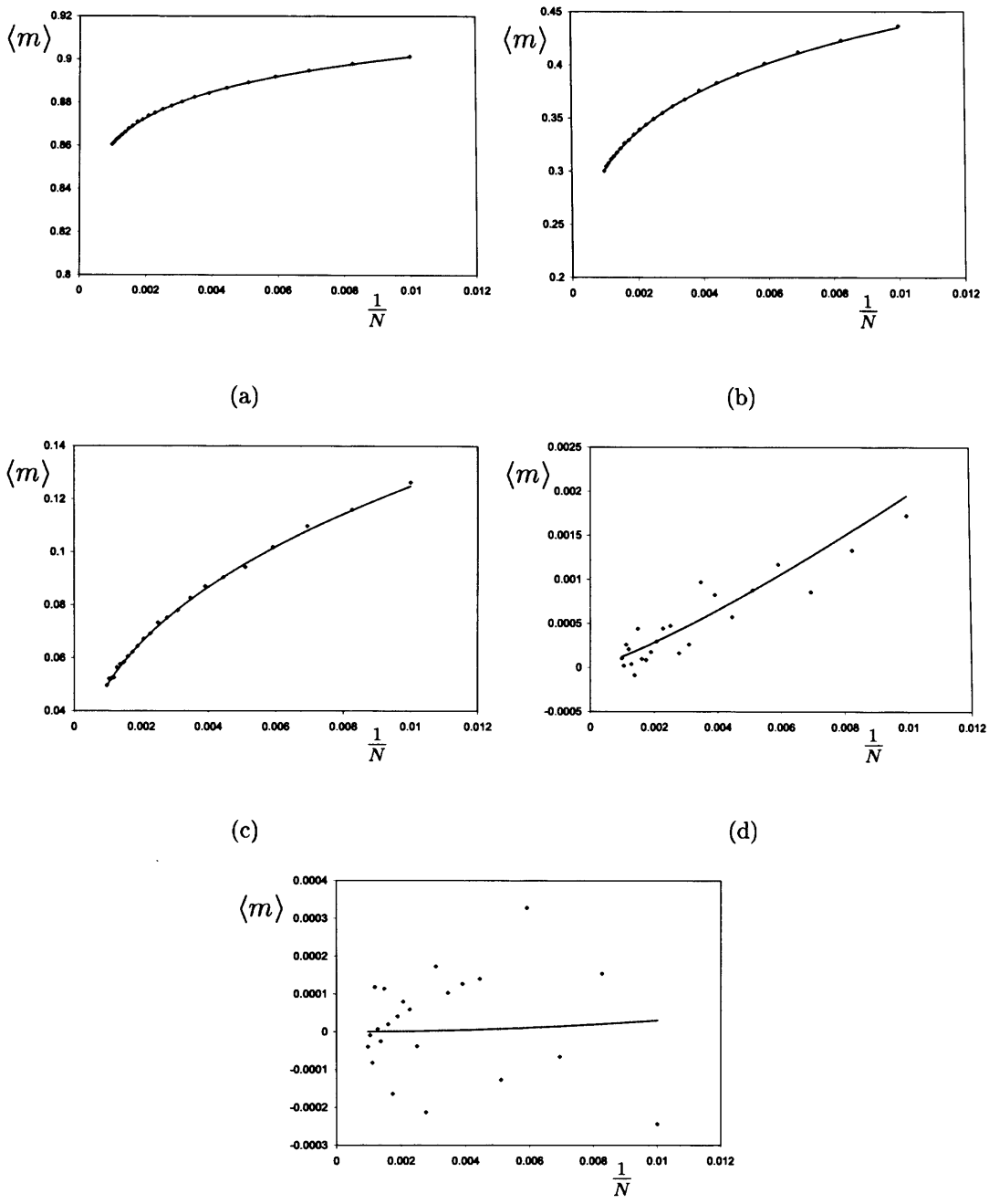

Figure 4.15: The Variation of $\langle m \rangle$ with N: (a) $T/J = 0.5$, (b) $T/J = 4.0$, (c) $T/J = 10.0$, (d) $T/J = 30.0$, (e) $T/J = 50.0$. The blue diamonds are the results of MC calculations; the solid (pink) line is the theoretical predicition from spin wave theory (equation (4.27)). At low temperatures the correlation is very good, however as T is increased the agreement collapses for the reasons discussed in the text.

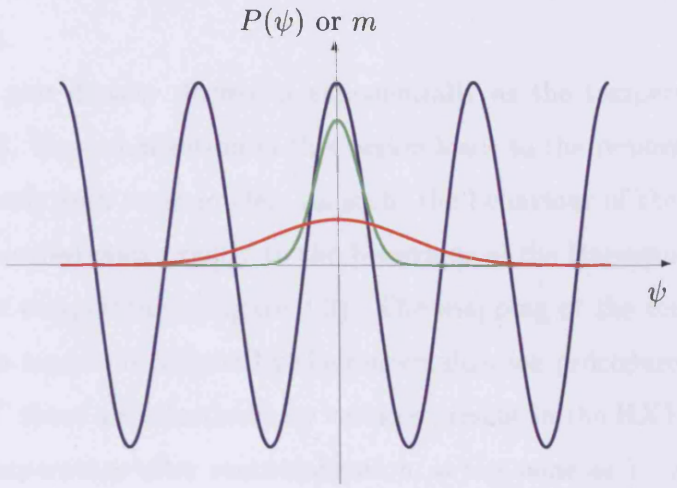

Figure 4.16: A Comparison Between $P(\psi)$ and m: The blue periodic function represents m as defined in (4.26) (note that this has been scaled by half for clarity). The green line shows the Gaussian distribution of ψ at low temperatures, where neighbouring spins differ little from each other and ψ is generally small. At higher T (red line) ψ variables may be excited to high energy states, spanning multiple periods of the magnetization function.

However, if N is small it is possible that the the number of $\psi_{\mathbf{r}}$ contributing to m may be insufficient to accurately reflect the distribution of the spin variables. In this case, as the disparity grows, one ends up with an effectively random distribution of $\psi_{\mathbf{r}}$ with equal probability of positive and negative $\langle m \rangle$. As this problem does not arise until well above the temperature at which one starts to observe Gaussian behaviour for the order parameter, there is no need to modify the conclusions regarding the temperature dependence of $\Pi(z)$.

4.5.2 Temperature Dependence in the HXY Model

Having established that the order parameter for the Harmonic model exhibits temperature dependence, the inference must be that the same is true of the vortex-free region of the HXY model. In this case there is a much smaller range of temperatures available for simulation. Not only must T be less than the Kosterlitz Thouless transition temperature, but it should also be low enough to effectively exclude bound

pairs of vortices.

The vortex pair density decreases exponentially as the temperature is lowered below T_{KT} [110]. Renormalization in this region leads to the removal of all vortices, recovering a purely spin wave model. As such, the behaviour of the HXY model at some $T < T_{KT}$ corresponds exactly to the behaviour of the Harmonic model at some generally higher temperature (Figure 4.3). The mapping of the temperature scales between the two models is defined by the renormalization procedure [59] and is non-linear. At low T there are effectively no vortices present in the HXY model and T_{eff}, the effective temperature after renormalization, is the same as T. As the transition temperature is approached, the rapid increase in the number of vortex pairs leads to a rapid divergence in T_{eff}, which becomes infinite at T_{KT}.

Using the results of [59], the value of the effective temperature has been calculated for T from 0.075 to 2, for a system with $L = 16$ (Table 4.1) [113]. It can be seen that the original and renormalized temperature scales coincide exactly for $T \leq 0.9$. We have performed simulations of the HXY model in this range and the results show a clear change in the skewness of the magnetization distribution as T is varied. Given that there are demonstrably no vortices present in the system, it is concluded that the temperature dependence has the same origins as in the Harmonic model, namely the multiple loop graphs in the moment expansion. The plot of $\gamma_3(T)$ for the harmonic model shows an essentially linear dependence at low temperatures (Figure 4.17(a)). According to the arguments above it is expected that a very similar form should be observed for the HXY simulations. This is indeed the case as shown in Figure 4.17(b), and both models have a low temperature variation of γ_3 described by

$$\gamma_3 = 0.13T - 0.852. \tag{4.101}$$

T	K_{eff}	T_{eff}	y
0.075	13.333	0.075	0.000
0.1	10	0.1	0.000
0.125	8	0.125	0.000
0.15	6.667	0.15	0.000
0.175	5.714	0.175	0.000
0.2	5	0.2	0.000
0.225	4.444	0.225	0.000
0.25	4	0.25	0.000
0.275	3.636	0.275	0.000
0.3	3.333	0.3	0.000
0.325	3.077	0.325	0.000
0.35	2.857	0.35	0.000
0.375	2.667	0.375	0.000
0.4	2.5	0.4	0.000
0.425	2.353	0.425	0.000
0.45	2.222	0.45	0.000
0.475	2.105	0.475	0.000
0.5	2	0.5	0.000
0.525	1.905	0.525	0.000
0.55	1.818	0.55	0.000
0.575	1.739	0.575	0.000
0.6	1.667	0.6	0.000
0.625	1.6	0.625	0.000
0.65	1.538	0.65	0.000
0.675	1.481	0.675	0.000
0.7	1.429	0.7	0.000
0.725	1.379	0.725	0.000
0.75	1.333	0.75	0.000
0.775	1.29	0.775	0.000
0.8	1.25	0.8	0.000
0.825	1.212	0.825	0.000
0.85	1.176	0.85	0.000
0.875	1.143	0.875	0.000
0.9	1.111	0.9	0.000
0.925	1.08	0.926	0.000
0.95	1.052	0.951	0.000
0.975	1.025	0.976	0.000
1	0.999	1.001	0.001
1.025	0.974	1.027	0.001
1.05	0.95	1.053	0.001
1.075	0.927	1.078	0.001
1.1	0.905	1.105	0.002
1.125	0.884	1.131	0.002
1.15	0.864	1.158	0.003
1.175	0.844	1.185	0.004
1.2	0.825	1.213	0.004
1.225	0.806	1.241	0.005
1.25	0.787	1.271	0.007
1.275	0.769	1.301	0.008
1.3	0.75	1.333	0.01
1.325	0.732	1.366	0.012
1.35	0.714	1.401	0.014
1.375	0.695	1.438	0.017
1.4	0.677	1.478	0.02
1.425	0.657	1.521	0.023
1.45	0.638	1.568	0.028
1.475	0.617	1.621	0.032
1.5	0.596	1.679	0.038
1.525	0.574	1.744	0.045
1.55	0.55	1.817	0.052
1.575	0.526	1.902	0.061
1.6	0.5	2	0.071
1.625	0.473	2.113	0.082
1.65	0.445	2.247	0.096
1.675	0.416	2.405	0.111
1.7	0.386	2.592	0.129
1.725	0.355	2.817	0.15
1.75	0.324	3.086	0.174
1.775	0.293	3.411	0.201
1.8	0.263	3.804	0.232
1.825	0.234	4.28	0.267
1.85	0.206	4.855	0.306
1.875	0.18	5.55	0.351
1.9	0.157	6.388	0.401
1.925	0.135	7.395	0.456
1.95	0.116	8.601	0.516
1.975	0.1	10.037	0.583
2	0.085	11.74	0.655

Table 4.1: Equivalent Temperature Scales for the HXY and Harmonic Models with $L = 16$: The temperature of the HXY model is given as T. T_{eff} and K_{eff} are the effective temperature and spin wave stiffness respectively – i.e. relating to the Harmonic model in which all vortices have been renormalized out. The RG expansion parameter y is a measure of the vortex density.

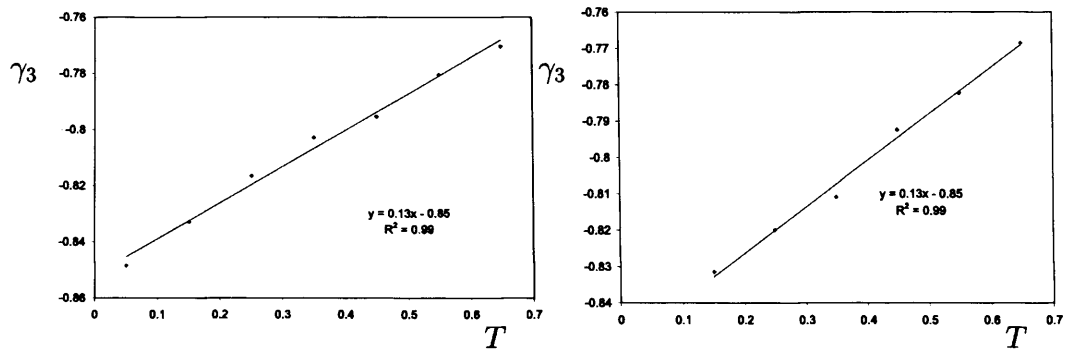

(a) (b)

Figure 4.17: $\gamma_3(T)$ at Low Temperatures: This figure shows the variation of the skewness at low temperatures for (a) the Harmonic and (b) HXY models. The dependence is linear in both cases with essentially the same form. Given that the HXY vortex density in this region is effectively zero, the implication is that the corrections to universality described in the text must arise from MLGs.

4.5.3 Vector, Cosine and Quadratic Order Parameters

There are two definitions of the order parameter in §4.3,

$$m = \frac{1}{N}\sqrt{\left(\sum_{\mathbf{r}} \mathbf{S}_{\mathbf{r}}\right)^2} \tag{4.102}$$

and

$$m = \frac{1}{N}\sum_{\mathbf{r}} \cos\psi_{\mathbf{r}}. \tag{4.103}$$

These will be referred to these as the vector and cosine order parameters respectively. Another version of m is obtained by expanding the cosine form as a power series and discarding all terms higher than the quadratic,

$$m = 1 - \frac{1}{2N}\sum_{\mathbf{r}} \psi_{\mathbf{r}}^2. \tag{4.104}$$

This is referred to in the literature, perhaps surprisingly given the quadratic nature of the expression, as the linearized order parameter[6] – for consistency the same nomenclature is used in this work.

The cosine order parameter is necessary for analytical development of spin wave theory and, as has been metioned before, differs only slightly from the more traditional

vector definition. To enable direct comparison with the spin wave predicitions, this form has been used in all the simulations discussed above.

The Vector Order Parameter

A cautionary word regarding the name of this form of the order parameter. The 'vector' is used to emphasize the role of the vector spins in this definition of m. *The magnetization itself remains a scalar.* Using the vector order parameter in the Monte Carlo simulations does not alter the results for the XY and HXY models in any noticeable way. However, simulations of the Harmonic model reveal a different pattern of behaviour. At low temperatures the PDF is found to be BHP like as expected, and the skewness is even seen to vary with T in a similar manner to before (Figure 4.18). However, as the temperature is increased, the PDF does not tend towards a Gaussian, but becomes Maxwellian as in the XY and HXY models. This ties in with the discussions in §4.5.1 regarding the effect of negative values of m. It was argued that the appearance of a Gaussian high temperature distribution was the result of a balancing effect between positive and negative m, possible only in the Harmonic model. The vector order parameter is necessarily always positive and so has the same effect as constraining the spin variables to within the positive range of the cosine function in (4.26), explaining the observed Maxwell distribution.

The problem with this explanation is that negative values of m only become relevant at temperatures when the distribution is already Gaussian. In fact, our simulations reveal that while at $T/J = 20$ over 40% of the observed values of m are negative, this drops to below 1% for $T/J = 7$, even though the magnetization remains very nearly normally distributed. The observations may be rationalized by considering three temperature regions. At low T, where there are no vortices present in any model and no possibiliy of negative m, one expects essentially the same behaviour of the PDF across all models for both the vector and cosine order parameters. This is indeed the case. At high temperatures where the microscopic interactions are outweighed by entropic effects, one expects a random distribution of the magnetization. This manifests itself as a Maxwell distribution of speeds when m is constrained to be

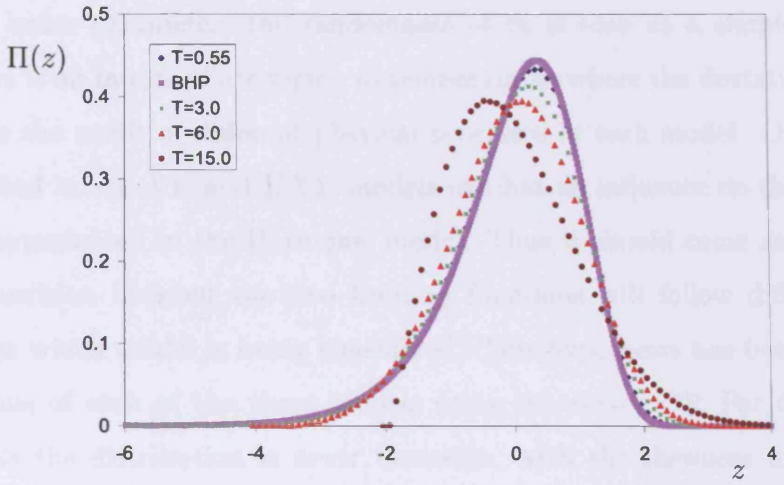

(a)

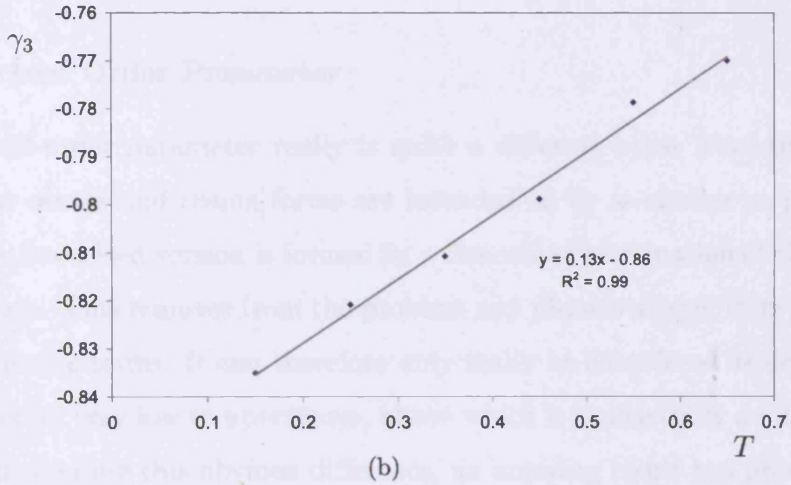

(b)

Figure 4.18: Monte Carlo Results for the Harmonic Model with Vector Order Parameter ($L = 16$): Part (a) shows the variation of the distribution as a function of temperature. At low T the curve closely approximates the BHP form, but it becomes Maxwellian at high temperatures. Unlike the XY and HXY models, the intermediate functions pass very close to a Gaussian (see $T = 6.0$). Part (b) shows the low temperature variation of the skewness as a function of T. The least squares fit through the data is functionally very similar to that seen for the cosine order parameter - the small deviations being attributable to the differences between the two OPs for small N and fluctuations in γ_3.

positive, either by restricting the spin variables or using the vector order parameter. In the unique case where m can take negative values, that is the Harmonic model with cosine order parameter, the randomness of m is seen as a simple Gaussian. Finally, there is an intermediate region of temperatures where the deviation from the BHP form is the result of different phsyical processes in each model. Once vortices start to unbind in the XY and HXY models one has an influence on the PDF that can not be experienced in the Harmonic model. Thus it should come as no surprise that the transition between the two limiting functions will follow different paths depending on which model is being considered. This hypothesis has been confirmed by simulations of each of the three models using the vector OP. For the XY and HXY models the distribution is never Gaussian, with the skewness and defect of kurtosis being zero at different temperatures. For the Harmonic model with vector order parameter the transition from BHP (low T) to Maxwellian (high T) does pass through an approximately Gaussian form.

The Linearized Order Parameter

The linearized order parameter really is quite a different beast from the other two options. The vector and cosine forms are intended to be as similar as possible. By constrast the linearized version is formed by a Draconian termination of the expanded cosine function. This removes from the problem any physics arising from the analytic but non-harmonic terms. It can therefore only really be considered as describing the magnetization at very low temperatures, above which it is physically a different quantity. Notwithstanding this obvious difference, an amazing result has previously been derived showing that, for the Harmonic model, the distribution of the linearized order parameter is *analytically identical* to the BHP function [6] as is shown in Chapter 5.

Simulations of the Harmonic model using the linearized order parameter have been performed over range of temperatures for a system with $N = 1024$. The results are in stark contrast to those seen for either the vector or cosine forms. The BHP distribution is again seen at low temperatures, however as T is increased there is no observable change in $\Pi(z)$ which always remains BHP like.

This leads to the conclusion that the equivalence of the distributions derived for the cosine and linearized order parameters is the result of making low temperature approximations in each case. For the linearized order parameter the neglect of higher order terms in the expansion of the cosine may be thought of as a low temperature approximation. At low T the $\psi_{\mathbf{r}}$ variables are generally small and the linearized form more closely approximates the cosine function. What was remarkable about the results in [6] was that the equivalence of the two distributions was valid even at high T when this argument breaks down.

The work presented here sheds light on this apparent anomaly. The neglect of multiple loop graphs in the derivation of the BHP function leads to a temperature independent distribution. However, we have shown that this approach removes contributions to the moments from higher powers of T. In this way the neglect of MLGs is interpreted as a fundamentally low temperature approximation. In other words, one can impose a low temperature on the Harmonic model either by approximating the moments, or by directly simplifying the order parameter. Whichever method is used, the result is the same, temperature independent, distribution of m.

It should be emphasized that arriving at the same $P(m)$ via these two approximations is, in itself, something remarkable. The non-universality of the BHP function with respect to temperature is now clear. However, there is no immediate analytical equivalence between neglect of MLGs and use of the linearized order parameter - only a heuristic argument regarding low temperatures. On this basis it is a significant, and very interesting, result that one rigorously obtains the same PDF in each case.

The restriction to SLGs was originally useful as it provided a route through an otherwise apparently intractable problem. In using such partial summations the hope is always that one retains the most significant physics, at least to first order. It is tempting to conclude that the MLGs represent the higher order terms in the cosine order parameter, with SLGs corresponding to only harmonic contributions. This has not been shown directly, but there is certainly evidence to this effect. If true there are possible implications for the use of partial graph summations in other contexts.

For completeness we report that the results of simulations on the 2dXY and HXY

models with linearized order parameter recover the BHP function only at very low temperatures, below about $T/J = 0.1$.

4.5.4 Is There Phase Transition in the Harmonic Model?

The Kosterlitz-Thouless transition separates two phases with distinct behaviour of the susceptibility. In the case of the 2dXY model, one phase is entirely critical and the other paramagnetic. The results presented here regarding the Harmonic model therefore pose some interesting questions. At low T the statistics are clearly non-Gaussian, indicative of a critical system with a high degree of correlation. However above $T/J \approx 4\pi$ the onset of a new regime is seen with normally distibuted m for all N and T. Equally, the susceptibility remains divergent at low temperatures, but this behaviour changes, to a first approximation, at $T/J = 4\pi$, above which the susceptibility approaches zero with increasing N (see (4.40)). There is, however, no change in the behaviour of the magnetization as one passes through this point as one would expect for a true phase change.

On the critieria used by Kosterlitz and Thouless it appears as though a change in regime occurs. Certainly the statistics are manifestly different in the two regions. The susceptibility data is slightly ambiguous though, as it depends on the N and T dependence given in §4.3.2 which is only a first approximation. What is fair to say is that the Harmonic model appears to be non-critical at high temperatures suggesting that thermal excitation of very high energy spin waves destroys long distance correlations.

The KT transition is associated with the onset of topoligical order, which suggests that, if such a transition were to occur in the Harmonic model, a suitable topological defect must be found. We have identified one such defect, and, rather surpringly, it is a spin vortex. Care must be taken here as to the definition of what constitutes a vortex when the spin variables are not periodic. The standard definition in the 2dXY model is a region of spins around which tracing a closed path results in a change in angle of $2n\pi$ where n is the vorticity. To calcuate the 'change in angle' one evaluates $\theta_{\mathbf{r}} - \theta_{\mathbf{r}'}$ for each neighbouring pair of spins on the closed path, making

sure to correct each of these differences such that they lie in the range $\pm\pi$ [110]. When the spins are freely varying this 'correction' is meaningless, however without it, simply summing the differences will always lead to zero. We propose that a suitable method for evaluating vortices in this case is to consider the relative 'windings' of neighbouring spins on the path. For example, if two spin variables have a difference of more than π, the winding number of that pair is simply the integer number of times 2π must be subtracted to bring the difference into the range $\pm\pi$. Similarly, if the difference is less than $-\pi$ the winding number is the negative of the number of time 2π must be added. Summing the winding numbers of each pair on the closed path then defines the vorticity. It is readily seen that when the spins are confined as in the 2dXY and HXY models our approach reduces to the usual form.

Simulations of the Harmonic model with $N = 3600$ reveal a surprising pattern of behaviour. The results are presented in the form of lattices showing the location of spin vortices in Figure 4.19. At low temperatures there are no vortices – which is as expected given that the Hamiltonian for this model explicitly includes only harmonic spin waves. However, at $T/J = 1.5$, the presence of a tightly bound vortex/anti-vortex pair can be seen. As the temperature is raised slightly the number of such pairs increases, sometimes occuring close together forming small clumps of vortices (each with overall neutrality). At $T/J = 3$ there is the first evidence of unbinding with two vortex pairs separating, each by just a single lattice spacing. However, as the temperature is raised one only sees this limited separation before the vortex density becomes so high that it is hard to identify distinct clusters.

These observations pose several questions, not least of which is the origin of vortices in a 'vortex-free' model. The explanation of this is made easier by the fact that there appears to be only one way in which the vortices can occur. The Harmonic model Hamiltonian includes only harmonic spin waves; as such it must be the case the vortices we observe are the result of a superposition of these waves, indicating that the two are not seperable. This result, whilst interesting, should not affect any of the previous low temperature work done on the Harmonic model, or indeed the 2dXY, Villain or HXY models. In these cases, where necessary, the spin wave contribution

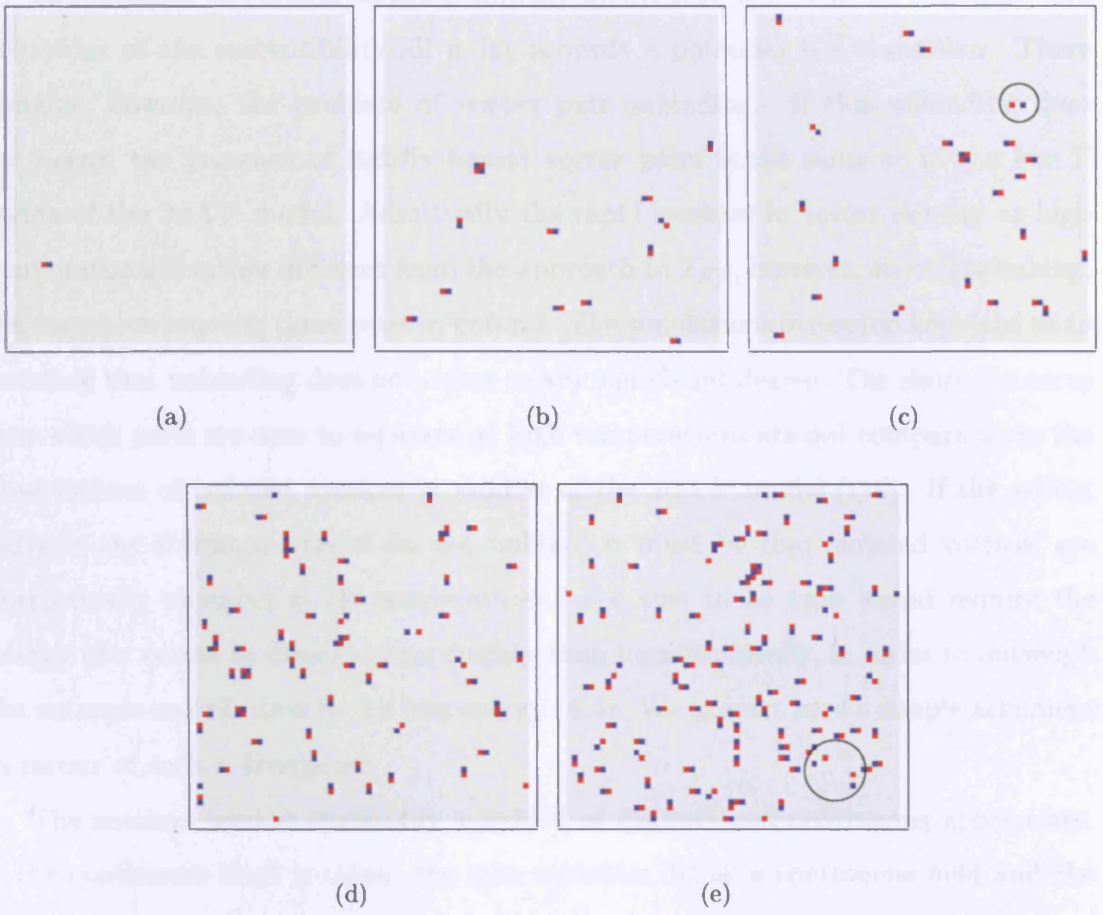

Figure 4.19: Vortices in the Harmonic Model: These figures are snapshots of the Harmonic model with $N = 3600$ at (a) $T/J = 1.5$, (b) $T/J = 2.0$, (c) $T/J = 2.5$, (d) $T/J = 3.0$ and (e) $T/J = 3.5$. At low temperatures one sees the surprising emergence of a tightly bound vortex/anti-vortex pair. As T is increased the number of such pairs also goes up, until, at $T/J = 2.5$, there is evidence of pair unbinding (circled). There are further examples of this unbinding at higher T - the circle in (e) shows a 'group' of free vortices apparently stabilized by the high density of vortex pairs in the surrounding region - however the separation distances are only ever very small. By the time the temperature reaches $T/J = 4.0$ the vortex density is so high it hard to dinstinguish between clusters of vortices. Here the blue squares represent a vorticity of -1, the red squares a vorticity of +1.

to the energy was regarded as a perturbation to the vortex minima. The temperatures considered were never sufficient to excite vortices in the spin wave component.

The presence of vortices in the Harmonic model together with the statisitics and behaviour of the susceptibility all point towards a potential KT transition. There remains, however, the problem of vortex pair unbinding. If this unbinding does not occur, the presence of tightly bound vortex pairs is the same as in the low T region of the 2dXY model. Admittedly the rapid increase in vortex density at high temperatures is rather different from the approach to T_{KT}, however, strictly speaking, the transition requires these pairs to unbind. The simulations presented here lead us to conclude that unbinding does not occur to any significant degree. The short distances over which pairs are seen to separate at high temperatures are not comparable to the observations of isolated vortices in studies of the 2dXY model [110]. If the vortex pairs in the Harmonic model do not unbind, it must be that isolated vortices are energetically unstable at all temperatures. For this to be true would require the energy of a vortex to diverge more quickly than logarithmically, in order to outweigh the entropic contribution to the free energy (4.4). We present here a simple argument in favour of such a divergence.

The method used is essentially a hybrid of discrete and continuous approaches. If the continuum limit is taken, the spin variables define a continuous field and the Hamiltonian becomes

$$H = \frac{J}{2}\int (\nabla\theta)^2 \, \mathrm{d}^2\mathbf{r}. \tag{4.105}$$

For a configuration consisting of only a single vortex the only contribution to the energy is from that vortex. Thus E_{vor} may be found by simply evaluating $\nabla\theta$, converting to polar coordinates and integrating. This works well for periodic spins, however when the spins are inifinitely variable there is a discontinuity in $\nabla\theta$ within the range of integration. This is where the recognition of the discrete nature of the lattice becomes useful.

It is assumed that, within the continuous picture one can draw circular paths around the vortex core. One then considers these paths to be the limit of a series of discrete steps. All spins lying on the same radial line emanating from the vortex core

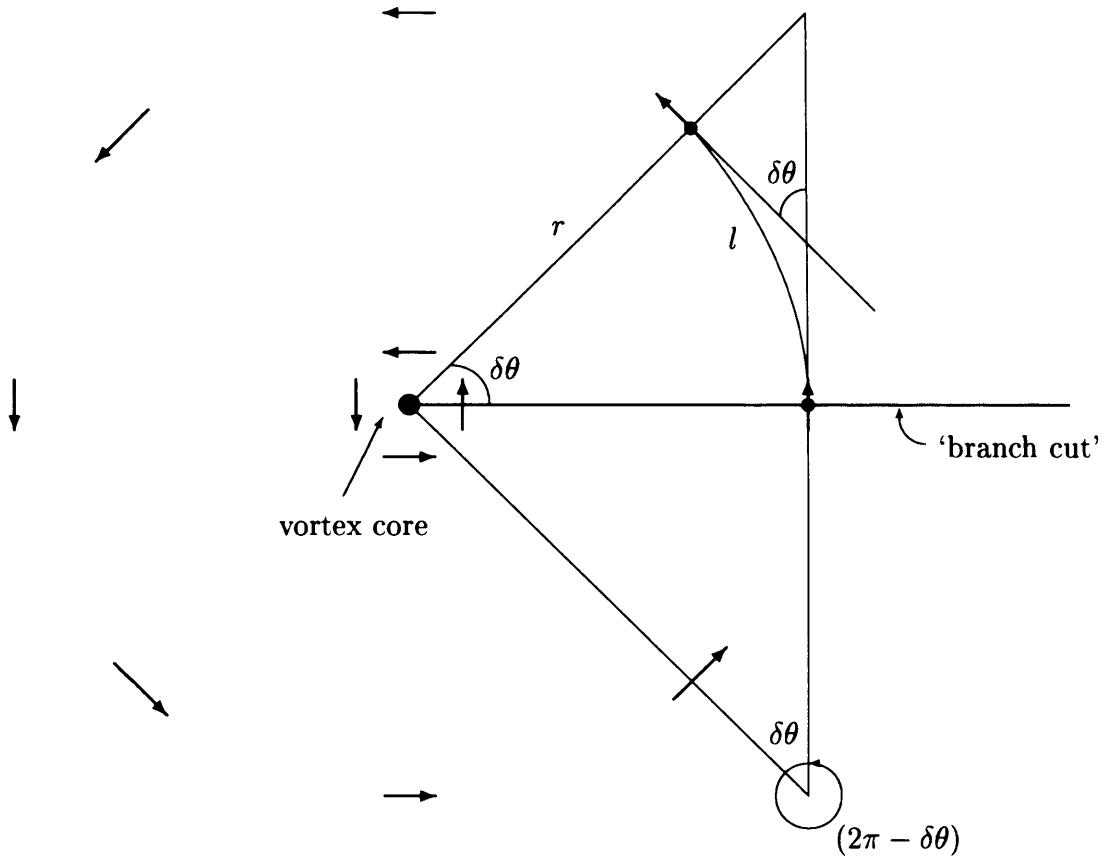

Figure 4.20: Energy of an Isolated Spin Vortex: This Figure is a schematic representation of the construction used to determine the energy of a vortex, as discussed in the text. Starting at one spin and tracing a circular path around the vortex core introduces contributions to the energy from the small angular displacements beteen neighbouring spins. The absolute difference between the first and last spins on the path is not, however, small. For periodic spins this makes no difference as the differences are considered modulo 2π, however for non-periodic spins the large contribution to the energy must be included explicitly. The 'branch cut' therefore marks the line across which $\nabla\theta$ is discontinuous in the limit of a continuum approximation for the field defined by the spin variables. In this diagram a periodic spin would be in the range $(0, 2\pi)$, rather than $(-\pi, \pi)$, though this is just a shift in the origin and has no effect on the energy.

can be assumed to be pointing in the same direction - thus there is no contribution to the energy from interactions between circular paths. All that remains in determining E_{vor} is to evaluate the energy associated with each circular path around the core, and to integrate over r.

Along each path the contribution to the energy from neighbouring pairs of spins is

$$\delta E = J\frac{(\delta\theta)^2}{2}, \tag{4.106}$$

where $\delta\theta$ is the (discrete) angular change in variable on going from one spin to the next. Also the arc length around the circular path between two neighboring spins is a constant, say l, of the order of the lattice spacing a, thus

$$\delta\theta = \frac{l}{r}. \tag{4.107}$$

This is true for all but the last step on the path where the difference between the first and last spins is

$$\theta_{\text{last}} - \theta_{\text{first}} = 2\pi - \delta\theta. \tag{4.108}$$

For periodic spins the difference $\theta_{\mathbf{r}} - \theta_{\mathbf{r}'}$ is required to be in the range $\pm\pi$ reducing the RHS of (4.108) to simply $\delta\theta$ - the same as for all the other 'steps' around the path.

Given that there are $2\pi/\delta\theta$ pairs of spins on a path, the energy of each path is given by

$$\Delta E = J\frac{2\pi}{\delta\theta}\frac{(\delta\theta)^2}{2} \tag{4.109}$$

$$= J\pi\frac{l}{r}. \tag{4.110}$$

The energy of the vortex therefore goes as

$$E_{\text{vor}} = J\pi l\int_a^L \frac{\mathrm{d}r}{r} \tag{4.111}$$

$$= J\pi l \ln\left(\frac{L}{a}\right), \tag{4.112}$$

which, setting $l = a = 1$ is the same result as (4.2), derived in a purely continuous context. Our approximations are quite drastic. It is not possible to draw circular

paths between neighbouring spins on a discrete square lattice. Furthermore the lack of interaction between circular paths assumes neighbouring spins lie on the same radial lines. Despite this, the fact that this method yields the same result as is obtained (more rigorously) using a consistent continuum approach provides *a posteriori* justification of our approximations.

On this basis we modify the results for the case of infinitely variable spins. There is now no possibility of 'winding back' spins so that differences lie in specific range. Thus the last step around a path must be expressed as in (4.108) and summing the energy around a path gives,

$$\Delta E = J\left(\frac{2\pi}{\delta\theta} - 1\right)\frac{(\delta\theta)^2}{2} + \frac{(2\pi - \delta\theta)^2}{2} \tag{4.113}$$

$$= J(2\pi^2 - \pi\delta\theta). \tag{4.114}$$

Integration over r gives

$$E_{\text{vor}} = J\pi\int_a^L \left(2\pi - \frac{l}{r}\right) \mathrm{d}r \tag{4.115}$$

$$= 2J\pi^2(L-a) - J\pi l \ln\left(\frac{L}{a}\right). \tag{4.116}$$

Thus the vortex has an energy which diverges as $\sqrt{N}$ and so is unstable at all temperatures. The cause of this instability is a line radiating from the vortex core across which $\nabla\theta$ is not analytic, analogous to a branch cut. For convenience we have chosen this line to be along $\theta = 0$, however it can point in any direction.

The only way to stabilize a vortex is to truncate the line by introducing a vortex of opposite vorticity, thereby creating a vortex pair. For paths of radius r encircling a vortex pair with separation R, the effects of the two vortices cancel out for $r \gg R$, and so the energy of the vortex pair is determined by the energy of interaction between the two cores. If an isolated vortex is viewed as part of a pair with $R \sim \mathcal{O}(L)$, given that the line of discontinuous $\nabla\theta$ is responsible for the leading order terms in E_{vor}, it is clear that

$$E_{\text{pair}} \sim \mathcal{O}(R - \ln(R)). \tag{4.117}$$

Isolated vortices are energetically unstable for all T in the Harmonic model. Our simulations reveal that the superposition of high energy spin waves is sufficient to create topological defects in the form of spin vortices. However these defects occur only in tightly bound pairs with energies that scale linearly with the distance between the cores. The minor degree of unbinding that is seen in our simulations may be ascribed to the relaxation of one pair in the field of numerous surrounding vortices. Thus it must be concluded that, despite the evidence from statistics and the behaviour of the susceptibility, no Kosterlitz-Thouless transition can occur for the Harmonic model.

4.6 Conclusion

The original result of [6] was a PDF which was truly universal and had been seen to describe the statistics of a range of critical systems. In the light of the work presented here it must be concluded that strict universality does not hold. However the observed dependence on temperature is very weak. From a visual point of view the distribution looks essentially the same throughout the vortex free region of the 2dXY model. One must employ a semi-log plot to see the variation with T which is evident only in the wings. It remains a very interesting result that the general functional form of the distribution is observed for a wide array of critical and self-organized critical systems from a variety of universality classes.

Despite the weakness of the temperature dependence, we feel that the confirmation of its existence is an important result. Much literature has grown up around the unusual behaviour of fluctuations in the 2dXY model. Our findings should help guide the search for universality in other systems, as well as preventing the need for any physical explanation of the apparent universality in this one.

We have highlighted the need for careful definition of the order parameter and the effect this may have on the statistics one obtains from simulations. This goes hand in hand with the ever present difficulties concerning the range of the spin variables. Most significantly it has been shown that equivalence between the distributions obtained

using the cosine and linearized order parameters is the result of the imposition of low temperature in both cases – by neglect of MLGs and anharmonic terms respectively.

We conclude the assertion that the Harmonic model is 'vortex free' is true only in the sense that vortices do not appear explicitly in the Hamiltonian. However, by introducing a definition of vortices consistent with infinitely variable spins, we have identified tightly bound vortex pairs at high temperatures which we conclude are the result of the superposition of high energy spin waves. The crossover to a Gaussian statistical regime at $T \approx 4\pi$ for the Harmonic mode, coupled with the fact that the susceptibility appears not to diverge above this point, are suggestive of a Kosterlitz-Thouless transition. However, this would require the unbinding of vortex pairs and we have shown that such a phenomenon is not energetically viable.

Chapter 5

One Dimensional Critical Models

In Chapter 4 it was shown that the magnetization distribution for the 2dXY model was not, as was once thought, a single universal function, but is weakly dependent on temperature. There are, therefore, distinct PDFs for each of the $\eta(T)$ dependent universality classes represented in the critical region – though the functional forms of these distributions are seen to be very similar. Distributions of this general form have been observed for quantities belonging to a range of universality classes, resulting from physical experiments and numerical simulations [18–21, 29, 33–41, 48]. We know that there is no critical equivalent of the Gaussian distribution toward which PDFs tend when the CLT breaks down. However, the similarity of distributions from so many different critical systems suggests the possibility that there may be a general functional form, or at least certain constraints on the shape of their PDFs.

This chapter examines the conditions that must be met for a system to be deemed critical, and, following [48] and [25] a reciprocal space model is identified which we argue may be considered critical in general dimension d. The cumulants of these systems may be determined numerically to arbitrary precision and the similarity of the distributions for the first three dimensions is highlighted. In the case $d = 1$ it is possible to revert to direct space and obtain a Hamiltonian model with infinite range interactions; two such models are derived and analysed. A link with the field of extremal statistics is discussed, as are the contributions to the critical PDFs from different regions of the Brillouin zone.

5.1 The Origins of Non-Gaussian Fluctuations in the 2dXY Model

The linearized order parameter for the two dimensional XY model was defined in Chapter 4 as

$$m = 1 - \frac{1}{2N}\sum_{\mathbf{r}} \psi_{\mathbf{r}}^2. \tag{5.1}$$

Remarkably, using this definition together with the Harmonic model Hamiltonian gives rise to the same magnetization distribution as is arrived at by neglecting multiple loop graphs in the expansion of the moments of the related cosine form of m (4.26) [6]. This is most easily seen by deriving expressions for the cumulants in each case and showing that they are the same.

The BHP function, derived in Chapter 4 using the cosine order parameter, may be expressed as

$$P(m) = \int_{-\infty}^{\infty} \frac{\mathrm{d}x}{2\pi\sigma} \exp\left[ix\frac{m - \langle m\rangle}{\sigma} + \sum_{k=2}^{\infty} \frac{g_k}{2k}\left(ix\sqrt{\frac{2}{g_2}}\right)^k\right]. \tag{5.2}$$

Comparing this with the definition of the characteristic function, $\phi(s)$,

$$P(x) = \int_{-\infty}^{\infty} \frac{\mathrm{d}s}{2\pi} e^{isx}\phi(s), \tag{5.3}$$

it is seen that

$$\phi(x) = \exp\left\{\sum_{k=2}^{\infty} \frac{g_k}{2k}\left(ix\sqrt{\frac{2}{g_2}}\right)^k\right\} \tag{5.4}$$

is the characteristic function of the normalized BHP distribution. Therefore,

$$\ln(\phi(x)) = \sum_{k=2}^{\infty} \frac{(ix)^k}{k!}\frac{(k-1)!g_k}{2}\left(\frac{2}{g_2}\right)^{\frac{k}{2}}, \tag{5.5}$$

and the k^{th} normalized cumulant of the distribution is

$$\kappa_k = \frac{(k-1)!g_k}{2(g_2/2)^{k/2}}. \tag{5.6}$$

The reciprocal space form of the Harmonic model Hamiltonian,

$$H = \frac{J}{2}\sum_{\mathbf{q}\neq 0} |\gamma_{\mathbf{q}}||\psi_{\mathbf{q}}|^2, \tag{5.7}$$

shows the system to be phase independent, so the modulus notation may be dropped with regard to the spin variable, where it is understood that $\psi_{\mathbf{q}}$ represents a real function defined on the interval $\pm\infty$. Parseval's theorem then allows the magnetization (5.1) to be expressed as

$$m = 1 - \sum_{\mathbf{q}\neq 0} m_{\mathbf{q}}, \tag{5.8}$$

where $m_{\mathbf{q}} = \frac{1}{2N}\psi_{\mathbf{q}}^2$. On this basis, $\psi_{\mathbf{q}}$ is Gaussian with zero mean and $P(m_{\mathbf{q}})$ becomes $\Gamma_{\frac{1}{2}}$ distributed (Appendix B),

$$P(m_{\mathbf{q}}) = \sqrt{\frac{\beta J N q^2}{\pi}} m_{\mathbf{q}}^{-1/2} e^{-\beta J q^2 N m_{\mathbf{q}}}, \tag{5.9}$$

where $\beta = 1/T$ and the approximation $\gamma_{\mathbf{q}} \approx q^2$ has been used, which is reasonable given the dominance of the low frequency modes.

Fourier transforming (5.9) yields expressions for the cumulants of the distribution of a single mode. Given the independence of the $m_{\mathbf{q}}$, the cumulants of m are then found by summing these expressions over $\mathbf{q}$. This is shown in detail in Appendix B, the result for the k^{th} normalized cumulant being

$$\kappa_k = \frac{\frac{1}{2}(k-1)! \sum_{\mathbf{q}\neq 0} \left(\frac{1}{|\mathbf{q}|^2}\right)^k}{\left(\frac{1}{2}\sum_{\mathbf{q}\neq 0}\left(\frac{1}{|\mathbf{q}|}\right)^4\right)^{k/2}}. \tag{5.10}$$

Recalling that $g_k = (1/N^k)\sum_{\mathbf{q}\neq 0}\gamma_{\mathbf{q}}^{-k}$, with $\gamma_{\mathbf{q}} \approx |\mathbf{q}|^2$, reveals that (5.6) and (5.10) are the same. It has been demonstrated in the previous chapter that this remarkable result arises from the 2dXY model as a consequence of imposing low temperatures. This is explicit in the case of the linearized order parameter as the neglect of anharmonic terms may be considered a fundamentally low temperature approximation. For the cosine OP the effect is more subtle, arising from the neglect of multiple loop graphs in the expansion of the moments. Given that these two approximations have not been shown to be the same analytically, it is interesting that they give rise to the same distribution. Furthermore this function is undoubtedly independent of temperature and can be viewed as representing magnetization fluctuations in the 2dXY model as $T \to 0$.

Viewing the magnetization in reciprocal space like this provides a useful insight into the origins of the non-Gaussian behaviour of m [6], with the central limit theorem being violated in both direct and reciprocal space. Infinite correlations in direct space mean that the critical 2dXY model can not be broken into mesoscopically independent regions. The failure of the CLT in reciprocal space is for an entirely different reason. Here the model is diagonalized into independent normal modes. However the requirement that the microscopic degrees of freedom be individually negligible [1] does not apply. This criterion is broken as a consequence of the dispersion in amplitudes of the normal modes. For example, the lowest frequency modes near $\mathbf{q} = 0$ have wavevectors with modulus $|\mathbf{q}| = 2\pi/L$ which make contributions of $\mathcal{O}(1)$ to the magnetization. Compare this with the microscopic amplitudes of the modes near the boundaries of the Brillouin zone, and it is seen that the low frequency modes are individually significant.

The average of the linearized order parameter is [6]

$$\langle m \rangle = 1 - \sum_{\mathbf{q} \neq 0} \langle m_{\mathbf{q}} \rangle \tag{5.11}$$

$$\sim \int_{\mathrm{BZ}} \frac{\mathrm{d}\mathbf{q}}{q^2}. \tag{5.12}$$

Therefore $\langle m \rangle$ diverges logarithmically for $d = 2$ and the upper and lower limits of the integral are both important, in much the same way as was seen when deriving g_k in Chapter 4. Contrast this with the case for $d = 1$ in which the magnetization depends strongly on the lower limit but the upper limit may be set to infinity without loss of generality. Or, in three dimensions, where the upper limit dominates and the lower limit may be set to zero.

In both these situations an exponential tail to the PDF is still observed, but not as a result of criticality, highlighting that non-Gaussianity of a global quantity is not sufficient evidence to infer critical fluctuations. In the case of the 1d Harmonic model with linearized order parameter, the average magnetization and standard deviation scale as [6]

$$\langle m \rangle \sim N \qquad \text{and} \qquad \sigma \sim \langle m \rangle^2, \tag{5.13}$$

so m cannot be normally distributed. However, a quantity $w \sim \sqrt{1-m}$ will have $\sigma_w \sim \sqrt{N}$ and is therefore a suitable central limit theorem variable. Another way to view this is that while the constituents of one global quantity, such as w, may obey the criteria of independence and individual negligibility, another global quantity need not. Indeed, if $w = \sum_i w_i$ and $w^2 = \sum_i w_i'$, then if the w_i are independent, the w_i' are necessarily correlated.

In reciprocal space where the magnetization is a sum over explicitly independent normal modes, the dispersion of these modes violates the criterion of individual negligibility in one dimension, just as it does for $d = 2$. However, the fact that only the lower limit of the integral (5.12) is important is an indication that only a few modes with low frequency are needed to define m. The magnetization is then no longer a sum over a large number of elements and the CLT does not apply.

In three dimensions the system is able to support long range order, with a non-critical low temperature region. However, T is now a dangerously irrelevant variable near the $T = 0$ fixed point [114], and at low temperature the low frequency modes retain some influence over the PDF. This results in $\sigma / \langle m \rangle \sim 1/N^{1/3}$ and the longitudinal susceptibility is weakly divergent throughout the ordered phase [6, 16]. In this case the non-Gaussianity is caused specifically by the Goldstone modes [64] and does not arise from many body effects.

Thus the critical nature of the two dimensional model is best characterized, not by evidence of non-Gaussian behaviour of the order parameter *per se*, but by the explicit many body nature of m coupled with the relevance of fluctuations on all length scales.

Discussions of critical probability density functions can sometimes appear to contain conflicting arguments. An important example is the conclusion that the PDF of the linearized order parameter in the two dimensional Harmonic model relies on all modes, despite the fact that the approximation $\gamma_{\mathbf{q}} \approx |\mathbf{q}|^2$ is regularly invoked because of "the dominance of the low frequency contributions". It has been shown that the PDF is not recovered quantitatively by considering just the smallest $\mathbf{q}$ behaviour [64]. However, the same study demonstrated that a good fit to the eye can be obtained

using only a small fraction, N_{eff}, of the modes, provided N is large. For $N \gg N_{\text{eff}}$ the error in the fit, δ, is independent of N. Importantly the many-body nature of the problem manifests itself in the requirement that the number of modes included must diverge for the error in the fit to go zero. That δ depends on only N_{eff} is consistent with the approximation $\gamma_{\mathbf{q}} \approx |\mathbf{q}|^2$, however it suggests that only the centre of the Brillouin zone is important. In contrast the fact that N_{eff} must be arbitrarily large to accurately reproduce the PDF indicates that the magnetization is truly a many-body quantity. Indeed, as argued in [64], the approach to a Gaussian form for a central limit theorem variable is a function of only N_{eff} for $N \gg N_{\text{eff}}$. These two observations are not inconsistent but they do mean that care must be taken to understand the origins of non-Gaussian fluctuations before deciding that they imply critical behaviour. For example, in the three dimensional Harmonic model the asymmetry of the PDF arises almost entirely from the softest modes [64] indicative of the general result for continuous spin models for $d = 3$ that the Goldstone modes, rather than any underlying criticality, lead to a departure from normal statistics.

5.2 Critical Fluctuations in d Dimensions

The Harmonic model approximation to the 2dXY model is directly equivalent to the Edwards-Wilkinson model of interface growth [21, 51]. The linearized order parameter relates to the 'width square' of the interface, w, as $m = 1 - w^2$, and studies of $P(w^2)$ show good qualitative agreement with the BHP function [46]. In many ways it is more reasonable to associate the linearized order parameter with an interface model than with a spin system. Unlike the vector (4.22) and cosine (4.26) forms of the magnetization the linearized m has lost all periodicity and is no longer constrained between limits. This is physically acceptable for an interface that is free to grow unbounded, but not for a magnetic system with spin variables in high energy configurations.

Thus it is worth generalizing the analysis somewhat, moving away from specifically magnetic models, and considering arbitrary dimension d. Following the analysis

in [25], the distribution function (5.9) is seen to be of the form

$$g(s_{\mathbf{q}}) = \frac{a_{\mathbf{q}}^{\gamma}}{\Gamma(\gamma)} s_{\mathbf{q}}^{\gamma-1} e^{-a_{\mathbf{q}} s_{\mathbf{q}}}, \tag{5.14}$$

where $s_{\mathbf{q}}$ replaces $m_{\mathbf{q}}$ as a general intensive gamma distributed variable depending on $\mathbf{q}$, a non-zero d dimensional vector with integer elements. Also $a_{\mathbf{q}}$ replaces $\gamma_{\mathbf{q}}$ as the mode weighting factor. By analogy with (5.9), the case of interest here has $\gamma = 1/2$ and $a_{\mathbf{q}} = \beta|\mathbf{q}|^{\alpha}$. When $\mathbf{q}$ is a wavevector it does not have integer elements, rather its elements are integer multiples of $2\pi/L$. As this extra factor may be taken outside the sum over $\mathbf{q}$, and disappears on normalization, the distinction can be ignored here.

Comparing (5.14) with (5.7) and (5.9) shows that the reciprocal space Hamiltonian which gives rise to the distribution (5.14) is

$$H = J \sum_{\mathbf{q}\neq 0} |\mathbf{q}|^{\alpha} \psi_{\mathbf{q}}^2, \tag{5.15}$$

where now $s_{\mathbf{q}} = (1/N)\psi_{\mathbf{q}}^2$ and it is again understood that $\psi_{\mathbf{q}}$ may be taken as a real variable defined on the interval $\pm\infty$, and is Gaussian with zero mean.

Defining the global quantity whose PDF is to be determined as $S = \sum_{\mathbf{q}\neq 0} s_{\mathbf{q}}$, where the sum is over N statistically independent $\Gamma_{\frac{1}{2}}$ variables, the r^{th} cumulant of $P(S)$ is (see Appendix B),

$$\kappa_r(S) = \frac{1}{2}(r-1)! \sum_{\mathbf{q}\neq 0} \left(\frac{1}{|\mathbf{q}|^{\alpha}}\right)^r. \tag{5.16}$$

As usual, the variate must be normalized by its standard deviation giving,

$$\kappa_r\left(\frac{S}{\sigma_S}\right) = \frac{\frac{1}{2}(r-1)! \sum_{\mathbf{q}\neq 0} \left(\frac{1}{|\mathbf{q}|^{\alpha}}\right)^r}{\left(\frac{1}{2}\sum_{\mathbf{q}\neq 0} \left(\frac{1}{|\mathbf{q}|}\right)^{2\alpha}\right)^{r/2}}, \tag{5.17}$$

so the nature of the PDF is governed by two parameters, the mode weighting α and the dimension d [25, 49]. As discussed by Antal *et al.* [49], the balance between these parameters may be used as a signature for different types of statistical regimes. One extreme has small d and large α. This scenario essentially negates the majority of contributions to the sums and reduces the problem to one where only the smallest $|\mathbf{q}|$ modes are important. The PDF then becomes a χ^2 distribution with $2d$ degrees

of freedom. At the other end of the scale, if α is small and d large, the sums are dominated by the many large $|\mathbf{q}|$ contributions. This makes the second cumulant large relative to the others, and the normalized PDF becomes Gaussian. Specifically, Gaussianity is seen for $d > 2\alpha$ as it is in this region that the variance dominates the higher cumulants [49].

It is the intermediate region that is of most interest in this study. Specifically, when $d = \alpha$ the average of the global quantity S diverges logarithmically with the size of the system. This raises questions regarding the definition of criticality. The usual signatures of critical systems include power laws and scaling behaviour. However, in the case of the Harmonic model with linearized order parameter, the average magnetization scales logarithmically. Furthermore, setting $d = \alpha = 2$ in (5.17) recovers (5.10) and it is seen that the while normalizing with respect to σ gives size independent cumulants for $r \geq 2$, the ratio $\langle m \rangle / \sigma \sim \mathcal{O}(\ln N)$ and hyperscaling is not obeyed. Yet we know that the two dimensional Harmonic model is inherently critical, in theory at all temperatures, as is demonstrated by the behaviour of the cosine order parameter, for which $\langle m \rangle$ scales as a power law and $\langle m \rangle / \sigma \sim \mathcal{O}(1)$. This returns to the point that the criticality, or otherwise, of a system, is governed by its Hamiltonian. In order to observe critical behaviour one must be looking at the correct quantity.

The infinite correlation length in critical systems leads to scale invariance and power laws of appropriate global measures, but there are other signs too. As mentioned above, the logarithmic divergence of $\langle m \rangle$ necessitates the explicit inclusion of both limits when integrating over the Brillouin zone, which we interpret as an indication of critical behaviour. The power law variation of the cosine form of m has an exponent that is directly proportional to the temperature. Given that

$$\log\left(\frac{1}{x}\right) = \lim_{y \to 0+} \frac{1}{y}(x^{-y} - 1), \tag{5.18}$$

a logarithmically varying global quantity may be interpreted simply as the low T limit of another measure varying as a power law with an exponent proportional to T. This is readily seen to be true for the magnetization, where the linearized form ignores

terms in the expansion of the cosine form which are relevant only as T increases.

In conclusion, setting $d = \alpha$ in (5.17) gives the cumulants of a distribution of a global quantity exhibiting critical fluctuations in the limit of low temperature. Thus the Hamiltonian (5.15) generates an inherently critical system for which a suitable order parameter will scale as a power law with a temperature dependent exponent.

5.2.1 Skewness-Kurtosis Space – Locations of Critical Distributions

The fact that we interpret setting $d = \alpha$ in (5.17) as defining a critical system means that the corresponding PDFs should be non-Gaussian – though this behaviour is not solely the preserve of critical systems, as discussed above. Given the proposal that critical statistics may have similar functional forms [19], it is expected that the distributions of S for $d = \alpha = 1, 2, 3$ should look relatively alike. A good illustration that this is so comes from a plot of defect of kurtosis against skewness as shown in Figure 5.1. The plot shows points in three series corresponding to the three dimensions, each with $\alpha = 0 - 20$, calculated with $N^{1/d} = 100$. The series overlap, covering only a narrow region of the available space. There is rapid convergence with increasing m, with the appropriate χ^2_{2d} limits being quickly reached.

The three points of interest, representing the critical systems with $d = \alpha$, are circled. Taking Figure 5.1 in isolation, there are two ways to interpret the positions of these points. The first is to be optimistic and observe that the three points occupy roughly the same region of the available space. Certainly, if one were to plot just these points on a plane whose boundaries defined the maximum possible skewness and defect of kurtosis for the three dimensions, they would have the appearance of a small cluster. Accepting this, their proximity to each other must imply a similarity of distributions, given that γ_3 and γ_4 describe the shape of the normalized PDF to a good first approximation.

It is perhaps a little unjustified to draw such conclusions and ignore the presence of numerous other nearby points. Many of these are fairly irrelevant as very large values

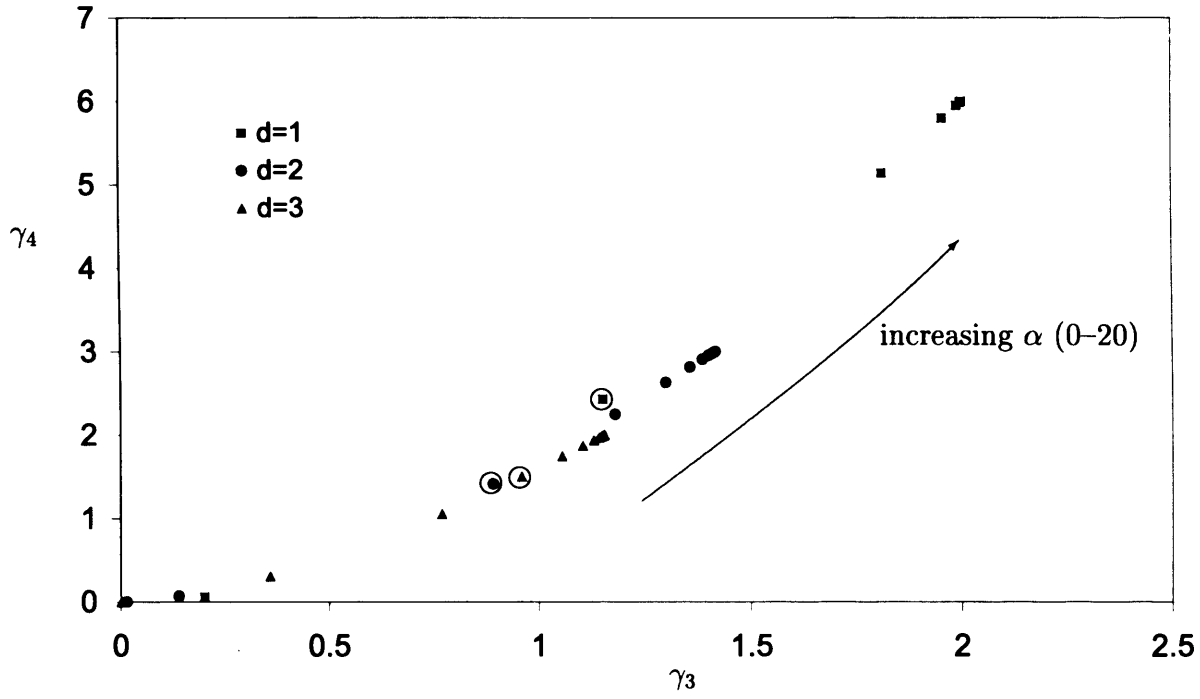

Figure 5.1: 'Skewness-Kurtosis' Space: The points are in three series for dimension $d = 1, 2, 3$ each having α in the range 0–20. The values of the skewness and defect of kurtosis were determined numerically from (5.17) with $L = N^{1/d} = 100$. The circled points correspond to the three critical systems with $d = \alpha$. Note that the finite size of the systems becomes evident for small α – although the numerical evaluations have converged, there are insufficient numbers of degrees of freedom for the Gaussian limit to be reached for $\alpha \leq d/2$ other than in three dimensions.

of α indicate such a dispersion of normal modes that effectively the χ^2_{2d} limit has been reached. In fact, the plot shows that the requirement of $\alpha \gg d$ for this to happen can reasonably be approximated by $\alpha - d \gtrsim 3$. However, this still leaves a number of potentially significant non-critical, non-Gaussian distributions. The presence of these ties in with the discussion in §5.1 and the conclusion that non-Gaussian statistics alone are insufficient to infer criticality.

It seems that the following conclusions can be drawn. Firstly, out of the range of available values, the three critical distributions do have similar skewnesses and defects of kurtosis, suggesting similar PDFs. This is in keeping with the idea that distributions of critical quantities obey functionally similar statistics. Secondly, there exist certain theoretical systems which, though not critical, have global quantities whose distributions occupy the same region of skewness-kurtosis space as the models with $d = \alpha$. This in no way negates the arguments regarding the statistical behaviour of the critical systems, but it does raise questions about the usefulness of these PDFs. For example, if an experiment yields values of the skewness and kurtosis within the ranges of the critical systems, it may be that the experimental system is itself critical, or simply that it is described by some other non-critical, non-Gaussian PDF that looks similar. A possible saving grace in this regard may be that the non-critical models in this region are purely mathematical toys and do not correspond to any physical system. This seems more likely as α becomes large, but there is really no reason to suppose that a system with, say, $d = 3$, $\alpha = 4$, should not exist. We discuss this point further in §5.7.

5.2.2 $d = \alpha = 1$: The Fisher-Tippet-Gumbel (FTG) Distribution

In order to see visually just how similar the three $d = \alpha$ critical PDFs are, it is necessary to have some means of determining their analytical form. The $d = \alpha = 2$ case is already known to be the BHP function. It is a remarkable, and in many ways intrigu-

ing, fact that setting $d = \alpha = 1$ yields the Fisher-Tippet-Gumbel distribution [48],

$$P(x) = be^{-(bx+\gamma)-e^{-(bx+\gamma)}}, \tag{5.19}$$

from the field of extremal statistics (where $\gamma \approx 0.577$ is Euler's constant and $b = \pi/\sqrt{6}$). Extreme value statistics (EVS) deal with the behaviour of global quantities whose constituent elements are drawn from the extremities of their own range of values – yet no extreme quantities were used in the derivation in [48]. We return to this interesting link in §5.5.

The question of immediate interest is how similar in shape the FTG and BHP functions are. The answer is really quite similar, the main differences being far out in the wings of the distribution, corresponding to very rare events. Figure 5.2 shows the two functions plotted on semi-log axes, highlighting the deviation for large fluctuations. It is certainly possible to distinguish between the analytical functions. However, the errors associated with experimental distributions may make it hard to be sure which form is being observed [115]. Certainly one would required good statistics to accurately represent the tails.

5.2.3 $d = \alpha = 3$ Distribution

Unlike in one dimension there is no known analytical form for the distribution function for the three dimensional critical system. Thus we are without a function to plot against the BHP and FTG distributions for comparison. To circumvent this problem it is possible to obtain an approximate PDF using a technique due to Pearson [91]. His method relies on the fact that two distributions whose first four moments are the same, are approximately coincident for a few standard deviation each side of the mean. As this is the region of greatest experimental interest one can reasonably describe the shape of a distribution with just these moments.

Pearson's analysis begins with the differential equation,

$$\frac{\mathrm{d}\ln P}{\mathrm{d}x} = -\frac{x + b_1}{b_0 + b_1 x + bx^2}. \tag{5.20}$$

When $P(x)$ is a probability density function, the constants b, b_0 and b_1 can be shown to be functions of the first four principle moments. Exactly what these functions are,

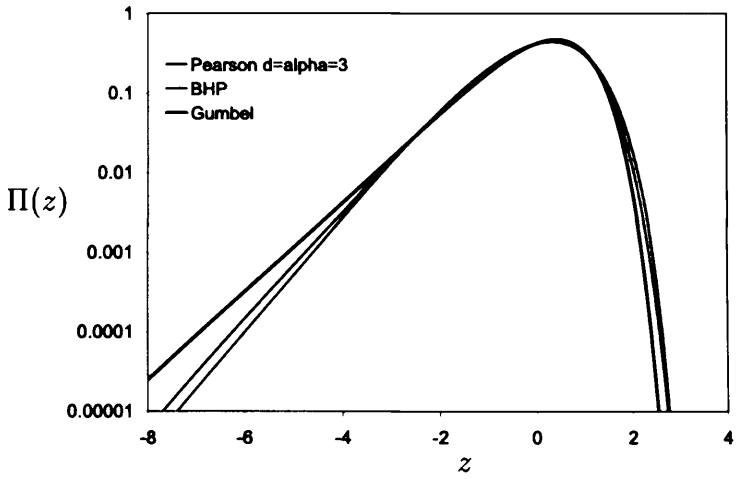

Figure 5.2: Comparison between $d = \alpha$ Critical Distributions: For $d = 1$ (Fisher-Tippett-Gumbel), $d = 2$ (Bramwell-Holdsworth-Pinton) and $d = 3$ (using a Pearson fit). The similarity is striking for several σ either side of the mean and the three functions may be difficult to distinguish experimentally. As usual, $z = (m - \langle m \rangle)/\sigma$ and $\Pi(z) = \sigma P(m)$.

and how they may be used to determine $P(x)$ is discussed in Appendix D. The result of the analysis for the $d = \alpha = 3$ model is,

$$P(\xi) = P_0 \left(1 - \frac{\xi}{\alpha}\right)^{p\alpha} \left(1 - \frac{\xi}{\beta}\right)^{p\beta}, \tag{5.21}$$

where there has been a shift in origin, $\xi = x - 0.35195$, and $P_0 = 0.43986$, $\alpha = 2.98404$, $\beta = 12.74363$ and $p = 4.78369$.

Looking back at the plot of skewness-kurtosis space one sees that the point corresponding to $d = \alpha = 3$ is much closer to the BHP function than is the FTG point. Therefore it is expected that the three dimensional model has a distribution which is even closer to the BHP form. The Pearson curve (5.21) is plotted against the other two in Figure 5.2 and indicates that this is so. It must be concluded, therefore, that it is likely to be hard to experimentally distinguish between the two. The BHP function and the distribution of power consumption in a turbulent flow have been observed to be very similar. Given that the latter is three dimensional it may be more fruitful to consider the similarity with the $d = \alpha = 3$ model.

5.2.4 Implications of the Functional Similarity

The consequences of the similarity of the three critical distributions are most important in the context of interpreting experimental and numerical data. First we note that the hypothesis of a general functional form for critical distributions, whilst not proved, is lent weight by the three examples cited here. The three all have an exponential tail for large fluctuations and can each be approximated to a reasonable degree by a generalized FTG distribution (see [6]),

$$P(x) = w\left(e^{b(x-s)-e^{b(x-s)}}\right)^a, \tag{5.22}$$

where

$$w = \frac{a^a b}{\Gamma(a)} \tag{5.23}$$

$$b = \sqrt{\frac{1}{\Gamma(a)}\frac{\partial^2\Gamma(a)}{\partial a^2} - \left(\frac{1}{\Gamma(a)}\frac{\partial\Gamma(a)}{\partial a}\right)^2} \tag{5.24}$$

$$s = \frac{1}{b}\left[\log(a) - \frac{1}{\Gamma(a)}\frac{\partial\Gamma(a)}{\partial a}\right]. \tag{5.25}$$

For the BHP function, as already mentioned, a takes the non-integer value of approximately $\pi/2$. For $d = \alpha = 1$ the FTG function is recovered, by definition, by setting $a = 1$. For $d = \alpha = 3$ the best fit requires $a \approx 1.84$.

If one observes a distribution experimentally that fits a generalized FTG function with a reasonable value of a, the associated errors may make it difficult to tie it specifically to one out the three distributions discussed here. There is also no guarantee that observing a distribution of this type implies an underlying criticality, as there are a number of possible non-critical models giving rise to similar non-Gaussian PDFs. As a result great care must be taken when drawing conclusions about the physics of a system based solely on the observation of a given probability distribution – even on such a coarse level as merely inferring critical behaviour.

5.3 A Direct Space Hamiltonian for the $d = \alpha = 1$ Model

Having identified a family of Hamiltonians in reciprocal space that represent critical systems, we now turn our attention to finding the corresponding direct space models. In two dimensions this means, as already stated, the low temperature limit of the 2dXY model. To find the appropriate direct space Hamiltonians in one and three dimensions involves Fourier transforming the reciprocal space expression (5.15). This is difficult in three dimensions, however for $d = 1$ the process is relatively straightforward. In fact, we have been able to identify two suitable direct space Hamiltonians which are so different in form that it is unlikely they would be linked other than via this method.

Before considering these models we note the approach taken by Antal *et al.* in their studies of $1/f^{\alpha}$ noise [48, 49]. They constructed an action

$$S(\{c_n\}) = 2\sigma T^{1-\alpha} \sum_{n=1}^{N} n^{\alpha} |c_n|^2, \tag{5.26}$$

designed such that the power spectrum of the associated time signal was of the required Gaussian $1/f^{\alpha}$ form. For $\alpha = 1$ they showed that the scaling function of the roughness of their signal is explicitly the FTG distribution [48]. It is no surprise then that our $d = \alpha = 1$ critical model also yields the FTG function [25] as the reciprocal space Hamiltonian (5.15) may be directly mapped onto (5.26). This is discussed in more detail in Chapter 6.

5.3.1 $d = \alpha = 1$ Spin Model 1

Our aim is to establish a model spin system in one dimensional direct space whose magnetization is FTG distributed. We have derived two such systems and begin with the more traditional approach. In general [116], a direct space Hamiltonian of the form

$$H = \frac{1}{2} \int \mathrm{d}\mathbf{r} \int \mathrm{d}\mathbf{r}' \, \theta(\mathbf{r}) G(\mathbf{r} - \mathbf{r}') \theta(\mathbf{r}'), \tag{5.27}$$

Fourier transforms to give,

$$H = \frac{1}{2} \sum_{\mathbf{q} \neq 0} G(\mathbf{q}) |\psi_{\mathbf{q}}|^2, \tag{5.28}$$

where $\psi_{\mathbf{q}}$ is the Fourier transform of $\theta(\mathbf{r})$, and,

$$G(\mathbf{q}) = \int \mathrm{d}\mathbf{r}\, G(\mathbf{r}) e^{i\mathbf{q}\cdot\mathbf{r}}. \tag{5.29}$$

Using an analogous set of equations for a discrete real lattice, a Hamiltonian

$$H = \sum_{r} \sum_{x=-L}^{L} c_x \theta_r \theta_{r+x}, \tag{5.30}$$

should produce the correct reciprocal space form when

$$|q| = c_0 + 2 \sum_{x=1}^{L} c_x \cos(qx). \tag{5.31}$$

For this to be true requires

$$c_0 = \frac{1}{\pi} \int_0^{\pi} |q|\, \mathrm{d}q \tag{5.32}$$

$$= \frac{\pi}{2} \tag{5.33}$$

$$c_{x \neq 0} = \frac{1}{\pi} \int_0^{\pi} |q| \cos(qx)\, \mathrm{d}q \tag{5.34}$$

$$= \frac{\cos(\pi x) - 1}{\pi x^2}. \tag{5.35}$$

Equation (5.30) contains contributions from all possible pairs of spins with a coefficient depending on their separation. Given that x must be an integer, the coefficients $c_{x \neq 0}$ are zero for even values of x (5.35). For odd x the values fall off as x^{-2} and are all negative. There are effectively two interpenetrating sub-lattices with no intra-lattice coupling and with ferromagnetic inter-lattice interactions. We do not know of any system for which this Hamiltonian is a suitable representation of the microscopic interactions. However, it is perhaps not unreasonable to suppose that a system of this type could be contrived. The predicted critical behaviour resulting from algebraically decaying long-range interactions is also reminiscent of the one dimensional Ising model with interactions going as $1/r^{1+\sigma}$. This model is known to have a finite

temperature phase transition for $0 < \sigma \leq 1$ [117–119]. It would be interesting to study further a possible link between such a system and our model which is critical for all T.

Monte Carlo simulations using a standard Metropolis algorithm have been performed on this model for $L = 10, 50$ at high and low temperatures for both the linearized and cosine order parameters – the results are shown in Figure 5.3. For both OPs the size dependence in negligible, the fits to the FTG function being extremely good at low T even for the very small $L = 10$ systems.

For the linearized order parameter the distribution remains FTG like as the temperature is increased – as was observed for the two dimensional Harmonic model. The cosine form shows a deviation from the FTG function with increasing T, eventually becoming Gaussian at around $T/J \approx 2\pi$. This is again very similar to the behaviour of the $d = 2$ Harmonic model where Gaussian fluctuations are observed at $T/J = 4\pi$, above which the susceptibility was convergent. For our model the susceptibility converges above $T/J \approx 2\pi$ and the parallels are obvious. Following the same arguments put forward in Chapter 4, this is suggestive of some sort of phase transition, though not of a sharp thermodynamic type.

5.3.2 $d = \alpha = 1$ Spin Model 2

The second model is more unusual, both in terms of its derivation and the resulting Hamiltonian. Rather than simply inverse Fourier transforming the reciprocal space Hamiltonian, this model was derived by hypothesizing a form for the direct space model and recognizing that its coefficients could be chosen such that (5.15) was recovered. A one dimensional system with continuous symmetry and finite range interactions can not support long range order [100]. Thus, for critical fluctuations to be possible the interactions in our model had to be infinite in range. Also, as the reciprocal space model consists of harmonic normal modes, the direct space model had to be based around a quadratic form. The proposal was,

$$H = \sum_{r=1}^{N} \left(\sum_{x=-L}^{L} c_x \theta_{r+x} \right)^2 , \tag{5.36}$$

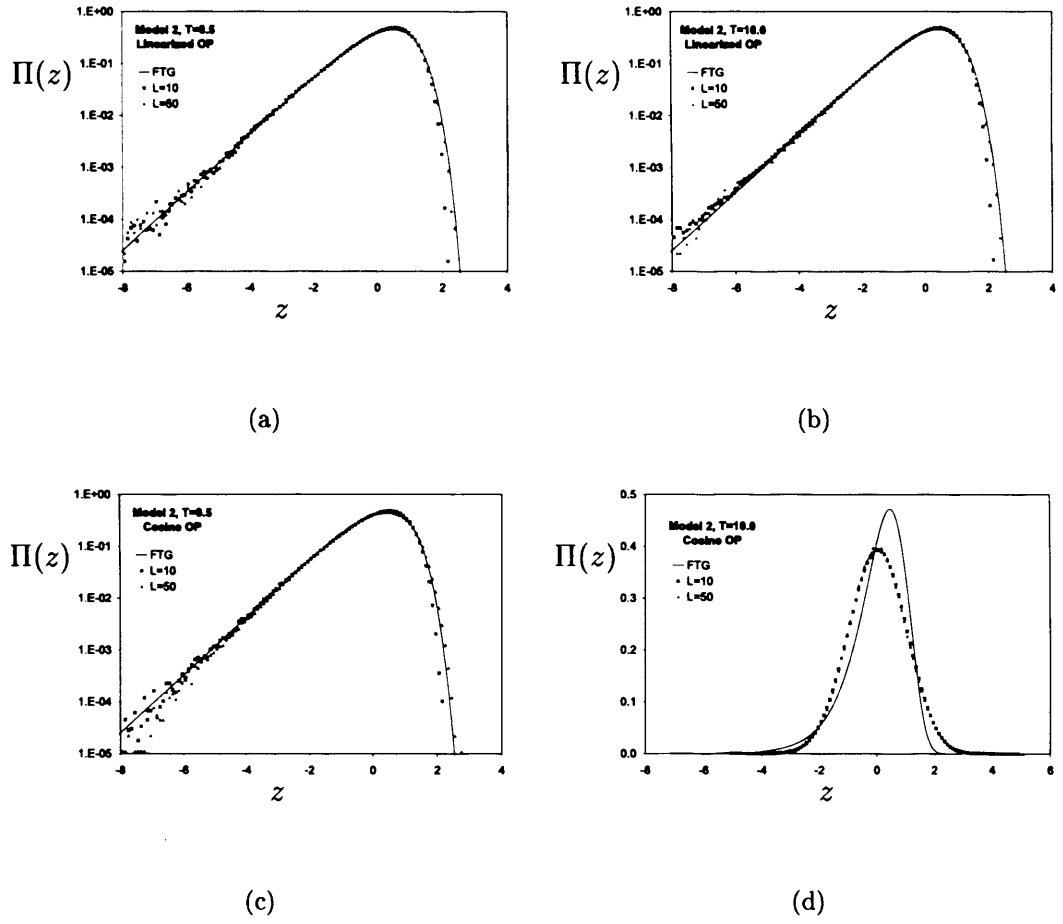

Figure 5.3: Monte Carlo Simulations of $d = \alpha = 1$ Model 1: (a) and (b) show results for the linearized order parameter at low and high T respectively. The fit to the FTG function is very good in both cases – particularly considering the size of the systems and length of the simulations (10^6 MCS/s). For the cosine OP, the low temperature results, (c), are an excellent fit to the FTG distribution, and as expected, at high T the fluctuations become Gaussian, hence (d) is plotted on linear axes rather than the semi-log plots of (a)–(c). Two system sizes are shown in each graph, $L = 10$ and $L = 50$. The fit to the exponential tail is good even for the smaller system, however an improvement in the double exponential wing is clear for the larger value of L. As usual, $z = (m - \langle m \rangle)/\sigma_m$ with m defined in (5.1).

where θ_r is the spin at site r on a one dimensional lattice of size $N = 2L + 1$ such that

$$\theta_r = \frac{1}{\sqrt{N}} \sum_q e^{-iqr} \psi_q. \tag{5.37}$$

The c_x are coefficients whose values are to be determined. The contents of the brackets in (5.36) may be expressed as

$$\sum_{x=-L}^{L} c_x \theta_{r+x} = \sum_{x=-L}^{L} c_x \frac{1}{\sqrt{N}} \sum_q e^{-iq(r+x)} \psi_q \tag{5.38}$$

$$= \frac{1}{\sqrt{N}} \sum_q \left(e^{-iqr} \psi_q \sum_{x=-L}^{L} c_x e^{-iqx} \right). \tag{5.39}$$

Therefore,

$$H = \sum_r \frac{1}{N} \sum_q \sum_{q'} e^{-i(q+q')r} \left(\sum_{x=-L}^{L} c_x e^{-iqx} \right) \left(\sum_{x=-L}^{L} c_x e^{-iq'x} \right) \psi_q \psi_{q'} \tag{5.40}$$

$$= \sum_q \left(\sum_{x=-L}^{L} c_x e^{-iqx} \right) \left(\sum_{x=-L}^{L} c_x e^{iqx} \right) |\psi_q|^2 \tag{5.41}$$

where (5.41) follows because $\sum_r e^{iqr} \overset{N \to \infty}{=} N\delta(q)$, introducing the requirement that $q' = -q$. By symmetry it is physically reasonable to fix $c_x = c_{-x}$, and so

$$\sum_{x=-L}^{L} c_x e^{-iqx} = \sum_{x=-L}^{L} c_x e^{iqx} = \sum_{x=-L}^{L} c_x \cos(qx), \tag{5.42}$$

where the sum over all x results in a cancelling of the sine terms. Thus, substituting (5.42) into (5.41) gives,

$$H = \sum_q f(q)^2 |\psi_q|^2, \tag{5.43}$$

with

$$f(q) = \sum_{x=-L}^{L} c_x \cos(qx). \tag{5.44}$$

Comparison of (5.43) with (5.15) shows that, ideally, $f(q) = \sqrt{|q|}$. Fortunately, $f(q)$ as given in (5.44) is in the form of a 'real to real' Fourier transform, with c_x being the Fourier coefficients. Thus,

$$\sqrt{|q|} = \sum_{x=-L}^{L} c_x \cos(qx) \tag{5.45}$$

$$= c_0 + 2\sum_{x=1}^{L} c_x \cos(qx), \tag{5.46}$$

where q is defined over the first Brillouin zone such that $-\pi \leq q < \pi$, giving q a period of 2π. Hence,

$$c_0 = \frac{1}{\pi}\int_0^{\pi} \sqrt{|q|}\, \mathrm{d}q \tag{5.47}$$

$$= \frac{2}{3}\sqrt{\pi} \tag{5.48}$$

$$c_{x\neq 0} = \frac{1}{\pi}\int_0^{\pi} \sqrt{|q|}\cos(qx)\, \mathrm{d}q \tag{5.49}$$

$$= -\frac{1}{\sqrt{2\pi}}\frac{S_f(\sqrt{2x})}{x^{3/2}}. \tag{5.50}$$

Here the function $S_f(z)$ is the Fresnel Sine integral,

$$S_f(z) = \int_0^z \sin\left(\frac{\pi}{2t^2}\right)\, \mathrm{d}t. \tag{5.51}$$

This function oscillates but quickly approaches the limit $S_f(\infty) = \frac{1}{2}$ at which point the coefficients go as $x^{-3/2}$.

Hence the postulated form (5.36) does give rise to the required reciprocal space Hamiltonian when the coefficients c_x are defined by (5.47) and (5.50). It is unfortunate that the direct space Hamiltonian is difficult to interpret physically. Once again we have thus far been unable to identify any known physical system whose microscopic interactions it describes. However, the algebraic decay of the interactions again points to a possible link with critical one dimensional Ising systems [119].

The Monte Carlo simulations performed for Model 1 were repeated for this model; the data is shown in Figure 5.4. As would be expected the results show exactly the same patterns of behaviour as before and need no further discussion.

5.4 Reciprocal Space Analysis of $d = \alpha = 1$ model

The spin wave analysis used to study the Harmonic model in Chapter 4 may equally well be applied to the one dimensional model introduced here. We note also that

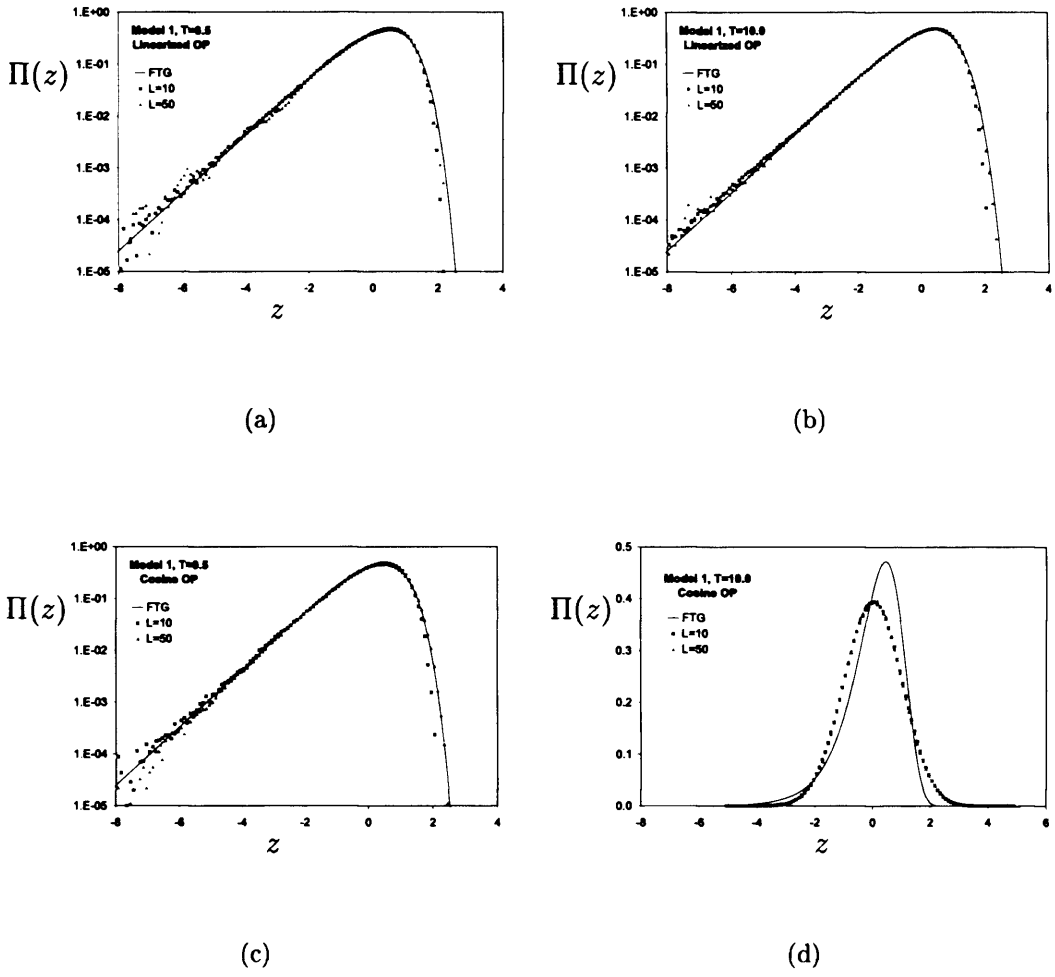

Figure 5.4: Monte Carlo Simulations of $d = \alpha = 1$ Model 1: This figure is a repeat of Figure 5.3 but resulting from simulations of the second version of our one dimensional model. The results are, as expected, essentially identical both qualitatively and quantitatively. As before $z = (m - \langle m \rangle)/\sigma_m$ with m defined in (5.1).

it is possible to force Models 1 and 2 above to yield a reciprocal space Hamiltonian $H = \sum_q |\gamma_q| \psi_q^2$ with $\gamma_q = 2\sin(q/2)$, i.e. an inherently periodic mode weighting more akin to the cosine function in (4.24). We don't pursue this line, however, as its main effect is to introduce a restricted range of temperatures over which the critical PDF may be observed.

In a move analogous to the study of the $d = 2$ Harmonic model, a set of constants

$$g_k = \frac{1}{N^k} \sum_{q \neq 0} \frac{1}{q^k}, \tag{5.52}$$

is defined, and $g_1 = 2G(0)$ where $G(r)$ is the spin-spin correlation function*. Therefore,

$$g_1 = \frac{1}{N} \sum_{q \neq 0} \frac{1}{q} \tag{5.53}$$

$$\approx \frac{1}{\pi} \int_{q_{min}}^{q_{max}} \frac{\mathrm{d}q}{q}. \tag{5.54}$$

The discrete wavevector $q = (2\pi/N)n$ is constrained by the integer nature of n, however each value is better thought of as being at the centre of a one dimensional 'volume' of size $(2\pi/N)$. Thus, on taking the continuum limit, the limits of the Brillouin zone integral should be taken from the extremes of the volumes of the smallest and largest n. That is, $q_{min} = \pi/N$ and $q_{max} = \pi$, and hence

$$G(0) = \frac{1}{\pi} \ln(N). \tag{5.55}$$

Though the integral approximation made here is not a bad one, comparison with numerical results from the discrete sum reveals a noticeable difference (Figure 5.5). A more accurate result is obtained using a standard result for the discrete sum in the case of large but finite N. We re-derive this result by applying the Abel-Plana formula [120] which yielded a very accurate result in the two dimensional case [6]. This provides a straightforward introduction to this method which we use again in

*Due to the slightly different ways in which the Hamiltonians are defined there is an extra factor of 2 in the one dimensional definition of $G(0)$ relative to the same expression for the $d = 2$ Harmonic model. This can be seen by considering the variance of $\psi_{\mathbf{q}}$ in each case.

Chapter 6. To begin, the sum over q is changed to a sum over the integer n,

$$g_1 = \frac{1}{N}\sum_{q\neq 0}\frac{1}{q} \tag{5.56}$$

$$= \frac{2}{N}\sum_{n=1}^{L}\frac{1}{\left(\frac{2\pi}{N}\right)n} \tag{5.57}$$

$$= \frac{1}{\pi}\sum_{n=1}^{L}\frac{1}{n}. \tag{5.58}$$

Obviously the sum over n does not converge as $L \to \infty$, however the Abel-Plana formula,

$$\sum_{i=p}^{q} f(i) = \int_p^q f(x)\,\mathrm{d}x + \frac{1}{2}f(p) + \frac{1}{2}f(q) + 2\int_0^\infty \frac{\mathrm{Im}[f(q+ix) - f(q-ix)]}{e^{2\pi x}-1}\,\mathrm{d}x, \tag{5.59}$$

may be used to evaluate it for large L.

$$g_1 = \frac{1}{\pi}\left\{\int_1^L \frac{\mathrm{d}x}{x} + \frac{1}{2} + \frac{1}{2L} + 2\int_0^\infty \frac{\mathrm{Im}\left[\frac{1}{L+ix} - \frac{1}{L-ix}\right]}{e^{2\pi x}-1}\,\mathrm{d}x\right\} \tag{5.60}$$

$$\overset{L\to\infty}{=} \frac{1}{\pi}\left\{\int_1^L \frac{\mathrm{d}x}{x} + \frac{1}{2} + \frac{1}{2L} + 2\int_0^\infty \frac{x\,\mathrm{d}x}{(1+x^2)(e^{2\pi x}-1)}\right\} \tag{5.61}$$

This expression is considerably simplified by the identity

$$2\int_0^\infty \frac{x\,\mathrm{d}x}{(1+x^2)(e^{2\pi x}-1)} = \gamma - \frac{1}{2}, \tag{5.62}$$

where $\gamma \approx 0.577...$ is Euler's constant. And so, substituting $N = 2L+1$ and (5.62) into (5.61) gives,

$$g_1 = \frac{1}{\pi}\left\{\ln\left(\frac{N-1}{2}\right) + \frac{1}{N-1} + \gamma\right\}, \tag{5.63}$$

which is in excellent agreement with numerical results (Figure 5.5).

There are different expressions for the magnetization and susceptibility depending on which order parameter one uses. For the cosine order parameter we have, from spin wave analysis (Appendix C),

$$\langle m\rangle = \exp\left(-\frac{TG(0)}{2J}\right), \tag{5.64}$$

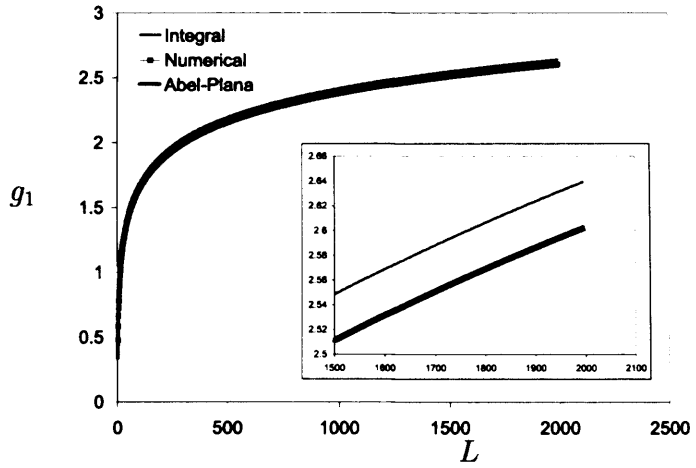

Figure 5.5: Divergence of g_1 for $d = \alpha = 1$: The approximate method of integrating over the Brillouin zone is clearly very good, however the Abel-Plana formula gives a much better fit to the numerical data, the two curves remaining overlapped even on the much larger scale of the inset.

and

$$\chi \approx \frac{T \langle m \rangle^2 N}{2J^2} g_2. \tag{5.65}$$

Therefore,

$$\langle m \rangle = \left(\frac{N-1}{2}\right)^{-\frac{T}{4\pi J}} \exp\left(-\frac{T}{4\pi J}\left(\gamma + \frac{1}{N-1}\right)\right). \tag{5.66}$$

Figure 5.6 shows $\langle m \rangle$ as a function of system size. The numerical results are from Monte Carlo simulations of Model 1 at $T/J = 1.0$. The fit to the predicted form is excellent, particularly considering the small systems and comparatively few MCS/s (10^6).

As the constants g_k are once again independent of N (e.g. $g_2 = 1/12$), the ratio $\sigma / \langle m \rangle \sim \mathcal{O}(1)$ and hyperscaling is obeyed. The exponential factor in (5.66) becomes constant very rapidly with N and so the magnetization can be seen to vary as a power law with $\beta/\nu = T/(4\pi J)$ - further evidence of the critical nature of the system. The susceptibility displays the same intriguing property as for the Harmonic model in two dimensions, namely an apparent limit to the temperature at which it will diverge. As

$$\chi \sim N^{1-\frac{T}{2\pi J}} \tag{5.67}$$

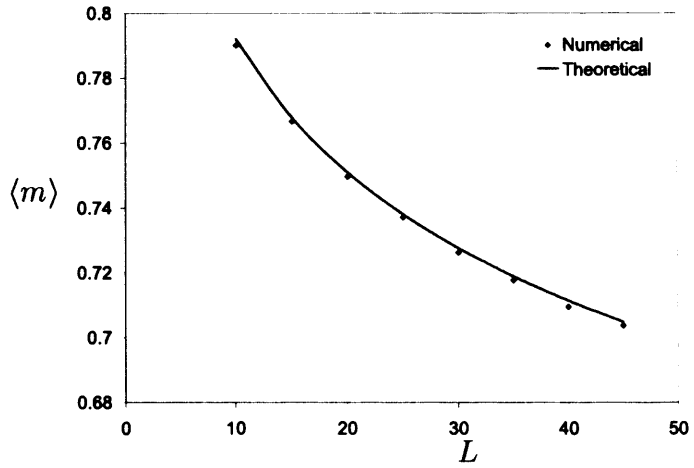

Figure 5.6: $\langle m \rangle$ as a Function of L for the Cosine Order Parameter for $d = \alpha = 1$: Numerical data from MC simulations of Model 1 shows very good agreement with the theoretically predicted form (5.66).

for large N, the susceptibility remains divergent only below $T/J \approx 2\pi$. It must be born in mind however that as (5.65) is derived using an effectively low T approximation, it is possible that the susceptibility could remain weakly divergent at all T. However the statistics do become Gaussian above $T \approx 2\pi$, indicating a finite correlation length and the possible onset of the central limit theorem.

For the linearized order parameter the average magnetization scales, by design, logarithmically,

$$\langle m \rangle = \frac{T}{J} G(0) \tag{5.68}$$

$$= \frac{T}{2\pi J} \left\{ \ln\left(\frac{N-1}{2}\right) + \frac{1}{N-1} + \gamma \right\}, \tag{5.69}$$

hyperscaling is violated and the distribution of the OP is strictly temperature independent.

5.5 $d = \alpha = 1$ – The link with Extremal Statistics

As stated above, extreme value statistics deal with the distribution of the largest (or smallest) of a set of independent, identically distributed random numbers. The fact that the Fisher-Tippett-Gumbel distribution [61], one of only three possible non-Gaussian EVS limit functions [60], should describe fluctuations in a highly correlated system [48] is of great interest – particularly as a link between EVS and criticality is so appealing [62, 63]. Considering the a^{th} largest (or smallest) member of the sample one obtains a generalized FTG distribution, characterized by the parameter a. This provides a link to the BHP function which is seen to be a good fit to a generalized FTG curve with $a = \pi/2$, though such a non-integer value for a is difficult to interpret in this context.

An explanation for the apparent FTG – critical link in terms of extremes of physical quantities has not yet been found [6, 64, 69]. The extremes of the independent normal modes in the 2dXY model do not follow a BHP distribution [64], thus for extremal statistics to be relevant it seems likely they will relate to correlated many body quantities [21]. If true, the BHP function could be viewed as analogous to the FTG distribution in the case of highly correlated variables. For a system with strong correlations, it would therefore be hoped that the statistics of the largest of sample of correlated variables would approximate the BHP function (rather than the FTG form) in the limit of large N. Some evidence to this effect has come from studies of the Sneppen depinning model, where the distribution of the largest avalanche is BHP like over a range of time and length scales [42]. By contrast, generating uncorrelated variables with the same microscopic distributions as the correlated ones, leads, as would be expected, to the FTG function. Further weight is given to this argument by the renormalization group study of Carpentier and Le Doussal [65] who demonstrated that the EVS of $1/f$ correlated signals had a tail of the form $y\exp(-y)$ for $y = x - \langle x \rangle \gg 0$. This indicates that the logarithmic correlations alter the exponential of the uncorrelated FTG form to precisely the large fluctuation asymptote of the BHP distribution (1.4).

After so much debate, it is interesting that a highly correlated, and we would argue critical, system has been identified where the limit function is explicitly the $a = 1$ FTG distribution [25, 48]. Even in this case it is not clear which quantity, if any, is extreme [69]. The normal modes of the $d = \alpha = 1$ model satisfy the requirements of independence, though they are not uniformly dispersive. For strong enough dispersion the largest mode will always be one of only a few possibilities near to the Goldstone mode. This severely restricts the effective size of the ensemble and there is no reason to expect the FTG asymptote to apply. The question then is whether the $1/q$ dispersion is sufficient for this to be true.

The easiest way to answer this question is to simulate our model and evaluate $P(\max(m_{\mathbf{q}}))$ to see whether it is FTG like. We have used Model 1 (above) for the Monte Carlo simulations (Metropolis, 10^6 MCS/s) in direct space, with the maximum normal mode being identified by Fourier transform[†] at each observation time. The results are shown in Figure 5.7(a) and clearly indicate that the two functions are distinct across all ranges. Thus we can find no link between the order parameter fluctuations in our model and the extreme values of a suitable independent quantity.

We have approached the question of extremal statistics in the context of an equilibrium model which has been shown to be critical and have concluded on the basis of numerical simulations that no simple link with criticality is possible. Since performing these simulations we have become aware of a much more rigorous demonstration of this result in the detailed work of Györgyi *et al.* [69], studying fluctuations of the roughness of $1/f^{\alpha}$ noise signals (directly analogous to the models discussed here – see Chapter 6). They performed a thorough analytical treatment of the the distribution of extreme values for general d and α. It was concluded unequivocally that the roughness PDF could not be recovered by simply observing the largest mode, even in the case $d = \alpha = 1$ where the former is inherently an extreme value distribution. Furthermore it was seen that the strong dispersion leading to the failure of the CLT

[†]All the Fourier transforms performed in our Monte Carlo simulations use the excellent "Fastest Fourier Transform in the West" (FFTW) version 3.0.1 [121] available from www.fftw.org.

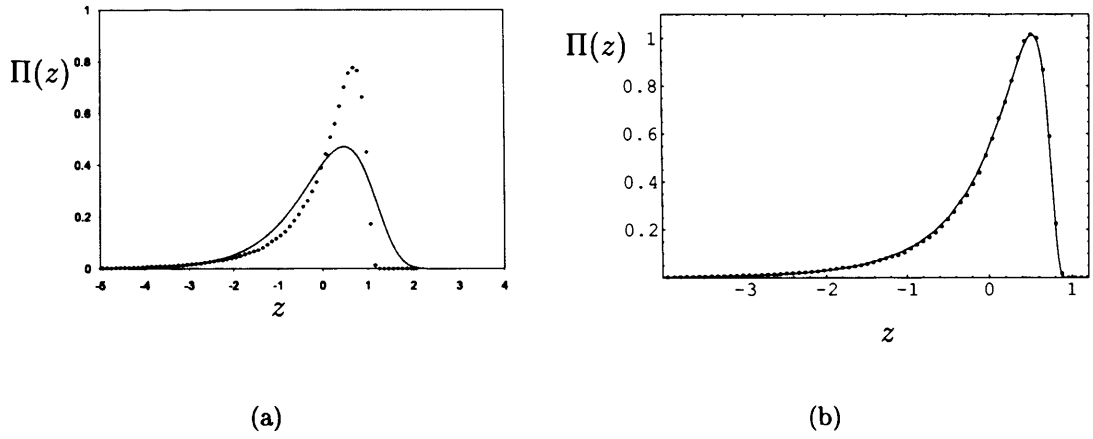

(a) (b)

Figure 5.7: Distribution of the Largest Normal Mode: (a) and (b) shows the distribution of $|\max(\psi_q)|^2$ normalized to the standard deviation and average respectively. In (a) the FTG distribution has been included for comparison, showing categorically that the largest mode does not have EVS fluctuations. Here $z = (m' - \langle m' \rangle)/\sigma'_m$. In (b), $z = (m' - \langle m' \rangle)/\langle m' \rangle$, to enable comparison with the theoretical results from [69] (solid line). In both cases $m' = 1 - |\max(\psi_q)|^2$.

was also responsible for the exclusion of EVS limit functions.

In the light of these findings our simulations do not reveal anything new but serve as a numerical confirmation of the analytical result. Comparison of our results with Figure 1 in [69] requires that our data be normalized to the average rather than our usual choice of the standard deviation. As hyperscaling is not obeyed this results in a different form of the scaling function, shown in Figure 5.7(b).

5.6 The Contributions to $P(m)$ from Soft Modes

In studies of the 2dXY model it proved interesting to consider the contributions to the PDF coming from different regions of the Brillouin zone [64]. The results demonstrated that the asymmetry of the BHP distribution arises from the soft modes near the zone centre. The first twenty-four modes alone are sufficient to give a good fit to the exponential tail, and summing all but these modes leads to an almost Gaussian form. However to reproduce the BHP function across the entire range of m (i.e. to fit both tails) requires more modes to be included in the sum. As discussed in §5.1 this

is interpreted as indicating the essential many-body origins of the non-Gaussianity.

We have performed a similar analysis in the case $d = \alpha = 1$ using Model 1 as described above. Given the one dimensional nature of the system it seems reasonable to assume that the $1/q$ dispersion will lead to a less dominant zone centre than is the case for $d = 2$. Our results confirm this, being qualitatively similar to those for the 2dXY model but with a larger range of $|\mathbf{q}|$ required to get an approximate fit to the FTG function. Monte Carlo simulations were performed for a system with $L = 50$ at $T/J = 1.0$. The quantity we studied was

$$m_n = 1 - \sum_{q=1}^{n} m_q, \tag{5.70}$$

where m_n indicates the contribution to magnetization from the first n modes with $q \neq 0$.

It is also possible to obtain theoretical predictions of the distribution formed from different sets of normal modes. This is most easily seen in terms of the inverse Laplace transform of the moment generating function, $G(s)$, for the distribution, where for a general PDF, $P(x)$,

$$G(s) = \int_0^\infty P(x)e^{-sx}\,\mathrm{d}x. \tag{5.71}$$

Setting $J = 1$ and $\alpha = 1$ in (5.15) leads to (see [48])

$$G(s) = \prod_{j=1}^{L} \left(1 + \frac{s}{j}\right)^{-1} \tag{5.72}$$

and if m is the magnetization summed over the whole BZ then

$$\sigma = \sqrt{\langle m^2 \rangle - \langle m \rangle^2} = \frac{\pi}{\sqrt{6}}. \tag{5.73}$$

Rescaling the magnetization to its standard deviation and taking the limit $L \to \infty$ then yields the scaling function [48]

$$\Pi(z) = \sigma P(m) \tag{5.74}$$

$$= \int_{-i\infty}^{i\infty} \frac{\mathrm{d}s}{2\pi i} e^{zs} \prod_{j=1}^{\infty} \frac{e^{\frac{s}{aj}}}{1 + \frac{s}{aj}} \tag{5.75}$$

$$= a e^{-(ax+\gamma)-e^{-(ax+\gamma)}}, \tag{5.76}$$

where, as usual,

$$z = \frac{m - \langle m \rangle}{\sigma}. \tag{5.77}$$

The limits of the product in (5.75) may be changed to evaluate the contribution to the scaling function from specific parts of the Brillouin zone – though care must be taken to correctly normalize the magnetization. It is no longer appropriate to scale m to the standard deviation of the full distribution; one must evaluate σ_n corresponding to the partial system. Using equation (2.54) the moments of m_n are found by differentiating (5.72) and it is seen that

$$\sigma_n = \sqrt{\sum_{j=1}^{n} \frac{1}{j^2}}, \tag{5.78}$$

which, letting $n \to \infty$ simply yields a. Hence we define

$$z_n = \frac{m_n - \langle m_n \rangle}{\sigma_n}, \tag{5.79}$$

and make use of the general result that if $G_x(s)$ is the moment generating function of a variable x,

$$G_{\frac{(x-a)}{b}}(s) = e^{at/b} G_x\left(\frac{s}{b}\right), \tag{5.80}$$

to give

$$\Pi(z_n) = \int_{-i\infty}^{i\infty} \frac{\mathrm{d}s}{2\pi i} e^{zs} \prod_{j=1}^{n} \frac{e^{\frac{s}{\sigma_n j}}}{1 + \frac{s}{\sigma_n j}}. \tag{5.81}$$

The σ_n may always be evaluated exactly numerically from (5.78), and the integral is found in closed form for each n in turn. The general form of the result is

$$\Pi(z_n) = n\sigma_n e^{-n\sigma_n\left(\frac{c_n}{\sigma_n}+z\right)} \left(-1 + e^{\sigma_n\left(\frac{c_n}{\sigma_n}+z\right)}\right)^{n-1} H\left(\frac{c_n}{\sigma_n} + z\right), \tag{5.82}$$

where c_n is a constant dependent on n, and $H(x)$ is the Heaviside or unit step function.

Figure 5.8 shows the results of the MC simulations for $n = 1-5, 15$ plotted against the respective theoretical curves. Also, Figure 5.9 shows the results of letting $n \to \infty$ but excluding the first 5 and 15 modes. For comparison between dimensions it is better to discuss 'shells' in the Brillouin zone rather than individual modes. It is readily seen that the soft modes are responsible for the asymmetry of the distribution as excluding these low frequency contributions yields an essentially Gaussian form.

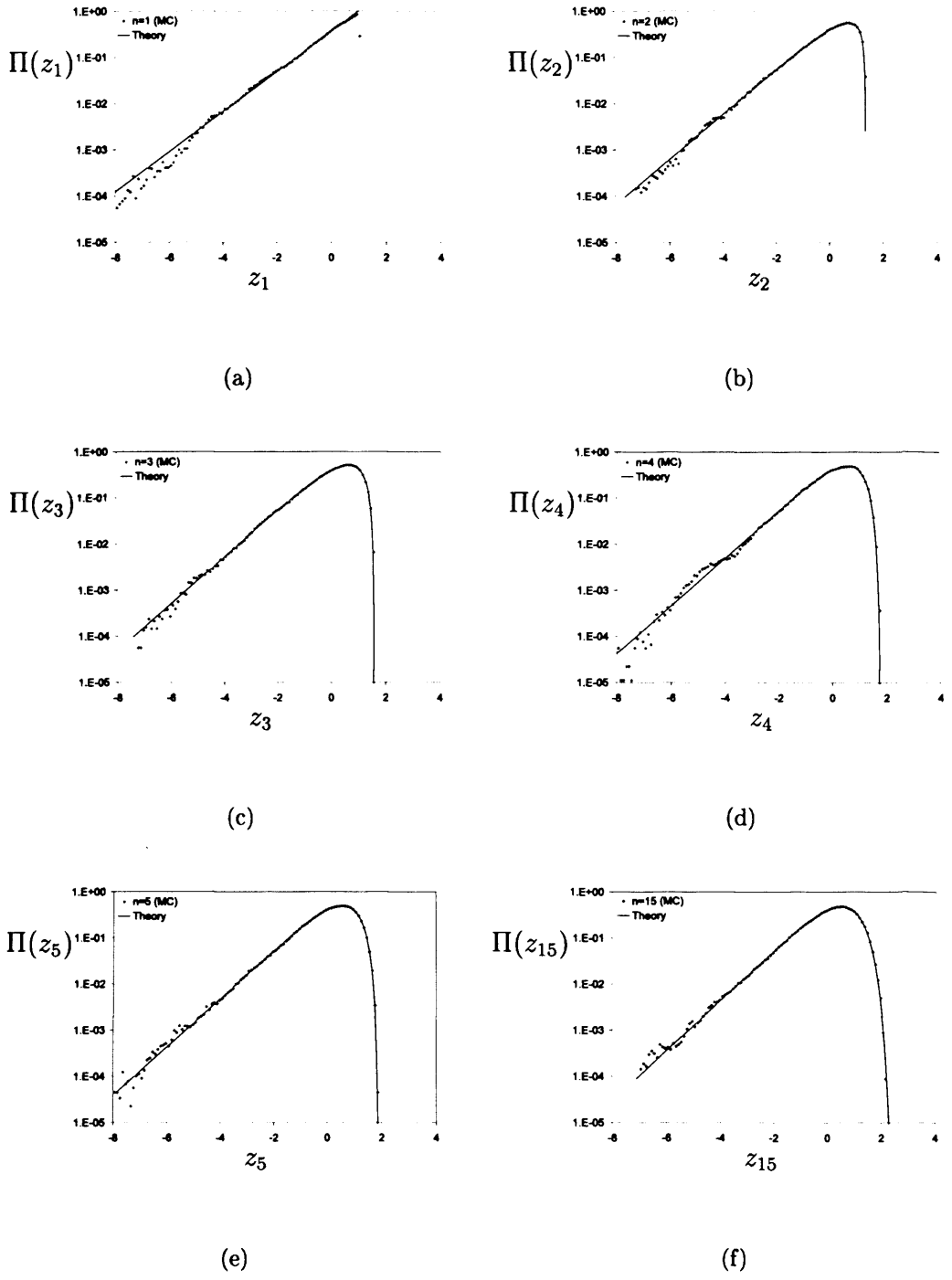

Figure 5.8: Contributions to the Distribution Function from Restricted Sets of Normal Modes: Each $\Pi(z_n)$ is the contribution to the distribution of the linearized order parameter from the first n shells of the BZ. The solid lines are the theoretical results from (5.81).

However, whilst in two dimensions (XY model) excluding only 5 shells produced a reasonably Gaussian PDF, many more are required in the one dimensional case. This is also reflected in the approach to the FTG limit as n is increased. To recover the exponential tail in the BHP distribution requires the inclusion of only the first four shells [64]. In contrast 15 or more one dimensional shells are needed to reasonably approximate the FTG function.

In conclusion it is clear that, whilst the soft modes are largely responsible for the asymmetry of the magnetization PDF, many modes are required to obtain the full FTG distribution. This is a consequence of the many body nature of the magnetization and the effect is more pronounced than for the equivalent two dimensional system. Despite this, the fact that a reasonable approximation to the limit function is obtained with $n < N$ provides some explanation as to why γ_q may be replaced by q in many instances.

5.7 Conclusions

The work in this chapter stems from two remarkable results: the observation of [6] that the linearized and cosine order parameters of the Harmonic model appeared to give rise to the same PDF, and the analytical link between a related model in one dimension and the field of extreme value statistics [48]. Coupled with the work presented in Chapter 4, we have rationalized the first of these as a direct consequence of low temperature approximations. We suggest that a logarithmically diverging average of a global measure is direct evidence of critical behaviour and represents the low temperature limit of a critical quantity with a power law dependence and exponent proportional to T. The logarithmic behaviour is then interpreted as an indication that all length scales must be included to accurately describe the system, implying an infinite correlation length.

On this basis we have identified a family of model systems in reciprocal space, depending on dimensionality d and a mode weighting parameter α, which, for $d = \alpha$ we recognize as critical. For $d = \alpha = 1$ it has been possible to derive two direct

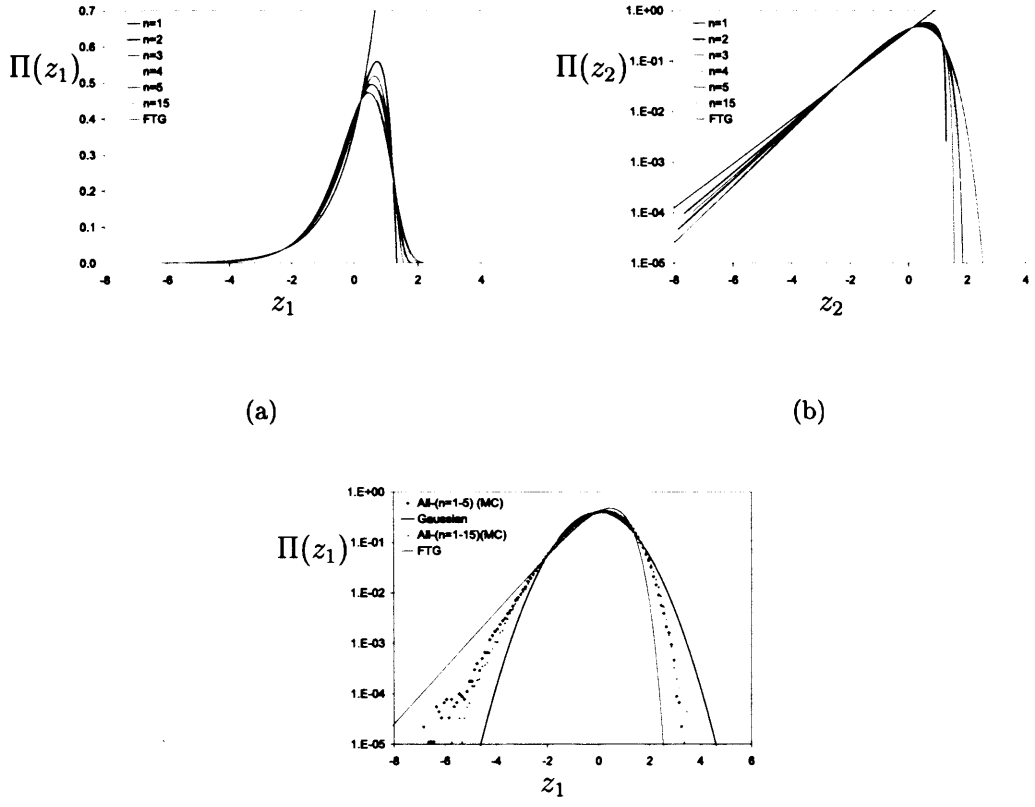

Figure 5.9: Restricted Shells - The Approach to the FTG Distribution: (a) The theoretical curves for $\Pi(z_n)$, $n = 1, 2, 3, 4, 5, 15$, plotted against the FTG distribution. Even for $n = 15$ there is a noticeable deviation from the limiting form. The same functions are plotted in (b) on semi-log axes to highlight the wings. The exponential tail is approached quickly however the double exponential tail requires the inclusion of many more modes. Part (c) shows the effect of neglecting the first 5 and 15 shells when evaluating the order parameter.

space Hamiltonians which would be difficult to relate any other way. Simulations of these models show excellent agreement with the theoretical limit (FTG) function even for relatively small systems. Unfortunately it has not been possible to identify any physical systems for which our Hamiltonians are a good description of the microscopic interactions. We note however that a direct space quantum model of linearly (nearest neighbour) coupled harmonic oscillators has been shown to give rise to FTG statistics for the displacement fluctuations [122]. Our argument regarding criticality is confirmed by the behaviour of the order parameter of the $d = \alpha = 1$ models. The average of a linearized form of the order parameter varies, by design, logarithmically, however a related cosine form varies as a power law with an exponent proportional to T.

As the scaling function for the linearized OP is analytically the FTG distribution from extreme value statistics we have analysed $P(\max(m_q))$, to try and establish any simple link with an extreme quantity. This is a contribution to a long running debate regarding the link between critical systems and EVS and ties in well with the analytical work in [69]. Our simulations agree extremely well the theoretical predictions and confirm that the distribution of the largest mode is not the FTG function. Thus the question of how, and if, EVS relate to critical systems in a physical sense, remains open.

Simulations of partial order parameters have shown the asymmetry of the FTG distribution arises, in this context, primarily from the soft normal modes. The results of these simulations are in excellent agreement with theoretical predictions, and are qualitatively similar to the behaviour of the 2dXY model [64]. The fact that a limited number of modes is required to approximate the FTG distribution accounts for the ability to assume $\gamma_q \approx q$, but is not, for the same reasons argued in [64], sufficient justification for neglecting harder modes when calculating averages.

Perhaps most significantly we have addressed the question of functional similarity in critical scaling functions. The family of models studied provides an excellent means for determining PDFs arising from distinct universality classes. The three functions, the BHP, FTG, and $d = \alpha = 3$ Pearson curve, are remarkably similar in shape. In fact

it may be hard to distinguish between them experimentally (particularly between the curves for $d = 2, 3$). This similarity is suggested by the proximity of the distributions in skewness-kurtosis space. The fact that a number of non-Gaussian distributions of global measures in non-critical systems occupy the same region of this space leads us to two conclusions. Firstly, the prediction that order parameter fluctuations in critical systems would have functionally similar PDFs is seen, for the systems studied, to be true. Secondly, if a PDF with the general form of one of our critical distributions is observed experimentally, it is difficult to say to which universality class it belongs. Furthermore it is may not even be sufficient evidence to infer that the system being observed is truly critical.

Let us assume that we are restricted experimentally to $d = 1, 2, 3$. Figure 5.1 shows that $d = 1$ enables the PDF to be a relatively robust measure of criticality. For $\alpha = 0$ the distribution is effectively Gaussian, whilst for $\alpha \geq 2$ the PDF appears very close to the χ^2 limit. The $d = \alpha = 1$ model has a distribution in a region of skewness-kurtosis space well away from these two extremes and is therefore clearly identifiable. As d increases the relevant χ^2_{2d} distribution becomes more Gaussian and so the range of available skewness and kurtosis is diminished. For $d = 2$ the $\alpha = 0, 1$ functions are very close approximations to Gaussians. For $\alpha \geq 4$ the points in skewness-kurtosis space are sufficiently far from the critical model that it is reasonable to assume they will be distinguishable from it. However the $\alpha = 3$ point is very close to the location of the FTG function which we already know is of a similar form to the BHP ($d = \alpha = 2$) distribution. This introduces the question of whether we can be certain that an experimentally observed (approximately) BHP or FTG distribution does not, in fact, correspond to the case $d = 2, \alpha = 3$? With just the PDF for reference it seems that the answer to this question is probably no.

It appears that PDFs must be used in conjunction with other sources of information. If it is known in advance that the system is critical then substantial simplification is possible. An example of this is the case of turbulence where a good argument has been made for the essential criticality of the system, going some way toward explaining the empirical link with the low temperature 2dXY model [19]. Likewise if the

dimensionality, or effective dimensionality, is clear, then confusion between different pairs of d and α may not arise. The most difficult dimension is $d = 3$. Depending on the quality of the experimental data, one could argue that all $\alpha \geq 2$ may be hard to distinguish. This makes it difficult to establish criticality for a three dimensional system solely from the PDF. It is especially interesting that the $d = \alpha = 2$ and $d = \alpha = 3$ distributions are so similar (Figures 5.1 and 5.2). This may partly explain the apparent ubiquity of the BHP function, as it is possible that in some cases experimental observations were actually of the three dimensional system. This is a particularly troublesome problem as in both dimensions one is dealing with critical behaviour. Therefore even when one has sufficient knowledge of the system to argue its criticality, as was the case in the turbulence example, more information is required to distinguish between the possibilities.

We have focused on the third and fourth cumulants as being indicators of the shape of the PDF. Whilst this is generally a good approximation for a few standard deviations either side of the mean [91], we must accept that our conclusions may not be valid in all cases, especially for distributions with significant large scale fluctuations. Without wanting to be pessimistic, we feel that great care must be taken when using probability density functions as a measure of the underlying microscopic physics in a system. Viewed in isolation these functions may well lead to inaccurate inferences of critical behaviour, or at least to the mis-assignment of critical models.

Finally we note that our conclusions are based on the family of specifically equilibrium models discussed in the text. For non-equilibrium systems the news is perhaps a little more promising. The building of a gallery of non-equilibrium scaling functions for comparison with experimental data is ongoing [44]. The systems contributing to this gallery have power law temporal correlations providing an analogy with equilibrium critical behaviour and the concepts of universality. It appears that the scaling functions of these systems cover a wider range of functional forms than we observe at equilibrium, and the PDFs are generally more easily distinguishable [44, 49].

Chapter 6

$1/f$ Noise

6.1 Critical Dynamics

6.1.1 Temporal Fluctuations

In previous chapters our focus has been on static properties, described by probability density functions; as such the order of the collected data has not been important. If however the observations are viewed as a time series, it may be possible to extract information regarding the temporal evolution of the system. When the waiting time, t_w, between measurements is sufficiently short, the configuration of microscopic variables will generally change little between successive observations. The state of the system at time $t + t_w$ then depends strongly on the state at time t, whereas the state at time $t + Ct_w$ (where C is some large number) will probably not. This dynamical information is contained in the auto-correlation function (ACF) of the observable, say x, where

$$A(t', t) = \frac{\langle x(t')x(t'+t)\rangle - \langle x(t')\rangle^2}{\langle x(t')^2\rangle - \langle x(t')\rangle^2}, \tag{6.1}$$

with $\langle \ldots \rangle$ representing a time average. Systems at equilibrium may be considered statistically 'stationary'; probability distributions of their variables are constant with respect to time. Thus the averages $\langle x(t)^n \rangle$ simplify to $\langle x^n \rangle$ and the ACF becomes a function of a single variable, t.

It is often found empirically that $A(t) \propto e^{-t/\tau}$ where τ is some characteristic decay

time. As $T \to T_c$, τ is seen to diverge with the spatial correlation length as a power law [71],

$$\tau = \xi^z, \tag{6.2}$$

where z is the dynamical critical exponent. This divergence indicates that, at a critical point, correlations extend over all time scales and certain dynamical processes appear to have become limitingly slow – a phenomenon known as 'critical slowing down' [71].

Non-equilibrium systems have the added complication of time dependent statistics and an ACF that is explicitly a function of both t and t'. However it is possible that these systems can become stationary if they evolve into steady states. Even when this occurs the combination of spatial interactions and dynamical processes make it difficult to rigorously describe global fluctuations and non-equilibrium PDFs remain poorly understood [44].

The frequent observation of power laws (both spatial and temporal) across a range of non-equilibrium phenomena (see, for example, [66–68, 123]) is reminiscent of equilibrium critical behaviour. It has been proposed that this analogy may be exploited by characterizing non-equilibrium universality classes on the basis of statistical properties [44]. The resulting "picture gallery" of non-equilibrium PDFs from known systems could then be used for comparison with experimental data.

6.1.2 Power Spectra

A time signal, $x(t)$, may be characterized by the form of its power spectrum, $S(f)$ – a measure of the energy contained in each of the Fourier modes. Consider a signal consisting of N discrete measurements of the variable x, taken at regular intervals t_w, such that the total time is $T = Nt_w$. The normal modes are then restricted to integer multiples of $1/T$, and

$$x(t) = \sum_{f=-L}^{L} c_f e^{2\pi i t f/T}, \tag{6.3}$$

where $c_{-f} = c_f^*$ and $N = 2L + 1$. As the energy in a wave is proportional to the square of its amplitude, the power spectrum is most easily defined by the relation

$$S(f) \propto \left\langle |c_f|^2 \right\rangle, \tag{6.4}$$

where the average is over an ensemble of identical systems.

An alternative definition known, as the Wiener-Khintchine theorem, states that the power spectrum is equal to twice the Fourier transform of the auto-correlation function [124],

$$S(f) = 2\mathcal{F}\{A(t)\}, \tag{6.5}$$

and is thus the frequency domain representation of the temporal correlations.

6.1.3 $1/f$ Noise

There are many examples of physical systems having power spectra of the form

$$S(f) \sim \frac{1}{f}. \tag{6.6}$$

The natural association between this scale free power law behaviour and criticality, coupled with the ubiquity of this type of noise, have made it a popular topic both practically and theoretically (see [121] for a comprehensive bibliography of $1/f$ related work). First observed in studies of fluctuations in vacuum tube currents [66], $1/f$ noise has subsequently been seen in systems as diverse as the luminosity of stars [67], the occurrence of earthquakes [123] and the pitch and volume of a number of pieces of music spanning a range of genres [68]. Scale free power spectra in general are described by $S(f) \propto 1/f^\alpha$. The case $\alpha = 1$ is often considered particularly important as it represents a balance point where all modes make a significant contribution to the fluctuations (in the same way as we interpret the $1/q$ dispersion of modes in the $d = \alpha = 1$ model as indicating criticality). This is true because

$$\left\langle x^2 \right\rangle = \int_0^\infty S(f)\,\mathrm{d}f, \tag{6.7}$$

which diverges logarithmically for $\alpha = 1$.

The physical origins of $1/f^{\alpha}$ noise remain an open question. For equilibrium critical systems one can make a simple classical argument based on the spatial scale invariance resulting in perturbations propagating over all length scales, which in turn gives fluctuations with all possible lifetimes [43]. If the dynamical processes decay exponentially with characteristic times τ_k, the power spectrum of a single mode is

$$S(f_k) \propto \mathcal{F}\{e^{-t/\tau_k}\} \tag{6.8}$$

$$\propto \frac{\tau_k}{1+(f_k\tau_k)^2}, \tag{6.9}$$

where $\mathcal{F}$ denotes a Fourier transform. The full power spectrum is then the integral of this function over all time scales. Taking the continuum limit and assuming a power law distribution of τ, $\mathcal{D}(\tau) \sim \tau^{-a}$, gives

$$S(f) \sim \int \frac{\tau^{1-a}}{1+(f\tau)^2}\,\mathrm{d}\tau \sim f^{-2+a}. \tag{6.10}$$

It is likely, however, that the true origins of critical dynamic scaling are more complicated than this simple picture suggests [73, 125, 126].

For non-equilibrium systems it is even harder to determine the origins of $1/f^{\alpha}$ behaviour. One model, proposed in the now famous paper by Bak, Tang and Wiesenfeld (BTW), introduced the concept of 'self-organized criticality' (SOC) [43]. Their idea was that nonequilibrium systems with infinite spatial correlations would evolve under the influence of a driving force to the point at which the effect of that force can no longer be transmitted through infinite distances. This is true precisely when there is a scale free distribution of clusters – defined as regions over which small local perturbations can propagate. They argued that, in the spirit of the argument for equilibrium critical systems above, the presence of clusters of all sizes then translates directly into a distribution of fluctuations on all time scales. Taking the superposition of these processes then leads directly to (6.10).

Whilst there has been much work done in the field of self-organized criticality, the validity and range of applicability of the model remain uncertain [127]. In particular, both practical and analytical studies of sandpile models, such as that proposed by BTW, reveal power spectra varying as $1/f^2$ [128, 129]. This is significant because, of

all the values of α, 2 is perhaps the least interesting given that $1/f^2$ power spectra arise naturally from simple Brownian motion.

It is clear that if there is a universal mechanism operating in systems with $1/f^\alpha$ noise, it remains to be found.

6.2 $1/f$ Noise and Extreme Value Statistics

Our interest in $1/f$ noise began with the publication of a seminal paper by Antal *et al.* [48], detailing a link between these power law temporal fluctuations and the Fisher-Tippett-Gumbel distribution from extremal statistics. This link is intriguing and ties in with the work presented in Chapter 5 linking the FTG function to an inherently critical microscopic model.

The approach adopted in [48] was to consider fluctuations in the width square (or 'roughness')

$$w_2(h) = \left\langle h(t)^2 \right\rangle - \langle h(t) \rangle^2 , \tag{6.11}$$

of a one dimensional time signal $h(t)$. The averages are over the period of the experiment, T, and the nomenclature was chosen to highlight the analogy with the growth of an interface above a one dimensional substrate. It was stated that pure Gaussian, periodic $1/f$ noise with random phase could be generated by the Fourier space action

$$S = \sigma \sum_{n=-L}^{L} |n||c_n|^2, \tag{6.12}$$

where the c_n are the Fourier modes of the time signal and σ is a parameter making S dimensionless. This action was then used to determine the moment generating function which, after normalization, revealed the FTG distribution as the scaling function of the roughness. This is a particularly remarkable result as there was no reference to any extremal quantity in its derivation. It was concluded that Gaussian $1/f$ noise might therefore be the result of some undetermined extreme events [48].

Comparison of (6.12) with the reciprocal space Hamiltonian for the $d = \alpha = 1$ models described in Chapter 5,

$$H = J \sum_{\mathbf{q} \neq 0} |q||\psi_q|^2, \tag{6.13}$$

reveals that they the same, but for the transformations

$$\sigma \rightarrow J \tag{6.14}$$

$$n \rightarrow q \tag{6.15}$$

$$c_n \rightarrow \psi_q. \tag{6.16}$$

The time T becomes, for the spatial systems, the volume of the Brillouin zone, i.e. 2π, and N is, again, the system size. The values $h(t)$ are analogous to the microscopic (spin) degrees of freedom, θ_r, and so the width square is related to the linearized order parameter,

$$w_2(h) \rightarrow 1 - m. \tag{6.17}$$

It is therefore no surprise that m is FTG distributed. We think this mapping is potentially useful as an additional tool for interpreting the results of Antal *et al* [48]. They consider the temporal evolution of a system and derive the FTG function from a property of a time signal. For the $d = \alpha = 1$ model the FTG distribution is observed for a static global quantity. Comparison with [48] shows that this is a consequence of a $1/q$ dispersion of spatial normal modes. Antal *et al.* even explicitly relate their findings to a spatial system in the form of an interface model. We now turn our attention to the different merits of the temporal and spatial interpretations.

6.2.1 Dynamics and Statics: Two Interpretations of the $1/f$–FTG Link

The proven analytical relationship between Gaussian $1/f$ noise and the FTG distribution arose as part of the ongoing development of a picture gallery of non-equilibrium PDFs [44]. Apart from the interest this sparked in trying to identify any extremal origins of the distribution [69], it also provided the FTG function as a suitable member of that gallery. It is therefore interesting to to consider the implications of observing the FTG form experimentally.

We begin by noting that, although a Gaussian $1/f$ signal will have an FTG distributed roughness, observing such a roughness does not necessarily imply Gaussian $1/f$ behaviour. This is not a problem though. As we must have the time series in order to evaluate its roughness, we can determine its power spectrum and Gaussianity (or otherwise) directly, without the need to infer them from the PDF. At this point the striking universality of the result in [48] becomes manifest. It is true that *all* Gaussian $1/f$ signals have FTG distributed roughnesses, regardless of the microscopic physics giving rise to the time signal. A down side to this generality is that it makes it hard to use the FTG distribution as a signature of microscopic behaviour. Identifying extreme events as the the cause of the fluctuations would be a considerable step forward in this regard. However, as noted in [48], this is likely to be a difficult task and thus far it has not proved possible [69].

The main difference between the temporal and spatial models is the transparency of the power spectra. In the temporal model one has a time signal with a power spectrum and roughness that may be evaluated directly. They are both properties of the experimental data. For the spatial ($d = \alpha = 1$) model the experimental observations are of the magnetization – with no information about the individual normal modes (we assume a practical rather than a numerical experiment). The mode dispersion is therefore not experimentally accessible, so if we can infer it from the form of the PDF we have gained information. This would require the rather large assumption that an FTG distributed magnetization could not arise from other, non-$1/q$, systems. We cannot claim that this is so. However there is always the hope that the PDF, in conjunction with other information (suggestive of criticality, for example) may act as an indicator of unknown microscopic details. In this way the spatial approach provides us with extra information in a way that the temporal interpretation is perhaps unable to.

6.2.2 Experimental Implications

Consider an experiment in which some observable, x, is measured to give the time signal $x(t)$. If $P(x)$ is the FTG distribution there is no reason to expect the power

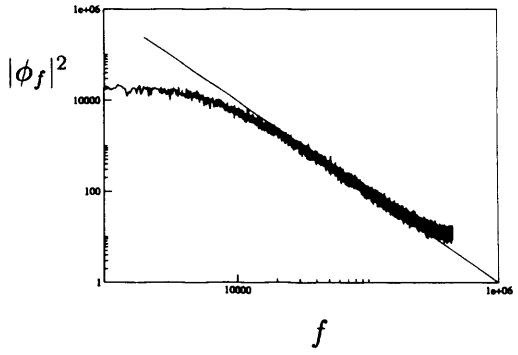

Figure 6.1: Example Power Spectrum of an FTG Distributed Signal: The power spectrum of the linearized order parameter from a MC simulation of the $d = \alpha = 1$ Model 1 from Chapter 5. This is $1/f^2$ noise (the straight guide line is proportional to $1/f^2$) over the majority of frequencies, as would be expected from the MC dynamics.

spectrum to go as $1/f$ because we have considered the statistics of the raw signal, not its roughness. An example of this is that the power spectrum of the magnetization from a Monte Carlo simulation of the $d = \alpha = 1$ model reveals $1/f^2$ dynamics (as would be expected for a single spin flip Markovian process [71]). The spectrum is shown in Figure 6.1. This highlights the fact that the signal having $1/f$ noise and the 'signal' (or data set) whose distribution is FTG like, are separate entities, and observations of an FTG distribution does not provide dynamical information. If the aim of an experiment is to study the observable x, we pose the question:

> Is it possible to observe the FTG function for $P(x)$ and to have $S_x(f) \propto 1/f$?

In other words, can a $1/f$ signal give rise to the FTG distribution without the averaging required to determine the width squared? If so, the two phenomena combine in a single signal and suggest a window into the microscopic physics of the system. This question is motivated in large part by observations [21, 42] of an approximately FTG distribution for fluctuations of simple global quantities (i.e. not width squared) with scale free power spectra ($\alpha \neq 1$). The combination of both these properties in a single signal was the result of restricting the resolution of the experiment, effectively pre-averaging the raw data. We are interested to know whether this is possible in the case of pure $1/f$ noise.

6.3 Numerical Investigations of $1/f$ Noise

6.3.1 Generating a Gaussian $1/f$ Noise Signal

Numerical simulations of noise signals require some means of generating data with the required statistics and temporal behaviour. In the case of Gaussian $1/f$ noise this is relatively straightforward. The first step is to generate a set of data with a Gaussian distribution, which is generally achieved by making use of the central limit theorem.

A large number, n, of values a_i are generated using a good random number generator*. As these values are all drawn from the same uniform distribution, their sum will be a Gaussian variable. Therefore

$$P\left(x = \sum_{i=1}^{n} a_i\right) = \frac{1}{\sigma\sqrt{2\pi}} e^{-\frac{(x-\mu)^2}{2\sigma^2}}, \tag{6.18}$$

where μ and σ are respectively the mean and variance of x. If a large number of x are independently generated in this way the resulting series $x(t)$ has a white noise ($\alpha = 0$) power spectrum. The mean and variance of the Gaussian distribution may be controlled by scaling and shifting the elements. For a signal generated from uniform random numbers in the range $0 \leq a \leq 1$,

$$x(t) \rightarrow \sqrt{\frac{12}{n}}\left(x(t) - \frac{n}{2}\right) \tag{6.19}$$

ensures that x has zero mean and unit variance.

To create the required power spectrum, the time signal is Fourier transformed into normal modes ϕ_f. These are complex variables which are themselves Gaussian, with

$$\langle \Re(\phi_f) \rangle = \langle \Im(\phi_f) \rangle = 0. \tag{6.20}$$

The real and imaginary parts are then scaled as

$$\Re(\phi) \rightarrow \frac{1}{\sqrt{f^\alpha}} \Re(\phi) \tag{6.21}$$

$$\Im(\phi) \rightarrow \frac{1}{\sqrt{f^\alpha}} \Im(\phi), \tag{6.22}$$

*For these and all other simulations presented in this thesis we have used `ran2()` from [130].

and so, on inverse Fourier transforming the resulting signal, the statistics of $x(t)$ remain Gaussian and the power spectrum has the form

$$S(f) \sim \left\langle |\phi_f|^2 \right\rangle \sim \frac{1}{f^\alpha}. \tag{6.23}$$

In §6.5.1 we discuss another method of generating $1/f^\alpha$ noise relating directly to a real physical process. In this section, however, we use the CLT method described above as this gives the best Gaussian $1/f$ behaviour over the whole range of frequencies.

When filtering the frequency spectrum by $1/f^{\alpha/2}$ there is a problematic divergence at $f = 0$. The easiest way to deal with this is to set $\phi_0 = 0$ which is equivalent to setting the mean of the corresponding time series to zero (which is often desirable anyway). Also, determining the power spectrum technically requires taking an ensemble average, which implies the need for many repetitions of the signal. In practice this is not always necessary. The linearity of a log–log plot of $|\phi_f|^2$ as a function of f generally gives a very clear indication of α. When the data is sufficiently scattered that the gradient of the mean is hard to ascertain, it is often possible to make considerable improvements by averaging $|\phi_f|^2$ over regions of f and plotting these averages against the mid-points of the ranges. This does not compromise the form of the power spectrum and can be remarkably effective in smoothing out the noise.

6.3.2 The $1/f$–FTG Link: A Simple Thought Experiment

The question at the end of §6.2.2 asks whether it is possible to observe $1/f$ noise and FTG statistics in a single signal. Our aim is to devise an experiment in which some property of a system has $1/f$ noise and is FTG distributed. This is not the case for the roughness of a Gaussian $1/f$ signal which, though having FTG statistics, has a white noise power spectrum (Figure 6.3.2).

Evaluating the roughness involves being able to calculate averages over the period of the signal. If a certain amount of experimental 'tuning' is allowed, it is possible to mimic the averaging process so that the observed values are themselves averages. This involves introducing a measuring time, t_m, which is defined as the finite time over

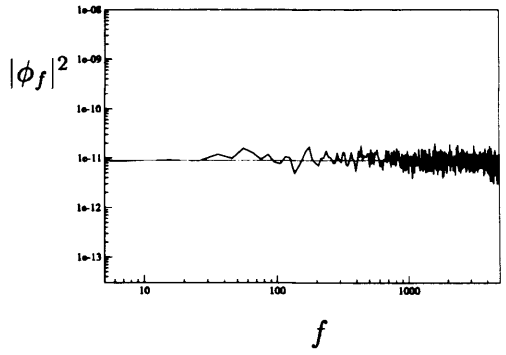

Figure 6.2: Power Spectrum of w_2 derived from $1/f$ Gaussian White Noise: The original signal had 10^6 elements and was split into sections of length 100 for each of which the roughness was evaluated. The power spectrum corresponds to the resulting roughness 'signal'. The straight guide line is proportional to f^0 (i.e. constant).

which each observation of the system is made. This time can be fixed by the temporal resolution of the apparatus or may be set by the experimenter. If the frequencies of some dynamical processes in the system are greater than T/t_m, then each observation of the system will see several different states, and the recorded value of the observable is the effective average

$$x'(t) = \frac{1}{t_m} \int_t^{t+t_m} x(t')\, \mathrm{d}t'. \tag{6.24}$$

The signal that is actually recorded must then be interpreted as being derived from the true $1/f$ signal with some of the high frequency behaviour having been integrated out. The effect of (6.24) on a Gaussian $1/f$ signal is to leave both the statistics and power spectrum unchanged (this is true because the convolution of two Gaussians is simply another Gaussian, and the noise is scale invariant by definition), however this is not so for other statistical regimes.

The roughness of a signal $x(t)$ is

$$w_{2_{(x)}} = \left\langle x(t)^2 \right\rangle - \left\langle x(t) \right\rangle^2. \tag{6.25}$$

Therefore, if $x(t)$ is Gaussian with zero mean, this reduces to

$$w_{2_{(x)}} = \left\langle x(t)^2 \right\rangle. \tag{6.26}$$

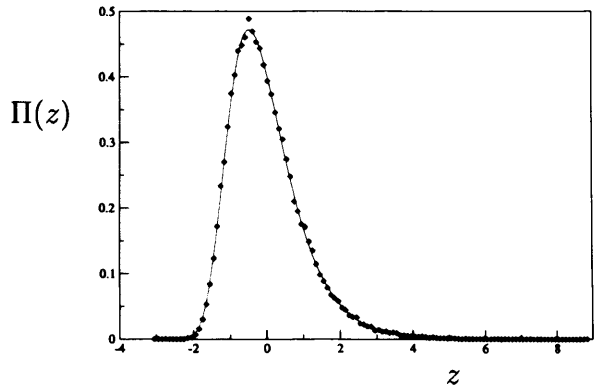

Figure 6.3: Distribution of the Ensemble Mean of $y(t)$: ...where $y(t)$ is a $\Gamma_{\frac{1}{2}}$ distributed signal formed from the squares of elements in Gaussian $1/f$ noise. In this case, $z = (\langle\mu\rangle - \mu)/\sigma_\mu$ where μ is the average value of $y(t)$ in any given signal. The data is an excellent fit to the FTG distribution (solid line).

Defining a new signal $y(t)$ such that

$$y(t) = x^2(t), \tag{6.27}$$

and assuming $x(t)$ has a $1/f$ power spectrum, it must be true that $\langle y(t)\rangle$ is FTG distributed [48]. To test this assertion we have generated 10^5 Gaussian, zero mean, $1/f$ noise signals. The elements of each signal were then squared to produce a new set of $\Gamma_{\frac{1}{2}}$ distributed signals, $y(t)$, which were analysed to give $P(\langle y(t)\rangle)$. As can be seen from Figure 6.3 the result is clearly the FTG distribution, and only 100 elements in each $x(t)$ were required for this level of fit.

The Power Spectrum of Gaussian $1/f$ Derived $\Gamma_{\frac{1}{2}}$ Signals

The signal $y(t)$ described above has a mean with the desired statistics, but our aim is to link this distribution specifically to $1/f$ noise. Taking $x(t)$ to be Gaussian with zero mean, and $1/f$, gives

$$x(t) = \frac{1}{\sqrt{N}} \sum_f e^{itf} \phi_f, \tag{6.28}$$

where N is the length of the signal and

$$\left\langle |\phi_f|^2 \right\rangle \sim \frac{1}{f}. \tag{6.29}$$

Squaring the elements of this signal produces the signal $y(t)$, the elements of which are $\Gamma_{\frac{1}{2}}$ distributed. We can also define

$$y(t) = \frac{1}{\sqrt{N}} \sum_f e^{itf} \psi_f \tag{6.30}$$

$$= \frac{1}{N} \sum_{f'} \sum_{f''} e^{i(f'+f'')t} \phi_{f'} \phi_{f''}, \tag{6.31}$$

which means,

$$\psi_f = \frac{1}{\sqrt{N}} \sum_t e^{-ift} y(t) \tag{6.32}$$

$$= \frac{1}{N^{\frac{3}{2}}} \sum_t e^{-ift} \left(\sum_{f'} \sum_{f''} e^{i(f'+f'')t} \phi_{f'} \phi_{f''} \right) \tag{6.33}$$

$$= \frac{1}{\sqrt{N}} \sum_{f'} \sum_{f''} \phi_{f'} \phi_{f''} \, \delta(f - (f' + f'')). \tag{6.34}$$

For a given value of f neither f' or f'' may be greater than f. Also, as the only non-zero contributions to ψ_f come from $f = f' + f''$, and $\langle \phi_0 \rangle = 0$,

$$\psi_f = \frac{1}{\sqrt{N}} \sum_{a=1}^{f-1} \phi_{f-a} \phi_a. \tag{6.35}$$

For complex z, if $Z = \sum_i z_i$,

$$|Z|^2 = \sum_i \sum_j z_i z_j^* \tag{6.36}$$

$$= \sum_i |z_i|^2 + 2 \sum_i \sum_{j \neq i} (\Re(z_i)\Re(z_j) + \Im(z_i)\Im(z_j)) \tag{6.37}$$

The power spectrum of $y(t)$ is therefore

$$\left\langle |\psi_f|^2 \right\rangle = \left\langle \frac{1}{N} \sum_{a=1}^{f-1} \left(|\phi_{f-a}|^2 |\phi_a|^2 \right) + 2 \sum_{a=1}^{f-1} \sum_{b=1}^{f-1} (\Re(\phi_{f-a})\Re(\phi_b) + \Im(\phi_{f-a})\Im(\phi_b)) \right\rangle. \tag{6.38}$$

It is assumed that these modes are indeed normal and therefore statistically independent. Also, by definition, the averages of the real and imaginary parts of ϕ are zero. Equation (6.38) then reduces to

$$\left\langle |\psi_f|^2 \right\rangle = \frac{1}{N} \sum_{a=1}^{f-1} \left\langle |\phi_{f-a}|^2 \right\rangle \left\langle |\phi_a|^2 \right\rangle \tag{6.39}$$

$$= \frac{1}{N}\sum_{a=1}^{f-1}\frac{1}{a\,(f-a)}, \tag{6.40}$$

where (6.40) follows from (6.29). The sum over a is interesting as it separates into two equal terms expressed in different ways.

$$\sum_{a=1}^{f-1}\frac{1}{a\,(f-a)} = \sum_{a=1}^{f-1}\frac{1}{af} + \sum_{a=1}^{f-1}\frac{1}{f\,(f-a)}. \tag{6.41}$$

Applying the Abel-Plana formula (5.59) gives the same results for both the sums on the RHS of (6.41). Though initially surprising, this can be seen by the fact that the arguments of the sums are the same function reflected and shifted relative to each other such that the area under each is the same between the specified limits.

$$\sum_{a=1}^{f-1}\frac{1}{a} = \sum_{a=1}^{f-1}\frac{1}{f-a} \overset{(\text{large}f)}{=} \left\{\ln(f-1) + \frac{1}{2(f-1)} + \gamma\right\}, \tag{6.42}$$

where γ is Euler's constant. Therefore the final expression for the power spectrum of $y(t)$ is

$$\left\langle|\psi_f|^2\right\rangle = \frac{2}{fN}\left\{\ln(f-1) + \frac{1}{2(f-1)} + \gamma\right\} \tag{6.43}$$

For large f this function is dominated by the $\ln(f-1)/f$ term which is very well approximated by $f^{-\alpha}$ with $\alpha \approx 0.9$ (Figure 6.4). In truth the value of α will necessarily vary with f, becoming closer to 1 as $f \to \infty$. This result is particularly interesting as $\Gamma_{\frac{1}{2}}$ $1/f$ noise cannot be generated by simply filtering $\Gamma_{\frac{1}{2}}$ white noise, due to the Fourier transform stages altering the statistics (eventually leading to a Gaussian form).

The analysis shows that squaring the elements of a Gaussian $1/f$ signal with zero mean leads to a $\Gamma_{\frac{1}{2}}$ distributed signal with a power spectrum very close to being $1/f$. It has also been shown that the distribution of the average of this signal is an excellent fit to the FTG function. Therefore $y(t)$ is an ideal choice for the study of a possible experimental, single signal, link between $1/f$ noise and FTG statistics. Our simulations to this point have recorded the ensemble statistics of $\langle y\rangle$, which is different from the average $\langle y(t)\rangle_{t_m}$ calculated from a single signal.

We have generated $y(t)$, a $\Gamma_{\frac{1}{2}}$ distributed, approximately $1/f$ signal with 10^6 elements from a parent Gaussian signal, $x(t)$, and split this into consecutive blocks of

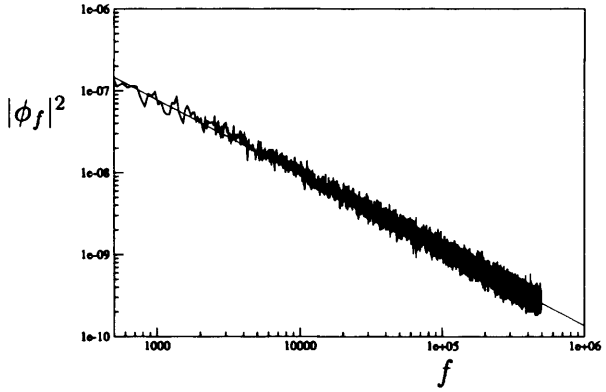

Figure 6.4: Power Spectrum of $\Gamma_{\frac{1}{2}}$ Noise Generated from Gaussian $1/f$ Noise: On squaring the elements of Gaussian $1/f$ signal with zero mean the power spectrum changes very little and can be fitted very well by $|\phi_f|^2 \sim 1/f^{\alpha}$ with $0.9 < \alpha < 1$. The red line here has a gradient of 0.92.

length $t_m = 100$. The average within each block was then evaluated giving 10000 values which, within the confines of our experiment, define the data set whose statistics are of interest. Importantly, from the point of view of our determination to compare the power spectrum and statistics of the same signal, scale invariance ensures that this 'raw' data retains the near $1/f$ temporal behaviour of $y(t)$. Figure 6.5 shows the PDF of $\langle y(t) \rangle_{t_m}$ which is clearly not the FTG distribution over any range of values.

The reasons behind this result demonstrate the importance of correlation and randomness in statistical sampling. If a Gaussian white noise signal of length N, having zero mean, has $n \ll N$ elements chosen at random, the distribution of the n elements will also be Gaussian with zero mean. If the n are not chosen at random but are, for example, the first n elements, the same also true. However, this is not the case if the signal is not uniformly dispersive but has $1/f$ noise (or some other non-uniform power spectrum). It remains true that a random sample may exhibit the statistics of the parent signal, however if the sample is taken simply as n contiguous points, the set $\{x_n\}$ will generally obey different statistics from the set $\{x_N\}$ [90]. If n is sufficiently long to cover all relevant time scales, this would not apply, however for $1/f$ noise this requires $n = N$ in which case there is no concept of sampling. In the context of our experiment, the Gaussian $1/f$ signal $x(t)$ has zero mean only over

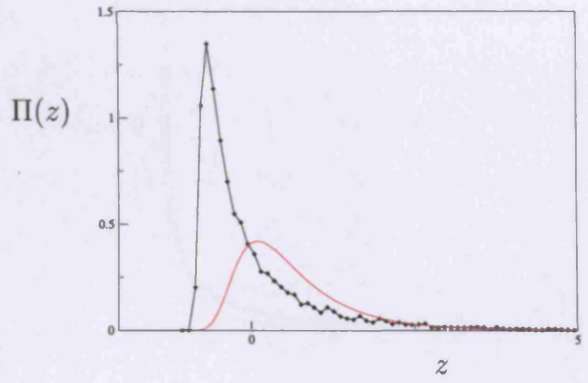

Figure 6.5: Distribution of $\langle y(t) \rangle$ from Sections of a Single Signal: The non-uniform mode dispersion makes this inherently different from taking an ensemble average – as discussed in the text. Again, $z = (\langle \mu \rangle - \mu)/\sigma_\mu$ where $\mu = \langle y(t) \rangle_{t_m}$ is evaluated over each section. The FTG function is also plotted (red line) to highlight the difference from the experimental data.

its entire length. For any individual section of length t_m, the average is non-zero and varies in a manner governed by the low frequency modes. Therefore, the signal $y(t)$ is $\Gamma_{\frac{1}{2}}$ distributed overall, but not within the t_m sections. The square of a Gaussian with finite mean, μ_G, and standard deviation σ_G has the normalized PDF (Appendix B)

$$P(x) = \frac{1}{\sigma_G \sqrt{2\pi}} x^{-\frac{1}{2}} \frac{\exp\left(-\frac{x}{2\sigma_G^2} + \frac{\mu_G \sqrt{x}}{\sigma_G^2}\right)}{\exp\left(\frac{\mu_G^2}{2\sigma_G^2}\right)\left(1 + \operatorname{erf}\left(\frac{\mu_G}{\sqrt{2}\sigma_G}\right)\right)}. \tag{6.44}$$

This is functionally quite similar to a $\Gamma_{\frac{1}{2}}$ distribution, especially for large x, and for a small data set it can be hard to distinguish between the two. Figure 6.6 shows the distribution of the first 10000 elements of our $y(t)$ signal, plotted together with the $\Gamma_{\frac{1}{2}}$ distribution and (6.44). It is clear that the numerical results are a much better fit to the latter. Therefore, as $y(t)$ is not $\Gamma_{\frac{1}{2}}$ on the interval defined by t_m, the derivation of (6.43) breaks down and there is no reason to expect $\langle y(t) \rangle_{t_m}$ to be FTG distributed.

We conclude that, even in our highly contrived thought experiment, we have been unable to directly observe a link between $1/f$ noise and the FTG distribution in a single experimental signal. One must have knowledge of the underlying microscopic degrees of freedom in order that their average may be removed from the problem. This highlights the distinction between a 'running average' evaluated over only part

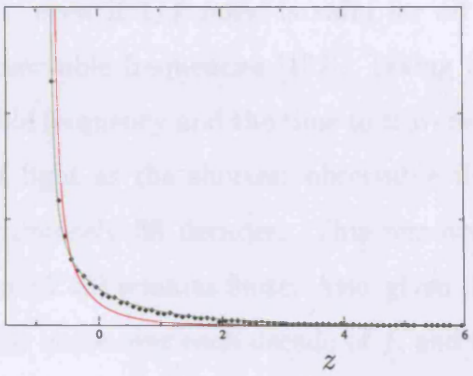

Figure 6.6: The Distribution of Elements in a Section of $y(t)$: Despite being $\Gamma_{\frac{1}{2}}$ distributed overall (red line), each section of $y(t)$ comes from a Gaussian signal with non-zero mean and is therefore distributed according to (6.44) (green line). The numerical data here is from the first 10^4 elements of a signal of length 10^6. The shape of the curve changes with the mean and standard deviation of the underlying Gaussian variables.

of a signal, and the global average $\langle x(t) \rangle$. We suggest that most insight may be gained from the former when dealing with cases such as interface problems, where the $1/f$ noise actually relates to spatial fluctuations.

6.4 Imperfect $1/f$ Noise

The Gaussian noise signals discussed in §6.3 were generated to be perfectly $1/f$ over all frequencies above $f = 0$. Such perfection in $1/f$ noise is practically feasible, as demonstrated by Pellegrini *et al.* in studies of voltage fluctuations across thin film resistors [131]. Their results showed $1/f$ power spectra extending over six decades of frequency, with no evidence of deviation from this behaviour even for the lowest values of f. However, if the power spectrum remains of this form to $f = 0$ it encounters a divergence, and as

$$\left\langle x^2 \right\rangle = \int_0^\infty S_x(f)\,\mathrm{d}f, \tag{6.45}$$

the fluctuations become unbounded. This has the potential for severe consequences in many physical situations and is essentially the reason for the interest in the wings of non-Gaussian distribution functions.

It has been argued that, even if $1/f$ noise is valid for all f, there are certain limits on experimentally observable frequencies [132]. Taking the inverse life of the universe as the lowest possible frequency and the time to traverse a Compton electron wavelength at the speed of light as the shortest observable time, gives a range of frequencies spanning approximately 38 decades. This removes the zero frequency divergence and the integral in (6.45) remains finite. Also, given the logarithmic nature of the integral, its value is the same over each decade of f, and thus fluctuations in x can be at most 38 times as big as the total fluctuations between, say, 1Hz and 10Hz.

Despite the occurrence of some very accurate $1/f$ signals, there are examples of systems where the noise is classed as $1/f$ even though this is strictly true over only a restricted range of frequencies. For example, earthquakes possess a $1/f$ power spectrum, but only over 3 decades of frequency, below which the spectrum flattens to approximately white noise [127]. More generally, $1/f$ noise formed by the superposition of dynamical processes with a distribution of relaxation times (discussed in more detail in §6.5) often has a white noise region at low frequency, and a high frequency $1/f^2$ 'roll off'. This introduces an interesting experimental question regarding the link between Gaussian $1/f$ noise and the FTG distribution. Does the $1/f$ noise signal have to retain its form for all f in order for the width square to remain apparently FTG distributed?

6.4.1 'Single Signal' Imperfect $1/f$ Noise

The answer to the question posed above depends on the manner in which the experiment is performed. We begin by addressing the case of a single Gaussian $1/f$ signal split into sections. This is the method used to numerically simulate the results in [48] and has the effect of introducing window boundary conditions (WBCs). The roughness of each section of length t_m is evaluated and it is the distribution of this quantity whose PDF is determined.

Modifying the High Frequency Region

For a perfectly $1/f$ signal it is well established that the distribution of w_2 measured in this manner is close to the FTG function. By altering the form of the power spectrum over a region of frequencies, it is reasonable to expect this to change. If the low frequency behaviour is left alone (i.e. remains $1/f$) and a region of $1/f^2$ behaviour is imposed above some frequency f_2 (see Figure 6.10), one sees some interesting results. The first significant observation is that f_2 can be very small relative to the highest frequency with no noticeable effect on the distribution of w_2. This can be understood by considering the relationship between f_2 and t_m, the time over which the roughness is measured.

In general, if one averages the signal over some time scale τ, the only modes that will contribute to that average must have frequencies greater than $f = t_N/\tau$. In our simulations, f is discrete, with the highest frequency process occurring every time step giving $f_{\max} = t_N$. However, the symmetry imposed by requiring the time signal to be real results in the highest frequency output from the Fourier transform being $t_N/2$. Thus f serves as an index for the modes rather than as a their absolute frequencies, and in reality, mode f has frequency $2f$. Evaluating w_2 involves taking the average over a period t_m. Thus the only modes that are relevant are those with $2f > t_N/t_m$. If the $1/f^2$ region is setup with $2f_2 \gg t_N/t_m$, the slower fall off and greater weighting of the $1/f$ modes in the region $t_N/(2t_m) < f < f_2$ will be expected to dominate, and w_2 should remain close to the FTG form. This leaves a lot of scope for defining f_2. For a perfectly $1/f$ signal, no improvement in the fit to the FTG function is seen beyond $t_m \approx 100$. A suitable value of f_2 is therefore anything significantly greater than about $t_N/100$, allowing the possibility of up to several decades of $1/f^2$ noise before $P(w_2)$ is affected.

To demonstrate this, Figure 6.7 shows $P(w_2)$ for a perfectly $1/f$ signal and a signal with a $1/f^2$ region at high frequencies. Both have $t_N = 10^6$ and the latter has $f_2 = 50000$ (meaning that 90% of the modes go as $1/f^2$); t_m is taken as 100. The plot shows that even this large modified region has little effect on the roughness

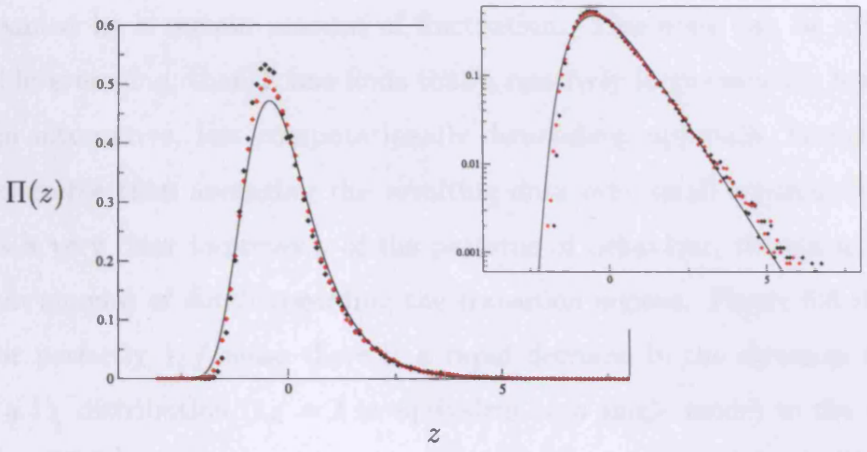

Figure 6.7: The Effect of High Frequency Modification on $P(w_2)$: The numerical data shows the normalized distribution of $z = (w_2 - \langle w_2 \rangle)/\sigma_{w_2}$ from 'pure' Gaussian $1/f$ noise (red points) and Gaussian $1/f$ noise with a $1/f^2$ high frequency region (black points). Both signals have $t_N = 10^6$ and $t_m = 100$. The modified signal has $f_2 = 50000$. The data is plotted against the FTG distribution (solid line); there is little difference between the two sets of numerical data despite the large range of modification. The discrepancy with the FTG function is also seen in [48] and arises from boundary considerations. The inset shows the same plot on semi-log axes.

distribution, what small differences there are being concentrated around the peak.

If the value of f_2 is lowered, the number of $1/f$ modes contributing to each value of w_2 is diminished and there is a cross over between statistical regimes. For pure $1/f^2$ noise $P(w_2)$ is the defined by the Wiener process [49] and is more skewed than the FTG function. By fixing f_2 at some suitably small value and varying t_m it would be expected that $P(w_2)$ should initially be controlled by the $1/f^2$ modes before gradually evolving to the approximately FTG form as the balance of the modes contributing to w_2 shifts in favour of $1/f$. In theory, the distribution corresponding to $1/f^2$ noise will dominate until $t_m \approx t_N/(2f_2)$, at which point the $1/f$ modes start to encroach on the individual sections of length t_m. Once there are sufficient $1/f$ modes contributing to w_2 to make $P(w_2)$ FTG like, further increasing t_m should lead to no change in the distribution.

A useful means of analysing this behaviour is to follow the skewness of $P(w_2)$ as

a function of t_m. The skewness is a relatively soft quantity and so the general trend is accompanied by a certain amount of fluctuation. This noise can be diminished by ensemble averaging, though one finds that a relatively large ensemble is required. We use an alternative, less computationally demanding, approach, averaging over a small ensemble then averaging the resulting data over small consecutive blocks. This gives a very clear impression of the patterns of behaviour, though at the cost of a certain amount of detail regarding the transition regions. Figure 6.8 shows the results; for perfectly $1/f$ noise there is a rapid decrease in the skewness from the value for a $\Gamma_{\frac{1}{2}}$ distribution ($t_m = 1$ is equivalent to a single mode) to the value for the limiting FTG like function. As a result of the window boundary conditions one never observes the actual FTG value of $|\gamma_3| \approx 1.14$, seeing instead a slightly more skewed distribution with $|\gamma_3| \approx 1.4$ [48]. Also included is a plot corresponding to distributions obtained from purely $1/f^2$ noise. The signals were of length $t_N = 10^6$, therefore setting $f_2 = 5000$ should fix γ_3 at the value corresponding to $1/f^2$ noise for, approximately, $t_m < 100$. Likewise, setting $f_2 = 2500$, the range of $1/f^2$ dominance should end at about $t_m = 200$. Above these values, $|\gamma_3|$ is expected to fall to the WBC corrected FTG value and remain there for all higher t_m. The general trends are confirmed by the numerical results shown in Figure 6.8, though our method of averaging the skewnesses makes it hard to confirm the predictions regarding the upper limits on t_m for $1/f^2$ dominance. More substantial simulations are required to look at this point detail, however it is clear that that predicted values are in the correct region. It is also apparent that there is a significant crossover period, so that the FTG limit is not approached until t_m is much greater than the point at which $1/f^2$ dominance breaks down.

It appears as though the limiting value of the skewness increases as f_2 decreases. This is perfectly reasonable as for $f_2 \to 0$ the distribution is markedly more skewed than the FTG function. The fact that the dominant low frequency $1/f$ modes do not completely mask this effect is an indication that the high frequency modes continue to play an important role in the value of w_2 even for large t_m.

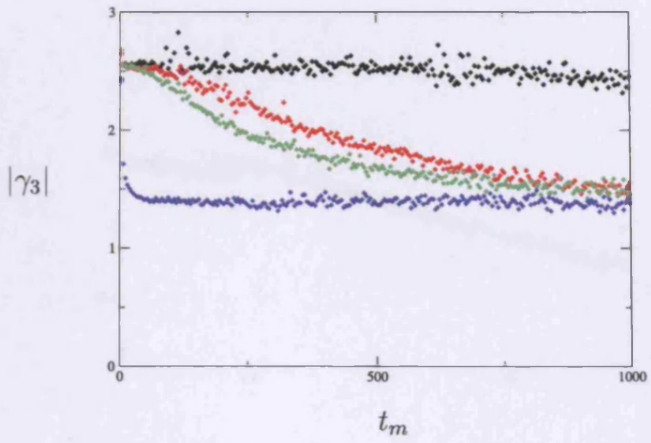

Figure 6.8: The Effect of High Frequency Modification on $|\gamma_3|$: A comparison between the evolution of the skewness of $P(w_2)$, with increasing t_m, of: $1/f^2$ noise (black), $1/f$ noise (blue), and $1/f$ noise with high frequency $1/f^2$ modification with $f_2 = 5000$ (green) and $f_2 = 2500$ (red).

Modifying the Low Frequency Region

The arguments regarding modifying the high frequency power spectrum can be applied directly to modifications at low f. Assuming the spectrum consists of two regions,

$$S(f) = \begin{cases} \frac{1}{f_1} & f \leq f_1 \\ \frac{1}{f} & f > f_1 \end{cases}, \tag{6.46}$$

the value of t_m controls the statistics of w_2. For $t_m < t_N/2f_1$ the roughness is dominated by modes with the desired $1/f$ spectrum. However, as the measuring time is increased w_2 starts to feel the effects of the white noise modes with frequencies below f_1. The roughness distribution of a white noise signal is Gaussian as the lack of correlation makes the central limit theorem valid. It is therefore expected that $P(w_2)$ will tend toward a Gaussian for $t_m \gg t_N/2f_1$.

The numerical results in Figure 6.9 appear to confirm this, showing a region of approximately FTG-like behaviour before a steady decline in the skewness as t_m is increased. The numerical data is from a signal with $t_N = 10^6$ and $f_1 = 1000$. It would thus be expected that the FTG region would end at $t_m \approx 500$, and this is

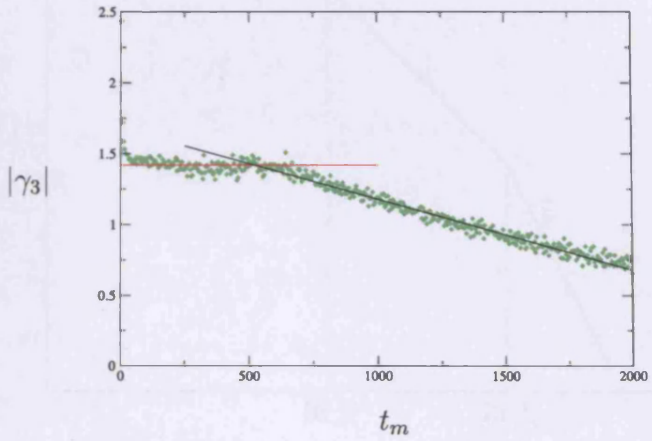

Figure 6.9: The Effect of Low Frequency Modification on $|\gamma_3|$: The evolution of the skewness of $P(w_2)$ as a function of t_m. The data is from a signal with $t_N = 10^6$ and $f_1 = 1000$. The solid lines are a guide to the eye, highlighting the approximately FTG region (red) and the deviation from this as the white noise modes force the skewness to zero (black).

seen to be the case. Although it appears that the skewness is tending toward zero for large t_m we have not actually seen this as the statistics become unreliable for small t_N/t_m. However, it is logical to conclude that this limit will be reached as, once the white noise dominates each w_2, the sections of length t_m may be split into mesoscopically independent regions at which point the CLT applies. For the largest t_m in our simulations there is no sign of a levelling off in $|\gamma_3|$.

Combined High and Low Frequency Modifications

Our theoretical experimental signal has a power spectrum represented schematically in Figure 6.10. It consists of a low frequency region of white noise, an intermediate $1/f$ region and finally $1/f^2$ noise at high frequencies. The consequences of the two non-$1/f$ regions differ, with the white noise region becoming more influential, and the $1/f^2$ region less so, for large values of t_m. Combining the results of the individual sectors, it is therefore expected that the statistics of w_2 will move from being $1/f^2$ dominated, through an FTG region and finally toward Gaussian behaviour as t_m is

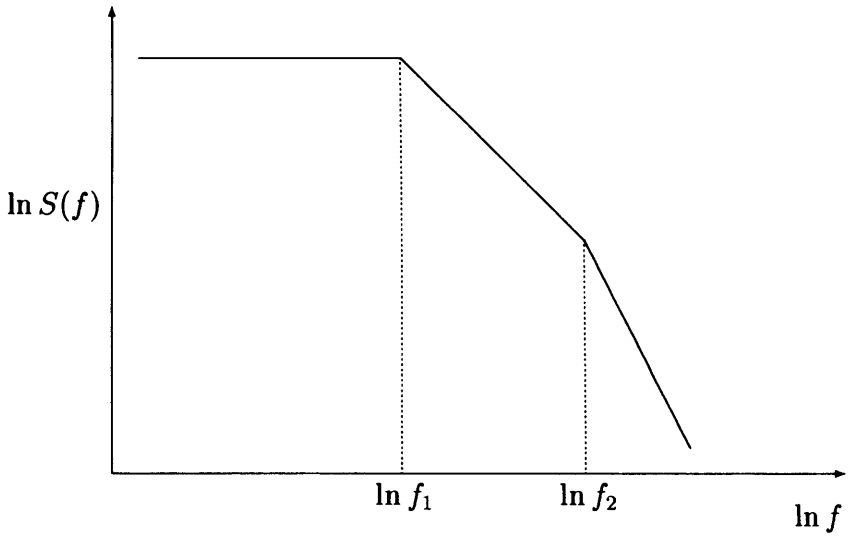

Figure 6.10: Schematic Power Spectrum for $1/f$ Noise Modified by Low Frequency White Noise and High Frequency $1/f^2$ Noise.

increased. In order to see the effects of all three regions, the values of f_1 and f_2 must be chosen carefully. Firstly, f_2 must be sufficiently small that the $1/f^2$ dominated region is represented. Secondly f_1 must be large enough to ensure that the FTG to Gaussian evolution occurs at a value of t_m for which reliable statistics are available. This is only a problem in terms of the computational constraints on t_N.

It is expected that w_2 will be approximately FTG distributed within a region defined by

$$\frac{t_N}{2f_2} \ll t_m < \frac{t_N}{2f_1}. \tag{6.47}$$

The requirement that t_m be much greater than the lower limit is a consequence of the transition between statistical regimes. As a result, if $f_2 - f_1$ is too small, the FTG region may appear transient with $|\gamma_3|$ steadily declining from the $1/f^2$ dominated value to the Gaussian value of zero.

Figure 6.11(a) shows a plot of $|\gamma_3|$ as a function of t_m for a signal of length $t_N = 10^6$, having a white noise region defined by $f_1 = 800$, and a high frequency $1/f^2$ region defined by $f_2 = 8000$. These values allow enough of a range of $1/f$ noise for an approximately FTG value of $|\gamma_3|$ to be observed over a range of t_m. The plot is on logarithmic axes to emphasize the different statistical regions. It is seen that

the $1/f^2$ dominance persists until around $t_m = 60$, after which there is a transition to FTG statistics which may reasonably be said to begin at $t_m \approx 400$ and continue to be observed until $t_m \approx 600$. This is in good agreement with the predicted value of $t_N/2f_2 = 625$. Beyond this there is a steady, and reasonably rapid, decrease in the skewness, though as before we have been unable to emphatically demonstrate the Gaussian limit of this decline.

Figure 6.11(b) shows the power spectrum of the high and low frequency modified signal, confirming that it has the required form. When constructing a signal with this type of power spectrum it is important to remember two points regarding the filtering of the modified regions. Firstly, the modes in the white noise region have no frequency dependent filtering, but must be multiplied by $1/f_1$ so that there is no discontinuity in $S(f)$. By the same logic, the $1/f^2$ modes must be filtered by $1/f$ with an extra factor of $\sqrt{f_2}$. Therefore the overall form is,

$$S(f) \propto \begin{cases} \frac{1}{f_1} & f < f_1 \\ \frac{1}{f} & f_1 \leq f < f_2 \\ \frac{\sqrt{f_2}}{f^2} & f \geq f_2 \end{cases} . \tag{6.48}$$

Experimental Implications

The results of this section demonstrate that our ability to observe experimentally the link between $1/f$ noise and the FTG distribution depends on the quality of the noise, or more precisely, the range over which it is $1/f$ like. For a region of non-$1/f$ behaviour at high frequencies there is relatively little effect on the roughness distribution providing the period over which w_2 is measured is suitably long. As an empirical rule it is fair to say that for high frequency modifications to become an issue, f_2 must be so low that the noise is unlikely to categorized as $1/f$ in the first place.

Low frequency white noise poses a different problem. Ideally t_m should be as large as possible and so the low frequency modes become more influential. The resulting deviation from FTG statistics occurs relatively slowly but steadily, and the result is

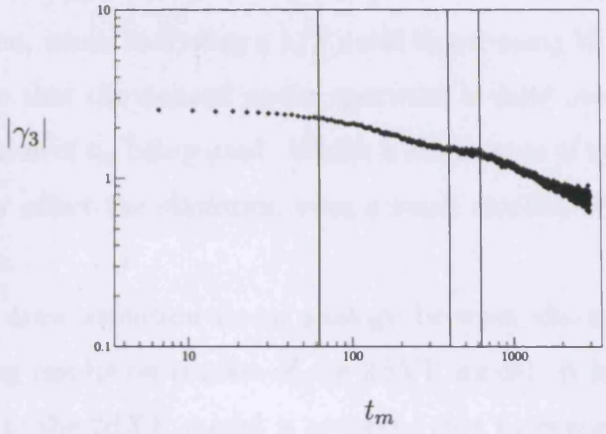

(a)

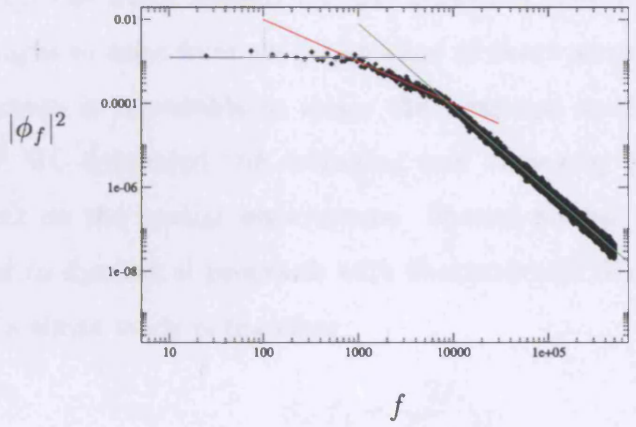

(b)

Figure 6.11: Combined High and Low Frequency Modified $1/f$ Noise: ... for a signal with $t_N = 10^6$, $f_1 = 800$ and $f_2 = 8000$. (a) The variation of the skewness as a function of t_m, in four sections (from left to right): $1/f^2$ dominated behaviour, transition region, FTG like statistics and decline to $\gamma_3 = 0$. Logarithmic axes are used to highlight the levelling off in the third region which is partly obscured on a linear scale. (b) The dependence of $|\phi_f|^2$ on f for the same signal. The solid lines are guides to the three regions: white noise (blue), $1/f$ noise (red) and $1/f^2$ noise (green).

ultimately a Gaussian $P(w_2)$. As t_m grows, very few white noise modes (relative to t_N) are needed to significantly alter the statistics of the roughness.

In conclusion, when analysing a $1/f$ noise signal using WBCs great care must be taken to ensure that the desired power spectrum is valid over a range of frequencies suited to the value of t_m being used. Whilst a large range of modified high frequencies will not unduly affect the statistics, even a small amount of low f white noise may have an impact.

Finally we draw attention to an analogy between the work presented here and some interesting results on studies of the 2dXY model. It has been seen that if the magnetization of the 2dXY model is averaged over t_m consecutive observations, the statistics of the resulting quantity, $\langle m \rangle_{t_m}$, vary with t_m. Initially the distribution is BHP, it becomes progressively more skewed as t_m is increased, approaching the FTG distribution at which point it becomes less skewed and tends toward a Gaussian for large t_m [133]. The exact reasons for this behaviour have not yet been established, but is is thought to arise from the integration of short wavelength modes out of the system. Because it is possible to relate the temporal modes to the spatial modes via the $1/f^2$ MC dynamics, the averaging over time may be thought of as having a direct effect on the spatial wavevectors. Spatial normal modes with wavevector $\mathbf{q}$ correspond to dynamical processes with characteristic frequency $\sqrt{f_s}$. The power spectrum of a single mode is therefore

$$S_s(f) = \frac{2f_s}{f_s^2 + f^2}, \tag{6.49}$$

which complicates the problem as the temporal modes are not independent. Integrating m over t_m effectively couples spatial modes in the Brillouin zone outside a circle of radius $q^* = \sqrt{f_m}$, where $f_m = t_m^{-1}$. When $q^* = 2\pi/L$ there is a reduction in the number of independent normal modes from N to approximately L; as the mean is not affected by this procedure, its logarithmic divergence might imply a change from $1/f^2$ to $1/f$ noise [134]. This would account for the appearance of the FTG function, given the Gaussian nature of the variables. Further increasing t_m means averaging over uncorrelated values of the magnetization which will eventually lead

to a Gaussian distribution. This can be thought of as being analogous to our modified $1/f$ noise results, where the FTG distribution emerges only when the period of integration corresponds to the range of $1/f$ behaviour.

6.4.2 $P(w_2)$ from Ensemble Averaging

When the roughness distribution is calculated from an ensemble of independent signals, all the frequencies present contribute to w_2 as, effectively, $t_m = t_N$. The roughness now has periodic boundary conditions (PBCs) and the different statistical regimes have functionally more similar PDFs – for a purely $1/f^2$ noise signal the PDF is considerably less skewed than its counterpart derived with WBCs [49]. Also, the dominance of the low frequency modes is manifest at all times, so the effect of different values of f_1 and f_2 should not be so dependent on t_N.

High Frequency $1/f^2$ Noise

As in the case of a single signal (WBC) evaluation of $P(w_2)$, the power spectrum has been modified to include a region of $1/f^2$ noise above some frequency f_2. The signals are considerably shorter for these simulations, however the ensemble contains 10^5 signals and the statistics are good. It is no longer appropriate to look at the skewness as a function of t_m (which remains fixed for a given t_N); instead we consider the form of the PDF as f_2 is varied. The results are given in Figure 6.12. As predicted, varying t_N for a given f_2 has little effect. Each value of f_2 is shown in a given colour for $t_N = 500$ (solid line) and $t_N = 100$ (discrete points). For all values of f_2 there is little distinction between these two plots, with the majority of points lying on the corresponding lines. For a purely $1/f^2$ power spectrum ($f_2 = 1$), the data is distinctly more skewed than the FTG distribution. However, including just a single $1/f$ mode, setting $f_2 = 2$, the PDF is already much closer to the FTG form than to that obtained with $f_2 = 1$. By the time $f_2 = 5$ the PDF is already very close to being FTG, and at $f_2 = 10$ it is essentially indistinguishable from it.

It is apparent that including very large numbers of $1/f^2$ modes has little effect on

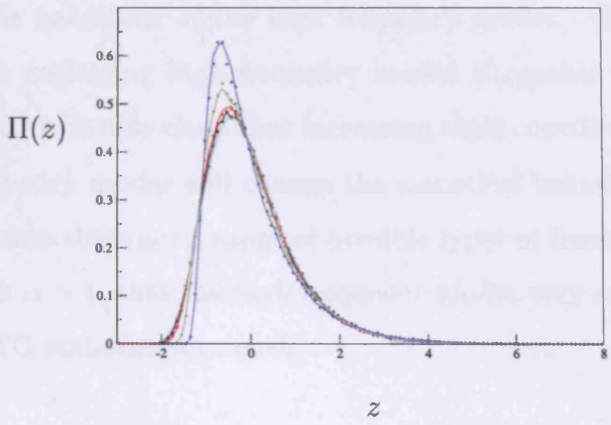

(a)

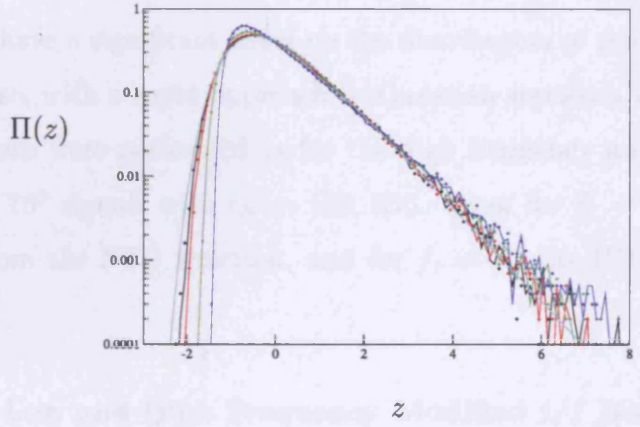

(b)

Figure 6.12: $P(w_2)$ from an Ensemble of $1/f$ Noise Signals with High Frequency $1/f^2$ Noise: All plots are for an ensemble of 10^5 signals; $z = (w_2 - \langle w_2 \rangle)/\sigma_{w_2}$ and $\Pi(z) = \sigma_{w_2} P(w_2)$. The solid lines correspond to $t_N = 500$ and the discrete points to $t_N = 100$. (a) The colours define different values of f_2 with: $f_2 = 10$ (black), $f_2 = 5$ (red), $f_2 = 2$ (green) and $f_2 = 1$ (blue). (b) As for (a) but plotted on semi-log axes, showing that the differences between the plots are almost entirely in the region below the mean. The FTG function (solid cyan line) is plotted for reference.

$P(w_2)$ provided a few low frequency $1/f$ modes are also present. The implications of this are that the dominance of the low frequency region allows for a degree of flexibility in the behaviour of the high frequency modes. We have already seen in Chapter 5 that neglecting high frequency modes altogether does have an effect on the distribution. It is also clear that increasing their contribution to be comparable to the low frequency modes will change the statistical behaviour. However between these two extremes there are a range of possible types of temporal behaviour, such as $1/f^{\alpha}$ noise with $\alpha > 1$, that the high frequency modes may adopt without obscuring the limiting FTG statistics too much.

Low Frequency White Noise

The explicit inclusion of all frequencies in evaluating w_2 necessarily leads to the dominance of low frequency behaviour when the power spectrum is of the general form $1/f^{\alpha}$. Thus the inclusion of a region of white noise near $f = 0$ would be expected to have a significant effect on the distribution of the roughness. This is seen to be the case, with a rapid approach to Gaussian statistics as f_1 is increased.

Simulations were performed as for the high frequency modified signals, using an ensemble of 10^5 signals with $t_N = 100, 500$. Even for $f_1 = 2$ there is a noticeable deviation from the FTG function, and for $f_1 = 10$ the PDF already appears very symmetrical.

Combined Low and High Frequency Modified $1/f$ Noise

When introducing both high frequency $1/f^2$ noise and low frequency white noise into our experimental signals, it is the white noise that has the most pronounced effect, as would be expected. This can be seen in Figure 6.14 (a) and (b) where, despite having $1/f^2$ noise for all modes above $f_2 = 10$, the PDF remains on the Gaussian side of the FTG function due to the white noise regions with $f_1 = 2$ and $f_1 = 5$ respectively. An interesting result is shown in Figure 6.14 (d), having $f_1 = 2$ and $f_2 = 3$. Despite having no $1/f$ behaviour, the combination of $1/f^2$ noise modified by a very small number of white noise modes at low frequency, is enough to generate an

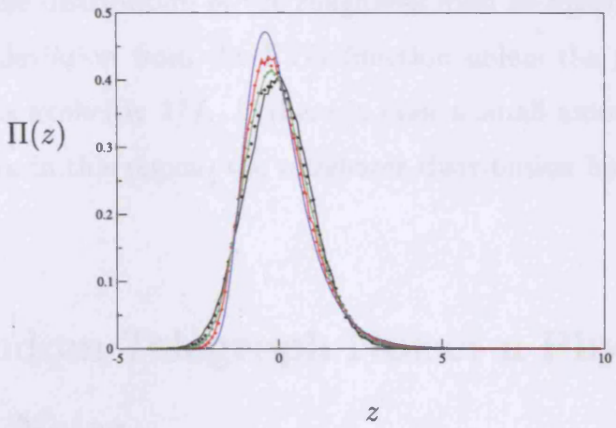

(a)

Figure 6.13: $P(w_2)$ from an Ensemble of $1/f$ Noise Signals with Low Frequency White Noise: All plots are for an ensemble of 10^5 signals; $z = (w_2 - \langle w_2 \rangle)/\sigma_{w_2}$ and $\Pi(z) = \sigma_{w_2} P(w_2)$. The solid lines correspond to $t_N = 500$ and the discrete points to $t_N = 100$. (a) The colours define different values of f_1 with: $f_1 =$ (black), $f_1 = 5$ (green) and $f_1 = 2$ (red). The FTG function (solid blue line) is plotted for reference.

almost perfect FTG distribution of the roughness over the full range of experimental interest.

Experimental Implications

As in the case of single signal (WBC) simulations, low frequency white noise is seen to be a bigger barrier to the observation of the FTG distribution than high frequency $1/f^2$ noise. In fact, the inclusion of all available modes in the evaluation of w_2 with PBCs makes the effect of the white noise region even more pronounced. Our results indicate that the distribution of the roughness from an ensemble of $1/f$ signals will show marked deviation from the FTG function unless the power spectrum of the lowest modes is explicitly $1/f$. If there is even a small amount of flattening of the power spectrum in this region, the roughness distribution becomes significantly less skewed.

6.5 Random Telegraph Noise: a Physical Route to $1/f$ Noise

As discussed above, the physical origins of $1/f$ noise remain an open question and it is unclear whether there a universal mechanism underlying all examples of this phenomenon. One proposal, stemming from the earliest studies of $1/f$ signals, relates the noise to the superposition of dynamical processes with a distribution of characteristic times. This approach started with Schottky's explanation for Johnson's observation of $1/f^{\alpha}$ noise in vacuum tube currents [66, 135]. Schottky proposed that the ability of the cathode to emit electrons would depend on the density of impurity atoms on its surface. He assumed that this density fluctuated as a result of diffusion and derived an expression for the mean square noise current per unit frequency interval (the power spectrum of the associated noise),

$$S(f) \sim \frac{\tau}{1+\tau^2 f^2}, \tag{6.50}$$

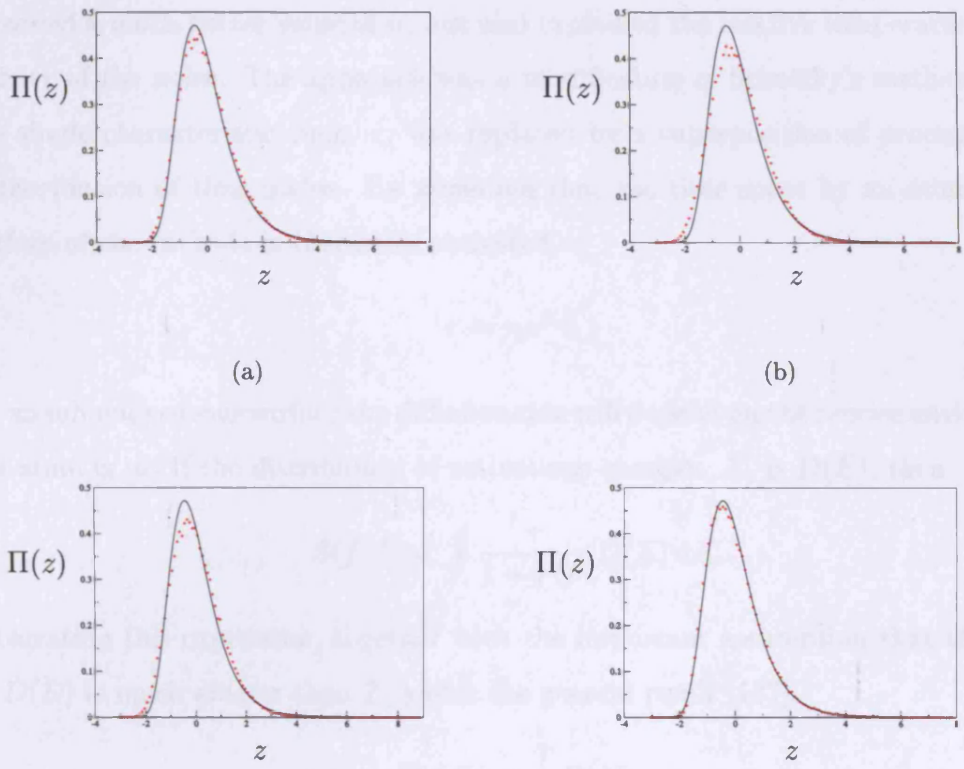

Figure 6.14: $P(w_2)$ from an Ensemble of High and Low Frequency Modified '$1/f$' Signals: The plots are of $\Pi(z) = \sigma_{w_2} P(w_2)$, with $z = (w_2 - \langle w_2 \rangle)/\sigma_{w_2}$. All numerical data is generated from an ensemble of 10^5 signals, each with $t_N = 500$, having white noise below $f = f_1$ and $1/f^2$ noise above f_2. (a) $f_1 = 2$, $f_2 = 10$; (b) $f_1 = 5$, $f_2 = 10$; (c) $f_1 = 5$, $f_2 = 6$; (d) $f_1 = 2$, $f_2 = 3$. The FTG function is included in each plot (solid line) for comparison.

where τ is the average time spent by an impurity atom on the surface of the electrode. This power spectrum is initially very flat and essentially $\sim 1/f^2$ at high frequencies. It therefore failed to accurately describe the empirical observations of $1/f^\alpha$ noise with $\alpha \approx 1.25$.

Many years later a mechanism was proposed by du Pré [136] which not only provided a much better value of α, but also explained the relative temperature insensitivity of the noise. The approach was a modification of Schottky's method, where the single characteristic time, τ, was replaced by a superposition of processes with a distribution of time scales. By assuming that the time spent by an atom on the surface of the cathode is thermally activated,

$$\tau = \tau_0 e^{E/T}, \tag{6.51}$$

for an inhomogeneous surface the diffusion rate will depend on the precise environment the atom is in. If the distribution of activations energies, E, is $D(E)$, then

$$S(f,T) \propto \int \frac{\tau}{1+\tau^2 f^2} D(E)\,\mathrm{d}E. \tag{6.52}$$

Integrating this expression, together with the important assumption that the width of $D(E)$ is much greater than T, yields the general result [137],

$$S(f,T) \propto \frac{T}{f} D(E). \tag{6.53}$$

Therefore $1/f$ noise is observed when the distribution of energies is constant, and in general, $1/f^\alpha$ noise is obtained for

$$D(E) \propto e^{(\alpha-1)E}. \tag{6.54}$$

6.5.1 $1/f$ Noise from Random Telegraph Signals

In 1953 Stefan Machlup demonstrated that random telegraph signals were a suitable representation of the dynamical processes underlying $1/f$ noise [138]. For an electron to contribute to the current in a vacuum tube, it must be free to move, and not held in a potential 'trap' such as those implied by Schottky's impurities. It is assumed that

each trap can hold at most one electron, and that the percentage of filled traps does not have large fluctuations (thereby ensuring their statistical independence). The state of each trap, empty or full, then defines a digital signal over time.

In the original work, an empty trap at time t gave the signal a value $x(t) = 0$, and a full trap was denoted by $x(t) = 1$. The use of 0 and 1 to define the states of the traps leads inevitably to a Gaussian with mean $1/2$ when many signals are combined. This results in non-$\Gamma_{\frac{1}{2}}$ variables when the combined signal elements, $X(t) = \sum_i x_i(t)$, are squared, which means the FTG distribution will not emerge from studies of the roughness. However it is seen that redefining the states to be ± 1 still produces $1/f$ noise, whilst also giving the required statistics.

To produce $1/f$ noise, the transition from -1 to $+1$ must occur with the same probability as the reverse process, namely

$$P_{-1,1} = P_{1,-1} = \frac{\mathrm{d}t}{\tau}, \tag{6.55}$$

for some short time $\mathrm{d}t$. Here τ is the mean lifetime of a state before a transition takes place, and, as this is the same for both possible states, the probability that a given trap is empty at any time is simply $P_{-1} = 1/2$. Obviously this also means that $P_1 = 1/2$. By letting $P_{a,b}(t)$ be the probability that the trap is in state b time t after having been in state a, the autocorrelation function for the signal becomes,

$$\begin{aligned} A(t) &= \langle x(t')x(t'+t)\rangle & (6.56)\\ &= \sum_{a,b} \frac{1}{2} x_a P_{a,b}(t) x_b & (6.57)\\ &= \frac{1}{2}\left((P_{-1,-1}(t) + P_{1,1}(t)) - (P_{-1,1}(t) + P_{1,-1}(t))\right) & (6.58)\\ &= P_{1,1}(t) + P_{1,-1}(t). & (6.59) \end{aligned}$$

$P_{1,1}(t)$ is the probability of an even number of transitions in time t. Given that $P_{1,-1}(t)$ must therefore be the probability of an odd number of transitions over the same length of time, we see that

$$P_{1,-1}(t) = 1 - P_{1,1}(t), \tag{6.60}$$

and therefore,

$$A(t) = 2P_{1,1}(t) - 1. \tag{6.61}$$

For a small increment of time $\mathrm{d}t$, the probability of an even number of transitions in time $t + \mathrm{d}t$ is equal to the probability of an even number of transitions in time t and no transitions in $\mathrm{d}t$, plus the probability of an odd number of transitions in time t and one transition in $\mathrm{d}t$ (where it is assumed that $\mathrm{d}t$ is so short that at most one transition can occur). We have already stated that the probability of a transition in some short time $\mathrm{d}t$ is equal to $\mathrm{d}t/\tau$, therefore

$$P_{1,1}(t + \mathrm{d}t) = P_{1,1}(t)\left(1 - \frac{\mathrm{d}t}{\tau}\right) + P_{1,-1}(t)\frac{\mathrm{d}t}{\tau}. \tag{6.62}$$

Substituting (6.60) into (6.62) and taking the limit $\mathrm{d}t \to 0$, yields the differential equation,

$$\frac{\mathrm{d}P_{1,1}}{\mathrm{d}t} + \frac{2P_{1,1}}{\tau} = \frac{1}{\tau}. \tag{6.63}$$

Together with the boundary condition that no transitions can occur in zero time ($P_{1,1}(0) = 0$), this leads to

$$P_{1,1}(t) = \frac{1}{2}\left(\exp\left(-\frac{2t}{\tau}\right) + 1\right), \tag{6.64}$$

and, from (6.61),

$$A(t) = \exp\left(-\frac{2|t|}{\tau}\right), \tag{6.65}$$

where the $|t|$ reflects the time symmetry of the system. This expression differs from that derived by Machlup [138], but only by a constant term. Therefore the change introduced by labelling the states ± 1 has no effect on the power spectrum other than for the zero frequency mode. The power spectrum is found by Fourier transforming the autocorrelation function, giving

$$S(f) \propto \frac{\tau}{1 + (\tau f)^2}. \tag{6.66}$$

This result is for a single trap with characteristic time τ, and corresponds precisely to Schottky's model. By allowing each trap to have a different energetic hold on the electrons, with thermally activated characteristic times

$$\tau = \tau_0 e^{E/T}, \tag{6.67}$$

the power spectrum becomes defined by (6.52) and $1/f$ noise is observed for uniform $D(E)$.

6.5.2 Numerical Simulations

We have simulated the generation of $1/f$ noise from the superposition of random telegraph signals (RTSs) – a mechanism that is gaining acceptance as the true origin of $1/f^{\alpha}$ noise in certain electrical systems [139]. In creating the individual RTSs one quickly encounters a difficulty in numerically applying the analytical equations. The differential equation (6.63) is derived in the limit $\mathrm{d}t \to 0$. However in numerical simulations time is discrete, t is therefore an integer and $\mathrm{d}t$ must equal 1. For low frequency modes this discrepancy is relatively unimportant. When the characteristic time for a process is long, it does not feel the effect of the discretization in any significant sense and (6.63) remains valid. Another way to interpret this is to replace the condition $\mathrm{d}t \to 0$ with $\mathrm{d}t/\tau \to 0$. For high frequency modes both of these conditions fail. The discrete nature of the numerical time scale therefore causes the analysis above to break down, and the power spectrum will not be $1/f$.

Taking $\tau_0 = 1$, a simulation of a signal of length $t_N = 10^5$ formed by the superposition of 1500 RTSs with activation energies uniformly distributed in the range $0.01 \leq E \leq 15.0$ (for $T = 1.0$) confirms that there is a problem at high frequencies. The power spectrum, shown in Figure 6.15, has quite good $1/f$ noise for many decades, but as f increases the noise is more accurately described by $1/f^{\alpha}$ with $\alpha > 1$. Eventually one encounters a high frequency tail where the modes becomes significantly larger than $1/f$. It was initially assumed that this anomaly was due to the high frequency modes compensating for the power lost by imposing a finite cut-off, $f_{\max}$. For the power spectrum of the compound signal $X(t)$ to behave in this manner, it was thought that the spectra of the individual RTSs would also show a slower than Lorentzian decline for large f. However, studies of $S_x(f)$ revealed a more fundamental reason for the problem. Initially, individual RT signals appeared to be good fits to the theoretical Lorentzians over most of the range of f, with, as expected, premature levelling off at very high frequencies (Figure 6.16(a) shows examples for

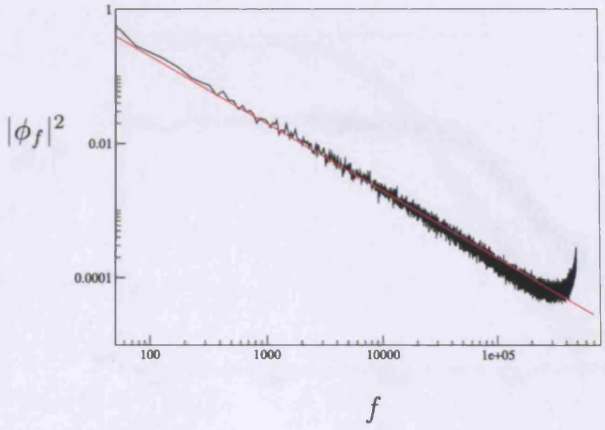

Figure 6.15: Mode Dispersion of Noise Generated from Superposition of Random Telegraph Signals, $\tau_0 = 1$: 1500 RTSs were used, with activation energies uniformly distributed over the range $0.01 \leq E \leq 15.0$, ($\tau_0 = 1$). Each signal had $t_N = 10^6$. The red line has a slope of $1/f$ which is clearly a good fit at low frequencies, however α starts to increase slightly for higher f before eventually collapsing giving rise to the high frequency 'tail'.

two signals with $E = 2.0, 4.0$ at $T = 1.0$). This turned out only to be true for high enough energies. As the energy was lowered the power spectra began to show marked deviations from the theory, eventually losing all semblance of a Lorentzian shape and for small E becoming increasing functions of f rather than declining. This is seen in Figure 6.16(b) corresponding to $E = 0.1$.

It is possible to rationalize this unusual behaviour by returning to the expression for the probability of an even number of transitions in a given time (6.64). As t becomes large, the exponential term tends to zero and the probability of an even number of transition in time t tends to $1/2$. This is logical, as two measurements separated by large t are effectively uncorrelated and $P_{1,1} \rightarrow P_1 = 1/2$. However, in a numerical simulation, there are difficulties for low energy systems. As $E \rightarrow 0$, for $\tau_0 = 1$ a transition in $\mathrm{d}t = 1$ is a certainty. Therefore

$$P_{11}(t) = \begin{cases} 1 & \text{for even } t \\ 0 & \text{for odd } t \end{cases}, \tag{6.68}$$

which is obviously different from the exponential decay derived analytically. Having

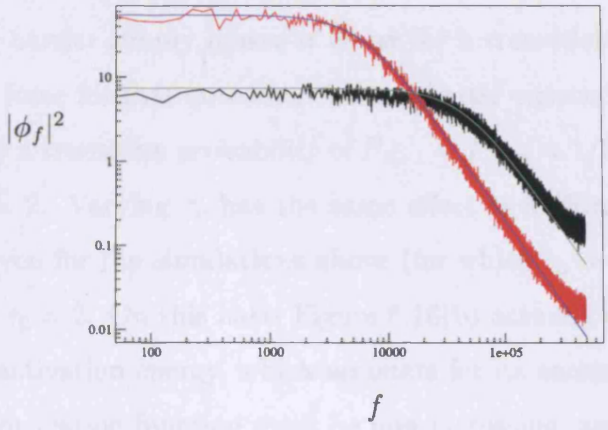

(a)

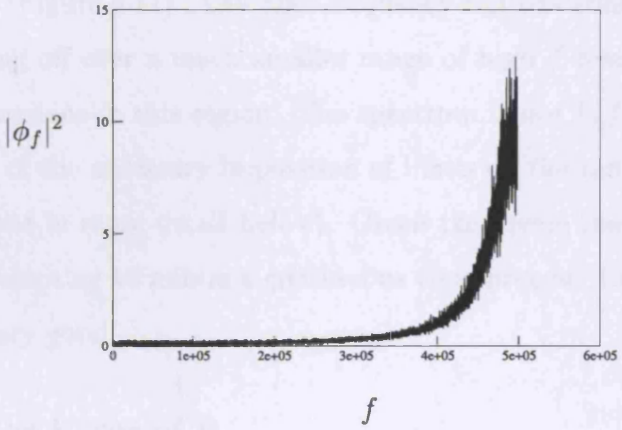

(b)

Figure 6.16: Mode Dispersion of Individual Random Telegraph Signals: (a) The effective power spectra of RT signals with $t_N = 10^6$. The black line corresponds to $E = 2.0$, the red line to $E = 4.0$. In both cases $\tau_0 = 1$. The numerical data is a good fit to theoretical Lorentzian curves (green and blue lines respectively) over a large range of f. A slight flattening occurs at high frequencies, presumably to compensate for power lost due to imposing a high frequency cut-off. Logarithmic axes are used for clarity. (b) As (a) but with $E = 0.1$ and plotted on linear axes. The rapidly increasing nature of the data for large f indicates an unexpected dominance of the high f modes.

a transition as a certain event seems physically questionable; even with zero energy barrier the two possibilities, transition or no transition, are still both feasible. The removal of the barrier simply makes it easier for a transition to occur, but is not in itself a driving force for that outcome. A much better constraint is for zero activation energy to imply a transition probability of $P_{1,-1} = P_{-1,1} = 1/2$, which can be achieved by setting $\tau_0 = 2$. Varying τ_0 has the same effect as shifting the energy scale, and the energies given for the simulations above (for which $\tau_0 = 1$) therefore correspond to $E - \ln 2$ for $\tau_0 = 2$. On this basis Figure 6.16(b) actually corresponds to a system with negative activation energy, which accounts for its anomalous behaviour.

The auto-correlation function must be non-increasing, and should be constant at zero energy. This ties in with the boundary condition that the transition probability in time t must tend toward $1/2$ as $t \to \infty$. These criteria are both met by setting $\tau_0 = 2$, which leads to a power spectrum for the compound signal which is much easier to understand (Figure 6.17). The high frequency tail has gone, however there is still a slight levelling off over a much smaller range of high f resulting from the slightly flattened Lorentzians in this region. The spectrum is not $1/f$ over all frequencies as a consequence of the necessary imposition of limits on the range of available energies (this is discussed in more detail below). Given the severe limitations of a numerical simulation attempting to mimic a continuous time process, the spectrum appears to be generally very good.

Restricting the Range of E

The activation energies for a transition from full to empty, or *vice versa*, must be evenly distributed for the addition of RTSs to lead to $1/f$ noise. Furthermore, as the power spectrum of $X(t)$ results from the integral over $\mathrm{d}E$, the separation of energy levels should be small. In both physical and numerical experiments there will be restrictions on the range of E. The power spectrum, $S_X(f)$, is therefore not $1/f$ for all frequencies, but has a form dependent on the boundaries $E_{\min}$ and $E_{\max}$.

$$S_X(f) \sim \int_{E_{\min}}^{E_{\max}} \frac{\tau}{1+(\tau f)^2}\,\mathrm{d}E \tag{6.69}$$

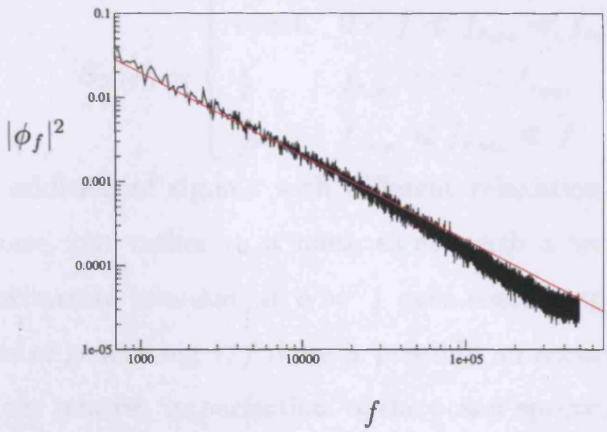

Figure 6.17: Mode Dispersion of Noise Generated from Superposition of Random Telegraph Signals ($\tau_0 = 2$): As for Figure 6.15, 1500 RTSs were used, with activation energies uniformly distributed over the range $0.01 \leq E \leq 15.0$, ($\tau_0 = 2$). Each signal had $t_N = 10^6$. The red line has a slope of $1/f$ which is again a good fit at low frequencies. There is the same tendency for α to increase slightly for higher f as was seen for $\tau_0 = 1$, however the high frequency tail has gone and is replaced by a much less severe levelling off.

$$\sim \int_{\tau_{\min}}^{\tau_{\max}} \frac{\mathrm{d}\tau}{1+(\tau f)^2} \tag{6.70}$$

$$\sim \int_{f_{s_{\min}}}^{f_{s_{\max}}} \frac{\mathrm{d}f_s}{f_s^2+f^2} \tag{6.71}$$

$$\sim \frac{1}{f}\left[\tan^{-1}\left(\frac{f_{s_{\max}}}{f}\right) - \tan^{-1}\left(\frac{f_{s_{\min}}}{f}\right)\right] \tag{6.72}$$

where f_s indicates the frequency associated with a single RT signal. Equation (6.72) defines $1/f^\alpha$ noise with a continuously varying exponent $0 \leq \alpha(f) \leq 2$. However, in three limiting cases, regions of approximately constant α can be identified,

$$S_X(f) \sim \begin{cases} \text{const.} & 0 < f \ll f_{s_{\min}} \ll f_{s_{\max}} \\ \frac{1}{f} & f_{s_{\min}} \ll f \ll f_{s_{\max}} \\ \frac{1}{f^2} & f_{s_{\min}} \ll f_{s_{\max}} \ll f \end{cases} . \tag{6.73}$$

Therefore the addition of signals with different relaxation times does not lead to perfect $1/f$ noise, but rather to a noise signal with a varying exponent α which remains approximately constant at $\alpha = 1$ over some range of frequencies. Given that this means of generating $1/f$ noise is possibly an accurate reflection of physical systems [139], the relative 'imperfection' of the power spectrum is a good justification for the need to consider modified spectra in §6.4.

For numerical simulations the effect of $f_{s_{\max}}$ is more noticeable than the effect of $f_{s_{\min}}$. For a discrete digital signal with t_N elements, the maximum possible frequency is $f_{\max} = t_N$, i.e. a transition occurs every time step. For the power spectrum to remain $1/f$ like up to $f_{\max}$, it must be the case that,

$$f_{\max} \ll f_{s_{\max}}. \tag{6.74}$$

However,

$$f_{s_{\max}} = \frac{t_N}{\tau_{\min}} \tag{6.75}$$

$$= \frac{t_N}{2e^{E_{\min}/T}}, \tag{6.76}$$

which takes its highest possible value for $E \to 0$, giving $f_{s_{\max}} = t_N/2$. Therefore the condition (6.74) can never be met. Instead numerical simulations can produce, at best, $1/f$ noise for $f \ll f_{\max}/2$.

By contrast, the lowest frequency mode contributing to $X(t)$ has $f_{\min} = 1$. However,

$$f_{s_{\min}} = \frac{t_N}{\tau_{\max}} \tag{6.77}$$

$$= \frac{t_N}{2e^{E_{\max}/T}}, \tag{6.78}$$

which may be made arbitrarily large, enabling the construction of $1/f$ noise to the lowest values of f.

Figure 6.18 shows power spectra for signals with $t_N = 10^6$ with different bounds on the activation energies of the underlying RTSs. In each case the spacing between energy levels was constant at $\Delta E = 0.01$. There is clearly a great degree of control of the form of $S_X(f)$ as $E_{\min}$ and $E_{\max}$ are varied. For $0.01 \leq E \leq 5.0$, the relatively low upper bound results in a significant region of white noise before the frequency is large enough to make the integral in (6.71) go as $1/f$. For $2.0 \leq E \leq 15.0$ the upper limit makes $f_{s_{\min}} \ll f_{\min}$ so no white noise is seen but the lower limit is relatively large and so, as the frequency increases, the $1/f$ behaviour fails. As $f_{s_{\max}} \approx 0.067 f_{\max}$ there is a region of high frequency where $f \gg f_{s_{\max}}$ and the noise becomes $1/f^2$.

6.5.3 $P(w_2)$ from RTS Derived $1/f$ Noise

We have studied the statistics of the roughness of signals formed from the addition of RTSs. Given that the power spectrum of these signals is not perfectly $1/f$ it would be expected that $P(w_2)$ will depend on the range of activation energies. In fact, given the limiting cases in (6.73) the general trends of §6.4 should apply.

Figure 6.19 shows the evolution of the skewness of $P(w_2)$ with increasing t_m of signals with $t_N = 10^6$ using WBCs. Three sets of numerical data are shown, corresponding to $0.01 \leq E \leq 15.0$, $0.01 \leq E \leq 6.0$ and $2.0 \leq E \leq 15.0$. The first of these has low enough $E_{\min}$ and high enough $E_{\max}$ that the power spectrum is about as close to $1/f$ noise as it is possible to generate with this method. The skewness declines steadily with increasing t_m before levelling out at a constant value. This value is slightly larger than was observed for the case of filtered Gaussian white noise

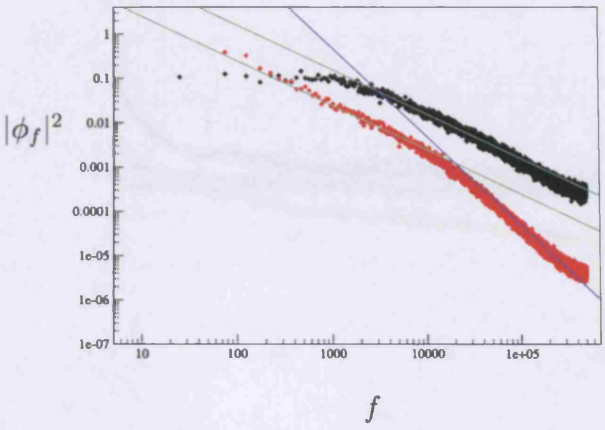

Figure 6.18: The Effect on $S_X(f)$ of Limiting the Range of E: Both sets of numerical data correspond to signals with $t_N = 10^6$. The spectrum in black has $0.01 \leq E \leq 5.0$, while the red points are for to $2.0 \leq E \leq 15.0$. The green lines both correspond to $1/f$ noise and the blue line to $1/f^2$ noise.

(shown in blue) presumably because the RTS method always leads to a range of modes with $\alpha > 1$ which contribute to w_2 and lead to a slightly more skewed distribution regardless of t_m.

Lowering the maximum activation energy increases the minimum RTS characteristic frequency, thereby leading to a region in $S_X(f)$ with $\alpha < 1$. As t_m increases the values of w_2 then become dominated by modes in the low frequency 'white noise' region and the skewness falls well below the FTG value. Unlike the spectrum in §6.4, the low frequency modes here are not strictly white noise but have $\alpha \to 0$ as $f \to 0$. As a result of this the correlation time remains of the order of t_N even for large t_N and the central limit theorem may not apply. The skewness is therefore expected to tend to a small, finite constant value as $t_m \to \infty$. Figure 6.19 also shows that the 'FTG region' for the signal with $E_{\max} = 6.0$ is barely distinguishable and the skewness diminishes fairly steadily as t_m is increased.

For an increased minimum activation energy the decline in the skewness becomes slower as the $\alpha > 1$ modes make their presence felt. Unlike the Gaussian derived signal, the region of $1/f^2$ dominated statistics is not seen, which may be attributed

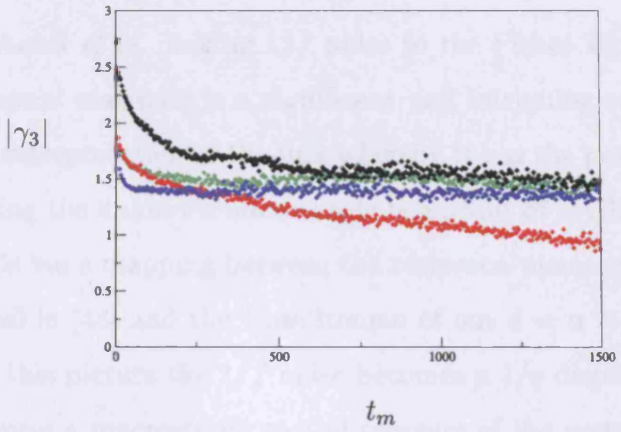

Figure 6.19: The Skewness of $P(w_2)$ as a Function of t_m: The data comes from signals with $t_N = 10^6$ derived from RTSs with energy ranges: $0.01 \leq E \leq 15.0$ (green), $0.01 \leq E \leq 6.0$ (red), $2.0 \leq E \leq 15.0$ (black). The same trends are observed as for signals formed from filtered Gaussian white noise. The data in blue is for 'perfect' $1/f$ noise derived from filtered Gaussian white noise.

to the effect of the flattening of $S_X(f)$ at very high frequencies. The continuous nature of $\alpha(f)$ makes it hard to precisely characterize the behaviour of the statistics. It appears that this plot has a region of t_m over which $1 < \alpha < 2$ dominates and there is a reasonably constant value of $|\gamma_3|$. Equally this may be an anomaly that would be ironed out with a larger ensemble of signals $X(t)$. In any case, for large t_m the skewness tends toward approximately the same constant value as seen for the signal with the largest range of E.

The data plotted in Figure 6.19 are for $t_m \leq 1500$ as above this value the statistics become unreliable. It would be interesting to perform larger scale calculations to confirm that the trends continue beyond this point. Indications from our simulations to $t_m = 3000$ appear to confirm that they do, with perhaps even greater convergence for the signals with no low frequency modifications.

6.6 Summary

The work by Antal *et al.* linking $1/f$ noise to the Fisher-Tippett-Gumbel distribution from extremal statistics is a significant and intriguing result. Here we present an alternative interpretation of the link whereby it has the potential to provide information regarding the unknown microscopic behaviour of equilibrium critical systems. Our approach is via a mapping between the reciprocal space action used to derive the $1/f$ noise signal in [48] and the Hamiltonian of our $d = \alpha = 1$ model introduced in Chapter 5. In this picture the $1/f$ noise becomes a $1/q$ dispersion of normal modes, and the roughness a macroscopic spatial measure of the system. We feel the spatial interpretation may be useful as it appears to be less universal than the temporal picture. In the latter the $1/f$–FTG link is so strong that it is independent of microscopic details. By contrast the spatial model specifically relates global fluctuations to microscopic interactions.

An attempt was made to design an experiment in which an FTG distributed global quantity had $1/f$ dynamics. This is clearly only possible for non-Gaussian systems and it appeared as though $\Gamma_{\frac{1}{2}}$ microscopic degrees of freedom might prove successful. It was shown that the power spectrum of the square of a zero mean Gaussian $1/f$ signal was itself approximately $1/f$. The ensemble average of the mean of the resulting signal, $y(t)$, was shown to be emphatically FTG. Therefore, introducing a finite measuring time, t_m, (in the spirit of [42]) the distribution of $\langle y(t) \rangle_{t_m}$ over a single signal was evaluated. However, even in this rather contrived thought experiment it was not possible to observe FTG statistics due to correlations between the various w_2.

To further investigate the experimental implications of the $1/f$–FTG link, the effect of introducing regions of non-$1/f$ behaviour into $S(f)$ were considered. Physically it is often seen that so called $1/f$ power spectra have white noise at low frequencies and a faster than $1/f$ roll-off at high frequencies. By artificially imposing these conditions on a signal we were able to characterize their effect on our ability to observe the FTG distribution for $P(w_2)$. In the case of both WBCs and PBCs it was seen

that the high frequency modifications caused little change in the PDF unless the parameter f_2 was very small compared with $f_{\max}$. However, for PBCs only a few low frequency white noise modes were needed to make the distribution significantly more Gaussian. For WBCs the low frequency modes only become significant for large enough t_m, however when they begin to contribute to w_2, their dominance quickly reduces $|\gamma_3|$.

An interesting result, the implications of which are not yet clear, is that we have been able to generate an almost perfect FTG distribution from the roughness of a signal with no $1/f$ character, as shown in Figure 6.14(d). By balancing the effects of low frequency white noise and high frequency $1/f^2$ noise it is possible to generate the required statistics.

Finally, we have numerically simulated $1/f$ noise from the superposition of random telegraph signals using an approach demonstrated analytically by Machlup [138]. This is gaining acceptance as the true mechanism giving rise to $1/f$ noise in certain electrical systems [139]. After discussing the consequences of the need for discrete time steps in numerical simulations, a signal was generated which was $1/f$ over many decades. The effects of limits on the range of activation energies of the individual RTSs was discussed, and it was seen that the resulting non-$1/f$ regions had much the same effect on $P(w_2)$ as was seen for the Gaussian derived signal.

Overall it is fair to say that experimental time signals require very accurate $1/f$ power spectra in the low frequency region before the distribution of the roughness will be recognized as being the FTG function.

Chapter 7

Conclusions

The nature of universal non-Gaussian fluctuations is one of the central questions in the study of critical phenomena [5]. In recent years the BHP (4.88) and generalized Fisher-Tippett-Gumbel distributions (5.22) have become popular choices of function in the fitting of such statistics. A good example is the behaviour of thin films near electrical breakdown. Under these conditions the resistance of the films fluctuate in a non-Gaussian manner, with $(\langle R \rangle - R)/\sigma$ being close to the BHP form [29]. The same is true for electrical breakdown in granular materials near the critical point [40] – further indication of the spanning of universality classes.

Other examples include turbulence, which has been associated with the BHP function since the work of Bramwell *et al.* [19]. More recently the generalized FTG form has been observed in studies of global fluctuations in decaying Burgers turbulence [36], a novel one dimensional turbulence model [34, 35] and the system average velocity in a system of self-driven particles – which incidentally also possesses a scale invariant power spectrum [140]. Similar results are seen for fluctuations in the power consumed by liquid crystals undergoing electroconvective flow [38], a quantity closely related to liquid crystal turbulence [37]. A magnetized torus has been shown to have non-Gaussian fluctuations for both the electron pressure and plasma potential [141]. At high pressures these are described by a generalized FTG distribution to a very good first approximation.

In general the use of extreme value distributions to describe highly correlated

many body fluctuations is becoming widely accepted [63] and has even been used to fit the statistics of goals in football matches [142]! Even in cases where the link has not been made explicitly, one can find examples in the literature of appropriate quantities with apparently generalized FTG fluctuations – such as the current fractions in non-equilibrium surface processing [143].

The prevalence of the BHP/FTG form provided the impetus behind the work presented in this thesis in the form of the question, "are there any constraints on the form that a distribution of a global quantity may take in a highly correlated system?". Earlier work on the 2dXY model had shown an apparent 'superuniversality' with the BHP function describing the fluctuations of a range of phenomena spanning universality classes [6, 16]. Of central importance to these observations was the analytical result that the BHP function was temperature independent, and therefore applied to the entire line of Gaussian fixed points controlling the low temperature critical region. By demonstrating that assumptions made in deriving this result are invalid we have shown analytically that the BHP function is in fact weakly dependent on T and is not therefore strictly universal. The function remains independent of the system size N however our analysis shows that it really represents the PDF in the limit $T \to 0$ and that the true order parameter PDF tends toward a Gaussian as T is increased. Numerical simulations confirm this and the skewness of the magnetization PDF is seen to be a well defined function of the temperature.

One of the more surprising consequences of the previously derived BHP universality was the rigorous equivalence between the PDFs of the cosine and linearized order parameters ((4.26) and (4.104) respectively) [6]. At high temperatures the linearized form is a poor approximation to an order parameter as it is not bound by 0 and +1. However, even when the linearized form represents a physical quantity quite different from m, the fluctuation distribution is precisely the BHP function. This may be understood in the context of our conclusion that $P(m)$ is dependent on T. The neglect of multiple loop graphs in the derivation of the BHP function is explicitly a low temperature approximation. Thus the BHP form must be interpreted

as the distribution of order parameter fluctuations in the limit $T \to 0$. Similarly the linearized form of the OP is a defined by neglecting terms which become more relevant at high temperatures. Therefore use of the linearized OP is equivalent to imposing low temperature constraints. It is an interesting result that these two low temperature approximations lead to precisely the same result, despite the fact that they are not evidently the same.

Our studies of the Harmonic model revealed the surprising appearance of vortices at high temperatures. It is assumed that these arise from the superposition of high energy spin waves. The identification of these topological defects, coupled with the change in statistical regime from non-Gaussian to Gaussian as T is increased, prompted speculation that there may be a Kosterlitz-Thouless transition in this model. However, whilst the vortex pair density increases rapidly with T, there is no evidence of unbinding. We have presented an argument for the energy of a vortex pair in the Harmonic model scaling linearly with separation, which would explain these observations.

The reciprocal space form of the Harmonic model Hamiltonian belongs to a family of systems defined by the dimension d and a mode weighting parameter α. For the linearized order parameter it is possible to derive a general expression for the cumulants of the models in this family [25, 49]. When $d = \alpha$, the average magnetization scales logarithmically with system size. This is an indication of an explicit dependence on all the normal modes. For a critical system one expects the order parameter to scale as a power law [71, 73]. However we argue that logarithmic behaviour is also a signature of underlying criticality. When a global property, X, of a highly correlated system scales logarithmically, if one can identify another global quantity, Y, such that $X \to Y$ as $T \to 0$ then Y is then expected to exhibit power law behaviour and the critical nature of the system is revealed. This is certainly true in the case of the low temperature 2dXY model where the logarithmic scaling of the linearized OP belies the power law behaviour of the cosine form.

We have derived two direct space Hamiltonians for spin systems which have Fisher-Tippett-Gumbel distributed magnetization fluctuations. Unfortunately the compli-

cated coupling schemes in these models mean we have been unable to identify physical systems whose microscopic interactions they describe. These systems correspond to the $d = \alpha = 1$ member of the family of models discussed above. Analysis in reciprocal space shows that the cosine order parameter scales as a power law for large N, in line with our assertion that these systems are critical. We have used Monte Carlo simulations to demonstrate that the largest normal mode is not FTG distributed. This is a numerical confirmation of the analytical results of Györgyi *et al.* [69]. Our investigations of the effect of different Brillouin zone shells shows that the bulk of the asymmetry in the PDF comes from the soft modes near the zone centre, however the many body nature of the magnetization is also confirmed.

Our analysis of a range of models in 'skewness-kurtosis' space is discussed in depth in Chapter 5. It is clear that one must take care when drawing conclusions regarding the underlying physics based solely on the shape of the order parameter PDF. Other knowledge of the system may be required to infer even quite coarse information such as the criticality or otherwise of the system.

The appealing link between $1/f$ noise and extreme value statistics [48] is intimately related to our critical $d = \alpha = 1$ models. This led us to consider the practical implications of the connection. There can be no dispute that periodic Gaussian $1/f$ noise signals have a roughness that is FTG distributed. Our question was how this manifests itself experimentally. The arguments presented in Chapter 6 are intended to provide an alternative way of viewing the same problem. We suggest that it is unlikely that analysis of the roughness of the time signal generated by experimental observation will provide insight into the physics of a system. The most promising means of observing the link is in studies of interface growth where the terminology '$1/f$ noise' may be replaced by '$1/q$ dispersion' of spatial normal modes. This ties in well with our one dimensional models. Our attempts to identify a single signal having both $1/f$ noise and FTG distributed elements were unsuccessful. We did, however, demonstrate that $\Gamma_{\frac{1}{2}}$ distributed signals derived from Gaussian $1/f$ noise have themselves very nearly $1/f$ power spectra.

We have considered the consequences of imperfections in the $1/f$ noise signals

for both periodic and window boundary conditions. It is generally seen that a large high frequency region may have $1/f^2$ behaviour without having a significant effect on the PDF. By contrast a few low frequency white noise modes will destroy the FTG fluctuations in the case of PBCs. Window boundary conditions are less sensitive and it is the relationship between the size of the white noise region and the measuring time, t_m, that is important.

Finally we provide numerical results confirming that superposition of random telegraph signals can generate good quality $1/f$ noise. The high and low frequency behaviour of the resulting signals acts as justification for the studies of the effects of imperfections in the power spectra.

7.1 Future Work

The studies of the Ising model discussed in Chapter 3 are at an early stage. The possibility of an exact solution in finite field is enticing; yet, as we have said, the computational barriers appear to be insurmountable. We intend to consider a system small enough such that our methods may be feasible, but still large enough to be beyond the realms of direct evaluation. This should act as a general confirmation of our approach. Our suggestion that finite size scaling may be investigated by means of the exact energy distribution is more promising. We intend to extend the rigour of our arguments and perform larger scale simulations to test the results.

We are currently looking at the 2dXY magnetization in the presence of a finite field. A particularly promising aspect of this work is the potential analogy between the approximation of neglecting multiple loop graphs in the expansion of $\langle m^p \rangle$ [6] and the Hartree approximation introduced by Pokrovsky and Uimin [144] to expand the field term in the Hamiltonian. We hope to use this to derive an analytical expression for the temperature dependence of the order parameter fluctuations.

Our simulations of $1/f$ noise were on a relatively small scale. We intend to improve on these to get a clearer picture of the limiting tendencies of the statistics as one varies the range of non-$1/f$ modes. We also hope to be able to treat this question analytically.

Appendix A

Gaussian Integration

A.1 Integration of a Gaussian Function in One Dimension

Consider the integral of a basic Gaussian function

$$I = \int_{-\infty}^{\infty} e^{-ax^2}\,\mathrm{d}x, \tag{A.1}$$

where $a > 0$. This equation occurs frequently in many branches of maths and science, due largely to the ubiquity of the Gaussian or normal probability distribution. It was famously solved by Laplace as follows:

$$I^2 = \int_{-\infty}^{\infty} e^{-ax^2}\,\mathrm{d}x \int_{-\infty}^{\infty} e^{-ay^2}\,\mathrm{d}y \tag{A.2}$$

$$= \int_{-\infty}^{\infty}\int_{-\infty}^{\infty} e^{-a(x^2+y^2)}\,\mathrm{d}x\,\mathrm{d}y \tag{A.3}$$

converting to polar coordinates gives

$$I^2 = \int_0^{2\pi}\int_0^{\infty} e^{-ar^2} r\,\mathrm{d}r\,\mathrm{d}\theta \tag{A.4}$$

$$= 2\pi \int_0^{\infty} r\,e^{-ar^2}\,\mathrm{d}r. \tag{A.5}$$

This integral is easily solved by making the substitution $r^2 = t$

$$I^2 = \pi \int_0^{\infty} e^{-at}\,\mathrm{d}t \tag{A.6}$$

$$= \pi \left[-\frac{1}{a} e^{-at} \right]_0^\infty \tag{A.7}$$

$$= \frac{\pi}{a}. \tag{A.8}$$

Thus

$$I = \int_{-\infty}^{\infty} e^{-ax^2} \, \mathrm{d}x = \sqrt{\frac{\pi}{a}}. \tag{A.9}$$

A.2 Averages and Gaussian Integration

The average of a quantity is defined as the sum over all its possible values, each value being weighted by the probability that it is observed. Thus for some function, $f(x)$, of a variable with the probability distribution $P(x)$, the average $\langle f(x) \rangle$ is given by

$$\langle f(x) \rangle = \int_{-\infty}^{\infty} f(x) \, P(x) \, \mathrm{d}x. \tag{A.10}$$

If $P(x)$ is a Gaussian, that is, if x is a Gaussian variable, the following important results can be derived.

A.2.1 Average of a Polynomial Function of a Gaussian Variable

Differentiating (A.9) with respect to the parameter a gives

$$\frac{\mathrm{d}I}{\mathrm{d}a} = -\int_{-\infty}^{\infty} x^2 e^{-ax^2} \, \mathrm{d}x = -\frac{1}{2} \frac{\sqrt{\pi}}{a^{3/2}}. \tag{A.11}$$

And so the average value of x^2, for Gaussian distributed x, is

$$\left\langle x^2 \right\rangle = \int_{-\infty}^{\infty} x^2 \, e^{-ax^2} \, \mathrm{d}x = \frac{1}{2} \frac{\sqrt{\pi}}{a^{3/2}}. \tag{A.12}$$

Repeated differentiation yields,

$$\left\langle x^{2n} \right\rangle = \int_{-\infty}^{\infty} x^{2n} \, e^{-ax^2} \, \mathrm{d}x = \frac{(2n-1)!!}{2^n} \frac{\sqrt{\pi}}{a^{(2n+1)/2}}. \tag{A.13}$$

The average of any odd power of x must be zero as $x^n \, e^{-ax^2}$ is an odd function for odd n. Hence, using (A.13), it is possible to evaluate the average of any polynomial function of a Gaussian variable x.

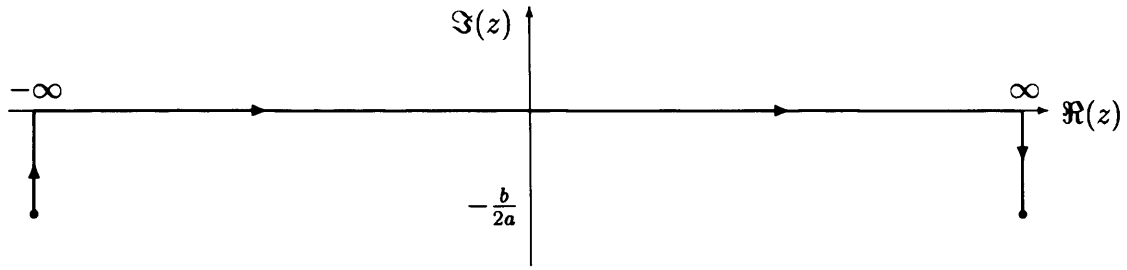

Figure A.1: Integration Contour for Evaluating Averages of Exponentials

A.2.2 Average of an Exponential Function of a Gaussian Variable

Another extremely useful result of Gaussian integration is the ability to determine the average of e^x or, more generally, e^{zx} where z may be complex. Consider the integral

$$I = \int_{-\infty}^{\infty} e^{-ax^2} e^{ibx}\,\mathrm{d}x \tag{A.14}$$

where i is the imaginary unit $i = \sqrt{-1}$. The trick is to complete the square.

$$I = \int_{-\infty}^{\infty} e^{-a(x-ib/2a)^2 - b^2/4a}\,\mathrm{d}x \tag{A.15}$$

$$= e^{-b^2/4a} \int_{-\infty}^{\infty} e^{-a(x-ib/2a)^2}\,\mathrm{d}x \tag{A.16}$$

$$= e^{-b^2/4a} \int_{-\infty-ib/2a}^{\infty-ib/2a} e^{-az^2}\,\mathrm{d}z \tag{A.17}$$

where the substitution $z = x - \frac{ib}{2a}$ has been made. The integration is then performed over the complex variable z. This task is made much easier by choosing to deform the contour of integration, which is perfectly acceptable provided no singularities are crossed. The easiest contour for this integral is that shown in Fig A.2.2. The contributions to the integral from the two purely imaginary sections of the path negate each other, so the problem reduces to one of integration of a real variable between $\pm\infty$,

$$I = e^{-b^2/4a} \int_{-\infty}^{\infty} e^{-az^2}\,\mathrm{d}z \tag{A.18}$$

$$= e^{-b^2/4a} \sqrt{\frac{\pi}{a}}. \tag{A.19}$$

A.3 Gaussian Integration in Multiple Dimensions

The usefulness of Gaussian integration extends to more than one dimension. Consider the integral

$$I = \int e^{-k\mathbf{x}^T\mathbf{A}\mathbf{x}+\mathbf{j}.\mathbf{x}}\,\mathrm{d}^N\mathbf{x}, \tag{A.20}$$

where $\mathbf{A}$ is a symmetric real matrix. The transformation to the reference frame in which $\mathbf{A}$ is diagonal is achieved by setting $\mathbf{x}' = \mathbf{O}\mathbf{x}$, where $\mathbf{O}$ is the (orthogonal) matrix of $\mathbf{A}$'s eigenvectors (see §A.4.1). This gives,

$$\mathbf{x}^T\mathbf{A}\mathbf{x} = \mathbf{x}^T\mathbf{O}^T\mathbf{O}\mathbf{A}\mathbf{O}^T\mathbf{O}\mathbf{x} \tag{A.21}$$

$$= \mathbf{x}'^T\mathbf{D}\mathbf{x}'. \tag{A.22}$$

Note that the volume of integration is left unchanged by this transformation (see §A.4.3), hence,

$$I = \int e^{-k\mathbf{x}'^T\mathbf{D}\mathbf{x}'+\mathbf{j}'.\mathbf{x}'}\,\mathrm{d}^N\mathbf{x}', \tag{A.23}$$

where the elements of $\mathbf{D}$ are $d_{ii} = \lambda_i$, the eigenvalues of $\mathbf{A}$.

The argument of the exponential may be expanded as

$$\sum_i \left(-k\lambda_i x_i'^2 + j_i' x_i'\right) = -\sum_i \left[\left(x_i'\sqrt{k\lambda_i} - \frac{j_i'}{2\sqrt{k\lambda_i}}\right)^2 - \frac{j_i'^2}{4k\lambda_i}\right] \tag{A.24}$$

$$= -\sum_i \left(z_i^2 - \frac{j_i'}{4k\lambda_i}\right) \tag{A.25}$$

with

$$z_i = \left(x_i'\sqrt{k\lambda_i} - \frac{j_i'}{2\sqrt{k\lambda_i}}\right). \tag{A.26}$$

This gives

$$\mathrm{d}x_i' = \frac{1}{\sqrt{k\lambda_i}}\,\mathrm{d}z_i, \tag{A.27}$$

and therefore

$$\mathrm{d}^N\mathbf{x}' = \frac{1}{k^{N/2}}\frac{1}{\sqrt{\lambda_1}}\,\mathrm{d}z_1\frac{1}{\sqrt{\lambda_2}}\,\mathrm{d}z_2\ldots \tag{A.28}$$

$$= \frac{1}{k^{N/2}}\left(\prod_i \frac{1}{\sqrt{\lambda_i}}\right)\mathrm{d}^N\mathbf{z} \tag{A.29}$$

$$= \frac{1}{k^{N/2}} \left(\prod_i \frac{1}{\lambda_i} \right)^{1/2} \mathrm{d}^N \mathbf{z}. \tag{A.30}$$

Given that the λ_i are the eigenvalues of $\mathbf{A}$, it follows that $(1/\lambda_i)$ are the eigenvalues of $\mathbf{A}^{-1}$, as

$$\mathbf{A}x_i = \lambda_i x_i \tag{A.31}$$

$$\mathbf{A}^{-1}\mathbf{A}x_i = \lambda_i \mathbf{A}^{-1} x_i \tag{A.32}$$

$$\frac{1}{\lambda_i} x_i = \mathbf{A}^{-1} x_i. \tag{A.33}$$

Hence, given that $\prod_i \lambda_i = \det \mathbf{D} = \det (\mathbf{O}^T \mathbf{A} \mathbf{O}) = \det \mathbf{A}$, and $\det \mathbf{A}^{-1} = \frac{1}{\det A}$,

$$\prod_i \frac{1}{\lambda_i} = \det \mathbf{A}^{-1}. \tag{A.34}$$

This leads to

$$\mathrm{d}^N \mathbf{x}' = \frac{1}{k^{N/2}} \sqrt{\det \mathbf{A}^{-1}}\, \mathrm{d}^N \mathbf{z}. \tag{A.35}$$

From which we get

$$I = \frac{1}{k^{N/2}} \sqrt{\det \mathbf{A}^{-1}} \int e^{-\sum_i z_i^2} e^{\sum_i \frac{j_i'^2}{4k\lambda_i}} \mathrm{d}^N \mathbf{z} \tag{A.36}$$

$$= \frac{1}{k^{N/2}} \sqrt{\det \mathbf{A}^{-1}} e^{\sum_i \frac{j_i'^2}{4k\lambda_i}} \prod_i \int e^{-z_i^2} \mathrm{d}z_i. \tag{A.37}$$

The argument of the exponential outside the product may be written in terms of the vector $\mathbf{j}'$ rather than its elements, as

$$\sum_i \frac{j_i'}{\lambda_i} = \mathbf{j}'^T \mathbf{D}^{-1} \mathbf{j}' \tag{A.38}$$

$$= \mathbf{j}^T \mathbf{A}^{-1} \mathbf{j}. \tag{A.39}$$

Thus, recalling the result from one dimension (A.9),

$$I = \sqrt{\frac{\pi^N \det \mathbf{A}^{-1}}{k^N}} e^{\frac{\mathbf{j}^T \mathbf{A}^{-1} \mathbf{j}}{4k}}. \tag{A.40}$$

This result is extremely useful in many areas of science. In particular, for a Gaussian variable $\mathbf{x}$, such that $P(\mathbf{x}) \propto \exp(-k\mathbf{x}^T\mathbf{A}\mathbf{x})$,

$$\left\langle e^{\mathbf{j}\cdot\mathbf{x}} \right\rangle = \frac{\int e^{\mathbf{j}\cdot\mathbf{x}} P(\mathbf{x})\, \mathrm{d}^N x}{\int P(\mathbf{x})\, \mathrm{d}^N x} \tag{A.41}$$

$$= e^{\frac{\mathbf{j}^T\mathbf{A}^{-1}\mathbf{j}}{4k}}. \tag{A.42}$$

Differentiating (A.42) twice with respect to elements of $\mathbf{j}$, then setting $\mathbf{j} = 0$, provides a direct link between the matrix $\mathbf{A}$ and the two point correlation function,

$$\left.\frac{\partial^2 \left\langle e^{\mathbf{j}\cdot\mathbf{x}} \right\rangle}{\partial j_a \partial j_b}\right|_{\mathbf{j}=0} = \left\langle x_a x_b e^{\mathbf{j}\cdot\mathbf{x}} \right\rangle\Big|_{\mathbf{j}=0} \tag{A.43}$$

$$= \frac{1}{2k} A^{-1}_{ab}. \tag{A.44}$$

A.4 Matrices

This section takes a look at some of the properties of matrices which are useful in deriving many of the formulae used in Gaussian integration. This is largely basic matrix manipulation but is included here for completeness to assist in the understanding of the previous sections.

Consider a matrix $\mathbf{M}$ which, on multiplying the vectors $\mathbf{v}_1$, $\mathbf{v}_2$,..., yields the vectors $\mathbf{w}_1$, $\mathbf{w}_2$..., *etc.* We can form a matrix $\mathbf{V}$ whose i^{th} column is simply the vector $\mathbf{v}_i$. Thus,

$$\mathbf{MV} = \mathbf{W} \tag{A.45}$$

where the i^{th} column of $\mathbf{W}$ is the vector $\mathbf{w}_i$.

A.4.1 Diagonalizing a Matrix

Let $\mathbf{M}$ be a square matrix of order n, having n normalized eigenvectors $\mathbf{x}_i$ corresponding to the eigenvalues λ_i such that

$$\mathbf{M}\mathbf{x}_i = \lambda_i \mathbf{x}_i. \tag{A.46}$$

Forming a matrix $\mathbf{X}$ whose columns are the eigenvectors $\mathbf{x}_i$, we see that

$$\begin{aligned}
\mathbf{MX} &= \mathbf{M}\begin{pmatrix} x_{11} & x_{12} & \cdots & x_{1n} \\ x_{21} & x_{22} & \cdots & \\ \vdots & & \ddots & \\ x_{n1} & & & \end{pmatrix} \\
&= \begin{pmatrix} \lambda_1 x_{11} & \lambda_2 x_{12} & \cdots & \lambda_n x_{1n} \\ \lambda_1 x_{21} & \lambda_2 x_{22} & \cdots & \\ \vdots & & \ddots & \\ \lambda_1 x_{n1} & & & \end{pmatrix} \\
&= \mathbf{X}\begin{pmatrix} \lambda_1 & 0 & \cdots & \\ 0 & \lambda_2 & & \\ \vdots & & \ddots & \\ & & & \lambda_n \end{pmatrix} \\
\mathbf{MX} &= \mathbf{XD}. \qquad \text{(A.47)}
\end{aligned}$$

where x_{ij} is the i^{th} element of the vector $\mathbf{x}_j$. Equation (A.47) defines the diagonal matrix $\mathbf{D}$ whose elements d_{ii} are the eigenvalues, λ_i, of $\mathbf{M}$.

Thus the matrix $\mathbf{M}$ is diagonalized on multiplication by the matrix of its eigenvectors.

A.4.2 Eigenvectors of Symmetric Matrices

An important property of real and Hermitian symmetric matrices is the orthogonality of their eigenvectors. Consider the case where $\mathbf{A}$ is a real symmetric matrix and $\mathbf{x}_1$ and $\mathbf{x}_2$ are two of its eigenvectors. We assume that $\det(\mathbf{X}) \neq 0$ (where $\mathbf{X}$ is as defined in §A.4.1, above) so all eigenvalues are distinct.

Multiplying $\mathbf{Ax}_1$ by the transpose of $\mathbf{x}_2$, then take the transpose of this product, we see that

$$\mathbf{Ax}_1 = \lambda_1 \mathbf{x}_1$$

$$\begin{aligned} \mathbf{x}_2^T \mathbf{A} \mathbf{x}_1 &= \lambda_1 \mathbf{x}_2^T \mathbf{x}_1 \\ \mathbf{x}_1^T \mathbf{A}^T \mathbf{x}_2 &= \lambda_1 \mathbf{x}_1^T \mathbf{x}_2 \\ \mathbf{x}_1^T \mathbf{A} \mathbf{x}_2 &= \lambda_1 \mathbf{x}_1^T \mathbf{x}_2 \end{aligned} \tag{A.48}$$

where we have made use of the symmetry $\mathbf{A} = \mathbf{A}^T$ and the general property of matrices that $(\mathbf{PQ})^T = \mathbf{Q}^T \mathbf{P}^T$.

It is also seen that

$$\begin{aligned} \mathbf{A} \mathbf{x}_2 &= \lambda_2 \mathbf{x}_2 \\ \mathbf{x}_1^T \mathbf{A} \mathbf{x}_2 &= \lambda_2 \mathbf{x}_1^T \mathbf{x}_2, \end{aligned} \tag{A.49}$$

and from (A.48) and (A.49)

$$(\lambda_1 - \lambda_2)\, \mathbf{x}_1^T \mathbf{x}_2 = 0. \tag{A.50}$$

The condition that $\det(\mathbf{X}) \neq 0$ imposes the constraint that $\lambda_1 \neq \lambda_2$, thus

$$\mathbf{x}_1^T \mathbf{x}_2 = 0, \tag{A.51}$$

and the eigenvectors must be orthogonal. Hence

$$\begin{aligned} \mathbf{X}^T \mathbf{X} &= \begin{pmatrix} \leftarrow & \mathbf{x}_1 & \rightarrow \\ \leftarrow & \mathbf{x}_2 & \rightarrow \\ & \vdots & \\ \leftarrow & \mathbf{x}_n & \rightarrow \end{pmatrix} \begin{pmatrix} \uparrow & \uparrow & & \uparrow \\ \mathbf{x}_1 & \mathbf{x}_2 & \cdots & \mathbf{x}_n \\ \downarrow & \downarrow & & \downarrow \end{pmatrix} \\ &= \begin{pmatrix} \mathbf{x}_1.\mathbf{x}_1 & \mathbf{x}_1.\mathbf{x}_2 & \cdots \\ \mathbf{x}_2.\mathbf{x}_1 & \ddots & \\ \vdots & & \end{pmatrix} \\ &= \mathbf{I}. \end{aligned} \tag{A.52}$$

A.4.3 Orthogonal Matrices

A matrix $\mathbf{O}$ is said to be orthogonal if $\mathbf{O}^T = \mathbf{O}^{-1}$; from equation (A.52) we can see that $\mathbf{X}$ fulfils this requirement. Such matrices enable transformations without a

change in length scale. Consider right multiplying the (orthogonal) matrix $\mathbf{X}$ by the vector $\mathbf{v}$ such $\mathbf{Xv} = \mathbf{v}'$. The elements of the new vector are then $\mathbf{v}'_a = \mathbf{x}_a.\mathbf{v}$ where $\mathbf{x}_a$ is the a^{th} row of $\mathbf{X}$. Then,

$$|\mathbf{v}'| = \sqrt{\sum_a (\mathbf{x}_a.\mathbf{v})^2} \tag{A.53}$$

where

$$\sum_a (\mathbf{x}_a.\mathbf{v})^2 = \sum_a \left(\sum_i x_{ai} v_i \right)^2 \tag{A.54}$$

$$= \sum_a \sum_i \sum_j x_{ai} v_i x_{aj} v_j \tag{A.55}$$

$$= \sum_a \sum_i \sum_j x^T_{ia} v_i x_{aj} v_j \tag{A.56}$$

$$= \sum_i \sum_j v_i v_j \delta_{ij} \tag{A.57}$$

$$= \sum_i (v_i)^2. \tag{A.58}$$

Thus

$$|\mathbf{v}'| = |\mathbf{v}| \tag{A.59}$$

and the transformation is seen to effect no change in length scale. More importantly, the volume of integration remains unchanged. Consider,

$$\mathbf{x}' = \mathbf{O}\mathbf{x} \tag{A.60}$$

$$\mathbf{x} = \mathbf{O}^{-1}\mathbf{x}' \tag{A.61}$$

$$= \mathbf{O}^T\mathbf{x}' \tag{A.62}$$

$$x_i = \mathbf{O}_i^T\mathbf{x}' \tag{A.63}$$

$$\mathrm{d}x_i = \sum_j \frac{\partial x_i}{\partial x'_j} \mathrm{d}x'_j \tag{A.64}$$

$$= \sum_j O^T_{ij} \mathrm{d}x_j'. \tag{A.65}$$

Thus

$$O_{ij}^{T} = \frac{\partial x_i}{\partial x'_j} \tag{A.66}$$

and so $\det(\mathbf{O})$ is the Jacobian for the transformation with,

$$\mathrm{d}^N\mathbf{x} = \det(\mathbf{O})\,\mathrm{d}^N\mathbf{x}' \tag{A.67}$$

$$= \mathrm{d}^N\mathbf{x}', \tag{A.68}$$

as the determinant of an orthogonal matrix is always 1 (or -1 in which case it is always possible to choose a matrix $\mathbf{P}$ such that $\mathbf{OP}$ diagonalizes $\mathbf{D}$ but has a positive unit determinant).

Appendix B

Probability Distributions Derived from Gaussians

Gaussian variables occur frequently in analytical work as they have a tendency to provide tractable solutions. In the case of the 2dXY and $d = \alpha$ models discussed in the main text, the quantity of interest, the order parameter, was defined in terms of the square of Gaussian variables therefore introducing another type of distribution.

B.1 Gaussians with Zero Mean

When x is a Gaussian with zero mean and standard deviation σ_x,

$$P_x(x) = \frac{1}{\sigma_x\sqrt{2\pi}} e^{-x^2/(2\sigma_x^2)}. \tag{B.1}$$

Defining $y = x^2$ to be a variable with PDF $P_y(y)$, we can make use of the general result,

$$\int P_a(x)\,\mathrm{d}x = \int P_b(x)\,\mathrm{d}x. \tag{B.2}$$

In this specific case there is actually an extra factor of 2 required to correctly normalize $P_y(y)$, arising from the fact that $P_y(y)$ is defined on only half the range of values of $P_x(x)$ – that is, y must be positive. Therefore, the distribution of y is found to be,

$$P_y(y) = 2\left|\frac{\mathrm{d}x}{\mathrm{d}y}\right| P_x(x) \tag{B.3}$$

$$= \frac{2}{x} P_x(x). \tag{B.4}$$

Substituting for x then gives

$$P_y(y) = \frac{1}{\sigma_x}\sqrt{\frac{1}{2\pi y}} e^{-y/(2\sigma_x^2)}. \tag{B.5}$$

This is the definition of a $\Gamma_{\frac{1}{2}}$ distribution with mean $\mu_y = \sigma_x^2$ and standard deviation $\sigma_y = \sigma_x^2\sqrt{2}$.

In line with our usual approach, this function can be shifted to zero mean and scaled by it standard deviation, by making the transformation

$$z = \frac{y - \langle y \rangle}{\sigma_y}. \tag{B.6}$$

Applying (B.2) then gives

$$P_z(z) = \frac{\sigma_y}{\sigma_x\sqrt{2\pi}}(\sigma_y z + \mu_y)^{-1/2} e^{-(\sigma_y z + \mu_y)/(2\sigma_x^2)}. \tag{B.7}$$

B.2 Gaussians with Non-Zero Mean

When the mean of the Gaussian distribution is non-zero, the change of variable to $y = x^2$ introduces an extra term in the argument of the exponential, and the resulting $P_y(y)$ is not $\Gamma_{\frac{1}{2}}$. If

$$P_x(x) = \frac{1}{\sigma_x\sqrt{2\pi}} e^{-(x-\mu_x)^2/(2\sigma_x^2)}, \tag{B.8}$$

then from (B.3),

$$P_y(y) = \frac{e^{-\mu_x/(2\sigma_x^2)}}{\sigma_x}\sqrt{\frac{1}{2\pi y}} \exp\left(-\frac{y}{2\sigma_x^2} + \frac{\mu_x y^{1/2}}{\sigma_x^2}\right). \tag{B.9}$$

Scaling and shifting the distribution as before leads to,

$$P_y(y) = \frac{\sigma_y e^{-\mu_x/(2\sigma_x^2)}}{\sigma_x\sqrt{2\pi(\sigma_y z + \mu_y)}} \exp\left(-\frac{(\sigma_y z + \mu_y)}{2\sigma_x^2} + \frac{\mu_x(\sigma_y z + \mu_y)^{1/2}}{\sigma_x^2}\right). \tag{B.10}$$

To be correctly identified as a probability density function, (B.10) must be normalized by its integral, yielding

$$P_y(y) = \frac{\sigma_y \exp\left(-\frac{(\sigma_y z + \mu_y)}{2\sigma_x^2} + \frac{\mu_x(\sigma_y z + \mu_y)^{1/2}}{\sigma_x^2}\right)}{\sigma_x e^{\mu_x^2/(2\sigma_x^2)}\sqrt{2\pi(\sigma_y z + \mu_y)}\left(1 - \mathrm{erf}\left(\mu_x/(\sigma_x\sqrt{2})\right)\right)}. \tag{B.11}$$

B.3 Cumulants of the Sum of Identical Γ_γ Variables

Consider a global quantity

$$S = \sum_{\mathbf{n}} s_{\mathbf{n}}, \tag{B.12}$$

where $s_{\mathbf{n}}$ is a general Γ_γ variable with distribution

$$P(s_{\mathbf{n}}) = \frac{{a_{\mathbf{n}}}^\gamma}{\Gamma(\gamma)} e^{-a_{\mathbf{n}} s_{\mathbf{n}}} s_{\mathbf{n}}^{\gamma-1}, \tag{B.13}$$

and $\mathbf{n}$ is a d dimensional vector with integer elements $\pm 1 \ldots \infty$. It is possible to determine an expression for the cumulants of S which may be summed numerically.

Fourier transforming (B.13) gives the characteristic function of a single $s_{\mathbf{n}}$,

$$\psi_{\mathbf{n}}(t) = \int_{-\infty}^{\infty} \frac{{a_{\mathbf{n}}}^\gamma}{\Gamma^\gamma} e^{-a_{\mathbf{n}} s_{\mathbf{n}}} s_{\mathbf{n}}^{\gamma-1} e^{its_{\mathbf{n}}} \, \mathrm{d}s_{\mathbf{n}} \tag{B.14}$$

$$= \frac{a_{\mathbf{n}}^\gamma}{\Gamma(\gamma)} \int_{-\infty}^{\infty} e^{s_{\mathbf{n}}(it - a_{\mathbf{n}})} s_{\mathbf{n}}^{\gamma-1} \, \mathrm{d}s_{\mathbf{n}} \tag{B.15}$$

Substituting $z_{\mathbf{n}} = s_{\mathbf{n}}(a_{\mathbf{n}} - it)$ then yields

$$\psi_{\mathbf{n}}(t) = \frac{a_{\mathbf{n}}^\gamma}{\Gamma(\gamma)(a_{\mathbf{n}} - it)^\gamma} \int_{-\infty}^{\infty} e^{-z_{\mathbf{n}}} z_{\mathbf{n}}^{\gamma-1} \, \mathrm{d}z_{\mathbf{n}}, \tag{B.16}$$

where the integral is simply the definition of $\Gamma(\gamma)$, hence

$$\psi_{\mathbf{n}}(t) = \frac{a_{\mathbf{n}}^\gamma}{(a_{\mathbf{n}} - it)^\gamma} \tag{B.17}$$

$$= \left(1 - \frac{it}{a_{\mathbf{n}}}\right)^{-\gamma}. \tag{B.18}$$

The r^{th} cumulant of a variable is equal to the coefficient of $(it)^r/r!$ in the expansion of the logarithm of its characteristic function, thus:

$$\log \psi_{\mathbf{n}}(t) = \sum_{r=1}^{\infty} \frac{(it)^r}{r!} \kappa_{\mathbf{r}}(s_{\mathbf{n}}) \tag{B.19}$$

$$\log \psi_{\mathbf{n}}(t) = -\gamma \log\left(1 - \frac{it}{a_{\mathbf{n}}}\right) \tag{B.20}$$

$$= -\gamma \left[-\frac{it}{a_{\mathbf{n}}} - \frac{1}{2}\left(\frac{-it}{a_{\mathbf{n}}}\right)^2 + \frac{1}{3}\left(\frac{-it}{a_{\mathbf{n}}}\right)^3 - \ldots + \right] \tag{B.21}$$

$$= \gamma\left[\frac{it}{a_{\mathbf{n}}} + \frac{1}{2}\left(\frac{it}{a_{\mathbf{n}}}\right)^2 + \frac{1}{3}\left(\frac{it}{a_{\mathbf{n}}}\right)^3 + \ldots +\right] \tag{B.22}$$

Comparison of (B.19) and (B.22) then shows that

$$\kappa_r(s_{\mathbf{n}}) = \gamma(r-1)!\frac{1}{a_{\mathbf{n}}^r}. \tag{B.23}$$

Assuming that the $s_{\mathbf{n}}$ are independent, the characteristic function of the global measure, S, is defined as

$$\Psi(t_1, t_2, \ldots) = \int_{-\infty}^{\infty} \ldots e^{it_1x_1 + it_2x_2 + \cdots} \mathrm{d}^N x \ldots \tag{B.24}$$

$$= \prod_{\mathbf{n}} \psi(t_{\mathbf{n}}) \tag{B.25}$$

Hence the r^{th} cumulant of S is the sum over $\mathbf{n}$ of the corresponding cumulants of $s_{\mathbf{n}}$,

$$\kappa_r(S) = \sum_{\mathbf{n}} \kappa_r(s_{\mathbf{n}}) \tag{B.26}$$

$$= \frac{1}{2}(r-1)! \sum_{\mathbf{n}} a_{\mathbf{n}}^{-r} \tag{B.27}$$

Scaling S with the transformation $S \to S/\sigma_S$ one finds

$$\kappa_r(S) = \frac{\frac{1}{2}(r-1)! \sum_{\mathbf{n}} a_{\mathbf{n}}^{-r}}{\left(\frac{1}{2}\sum_{\mathbf{n}} a_{\mathbf{n}}^{-2}\right)^{r/2}}. \tag{B.28}$$

Letting

$$a_{\mathbf{n}} = |\mathbf{q}|^{\alpha} \qquad \text{and} \qquad \gamma = \frac{1}{2}, \tag{B.29}$$

recovers the family of models discussed in Chapter 5. That the vector $\mathbf{n}$ becomes the wave vector $\mathbf{q}$, with non-integer elements $q_x = 2\pi L/n_x$, causes no problems as this only introduces constant factors multiplying the sums over integer elements and the constants cancel when scaling by σ.

Appendix C

Spin Wave Analysis of the XY Model

The derivations in this appendix follow the approach in [16] and are essentially a more explicit reproduction of the results therein.

C.1 The Reciprocal Space Hamiltonian in d Dimensions

The spin wave approximation to the XY model in d dimensions is defined by the Hamiltonian

$$H = -J\left(1 - \frac{1}{2}\sum_{\langle \mathbf{r},\mathbf{r}'\rangle}(\theta_{\mathbf{r}} - \theta_{\mathbf{r}'})^2\right), \tag{C.1}$$

where J is positive and the sum runs over all nearest neighbour pairs of spins, each of which is constrained to lie in the same two dimensional plane. The variable $\theta_{\mathbf{r}}$ represents the angle between the spin at site $\mathbf{r}$ and some arbitrary but fixed axis. It is assumed that the spins lie on the points of a hypercubic lattice of size $N = L^d$.

Defining the pair of Fourier transforms

$$\theta_{\mathbf{r}} = \frac{1}{\sqrt{N}}\sum_{\mathbf{q}} e^{i\mathbf{q}\cdot\mathbf{r}}\phi_{\mathbf{q}} \tag{C.2}$$

$$\phi_{\mathbf{q}} = \frac{1}{\sqrt{N}} \sum_{\mathbf{r}} e^{-i\mathbf{q}.\mathbf{r}} \theta_{\mathbf{r}}, \tag{C.3}$$

equation (C.2) can be substituted into (C.1) to give the reciprocal space form of the Hamiltonian. Firstly the contents of the brackets are expressed as,

$$(\theta_{\mathbf{r}} - \theta_{\mathbf{r}'}) = \frac{1}{\sqrt{N}} \sum_{\mathbf{q}} \left(e^{i\mathbf{q}.\mathbf{r}} - e^{i\mathbf{q}\mathbf{r}'} \right) \phi_{\mathbf{q}} \tag{C.4}$$

$$= \frac{1}{\sqrt{N}} \sum_{\mathbf{q}} e^{i\mathbf{q}.\mathbf{r}} (1 - e^{-i\mathbf{q}.(\mathbf{r}-\mathbf{r}')}) \phi_{\mathbf{q}}, \tag{C.5}$$

which squares to give

$$(\theta_{\mathbf{r}} - \theta_{\mathbf{r}'})^2 = \frac{1}{N} \sum_{\mathbf{q}} \sum_{\mathbf{q}'} e^{i(\mathbf{q}+\mathbf{q}').\mathbf{r}} \left(1 - e^{-i\mathbf{q}.(\mathbf{r}-\mathbf{r}')} \right) \left(1 - e^{-i\mathbf{q}'.(\mathbf{r}-\mathbf{r}')} \right) \phi_{\mathbf{q}} \phi_{\mathbf{q}'}. \tag{C.6}$$

Using the standard relation

$$\sum_{\mathbf{r}} e^{i\mathbf{k}.\mathbf{r}} \overset{N\to\infty}{=} N \delta_{\mathbf{k},0}, \tag{C.7}$$

and substituting (C.6) into (C.1), yields the Hamiltonian in the form,

$$H = -J \left[1 - \frac{1}{2} \sum_{\langle \mathbf{r},\mathbf{r}' \rangle} \frac{1}{N} \sum_{\mathbf{q}} \sum_{\mathbf{q}'} e^{i(\mathbf{q}+\mathbf{q}').\mathbf{r}} \left(1 - e^{-i\mathbf{q}.(\mathbf{r}-\mathbf{r}')} \right) \left(1 - e^{-i\mathbf{q}'.(\mathbf{r}-\mathbf{r}')} \right) \phi_{\mathbf{q}} \phi_{\mathbf{q}'} \right] \tag{C.8}$$

$$= -J \left[1 - \frac{1}{2} \sum_{\mathbf{q}} \sum_{x} (2 - 2\cos q_x) |\phi_{\mathbf{q}}|^2 \right] \tag{C.9}$$

Equation (C.9) follows because (C.7) forces $\mathbf{q} + \mathbf{q}' = 0$ and from (C.3) this implies $\mathbf{q}' = \mathbf{q}^*$. Also, the sum over nearest neighbours of $\mathbf{q}.(\mathbf{r} - \mathbf{r}')$ is equivalent to summing the components q_x over the dimensions x.

In two dimensions, i.e. the 2dXY model, we have,

$$H = -J \left[1 - \frac{1}{2} \sum_{\mathbf{q}} \gamma_{\mathbf{q}} |\phi_{\mathbf{q}}|^2 \right], \tag{C.10}$$

where

$$\gamma_{\mathbf{q}} = 4 - 2\cos q_x - 2\cos q_y. \tag{C.11}$$

C.2 The Magnetization in Two Dimensions

We wish to evaluate the thermal average of the order parameter, $\langle m \rangle$. Defining the instantaneous direction of the magnetization vector as

$$\bar{\theta} = \tan^{-1}\left(\frac{\sum_{\mathbf{r}} \sin\theta_{\mathbf{r}}}{\sum_{\mathbf{r}} \cos\theta_{\mathbf{r}}}\right), \tag{C.12}$$

it is possible to transfer to a reference frame in which the Goldstone mode is excluded, introducing the variable

$$\psi_{\mathbf{r}} = \theta_{\mathbf{r}} - \bar{\theta}. \tag{C.13}$$

This means that all sums over $\mathbf{q}$ must now exclude $\mathbf{q} = 0$. In these coordinates, the cosine form of the instantaneous scalar magnetization is,

$$m = \frac{1}{N}\sum_{\mathbf{r}} \cos\psi_{\mathbf{r}}. \tag{C.14}$$

To evaluate $\langle m \rangle$ requires that $|\psi_{\mathbf{r}}|$ is recognized as a Gaussian variable so that the methods of Gaussian integration may be applied. We must also determine the Green's function propagator

$$G(\mathbf{r}) = \frac{J}{T}\left\langle \psi_0 \psi_{\mathbf{r}} \right\rangle. \tag{C.15}$$

The Hamiltonian (C.9) shows that $|\phi_{\mathbf{q}}|$ is a Gaussian variable, as $H_{\mathbf{q}} \propto |\phi_{\mathbf{q}}|^2$, giving

$$P(|\phi_{\mathbf{q}}|) \propto \exp\left(-\frac{J}{2T}\gamma_{\mathbf{q}}|\phi_{\mathbf{q}}|^2\right). \tag{C.16}$$

Expressing $\phi_{\mathbf{q}} = \phi'_{\mathbf{q}} + i\phi''_{\mathbf{q}}$, we see that

$$|\phi_{\mathbf{q}}|^2 = \phi'^2_{\mathbf{q}} + \phi''^2_{\mathbf{q}}, \tag{C.17}$$

and therefore the real and imaginary parts of $\phi_{\mathbf{q}}$ must be Gaussian in their own right, as the convolution of two Gaussians is a Gaussian. In this context $\theta_{\mathbf{r}}$, and therefore $\psi_{\mathbf{r}}$, may be thought of as being the sum of two Fourier transforms of Gaussian variables. Since the Fourier transform of a Gaussian is itself a Gaussian, this means that $\psi_{\mathbf{r}}$ must be a Gaussian variable! As a result the methods discussed in Appendix A may be applied to averages of $|\phi_{\mathbf{q}}|$, most usefully in the form of Wick's theorem,

$$\left\langle \psi_0^{2i} \right\rangle = (2p-1)!! \left\langle \psi_0^2 \right\rangle^i. \tag{C.18}$$

The average of the order parameter is therefore,

$$\langle m \rangle = \left\langle \frac{1}{N} \sum_{\mathbf{r}} \cos \psi_{\mathbf{r}} \right\rangle \tag{C.19}$$

$$= \frac{1}{N} \sum_{\mathbf{r}} \left\langle \cos \psi_{\mathbf{r}} \right\rangle \tag{C.20}$$

$$= \langle \cos \psi_0 \rangle \tag{C.21}$$

$$= \sum_{i=0}^{\infty} \frac{(-1)^i}{(2i)!} \left\langle \psi_0^{2i} \right\rangle \tag{C.22}$$

$$= \sum_{i=0}^{\infty} \frac{(2i-1)!!}{(2i)!} \left[-\frac{T}{J} G(0) \right]^i \tag{C.23}$$

$$= \sum_{i=0}^{\infty} \frac{1}{2^i \times i!} \left[-\frac{T}{J} G(0) \right]^i \tag{C.24}$$

$$= \exp\left(-\frac{TG(0)}{2J} \right). \tag{C.25}$$

Equation (C.21) follows due to the translational invariance of the system. Equation (C.24) arises from the fact,

$$\frac{(2i-1)!!}{(2i)!} = \frac{(2i-1)(2i-3)(2i-5)\ldots}{(2i)(2i-1)(2i-2)(2i-3)\ldots} \tag{C.26}$$

$$= \frac{1}{(2i)(2i-2)(2i-4)\ldots} \tag{C.27}$$

$$= \frac{1}{2^i \times i!}. \tag{C.28}$$

C.2.1 Determining $G(\mathbf{r})$

Taking $\psi_{\mathbf{q}}$ to be the Fourier transform of $\psi_{\mathbf{r}}$,

$$G(\mathbf{r}) = \left\langle \frac{J}{NT} \sum_{\mathbf{q} \neq 0} \sum_{\mathbf{q}' \neq 0} e^{i\mathbf{q}.\mathbf{r}} \psi_{\mathbf{q}} \psi_{\mathbf{q}'} \right\rangle \tag{C.29}$$

$$= \frac{J}{NT} \sum_{\mathbf{q} \neq 0} \sum_{\mathbf{q}' \neq 0} e^{i\mathbf{q}.\mathbf{r}} \left\langle \psi_{\mathbf{q}} \psi_{\mathbf{q}'} \right\rangle. \tag{C.30}$$

And the variables $\psi_{\mathbf{q}}$ may be related to $\phi_{\mathbf{q}}$:

$$\psi_{\mathbf{q}} = \frac{1}{\sqrt{N}} \sum_{\mathbf{r}} e^{-i\mathbf{q}.\mathbf{r}} \psi_{\mathbf{r}} \tag{C.31}$$

$$= \frac{1}{\sqrt{N}} \sum_{\mathbf{r}} e^{i\mathbf{q}.\mathbf{r}} (\theta_{\mathbf{r}} - \bar{\theta}) \tag{C.32}$$

$$= \phi_{\mathbf{q}} - \frac{\bar{\theta}}{\sqrt{N}} \sum_{\mathbf{r}} e^{i\mathbf{q}.\mathbf{r}} \tag{C.33}$$

$$= \phi_{\mathbf{q}} - \bar{\theta}\sqrt{N}\delta_{\mathbf{q},0}. \tag{C.34}$$

The definition of the average magnetization direction given above is designed to maintain the periodicity of the spins in $\bar{\theta}$. Using the more conventional expression for the mean,

$$\bar{\theta} = \frac{1}{N} \sum_{\mathbf{r}} \theta_{\mathbf{r}}, \tag{C.35}$$

and given that

$$\phi_0 = \frac{1}{\sqrt{N}} \sum_{\mathbf{r}} \theta_{\mathbf{r}}, \tag{C.36}$$

equation (C.34) becomes

$$\psi_{\mathbf{q}} = \phi_{\mathbf{q}} - \phi_0 \delta_{\mathbf{q},0} \tag{C.37}$$

$$= \phi_{\mathbf{q}} (1 - \delta_{\mathbf{q},0}). \tag{C.38}$$

Therefore the Green's function may be expressed as

$$G(\mathbf{r}) = \frac{J}{NT} \sum_{\mathbf{q} \neq 0} e^{i\mathbf{q}.\mathbf{r}} \left\langle |\phi_{\mathbf{q}}|^2 \right\rangle. \tag{C.39}$$

Comparing (C.16) with the standard Gaussian form, $P(x) \propto \exp(-x^2/(2\sigma^2))$, shows that the variance of $|\phi_{\mathbf{q}}|$ is

$$\sigma^2_{|\phi_{\mathbf{q}}|} = \frac{T}{J\gamma_{\mathbf{q}}}, \tag{C.40}$$

and given that $\sigma_x^2 = \langle x^2 \rangle - \langle x \rangle^2$, and that we know $\langle |\phi_{\mathbf{q}}|^2 \rangle = 0$,

$$\left\langle |\phi_{\mathbf{q}}|^2 \right\rangle = \frac{T}{J\gamma_{\mathbf{q}}}. \tag{C.41}$$

The Green's function then becomes

$$G(\mathbf{r}) = \frac{1}{N} \sum_{\mathbf{q} \neq 0} \frac{e^{i\mathbf{q}.\mathbf{r}}}{\gamma_{\mathbf{q}}}. \tag{C.42}$$

For $\mathbf{r} = 0$, this sum may approximated by integrating over a circular Brillouin zone, as discussed in Chapter 4, or may be evaluated precisely using the Abel-Plana formula, as in Chapter 5. Both lead to

$$G(0) = \frac{1}{4\pi} \ln(CN), \tag{C.43}$$

with $C = 2$ and $C \approx 1.8456$ [6] respectively. Combining (C.25) and (C.43) then gives the power law variation of the magnetization,

$$\langle m \rangle = \left(\frac{1}{CN}\right)^{T/8\pi J}. \tag{C.44}$$

This result shows that the magnetization of the $d = 2$ Harmonic model (and, therefore, the critical region of the 2dXY model) is zero in the thermodynamic limit. However, the very slow decline in $\langle m \rangle$ as a function of N means that m is a physically relevant observable [31].

C.3 The Magnetic Susceptibility

Using the traditional definition of the magnetization,

$$m = \frac{1}{N} \sqrt{\left(\sum_{\mathbf{r}} \mathbf{S}_{\mathbf{r}}\right)^2}, \tag{C.45}$$

we can find the second moment of the magnetization distribution as

$$\left\langle m^2 \right\rangle = \left\langle \frac{1}{N^2} \sum_{\mathbf{r}} \sum_{\mathbf{r}'} \mathbf{S}_{\mathbf{r}} . \mathbf{S}_{\mathbf{r}} \right\rangle \tag{C.46}$$

$$= \frac{1}{N} \sum_{\mathbf{r}} \left\langle \mathbf{S}_0 \mathbf{S}_{\mathbf{r}} \right\rangle, \tag{C.47}$$

where (C.47) follows as a result of the translational invariance of the system. The magnetic susceptibility is therefore

$$\chi = \frac{N}{T}\left\{\left\langle m^2\right\rangle - \langle m\rangle^2\right\} \tag{C.48}$$

$$= \frac{N}{T}\left\{\left(\frac{1}{N}\sum_{\mathbf{r}}\left\langle \mathbf{S}_0\mathbf{S}_{\mathbf{r}}\right\rangle\right) - \langle m\rangle^2\right\}. \tag{C.49}$$

The sum over $\mathbf{r}$ of the average may be expressed in terms of the angles $\psi_{\mathbf{r}}$ as,

$$\frac{1}{N}\sum_{\mathbf{r}}\left\langle \mathbf{S}_0\mathbf{S}_{\mathbf{r}}\right\rangle = \frac{1}{N}\sum_{\mathbf{r}}\langle\cos(\psi_0 - \psi_{\mathbf{r}})\rangle \tag{C.50}$$

$$= \frac{1}{N}\sum_{\mathbf{r}}\left\langle e^{i(\psi_0-\psi_{\mathbf{r}})}\right\rangle, \tag{C.51}$$

which is possible because the sum results in the sine terms in the expansion of the exponential cancelling each other out. As $\psi_{\mathbf{r}}$ is Gaussian the average in (C.51) can be evaluated using the methods described in Appendix A. This gives

$$\left\langle e^{i(\psi_0-\psi_{\mathbf{r}})}\right\rangle = \left\langle \exp\left(i\sum_{a=1}^{2} J_a\psi_{(a)}\right)\right\rangle \tag{C.52}$$

$$= \exp\left(-\frac{1}{2}\sum_{a=1}^{2}\sum_{b=1}^{2} J_a A^{-1}_{ab} J_b\right) \tag{C.53}$$

$$= \exp\left(-\frac{1}{2}\left\{A^{-1}_{11} - A^{-1}_{12} - A^{-1}_{21} + A^{-1}_{22}\right\}\right), \tag{C.54}$$

where $J_1 = -1$, $J_2 = 1$, $\psi_{(1)} = \psi_0$ and $\psi_{(2)} = \psi_{\mathbf{r}}$, and

$$A^{-1}_{ij} = \left\langle \psi_i\psi_j\right\rangle \tag{C.55}$$

$$= \frac{T}{J}G_{ij}. \tag{C.56}$$

Combining (C.51), (C.54) and (C.56) gives

$$\frac{1}{N}\sum_{\mathbf{r}}\left\langle \mathbf{S}_0\mathbf{S}_{\mathbf{r}}\right\rangle = \exp\left[-\frac{T}{J}(G(0) - G(\mathbf{r}))\right] \tag{C.57}$$

Substituting (C.57) into (C.49) yields

$$\chi = \frac{N}{T}\left\{\frac{1}{N}\left(\sum_{\mathbf{r}}\exp\left[\frac{T}{J}(G(\mathbf{r}) - G(0))\right]\right) - \langle m\rangle^2\right\} \tag{C.58}$$

$$= \frac{N}{T}\left\{\frac{e^{-\frac{T}{J}G(0)}}{N}\left[\left(\sum_{\mathbf{r}} e^{\frac{T}{J}G(\mathbf{r})}\right) - N\right]\right\} \tag{C.59}$$

$$= \frac{\langle m\rangle^2}{T}\left\{\sum_{\mathbf{r}}\left(e^{\frac{T}{J}G(\mathbf{r})} - 1\right)\right\}. \tag{C.60}$$

Equation (C.60) follows from the definition of the magnetization in (C.25). At low temperatures the exponential may be expanded with higher terms being discarded,

$$\chi \approx \frac{T\langle m\rangle^2}{2J^2}\sum_{\mathbf{r}} G(\mathbf{r})^2. \tag{C.61}$$

Substituting (C.42) then gives

$$\chi \approx \frac{T\langle m\rangle^2}{2JN^2}\sum_{\mathbf{r}}\sum_{\mathbf{q}\neq 0}\sum_{\mathbf{q}'\neq 0}\frac{e^{i(\mathbf{q}+\mathbf{q}')\cdot\mathbf{r}}}{\gamma_{\mathbf{q}}} \tag{C.62}$$

$$\approx \frac{NT\langle m\rangle^2}{2J^2} g_2, \tag{C.63}$$

where g_2 is a constant (≈ 0.004) defined in Chapter 4. As $\langle m\rangle \sim N^{-T/(8\pi J)}$ (from (C.44), the susceptibility scales as

$$\chi \sim N^{1-T/(4\pi J)}. \tag{C.64}$$

Combining (C.48) and (C.63) then gives

$$\sigma \sim \sqrt{\frac{\chi}{N}} \tag{C.65}$$

$$\sim N^{-T/(8\pi J)} \tag{C.66}$$

$$\sim \langle m\rangle, \tag{C.67}$$

confirming that hyperscaling is obeyed. Furthermore, Berezinskiĭ demonstrated that, for sufficiently large systems, $\eta = T/(2\pi J)$ [56]. Combined with (C.44) and the finite size scaling result $m \sim N^{-\beta/2\nu}$, this implies that

$$\eta = \frac{2\beta}{\nu}, \tag{C.68}$$

and therefore the order parameter of the Harmonic model is dependent on a single temperature dependent critical exponent $\eta(T)$.

Appendix D

Pearson Analysis of the $d = m = 3$ Model

The shape of a probability distribution, $P(x)$, is largely governed by the values of its first four moments. Taking this as a starting point, Pearson developed a means for obtaining an analytical expression for a distribution using just these moments, via his eponymous differential equation,

$$\frac{\mathrm{d}\ln P(x)}{\mathrm{d}x} = -\frac{x + b_1}{b_0 + b_1 x + b x^2}. \tag{D.1}$$

It is assumed that $P(x)$ is a well behaved, normalized, probability density function. Choosing the origin to coincide with the average gives

$$\mu_0 = 1 \qquad \text{and} \qquad \mu_1 = 0. \tag{D.2}$$

The second, third and fourth moments are found as functions of the constants b_0, b_1 and b by rearranging (D.1), multiplying by the appropriate factor of x^r and integrating. This leads to,

$$b_0 = \frac{\sigma^2}{A}(4\beta_2 - 3\beta_1) \tag{D.3}$$

$$b_1 = \frac{\sigma\beta_1^{\frac{1}{2}}}{A}(\beta_2 + 3) \tag{D.4}$$

$$b = \frac{1}{A}(2\beta_2 - 3\beta_1 - 6), \tag{D.5}$$

where

$$A = 10\beta_2 - 12\beta_1 - 18. \tag{D.6}$$

Here the beta variables are related to the third and fourth normalized cumulants, that is the skewness and defect of kurtosis, as

$$\beta_1^2 = \gamma_3 \qquad \text{and} \qquad \beta_2 = \gamma_4 + 3. \tag{D.7}$$

Thus knowledge of the skewness and defect of kurtosis (we shall assume the distribution has been normalized by its standard deviation and take $\sigma = 1$) is sufficient to determine the constants b_0, b_1 and b. The solution of the differential equation depends on the behaviour of the 'auxiliary quadratic'

$$b_0 + b_1 x + b x^2 = 0. \tag{D.8}$$

There are a number of scenarios depending on the relative values of the roots of this quadratic. Here we consider only the case relevant to the solution of the $d = m = 3$ model discussed in Chapter 5. Other possibilities are discussed in detail in [145].

The skewness and defect of kurtosis for the $d = m = 3$ model may be evaluated numerically using (5.17). They are found to be

$$\gamma_3 = -0.769867 \qquad \text{and} \qquad \gamma_4 = 1.0543, \tag{D.9}$$

giving

$$\beta_1 = 0.59270 \tag{D.10}$$

$$\beta_2 = 4.0543 \tag{D.11}$$

$$A = 15.43066 \tag{D.12}$$

$$b_0 = 0.93574 \tag{D.13}$$

$$b_1 = -0.35195 \tag{D.14}$$

$$b = 0.02142. \tag{D.15}$$

Thus, substituting (D.13), (D.14) and (D.15) into (D.8) shows the roots of the quadratic are real and distinct. In this case it is convenient to shift the origin, introducing $\xi = x + b$, such that

$$\frac{\mathrm{d}\ln P}{\mathrm{d}\xi} = -\frac{\xi}{b\xi^2 + B_1\xi + B_0} \tag{D.16}$$

where

$$B_0 = b_0 + b_1^2(b-1) \qquad \text{and} \qquad B_1 = -b_1(2b-1). \tag{D.17}$$

If α and β are then the roots of the new auxiliary quadratic (setting the denominator of (D.16) to 0), then

$$B_0 = b\alpha\beta \qquad \text{and} \qquad B_1 = b(\alpha+\beta). \tag{D.18}$$

It is necessary to consider only the general case where $bB_1 < 0$ with $\alpha + \beta > 0$ and $|\alpha| < \beta$. Equation (D.16) may be written in the form

$$\frac{\mathrm{d}\ln P}{\mathrm{d}\xi} = \frac{p\alpha}{\xi - \alpha} - \frac{p\beta}{\xi - \beta} \tag{D.19}$$

where

$$p = \frac{1}{b(\beta - \alpha)}. \tag{D.20}$$

There are many solutions to (D.19) depending on the relative signs and magnitudes of the variables α, β and b. In our model, $0 < \alpha < \beta$ and $b > 0$ so the distribution takes the form

$$P = P_0\left(1 - \frac{\xi}{\alpha}\right)^{p\alpha}\left(1 - \frac{\xi}{\beta}\right)^{p\beta}. \tag{D.21}$$

Again, other possibilities are discussed in [145]. The only unknown is the normalizing factor P_0 which may be found in the usual manner by setting the integral of (D.21) to 1. For our model the final result is

$$P(\xi) = 0.43986\left(1 - \frac{\xi}{2.98404}\right)^{14.27472}\left(1 - \frac{\xi}{12.74363}\right)^{60.96151}, \tag{D.22}$$

remembering that $\xi = x - 0.35195$.

Bibliography

[1] L. D. Landau and E. M. Lifshitz, *Statistical Physics Vol. 1* (Pergamon, 1980).

[2] H. B. Callen, *Thermodynamics and an Introduction to Thermostatistics* (Wiley, New York, 1985), 2nd ed.

[3] I. N. Levine, *Quantum Chemistry* (Pearson, 1999), 5th ed.

[4] A. Y. Khinchin, *Mathematical Foundations of Statistical Physics* (Dover, 1949).

[5] K. G. Wilson and J. Kogut, *Phys. Rep.* **12**, 75 (1974).

[6] S. T. Bramwell, J.-Y. Fortin, P. C. W. Holdsworth, S. Peysson, J.-F. Pinton, B. Portelli, and M. Sellitto, *Phys. Rev. E* **63**, 041106 (2001).

[7] M. R. Spiegel, *Theory and Problems of Probability and Statistics* (McGraw-Hill, 1975).

[8] M. Cassandro and G. Jona-Lasinio, *Adv. Phys.* **27**, 913 (1978).

[9] G. H. Wannier, *Statistical Physics* (Dover, 1897).

[10] C. Garrod, *Statistical Mechanics and Thermodynamics* (Oxford University Press, 1995).

[11] R. S. Ellis, *Entropy, Large Deviations and Statistical Mechanics* (Springer-Verlag, 1985).

[12] J. Cardy, *Scaling and Renormalization in Statistical Physics* (Cambridge University Press, 1996).

[13] A. D. Bruce, *J. Phys. C* **14**, 3667 (1981).

[14] K. P. Binder, in *Computational Methods in Field Theory*, edited by H. Gausterer and C. B. Lang (Springer-Verlag, 1992), vol. 409 of *Lecture Notes in Physics*.

[15] R. Botet and M. Ploszajczak, *Phys. Rev. E* **62**, 1825 (2000).

[16] P. Archambault, S. T. Bramwell, and P. C. W. Holdsworth, *J. Phys. A* **30**, 8363 (1997).

[17] P. Archambault, S. T. Bramwell, J.-Y. Fortin, P. C. W. Holdsworth, S. Peysson, and J.-F. Pinton, *J. Appl. Phys.* **83**, 7234 (1998).

[18] V. Aji and N. Goldenfeld, *Phys. Rev. Lett.* **86**, 1007 (2001).

[19] S. T. Bramwell, P. C. W. Holdsworth, and J.-F. Pinton, *Nature* **396**, 552 (1998).

[20] S. C. Chapman, G. Rowlands, and N. W. Watkins (2003), ArXiv /cond-mat/0302624.

[21] S. T. Bramwell, K. Christensen, J.-Y. Fortin, P. C. W. Holdsworth, H. J. Jensen, S. Lise, J. López, M. Nicodemi, J.-F. Pinton, and M. Sellitto, *Phys. Rev. Lett.* **84**, 3744 (2000).

[22] B. Zheng and S. Trimper, *Phys. Rev. Lett.* **87**, 188901 (2001).

[23] S. T. Bramwell, K. Christensen, J.-Y. Fortin, P. C. W. Holdsworth, H. J. Jensen, S. Lise, J. M. López, M. Nicodemi, J.-F. Pinton, and M. Sellitto, *Phys. Rev. Lett.* **87**, 188902 (2001).

[24] S. T. Bramwell, K. Christensen, J.-Y. Fortin, P. C. W. Holdsworth, H. J. Jensen, S. Lise, J. M. López, M. Nicodemi, J.-F. Pinton, and M. Sellitto, *Phys. Rev. Lett.* **89**, 208902 (2002), (comment).

[25] S. T. Bramwell, T. Fennel, P. C. W. Holdsworth, and B. Portelli, *Europhys. Lett.* **57**, 310 (2002).

[26] K. Dahlstedt and H. J. Jensen (2003), ArXiv /cond-mat/0307300.

[27] P. C. W. Holdsworth and M. Sellitto, *Physica A* **315**, 643 (2002).

[28] N. W. Watkins, S. C. Chapman, and G. Rowlands, *Phys. Rev. Lett.* **89**, 208902 (2002).

[29] C. Pennetta, E. Alfinito, L. Reggiani, and S. Ruffo, *Semicond. Sci. Technol.* **19**, S164 (2004).

[30] G. Palma, T. Meyer, and R. Labbé, *Phys. Rev. E* **66**, 026108 (2002).

[31] S. T. Bramwell and P. C. W. Holdsworth, *J. Phys.: Condens. Matter* **5**, L53 (1993).

[32] S. T. Bramwell and P. C. W. Holdsworth, *Phys. Rev. B* **49**, 8811 (1994).

[33] B. Portelli, P. C. W. Holdsworth, and J.-F. Pinton, *Phys. Rev. Lett.* **90**, 104501 (2003).

[34] M. Peyrard, *Physica D* **193**, 265 (2004).

[35] M. Peyrard and I. Daumont, *Europhys. Lett.* **59**, 834 (2002).

[36] A. Noullez and J.-F. Pinton, *Eur. Phys. J B* **28**, 231 (2002).

[37] T. Toth-Katona and J. T. Gleeson, *Phys. Rev. E* **69**, 016302 (2004).

[38] T. Toth-Katona and J. T. Gleeson, *Phys. Rev. Lett.* **91**, 264501 (2003).

[39] W. I. Goldburg, Y. Y. Goldschmidt, and H. Kellay, *Phys. Rev. Lett.* **87**, 245502 (2001).

[40] C. Pennetta, E. Alfinito, L. Reggiani, and S. Ruffo, *Physica A* **340**, 380 (2004).

[41] P. Sinha-Ray, L. B. de Agua, and H. J. Jensen, *Physica D* **157**, 186 (2001).

[42] K. Dahlstedt and H. J. Jensen, *J. Phys. A* **34**, 11193 (2001).

[43] P. Bak, C. Tang, and K. Wiesenfeld, *Phys. Rev. Lett.* **59**, 381 (1987).

[44] Z. Rácz, *SPIE Proc.* **5112**, 248 (2003), Also at arXiv /cond-mat/0307490.

[45] R. Labbé, J.-F. Pinton, and S. Fauve, *J. Phys. II (France)* **6**, 1099 (1996).

[46] Z. Rácz and M. Plischke, *Phys. Rev. E* **50**, 3530 (1994).

[47] G. Foltin, K. Oerding, Z. Rácz, R. L. Workman, and R. K. P. Zia, *Phys. Rev. E* **50**, R639 (1994).

[48] T. Antal, M. Droz, G. Györgyi, and Z. Rácz, *Phys. Rev. Lett.* **87**, 240601 (2001).

[49] T. Antal, M. Droz, G. Györgyi, and Z. Rácz, *Phys. Rev. E* **65**, 046140 (2001).

[50] M. Plishcke, Z. Rácz, and R. K. P. Zia, *Phys. Rev. E* **50**, 3589 (1994).

[51] S. F. Edwards and D. R. Wilkinson, *Proc. R. Soc. Lond. A* **381**, 17 (1982).

[52] M. Kardar, G. Parisi, and Y.-C. Zhang, *Phys. Rev. Lett.* **56**, 889 (1986).

[53] E. Marinari, A. Pagnani, G. Parisi, and A. Rácz, *Phys. Rev. E* **65**, 026136 (2002).

[54] B. Zheng, *Phys. Rev. E* **67**, 026114 (2003).

[55] J. M. Kosterlitz and D. J. Thouless, *J. Phys. C: Solid State Phys.* **6**, 1181 (1973).

[56] V. L. Berezinskiĭ, *Sov. Phys. JETP* **32**, 493 (1971).

[57] J. M. Kosterlitz, *J. Phys. C: Solid State Phys.* **7**, 1046 (1974).

[58] J. Villain, *J. Physique* **36**, 581 (1975).

[59] J. V. José, L. P. Kadanoff, S. Kirkpatrick, and D. R. Nelson, *Phys. Rev. B* **16**, 1217 (1977).

[60] E. J. Gumbel, *Statistics of Extremes* (Columbia University Press, 1958).

[61] R. A. Fisher and L. H. C. Tippett, *Camb. Philos. Soc.* **28**, 180 (1928).

[62] J.-P. Bouchaud and M. Mézard, *J. Phys. A* **30**, 7997 (1997).

[63] S. C. Chapman, G. Rowlands, and N. W. Watkins, *Nonlinear Proc. Geoph.* **9**, 409 (2002).

[64] B. Portelli and P. C. W. Holdsworth, *J. Phys. A* **35**, 1231 (2002).

[65] D. Carpentier and P. le Doussal, *Phys. Rev. E* **63**, 026110 (2001).

[66] J. B. Johnson, *Phys. Rev.* **26**, 71 (1925).

[67] H. W. Press, *Astrophys.* **7**, 103 (1978).

[68] R. F. Voss and J. Clarke, *Nature* **258**, 317 (1975).

[69] G. Györgyi, P. C. W. Holdsworth, B. Portelli, and Z. Rácz, *Phys. Rev. E* **68**, 056129 (2003).

[70] B. Portelli, P. C. W. Holdsworth, M. Sellitto, and S. T. Bramwell, *Phys. Rev. E* **64**, 036111 (2001).

[71] J. Binney, N. J. Dowrick, A. J. Fisher, and M. E. J. Newman, *The Theory of Critical Phenomena* (Clarendon Press, Oxford, 1992).

[72] P. Ehrenfest, *Communic. Leiden Univ.* **20**, 628 (1933), Suppl. 756.

[73] H. E. Stanley, *Phase Transitions and Critical Phenomena* (Clarendon Press, Oxford, 1971).

[74] L. Onsager, *Phys. Rev.* **65**, 117 (1944).

[75] P. M. Chaikin and T. C. Lubensky, *Principles of Condensed Matter Physics* (Cambridge University Press, 1995).

[76] G. S. Rushbrooke, *J. Chem. Phys.* **43**, 842 (1963).

[77] R. B. Griffiths, *J. Chem. Phys.* **43**, 1958 (1965).

[78] R. B. Griffiths, *Phys. Rev. Lett.* **14**, 623 (1965).

[79] M. E. Fisher, *Phys. Rev.* **180**, 594 (1969).

[80] B. D. Josephson, *J. Phys. (C)* **2**, 1115 (1969).

[81] B. Widom, *J. Chem. Phys.* **43**, 3892 (1965).

[82] T. Andrews, *Phil. Trans. Royal Soc.* **159**, 575 (1869).

[83] See http://faraday.physics.uiowa.edu/optics/6A40.44.htm.

[84] H. Kawamura, *J. Phys.: Condens. Matter* **10**, 4707 (1998).

[85] M. Kolesik and M. Suzuki (1994), ArXiv /cond-mat/9411109.

[86] M. Hasenbsuch, K. Pinn, and S. Vinti (1998), ArXiv /hep-lat/9806012.

[87] M. Plischke and B. Bergersen, *Equilibrium Statistical Mechanics* (World Scientific, 1994), 2nd ed.

[88] R. J. Baxter, *Exactly Solved Models in Statistical Mechanics* (Academic, New York, 1982).

[89] L. P. Kadanoff, *Physics* **2**, 263 (1966).

[90] M. Kendall, A. Stuart, and J. K. Ord, *Kendall's Advanced Theory of Statistics*, vol. 1 (Griffin, London, 1987).

[91] K. Pearson, *Philos. Trans. R. Soc. London Ser. A* **216**, 429 (1916).

[92] W. Feller, *An Introduction to Probability Theory and Its Applications* (Wiley, 1971).

[93] G. R. Grimmett and D. R. Stirzaker, *Probability and Random Processes* (Oxford University Press, 1992).

[94] R. von Mises, *Mathematical Foundations of Statistical Mechanics* (Academic, 1964).

[95] E. Ising, *Z. Physik* **31**, 253 (1925).

[96] P. Beale, *Phys. Rev. Lett.* **76**, 78 (1996).

[97] B. Kaufman, *Phys. Rev* **76**, 1232 (1949).

[98] R. Peierls, *Proc. Cambridge Phil. Soc.* **32**, 477 (1936).

[99] A. E. Ferdinand and M. E. Fisher, *Phys. Rev.* **185**, 832 (1969).

[100] N. D. Mermin and H. Wagner, *Phys. Rev. Lett.* **17**, 1133 (1966).

[101] H. E. Stanley, *Phys. Rev. Lett.* **20**, 589 (1968).

[102] M. A. Moore, *Phys. Rev. Lett.* **23**, 861 (1969).

[103] F. Wegner, *Z. Phys.* **206**, 465 (1967).

[104] F. R. N. Nabarro, *Theory of Crystal Dislocations* (Pergamon, 1967).

[105] D. R. Nelson and J. M. Kosterlitz, *Phys. Rev. Lett.* **39**, 1201 (1977).

[106] W. Janke and T. Matsui, *Phys. Rev. B* **42**, 10673 (1990).

[107] V. L. Berezinskiĭ and A. Y. Blank, *Zh. Eksp. Teor. Fiz.* **64**, 725 (1973).

[108] H. J. Elmers, J. Hauschild, G. H. Liu, and U. Gradmann, *J. Appl. Phys.* **79**, 4984 (1996).

[109] J. Als-Nielsen, S. T. Bramwell, M. T. Hutchings, G. T. McIntyre, and D. Visser, *J. Phys.: Condens. Matter* **5**, 7871 (1993).

[110] J. Tobochnik and G. V. Chester, *Phys. Rev. B* **20**, 3761 (1979).

[111] S. Peysson, *Rapport de Stage*, ENS de Lyon, France (1997).

[112] N. Metropolis, A. Rosenbluth, M. Rosenbluth, A. Teller, and E. Teller, *J. Chem. Phys.* **21**, 1087 (1953).

[113] Data obtained using a code kindly supplied by S. T. Bramwell.

[114] N. Goldenfeld, *Lectures on Phase Transitions and the Renormalization Group* (Addison-Wesley, 1992).

[115] B. P. van Millgen, (private communication).

[116] S. A. Safran, *Statistical Thermodynamics of Surfaces, Interfaces and Membranes* (Addison-Wesley, 1994).

[117] F. J. Dyson, *Commun. Math. Phys.* **12**, 91 (1969).

[118] J. Frölich and T. Spencer, *Commun. Math. Phys.* **84**, 87 (1982).

[119] K. Uzelac, Z. Glumac, and A. Aničić, *Phys. Rev. E* **63**, 037101 (2001).

[120] F. W. Olver, *Asymptotics and Special Functions* (AKP Classics, 1997).

[121] M. Frigo and S. G. Johnson, *Proc. ICASSP 1998* **3**, 1381 (1998).

[122] F. van Wijland, *Physica A* **332**, 360 (2003).

[123] D. Sornette, *Critical Phenomena in Natural Sciences* (Springer-Verlag, Berlin, 2000).

[124] A. van der Ziel, *Noise in Measurements* (Wiley-Interscience, 1976).

[125] B. I. Halperin and P. C. Hohenberg, *Phys. Rev. Lett.* **19**, 700 (1967).

[126] B. I. Halperin and P. C. Hohenberg, *Phys. Rev.* **177**, 952 (1969).

[127] E. Milotti (2002), Physics/0204033.

[128] S. R. Nagel, *Rev. Mod. Phys.* **64** (1992).

[129] H. J. Jensen, K. Christensen, and H. C. Fogedby, *Phys. Rev. B* **40** (1989).

[130] W. H. Press, S. A. Teukolsky, W. T. Vetterling, and B. P. Flannery, *Numerical Recipes in C++* (Cambridge University Press, 2002), 2nd ed.

[131] B. Pellegrini, R. Saletti, P. Terreni, and M. Prudenziati, *Phys. Rev. B* **27**, 1233 (1983).

[132] I. Flinn, *Nature* **219**, 1356 (1968).

[133] P. C. W. Holdsworth, (private communication).

[134] S. T. Bramwell, (private communication).

[135] W. Schottky, *Phys. Rev.* **28**, 74 (1926).

[136] F. K. du Pré, *Phys. Rev.* **78**, 615 (1950).

[137] P. Dutta, P. Dimon, and P. M. Horn, *Phys. Rev. Lett.* **43**, 646 (1979).

[138] S. Machlup, *J. Appl. Phys.* **25**, 341 (1954).

[139] S. Kogan, *Electronic Noise and Fluctuations in Solids* (Cambridge University Press, 1996).

[140] C. Huepe and M. Aldana, *Phys. Rev. Lett.* **92**, 168701 (2004).

[141] K. Rypdal and S. Ratynskaia, *Phys. Plasmas* **10**, 2686 (2003).

[142] J. Greenhough, P. C. Birch, S. C. Chapman, and G. Rowlands, *Physica A* **316**, 615 (2002).

[143] M. A. Gosalvez and R. M. Nieminen, *Phys. Rev. E* **68**, 056116 (2003).

[144] V. L. Pokrovsky and G. V. Uimin, *Phys. Lett.* **45a**, 467 (1973).

[145] W. M. Smart, *Combination of Observations* (Cambridge University Press, 1958).